ISBN 978-82-471-2852-7 (printed ver.)
ISBN 978-82-471-2853-4 (electronic ver.)
ISSN 1503-8181

Doctoral theses at NTNU, 2011:154

Biao Su

# Numerical Predictions of Global and Local Ice Loads on Ships

Biao Su

Doctoral Thesis

NTNU
Norwegian University of
Science and Technology

Doctoral theses at NTNU, 2011:154

NTNU

**NTNU**
Norwegian University of
Science and Technology
Thesis for the degree of
philosophiae doctor
Faculty of Engineering Science and Technology
Department of Marine Technology

NTNU
Norwegian University of
Science and Technology

Biao Su

# Numerical Predictions of Global and Local Ice Loads on Ships

Thesis for the degree of philosophiae doctor

Trondheim, June 2011

Norwegian University of
Science and Technology
Faculty of Engineering Science and Technology
Department of Marine Technology

NTNU
Norwegian University of
Science and Technology

**NTNU**
Norwegian University of Science and Technology

Thesis for the degree of philosophiae doctor

Faculty of Engineering Science and Technology
Department of Marine Technology



ISBN 978-82-471-2852-7 (printed ver.)
ISBN 978-82-471-2853-4 (electronic ver.)
ISSN 1503-8181

Doctoral Theses at NTNU, 2011:154

Printed by Tapir Uttrykk

# Abstract

Ice loads represent the dominant load for ice-going ships, and it is important to estimate both global and local ice loads on ship hulls. The global ice load governs the ship's overall performance in ice, and it is an integrated effect of local ice loads over the hull area. Information on the distributions of local ice loads around the hull can be used for more effective design of ice-going ships both in terms of overall operation and from the structural point of view.

The present thesis focuses on a numerical model for simulating ice–hull interaction and ship maneuvers in level ice. This model is partly based on the empirical data, by which the observed phenomena of continuous icebreaking can be reproduced. In the simulation of a full-scale icebreaking run, the interdependence between the ice load and the ship's motion is considered, and the three degree-of-freedom (DOF) rigid body equations of surge, sway and yaw are solved by numerical integration. The thickness and strength properties of the ice encountered by the ship are assumed to be constant or predefined based on the statistical data. Accordingly the global and local ice loads on ship hulls can be obtained in a deterministic or probabilistic way.

The convergence tests are carried out to make sure that this numerical method can give a convergent solution of both global and local ice loads. The computation time is also examined with the purpose of determining a balance between the computation time and the convergence. The influences of the assumptions and simplifications made in this numerical model are analyzed by changing different parameters and comparing with an empirical method and the measured data.

The simulation results are discussed through three case studies, in which the global ice load effects on ship's performance, the probabilistic and spatial variations of local ice loads around the hull and the short-term distribution of maximum ice loads on a frame are respectively analyzed and compared with field measurements conducted in the Baltic Sea.

The ship's performance in level ice is usually described by the speed that the ship can attain in the ice of a certain thickness. A case study with an icebreaker, Tor Viking II, is carried out by using the simulation program. In this study, the ice encountered by the ship is assumed to be uniform. The ship's motion is obtained by solving the equations of motion in which the thrust and the global ice load both are identified. The speed that the ship can attain is then simulated in the ice of different thicknesses. The simulation

results agree well with the full-scale measurements. The turning circle diameter which is a measure of the ship's maneuverability in ice is also investigated by using the simulation program. Herein the ship is assumed to turn freely with a given rudder angle, and the simulated turning circles are comparable to the full-scale ice trials. It is also found that the ship's performance can be considerably affected by the geometry of simulated icebreaking patterns. If the shoulder crushing takes place (i.e. the ice is continuously crushed by hull shoulder without bending failure) both the forward speed and the turning rate of the ship will be significantly slowed down. This phenomenon is also observed in full-scale trials, but it is difficult to learn about its effect on ship's performance as the actual ice conditions in-service usually are uncontrollable. It is expected that numerical simulations can supplement full-scale tests in providing more details about the continuous icebreaking processes and the global ice load effects on ship's performance.

The local ice loading process has a clear stochastic nature due to variations in the ice conditions and in the icebreaking processes of ships. A case study with an icebreaking tanker, MT Uikku, is carried out by using the simulation program. In this study, the thickness and strength properties of the ice encountered by the ship are assumed to be constant or randomly generated using the Monte Carlo method. It is found that the variation of simulated ice loading process on a frame is noteworthy even if the ice properties are fixed. If the statistical variation of the ice conditions is considered, then the distributions of simulated load peaks are found to be comparable to the measured statistical distributions. In this case study, the spatial distribution of local ice loads around the hull is also investigated. The simulation results agree with previous experimental studies, that the turning operation may develop a high load level on the aft shoulder area.

Ice conditions and ship operations in ice vary in the short term from voyage to voyage and in the long term from winter to winter. Long-term ice load measurements conducted in the Baltic Sea consist mainly of 12-hour load maxima which are gathered during the normal operation of the ship over several years. A case study with a chemical tanker, MS Kemira, is carried out by using the simulation program. In this study, the statistical data on the strength properties of Baltic Sea ice are applied and the thickness of the ice encountered by the ship are classified referring to the full-scale measurements onboard MS Kemira. The 12-hour maximum ice loads on a frame are evaluated by fitting a Gumbel I asymptotic extreme value distribution to the simulated 10-min load maxima in a certain ice condition. It can be expected that if a reasonable variance of the ice thickness is defined, the simulation results can be used for a preliminary estimation of the maximum ice loads within a 12 hours' voyage in level ice. By applying the different ice thicknesses in simulations, the probable correlation between the simulated load maxima and the ice thickness is analyzed. A potential way to evaluate the long-term ice load statistics based on short-term simulations is then introduced.

Up to now the main source of knowledge about ice load statistics has been field measurement. While field measurements will continue to be important, numerical methods can provide useful information, since they can be easily used to study the effect of different parameters. As far as we know the present numerical model is the first one to deal with multiple subjects including the ice–hull interaction, the overall performance of icebreaking ships and the statistics of local ice loads around the hull. It is hoped that further studies on this numerical model can supplement the field and laboratory measurements in establishing a design basis for the ice-going ships, especially for ships navigating in first-year ice conditions.

# Acknowledgements

This work has been carried out at the Centre for Ships and Ocean Structures (CeSOS), sponsored by the Research Council of Norway, at Norwegian University of Science and Technology (NTNU).

I would like to express my sincere gratitude to my supervisors in the first place. I would like to thank Prof. Torgeir Moan for his excellent supervision during the whole period of my PhD study. The present work would not have been possible without the consistent guidance and support from him. I would like to thank Prof. Kaj Riska for his professional perspective and encouragement which inspire me a lot in promoting the work.

During my PhD study, I have received lots of help and suggestions from various persons. Among them, I would like to thank: Dr. Junji Sawamura at Osaka University for his support on the knowledge of fluid–ice interaction, finite element modeling and fruitful discussions; Dr. Xiangjun Kong and Xu Xiang for their assistance on hydrodynamic calculations; Dr. Zhen Gao for his specialized suggestions on statistical analysis; Mr. Uno Haraldsson at Rederi AB Transatlantic for the information about the rudders of Tor Viking II; Zhenhui Liu, Xiangyue Zhang, Li Zhou and Xiang Tan for the extensive discussions on various issues related to ice; and the crew of Swedish Icebreaker YMER for an impressive on-site observation of icebreaking process and ship operations.

I would also like to give my appreciation to all professors, research fellows and staffs at CeSOS and the Department of Marine Technology for creating a friendly and collaborative environment. The administrative assistance and help I received from Ms. Sigrid Bakken Wold, Ms. Marianne Kjølås, Ms. Karelle Gilbert, and Ms. Linda Grønstad are especially acknowledged.

I am grateful to all friends who contribute to my meaningful life in Norway. Among them, I would like to mention Dr. Yanlin Shao and Dr. Huirong Jia who introduced me to Norway and my room-mate, Limin Yang, Hamid Amini, Tan Hoi Nguyen, Nur Syahroni and Amir Rasekhi Nejad.

The last but not the least, my family in China is gratefully acknowledged for their consistent and unconditional support and encouragement!

Biao Su
April 12, 2011
Trondheim, Norway

# List of Appended Papers

This thesis is presented in the form of a collection of five papers. Three of the papers are published in journals and the rest are conference papers. The complete papers are presented in the Appendix, the following is a list of appended papers:

*Paper 1*:

**A numerical method for the prediction of ship performance in level ice**

Biao Su, Kaj Riska and Torgeir Moan

Published in *Cold Regions Science and Technology*, Vol. 60 (2010), pp. 177-188

*Paper 2*:

**Numerical simulation of ship turning in level ice**

Biao Su, Kaj Riska and Torgeir Moan

Published in the Proceedings of 29th International Conference on Offshore Mechanics and Arctic Engineering (OMAE 2010), Shanghai, China

*Paper 3*:

**Numerical simulation of local ice loads in uniform and randomly varying ice conditions**

Biao Su, Kaj Riska and Torgeir Moan

Published in *Cold Regions Science and Technology*, Vol. 65 (2011), pp. 145-159

*Paper 4*:

**Numerical study of ice-induced loads on ship hulls**

Biao Su, Kaj Riska and Torgeir Moan

Accepted for publication in *Marine Structures*, in press (2011)

*Paper 5*:

**Numerical simulation of ships operating in level ice**

Biao Su, Kaj Riska and Torgeir Moan

Submitted to 21st International Conference on Port and Ocean Engineering under Arctic Conditions (POAC 2011), Montreal, Canada

# Declaration of Authorship

All the five papers that serve as the core content of this thesis are co-authored, I am the first author and was responsible for establishing the models, performing the calculations, providing the results and writing all these papers, under the supervision of Prof. Kaj Riska and Prof. Togeir Moan. Prof. Kaj Riska has contributed to the initiating ideas, field data, validations and recommendations. Prof. Togeir Moan has contributed to the support, corrections and constructive criticism to increase the scientific quality of the publications, he also initiated *Paper 4*.

# Table of Contents

# Chapter 1

# Introduction

## 1.1 Background and motivation

The expected growth of oil and gas activities in Arctic and Sub-Arctic regions and shipping activities through the Northern Sea Route (NSR) will require dedicated designs of ice-going ships and planning of operations in ice. Ice is, depending on geographical locations, typically encountered in the form of level ice, ice ridges and icebergs. Fig. 1.1 indicates typical geographical regions where the ice actions are of current concern (Gürtner, 2009). The design of ice-going ships includes reaching an adequate performance, adequate hull and machinery strength and proper functioning of the ship in ice and in cold weather, which is constantly evolving to take account of technical and commercial progress. In the following, the historical development of ice-going ships and some aspects of ship design for ice (Riska, 2010a) will be briefly introduced.

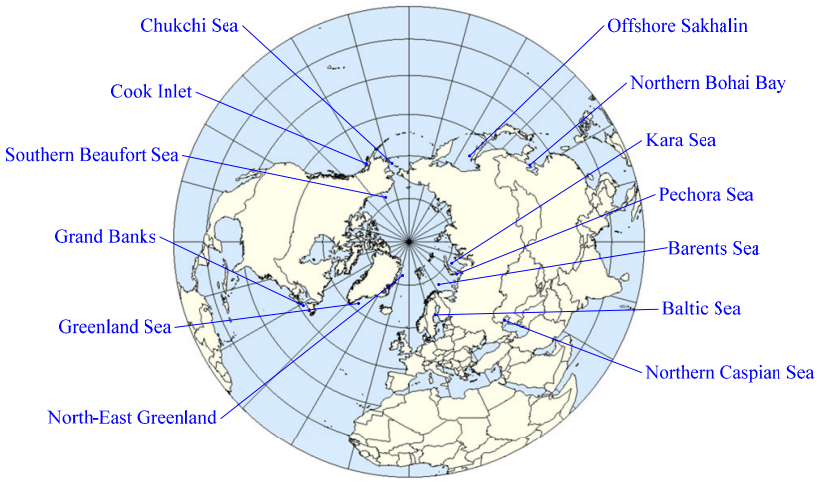


Fig. 1.1 Typical geographical regions where the ice actions are of current concern (Gürtner, 2009)

***Historical development of ice-going ships***

The history of ice-going ships may date back to the time when the icebreaking boats appeared in 1830's and 1840's in the Delaware River in the US and in the Elbe River in

Germany. The first dedicated icebreakers appeared in 1860's and 1870's in the St. Petersburg and Hamburg harbors. Before the turn of the century several dedicated sea-going icebreakers were in service. Fig. 1.2 shows the Russian Yermak, which was considered as the first modern polar icebreaker and sailed in heavy ice conditions for more than 1000 days from 1899 to 1911 (Marchenko, 2009). The development of merchant ships for ice started at the end of 19th century. The year-round navigation in the Baltic Sea started in 1877 with the introduction of the ship Express II sailing between the ports of Hanko and Stockholm. The hull design of this ship and many similar ones followed the design of icebreakers, only the machinery power was larger in icebreakers.

Fig. 1.2 Yermak, the first modern polar icebreaker (en.company.msco.ru)

Ships that were intended to sail independently in ice evolved in 1950's in the Soviet Union with the emergence of the Lena and Amguema series of ships (the latter is also called Kapitan Gotskij series). These ships had an icebreaking bow shape and a high strength for Arctic trade. Several series of Arctic ships were built to Soviet and Russian owners (e.g. Norilsk and Norilsk Nikel series) and to Finnish owners (Lunni series), the Canadian ships MV Arctic and MV Umiak I were also built.

The hull shape of the early icebreakers in the 19th century was characterized by a very small buttock line angle at the stem; values were usually smaller than 20º. The buttock lines and waterlines were rounded and the sides were inclined. The rounded stem was developed quite late (in the 1980's) as a sharp bow was long deemed favorable for icebreaking. The principle of hull lines design is and has been to make the flare angle as small as possible.

The general arrangement of ice-going ships has changed little during the years. The largest change in the arrangement took place in 1970's when the superstructure was changed into deck house (i.e. no accommodation was placed in the hull). The reason for this change was partly to increase the height of the bridge to improve the visibility and partly to avoid the noise and vibration caused by ice in the crew accommodation.

Machinery of icebreakers has experienced many changes since the early icebreakers with steam engines and fixed pitch propellers. The economy and torque capability of engines was improved much with the introduction of diesel-electric machinery (diesel

main engine with generators and electrical propulsion motors). The first diesel-electric icebreaker was the Swedish IB Ymer in 1933. The diesel-electric machinery is more expensive than a direct diesel drive but the torque performance of a fixed pitch propeller with a direct drive is not good. The solution for this is the use of controllable pitch (CP) propellers. These became common in early 1980's in merchant ships. In December 1957, the icebreaker Lenin was launched in Leningrad (St. Petersburg). It was the first nuclear powered icebreaker and represented a major technological achievement.

The bow propellers were introduced in icebreakers in the end of 19$^{th}$ century. The first European bow propeller icebreaker was the Finnish Sampo. The bow propeller improves the icebreaking capability by reducing the forces required to break ice and by reducing the friction. Only lately the bow propellers have been made superfluous by the introduction of so called azimuthing propulsion. The first icebreaker with azimuthing propulsion was the Finnish multi-purpose icebreaker Fennica. Since 1990 the major development of ice-going ships has been that of using Azipod units in ice with double acting tankers (DAT). The idea is to design an efficient icebreaking stern for the vessel, while keeping an efficient open water bow. Fig. 1.3 shows a DAT crude carrier going astern in ice.

Fig. 1.3 A DAT crude carrier, MT Tempera, owned by Neste Oil and built by Sumitomo Heavy Industries in 2003 (Jones, 2004)

Enormous technical progress has been made from the earliest icebreaking ships to double acting tankers. Ice will continue to be an important factor for dedicated ship design, as the expected growth of petroleum and shipping activities in Arctic and Sub-Arctic regions.

***Ice conditions***

The ice-covered seas are located mostly in the high latitudes where the temperatures are low and also the daylight hours are short in winter. Sea ice can, however, be found in surprisingly low latitudes like the Caspian Sea, Sea of Azov and the Bohai Bay. For many sea areas it is clear that multi-year ice does not exist as all ice melts during the summer (e.g. Baltic Sea, Sea of Azov, Caspian Sea and Bohai Bay) while in some other areas the existence of multi-year ice is a crucial factor for ship design.

As shown in Fig. 1.4, a typical first-year ice field is composed of some portion of open water and level ice with ice ridges scattered among the relatively level ice. The

description of ship transit through this kind of ice field requires the following data: (1) coverage of ice; (2) level ice thickness; (3) average thickness of ice ridges; and (4) density of ridges. Typical ice coverage in stationary ice field is about 90% and maximum level ice thickness typically in first-year ice areas is 1 m (Baltic) and 2 m in the Arctic. Average ridge thickness in the Baltic Sea is about 5 m and the ridge density varies from 4 to 10 ridges per kilometre.

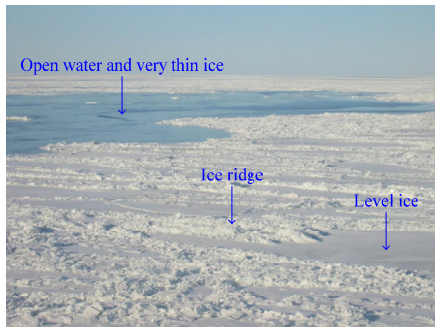


Fig. 1.4 A typical sea ice field with level ice, ice ridges and open water patches, a view from the Gulf of Finland (Riska, 2010b)

If ice survives the summer melting season, multi-year ice is created. More than half of the ice in the Arctic is multi-year ice. Growth continues from year to year until the ice thickness reaches a maximum of about 3 m, at which point summer melt matches winter growth and the thickness oscillates through an annual cycle (Wadhams, 2002). When a first-year ridge survives the summer melt, the voids in the ridge get filled with fresh water and the sail melts. This produces slightly wavelike top and bottom surfaces and quite uniform thickness, typically in excess of 5 m. These multi-year ridges can be quite large in horizontal extents, several hundred meters across.

The definition of design ice conditions is simplified in most cases by using the equivalent level ice thickness. Analysis of the ship performance and hull damages in the Baltic Sea shows that this definition gives a roughly good estimate on the severity of ice conditions (Riska, 2007a). Table 1.1 gives an example of the long-term statistics for the winter maximum equivalent level ice thickness. The effect of ice ridges is included by multiplying the mean level ice thickness with a factor, $k_r$, shown also in Table 1.1. This factor is obtained based on the occurrence probability, $P_r$, of ridges in an ice area (Kujala, 1994).

The drift of sea ice, forced by winds and currents, shifts the ice edge, opens and closes leads, and forms pressure zones, which are all important factors for navigation in ice-covered seas (Leppäranta, 2005). Also the hummocks and ridges resulting in local accumulation of ice volume and strength, as well as the drifting icebergs, may cause major problems to marine operations and constructions.

Table 1.1 Long-term statistics for the winter maximum equivalent ice thickness in various parts of the Baltic Sea (data from Kujala, 1994)

| Sea area | Level ice thickness | | Ice ridge effect | | Equivalent ice thickness | |
|---|---|---|---|---|---|---|
| | Mean (m) | Std. (m) | $P_r$ | $k_r$ | Mean (m) | Std. (m) |
| Bothnian Bay | 0.474 | 0.164 | 0.50 | 1.28 | 0.607 | 0.210 |
| Bothnian Sea | 0.414 | 0.153 | 0.25 | 1.21 | 0.501 | 0.185 |
| Gulf of Finland | 0.404 | 0.140 | 0.25 | 1.21 | 0.489 | 0.170 |
| Baltic proper | 0.336 | 0.136 | 0.10 | 1.12 | 0.376 | 0.152 |

### *Ship performance in ice*

Ship performance in ice consists of ability to break ice and to maneuver in ice. The ability to break ice is measured in uniform ice conditions by the speed that the ship can attain in the ice of a certain thickness, $h$, and in ridged ice conditions by the capability of ridge penetration which is sometimes coupled with level ice performance by using the equivalent level ice thickness (Riska, 2010b). The speed that the ship can attain in ice is determined by the propeller thrust available to overcome the ice resistance. The maneuvering performance is similarly determined by the transverse forces provided by the rudder(s) or azimuthing thruster(s) and the resisting forces mainly due to ice. It is thus clear that the performance in ice is influenced by the resisting forces and the propulsive forces, which can be improved (resisting forces minimized and propulsive forces maximized) by hull shape and propulsion design respectively.

Jones (2004) presented a historical review of the scientific literature on ship performance in ice (an updated version of the previous review – Jones, 1989). As mentioned in Jones (2004), the first scientific paper on icebreakers was published by Runeberg (1888/89) with particular reference to the Baltic, and it was claimed that the derived results agreed, “tolerably well”, with the actual performance of six ships. From 1900 to 1945, some empirical equations for determining the required power, displacement, length, and draught of an icebreaking ship, the importance of stem angle and the strength of ice in icebreaking, and a semi-empirical method for investigating continuous mode icebreaking resistance were introduced by Kari (1921), Simonson (1936) and Shimanskii (1938), respectively. From 1945 to 1960, Johnson (1946) described the U.S. Coast Guard’s icebreaking vessels and experience in detail; Vinogradov (1946) described some of Russian experience as well as giving an equation for the downward icebreaking force developed (paraphrased in Ferris (1959)); and German (1959) and Watson (1959) both reviewed the Canadian experience. A significant contribution to the literature was made by Jansson (1956a&b) with a major review article. He also discussed the science of icebreaking and gave a simple formula for the total ice resistance. The vast majority of the literature on ship performance in ice has been published since 1960. The development of model tests (e.g. Corlett and Snaith, 1964, Crago et al., 1971, Enkvist, 1972, Timco, 1986, and Ettema et al., 1987) and both analytical (e.g. White, 1970, Milano, 1973, and Carter, 1983) and numerical (e.g.

Valanto, 2001) methods have contributed significantly to the prediction of ship performance in ice. The detailed expressions for ice resistance were developed and improved (e.g. Kashteljan et al., 1968, Lewis and Edwards, 1970, Enkvist, 1972, Vance, 1975, Edwards et al., 1976, Lewis et al., 1982, Kotras et al., 1983, Zhan et al., 1987, and Lindqvist, 1989) based on physical analysis and model and full scale data, by characterizing the different components and influential factors of ice resistance (e.g. Johansson and Mäkinen, 1973, Mäkinen et al., 1975, Scarton, 1975, Virtanen et al., 1975, Poznak and Ionov, 1981, Bulat, 1982, Enkvist, 1983, Tatinclaux, 1984, and Kitagawa et al., 1986). As another key factor for ship performance, the thrust or propulsion efficiency in ice was also extensively investigated (e.g. Vance, 1980, Vance et al., 1981, Juurmaa and Segercrantz, 1981, and Lewis et al., 1982). At the end of Jones's review article, it was claimed that the modelling for ship performance in ice would continue to improve with emphasis on numerical simulations as well as physical modelling. This has been revealed in recent years (see e.g. Liu et al., 2006, Martio, 2007, Nguyen et al., 2009, Sawamura et al., 2010 and Lubbad and Løset, 2011).

As introduced above, most expressions for ice resistance are based on regression on model and full scale data. Ice resistance in level ice is the basis of all other ice resistance formulations (brash ice and ice ridges), and it is assumed to be linear with ship speed and consist of three components (see e.g. Lindqvist, 1989 and Riska et al., 1998):

$$R_{ice} = R_b + R_s + R_f \tag{1.1}$$

where $R_b$, $R_s$ and $R_f$ represent the breaking, submersion and friction components, respectively. The breaking component is attributed to the breaking of the ice (i.e. the crushing, bending and turning of the ice). The submersion component is attributed to pushing the broken ice down along the ship hull. The friction component is attributed to the sliding of the broken ice along the ship hull. Usually the velocity dependency of the ice resistance is attributed to the friction component.

The total resistance in ice, $R_{tot}$, is assumed to be the sum of pure ice resistance, $R_{ice}$, and open water resistance, $R_{ow}$:

$$R_{tot} = R_{ice} + R_{ow} \tag{1.2}$$

The net thrust concept, $T_{net}$, can then be used to define the propeller thrust available to overcome the ice resistance:

$$T_{net}(v) = T_{tot}(v)\left(1-t\right) - R_{ow}(v) \tag{1.3}$$

where $v$ is the ship speed, $T_{tot}$ is the total thrust at this speed, and $t$ is the thrust deduction factor. In early design, the net thrust can be estimated by (Juva and Riska, 2002):

$$T_{net}(v) = T_{pull} \cdot \left( 1 - \frac{1}{3}\frac{v}{v_{ow}} - \frac{2}{3}\left( \frac{v}{v_{ow}} \right)^2 \right) \qquad (1.4)$$

where $v_{ow}$ is the maximum open water speed, and $T_{pull}$ is the bollard pull of the ship.

Ship performance in level ice is described by ice thickness versus ship speed plots (i.e. h-v curve), in which the speed that the ship can attain in specified ice thicknesses at full power is plotted (see e.g. Fig. 1.5). In an early design phase, the h-v curve can simply be determined by solving the equation between the ice resistance and the net thrust. The calculation methods for both ice resistance and net thrust are at best semi-empirical and should be used cautiously, especially beyond the range of validity. These methods can not account for the details of hull shape. When the design proceeds, more exact calculations or model tests should be carried out to finalize the hull shape and to ensure an adequate maneuvering performance (e.g. the turning performance).

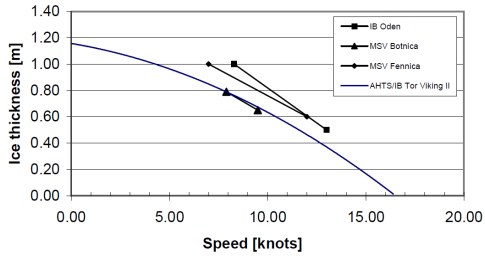


Fig. 1.5 The h-v curves determined from the full-scale tests of 4 vessels (Riska et al., 2001)

Turning performance in ice is measured by the diameter of the turning circle. Fig. 1.6 shows an example of the full-scale turning circle test. The turning ability is not the only measure for the maneuvering performance of an ice-going ship. It is important to perform different maneuvers (e.g. zigzag and star maneuvers) in shortest time possible. A good maneuvering performance can be achieved by a proper hull form design, having a large turning rate of the rudder(s) or azimuthing thruster(s) and providing a large transverse force.

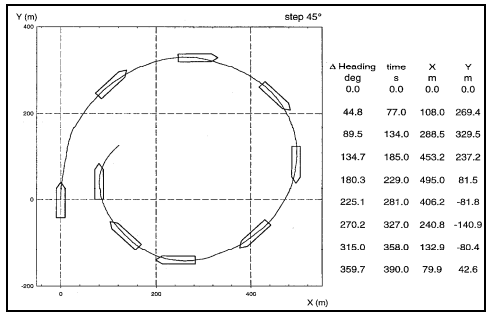


Fig. 1.6 An example of the recorded data of a full-scale turning circle test (Riska et al., 2001)

***Ice loads for hull strength assessment***

Design of ship hull structures requires knowledge of the ice loads acting on different regions of the hull. As ice loads arise from the contact with an ice edge, it is commonly assumed that the load acts mostly on a load patch which is narrow in vertical direction and long in horizontal direction. The load patch is thus idealized as rectangular for structural response calculation of local shell structures like plating, main frames, stringers and web frames. This simplification suggests that there are three quantities describing the local ice load: ice pressure, load height and load length.

Several different theories about ice pressure have been suggested. The earliest model for ice pressure is to treat it uniform and proportional to the compressive strength of ice (Korzhavin, 1971). Much research was done to clarify the proportionality factors (see e.g. Cammaert and Muggeridge, 1988) depending on the shape of contact surface and on the "quality of contact" whereas the dependence on ice temperature and strain rate was included in the definition of compressive strength. But when it was realized that the measured compressive strength of ice depends much on the testing method and specimen quality (see e.g. Kendall, 1978 and Tuhkuri, 1996), the use of Korzhavin's model diminished. Russian scientists analyzed the flow of crushed ice by assuming that the crushed ice is viscous fluid. Based on this assumption and Reynolds thin film fluid flow equations, another model for ice pressure was derived (Kurdjumov and Kheisin, 1976) and used to develop a formulation for ice force using energy principles in an impact between an ice feature and a ship. The drawback of this ice pressure formulation is that many assumptions have been made (e.g. viscosity, uniform film thickness, and uniform source of crushed ice). The third formulation used for ice pressure is based on observation that the average ice pressure, $p_{av}$, on an area is dependent on the magnitude of the area, $A$. Sanderson (1988) collected many different results and then suggested the pressure–area relationship as:

$$p_{av} = 8.1 \cdot A^{-0.57} \tag{1.5}$$

where $p_{av}$ and $A$ are in units of MPa and $m^2$. The constant and exponent in the pressure–area relationship has been studied for example by Riska (1987), Masterson and Frederking (1993), Frederking (1999), Frederking (2003), and Jordaan et al. (2005). The pressure–area relationship is the one used most, though it is empirical and little physical basis exists for the area dependence.

The dimensions of the load patch are difficult to determine for design purposes. In some cases an estimate of the load length or the load height can be given but usually the designer must assume most disadvantageous values for the dimensions. An example of the geometric reasoning for dimensions is given by the conceived load height in the Finnish-Swedish Ice Class Rules.

The resulting force or its normal component may thus be determined by analyzing the motion of the colliding bodies (ice and hull). Two cases for the calculation of ice force (and partly disregarding the load patch dimensions) have been given. The first one (Popov et al., 1968) investigates the collision of two bodies and deduces a one dimensional equation for the indentation along the normal to the contact surface. This model is essentially energy based and suitable for the so called oblique collision where the ship collides with a smaller ice floe and the collision area is on one side of the bow. This simplified model assumed a constant ice pressure, and Daley (2001) incorporated the pressure–area relationship into this model. Another case where the ice force has been calculated is the normal collision on a multi-year ice floe. This case includes crushing of the ice edge followed by the ship sliding up onto the ice. For a collision where the ice mass is assumed large as compared with the displacement of the ship, the force has been deduced by Riska et al. (1996). This calculation is based on the theory developed in Riska (1987) and can be used to calculate the shear forces and bending moments on the hull.

The ice loading process has a clear stochastic nature due to variations in the ice conditions and in the icebreaking processes of ships. Up to now, the main source of knowledge about ice load statistics is field measurement. There have been many ship–ice load measurement campaigns conducted in Canada, US, Germany, Japan, Russia and Finland, herein most of the data available for statistical analysis (e.g. Vuorio et al., 1979, Varsta, 1984, Kujala, 1996, and Kujala et al., 2009) are from the Finnish sources (see e.g. Hänninen, 2004 and Frederking et al., 2005). From the beginning, one objective of the measurements has been to establish a distribution for the observed loads. Such distribution could then be used to estimate the probability of extreme ice loads that may damage the hull. The applied distribution models are of two types. The observed loads follow some primary distribution for which a distribution model like exponential distribution is sought. On the other hand, the asymptotic extreme value distributions (i.e. Gumbel distributions of type I, II and III) are considered where the maximum ice load within a certain observation period is sought (Lensu, 2002).

The ice load is a statistical quantity and thus the design load value must in principle be determined assuming a probability level or a return period of occurrence for the load like once per lifetime, once per ice season, or once per voyage. The selected return period of the load must be in balance with the consequences of exceeding the allowable structural responses. This procedure of defining the design points requires thus (Riska, 2007b): (1) definition of the loads in probabilistic terms; (2) definition of the responses in terms of stresses, elastic deflections or permanent deflections; and (3) definition of the limit states in order to ensure a consequent risk implied by the failure of different structural components (e.g. shell plating and frames).

As even the description of the ice loads is not a simple task, the above procedure requires quite much work in fine tuning the final design loads and allowable structural

responses. Fig. 1.7 shows a schematic illustration of this procedure. It is based on the statistics of ice loads (right hand side of the sketch) and two design criterions which are illustrated by two different permanent deflections $w_0$ and $w_1$ of the plating. This illustration also shows how important it is to define an appropriate return period of the load in balance with the allowable structural response: a different definition would result in a quite different design value.

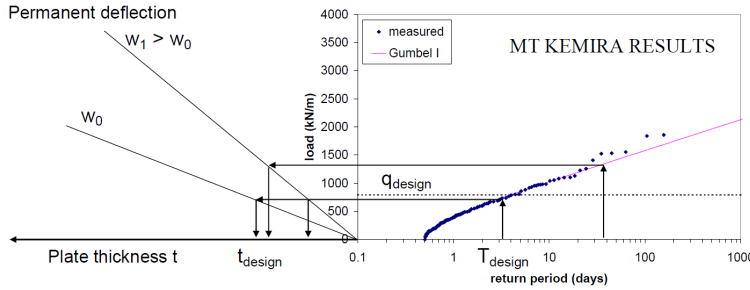


Fig. 1.7 Schematic illustration of the design point definition (Riska, 2007b)

***Ice loads for the assessment of propeller-machinery strength***

The propulsion machinery consisting of propellers(s), shafts, gears and couplings, and the main engine, all the shaft line components must have adequate strength to withstand the ice impacts. If the propeller is submerged at an adequate depth (i.e. has an adequate ice clearance), the propeller will not be in contact with unbroken ice. The ice loading on the shaft line is from impacts of broken ice floes on the propeller blades. The design point of the propeller blades is thus an impact with an individual ice floe.

The design forces of the propeller blades are determined by the size of the impacting ice floe. Several, mostly empirical investigations of the blade loading have been conducted (e.g. Koskinen and Jussila, 1991 and Marquis et al., 2008). Measurements have suggested a formulation for blade loading which has been adopted by several ice rules (see e.g. in FSICR 2008).

It is difficult to define the design torques for various components of shafts, only the loads on the propeller and the torque excitation (i.e. the design torque at the propeller) can be given (see e.g. in Browne and Norhamo, 2007). The designer must then do the detailed structural analyses for an individual design, and the principle of progressive strength should be followed in designing the shaft and its components. Herein the progressive strength means that the components along the shaft line get progressively stronger from the propeller towards the main engine (e.g. if the propeller fails, it acts as a “fuse” for other components).

Ice loads for the assessment of propeller-machinery strength are not followed up in this thesis.

***Winterization aspects***

Operation in cold weather places requirements for the general arrangement of the ship, especially for areas and spaces that are exposed to icing, snow and rain. Bridge, mooring equipment and lifting apparatus must be designed to guarantee adequate visibility. The construction materials for the ship hull and for all the exposed equipments must have proper strength and integrity in low temperatures. All these winterization aspects must also be taken into account in ship design, otherwise the operability and functioning of the ship may be impaired.

The winterization aspects are not followed up in this thesis.

***Ice class rules***

The classification societies and also some maritime authorities (e.g. Finnish and Swedish Maritime Administrations and Transport Canada) have developed rules for designing ice-going ships. These ice class rules define several different ice classes depending on the severity of ice conditions. Ice class rules define the scantlings of the hull and shaft line structures and give some requirements for ship performance in ice and structural arrangement. At present there are three main sets of ice class rules: the Finnish-Swedish Ice Class Rules (FSICR), the Russian Maritime Register of Shipping (RMRS) ice class rules and the unified Polar Class (PC) rules of the International Association of Classification Societies (IACS).

The FSICR have been adopted by most of the classification societies (all except RMRS) and described as an "industry standard" for first-year ice conditions even if they are intended only for ships navigating in the Baltic. The FSICR (2008) contain requirements for ship hull, ship machinery and also for ship performance in ice. Four different ice classes (IA Super, IA, IB and IC) are defined and also the open water ships have their own ice class notations (II and III). The classification societies follow their own notations, but the basic rules are the same as FSICR.

The RMRS ice class rules consist of nine ice classes and additionally four ice classes for icebreaker. They are mainly used for ships with the Russian flag or ships operating in Russian waters, and contain also the requirements for hull, machinery and powering. The powering requirements for the Baltic are the same as the corresponding FSICR ice classes.

The IACS ice class rules have been under development since mid 1990's and finally accepted in 2008. At the moment all IACS members are incorporating the unified rules into their own rule structure. There are seven polar classes (PC 1-7) in the IACS rules, where the ice description follows the World Meteorological Organization's practice. Hull design in PC classes is based on plastic structural limit and it has been stated that

the return period of the loads causing response up to the limit is one year. Machinery design in PC classes is based on the same theory of ice loads as in the FSICR.

Many ships having a Baltic ice class (IA Super or IA) have navigated in the Arctic successfully. This experience has prompted an action to parallel the lowest PC classes with the highest Baltic classes. This equivalency is recognized by the Baltic authorities and also by the Canadian authorities in the following form: "As an interim measure for navigation purposes, Transport Canada will consider that PC 6 and 7 vessels will be allowed to operate as Type A and B vessels (Baltic IA Super and IA construction) respectively." (Transport Canada Bulletin No. 04/2009)

An overview of the design aspects of ice-going ships is given above. Up to now, the ship's performance in ice and the strength of ship hull are still mostly designed based on the experiences from earlier ships and model tests. While the full-scale experiences and model tests will continue to be important, numerical methods can provide useful information, since they can be easily used to study the effect of different parameters.

## 1.2 Objectives and scope of the thesis

This thesis is presented in the form of a collection of five papers appended in the Appendix. The primary aim of this thesis is to introduce a numerical model for simulating ice–hull interaction and ship maneuvers in level ice, with focus on a deterministic or probabilistic assessment of both global and local ice loads on ship hulls. Tor Viking II, MT Uikku and MS Kemira, navigating in the Baltic Sea are selected for three specific case studies, in which the global ice load effects on ship's performance, the probabilistic and spatial variations of local ice loads around the hull and the short-term distribution of maximum ice loads on a frame are respectively analyzed and compared with field measurements. As far as we know the present numerical model is the first one to deal with multiple subjects including the ice–hull interaction, the overall performance of icebreaking ships and the statistics of local ice loads around the hull, which can be used to supplement the field and laboratory measurements in establishing a design basis for ice-going ships, especially for ships navigating in first-year ice conditions.

The scope of the present work is constituted by the following sub-tasks:

1) To reproduce the continuous icebreaking process of a ship moving forward and turning in level ice, by considering the interdependence between the ice loads and the planar motion (surge, sway and yaw) of the ship;

2) To determine the integrated ice load over the hull area and its effects on ship's performance;

3) To identify the origin of the probabilistic variation of local ice loads, by considering the variations in the external ice conditions and in the icebreaking processes of the ship;

4) To investigate the probabilistic distribution of ice-induced peak loads on a frame;

5) To gain improved understanding of the spatial distribution of local ice loads around the hull;

6) To analyze the correlation between the short-term distribution of maximum ice loads and the ice thickness;

7) To derive a preliminary approach for the evaluation of long-term ice load statistics based on short-term simulations.

## 1.3 Thesis outline

The present thesis is constituted by the following chapters:

After a brief introduction in **Chapter 1** concerning background, motivation and objectives of this thesis, **Chapter 2** describes the development of present numerical model, which is partly based on the empirical data. *Paper 1* and *Paper 3* are associated with this chapter. In *Paper 1*, the empirical estimates of the ice crushing force, ice bending failure and the submersion and friction components of ice resistance are clarified, respectively. The numerical method used to detect the ice–hull collision and the collision force is explained. The convergence tests are carried out to make sure that this numerical method can give a convergent solution of both global and local ice loads. The computation time is examined with the purpose of determining a balance between the computation time and the convergence. The influences of the empirical assumptions made in this numerical model are analyzed by changing different parameters and comparing with the measured data. In *Paper 3*, the numerical model is extended to more complex ice conditions by considering random ice thickness and strength properties. The procedure to randomize the ice encountered by the ship is also illustrated in this chapter.

**Chapter 3** deals with a specific case study on ship's performance in ice. *Paper 1* and *Paper 2* are associated with this chapter. In *Paper 1*, the speed that the ship can attain in ice is investigated, by comparing the simulation results with the h-v curves determined from field measurements. *Paper 2* focuses on the turning performance which is measured by the turning circle diameter.

**Chapter 4** deals with a specific case study on the probabilistic and spatial distribution of local ice loads around the hull. *Paper 3* and *Paper 4* are associated with this chapter. In *Paper 3*, the origin of the probabilistic variation of local ice loads is investigated, by

considering the variations in the external ice conditions and in the icebreaking processes of the ship. The probabilistic distribution of ice-induced peak loads on a frame is then analyzed and compared with field measurements. In *Paper 4*, the simulation results on the spatial distribution of local ice loads around the hull are presented.

**Chapter 5** deals with a specific case study on the short-term distribution of maximum ice loads on a frame. In *Paper 5*, the correlation between the short-term distribution of maximum ice loads and the ice thickness is analyzed. A potential way to evaluate the long-term ice load statistics based on short-term simulations is introduced.

In **Chapter 6**, the work carried out is summarized and several recommendations for future studies are given.

# Chapter 2

# Description of the Numerical Model

The development and validation of present numerical model are introduced in this chapter, based on *Paper 1* and *Paper 3*.

## 2.1 General

Research on the numerical modeling of ice–hull interaction and ship maneuvering in level ice can be found for example in Valanto (2001), Liu et al. (2006), Martio (2007), Nguyen et al. (2009), Sawamura et al. (2010) and Lubbad and Løset (2011). For the simulation of full-scale icebreaking runs, a more integrated model was developed and improved by Su et al. (2010a and 2011a – *Paper 1* and *Paper 3*). This model is partly based on the empirical data, and the simulation program has been established to reproduce the observed icebreaking patterns and the continuous ice loading processes in a uniform level ice and the ice with randomly varying thickness and strength properties.

The methodology and assumptions used in the ice–hull interaction model are:

1) The basic geometric model includes the full-size waterline of the ship and the edge of the ice both discretized;

2) The motions (surge, sway and yaw) of the ship on the horizontal plane are taken into account and the icebreaking forces are assumed to act on the waterline;

3) The contact zones around the hull and the resulting ice forces and icebreaking patterns are numerically determined based on the empirical estimates of ice crushing force and ice bending failure;

4) Ice forces induced after the ice wedges are broken from the ice edge are taken into account by the Lindqvist's ice resistance formula (Lindqvist, 1989);

5) The hydrodynamic effects on the ship's motion (drag and added mass) are derived from a numerical calculation before the simulation in ice;

6) Wave, wind and current forces in a level ice condition are neglected as they are minor forces compared to ice forces;

7) The rigid-body equations of motion are solved by numerical integration;

8) Iterations are performed at each time step to find a balance between the indentation into ice and the contact forces.

In the following section, the construction of present numerical model is described based on the above items.

## 2.2 Construction of the numerical model

As shown in Fig. 2.1, the ice forces encountered by a ship transiting a level sheet of ice depend primarily on the processes, by which its hull breaks and displaces ice. First, when the ice sheet contacts the hull, crushing happens. The crushing force will keep growing with an increasing contact area until its vertical component is large enough to cause a bending failure of ice. After the ice floes have been broken from the ice sheet, the advance of ship forces them to turn on edge until parallel with the hull. Then, the floes will become submerged and slide along the hull until they can not maintain contact with the hull. In some hull zones, typically at the very bow and at the shoulders which have large slope angles (almost vertical), crushing may be the only failure mode (Lindqvist, 1989). This can lead to a considerable ice resistance.

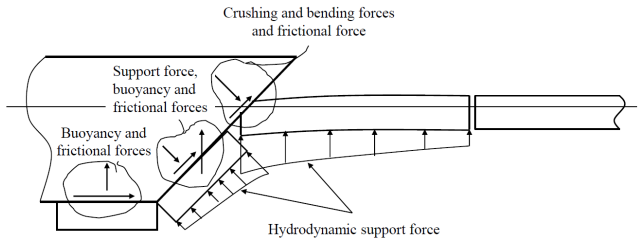


Fig. 2.1 The overall process of ice–hull interaction in level ice (Riska, 2010b)

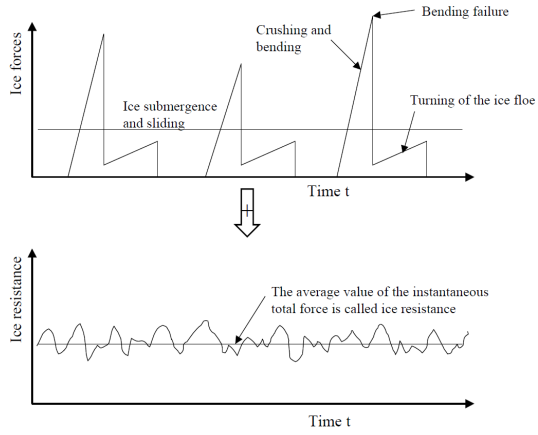


Fig. 2.2 Idealized time histories of ice forces and the definition of ice resistance (Riska, 2010a)

Early research on level ice resistance was usually carried out based on this break–displace process (see e.g. Fig. 2.2). Although it may be questionable (Enkvist et al., 1979), most of the ice resistance formulas were established on this assumption (e.g. Enkvist, 1972, Lewis, 1982, and Lindqvist, 1989). In the present numerical model, the icebreaking forces are numerically detected, while the ice forces induced after the ice wedges are broken from the ice edge are taken into account by the Lindqvist's ice resistance formula (the submersion and friction components given in Lindqvist (1989)).

### *2.2.1 Geometric model for ice–hull interaction*

The basic geometric model for ice–hull interaction includes the full-size waterline of the ship and the edge of the ice. As shown in Fig. 2.3, the waterline of the ship is discretized into a closed polygon and the edge of the ice is discretized into a polyline in the established simulation program. At each time step, the simulation program is set to detect the ice nodes which are inside the hull polygon. Then, each contact zone can be found. To check whether the ice node is inside the hull polygon, the specific geometric tools for computer graphics are adopted. The detailed algorithm can be found in Schneider et al. (2002).

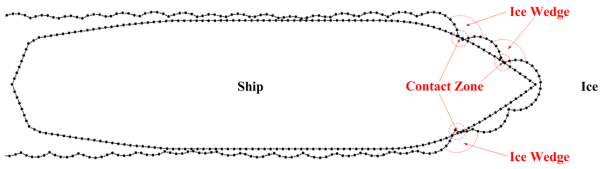


Fig. 2.3 Geometrical idealization of ice–hull interaction

At each contact zone shown in Fig. 2.3, it is assumed that the contact surface between ice and hull is flat, and the contact area, $A_c$, is simply determined by the contact length, $L_h$, and the indentation depth, $L_d$. Herein, $L_h$ is calculated from the distance between adjacent hull nodes, and $L_d$ is calculated from the perpendicular distance from the cusp of ice nodes to the contact surface (see e.g. in Fig. 2.4). As shown in Fig. 2.5, two cases must be considered in the calculation of contact area:

$$\begin{aligned} A_c &= \frac{1}{2} L_h \frac{L_d}{\cos(\varphi)} && \text{Case 1:} \quad L_d \cdot \tan(\varphi) \le h_i \\ A_c &= \frac{1}{2}\left( L_h + L_h \frac{L_d - h_i / \tan(\varphi)}{L_d} \right) \frac{h_i}{\sin(\varphi)} && \text{Case 2:} \quad L_d \cdot \tan(\varphi) > h_i \end{aligned} \tag{2.1}$$

where $h_i$ is the ice thickness, $\varphi$ is a slope angle of varying values at different hull zones (i.e. different locations of hull nodes).

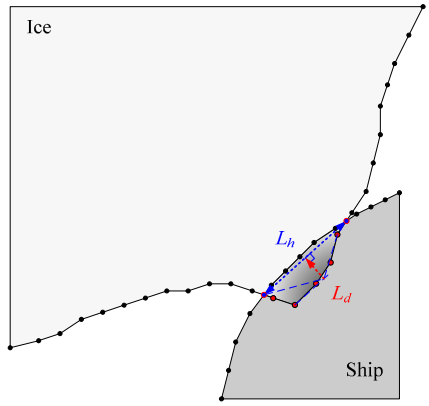


Fig. 2.4 Illustration of the contact length ( $L_h$ ) and indentation depth ( $L_d$ ) at each contact zone

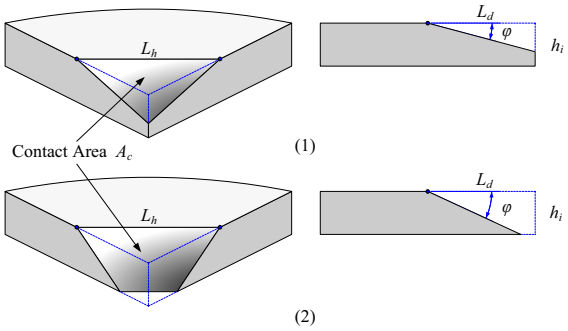


Fig. 2.5 Two cases for the calculation of contact area

### *2.2.2 Ice crushing force*

As shown in Fig. 2.6, it is assumed that the ice is uniformly crushed on the contact surface. The crushing force, $F_{cr}$ , is normal to the contact surface and calculated as the product of the effective ice crushing strength, $\sigma_c$ , and the contact area, $A_c$ :

$$F_{cr} = \sigma_c \cdot A_c \tag{2.2}$$

where the effective ice crushing strength, $\sigma_c$ , is derived from the measured ice crushing pressure on ship hull (Kujala, 1994).

Herein, the frictional force is also taken into account, which is divided into two components, $f_H$ and $f_V$ , according to the relative motion between ice and hull:

$$f_H = \mu_i \cdot F_{cr} \cdot v^{rel}{}_t \Big/ \sqrt{\left(v^{rel}{}_t\right)^2 + \left(v^{rel}{}_{n,1}\right)^2} \tag{2.3}$$

$$f_V = \mu_i \cdot F_{cr} \cdot v^{rel}{}_{n,1} \Big/ \sqrt{\left(v^{rel}{}_{t}\right)^2 + \left(v^{rel}{}_{n,1}\right)^2} \qquad (2.4)$$

where $\mu_i$ is the frictional coefficient, $v^{rel}$ is the relative velocity between ice and hull, and the decomposed force and velocity components are illustrated in Fig. 2.7.

The horizontal and vertical components, $F_H$ and $F_V$, of the total contact force are then calculated as:

$$F_H = F_{cr} \cdot \sin(\varphi) + f_V \cdot \cos(\varphi) \qquad (2.5)$$

$$F_V = F_{cr} \cdot \cos(\varphi) - f_V \cdot \sin(\varphi) \qquad (2.6)$$

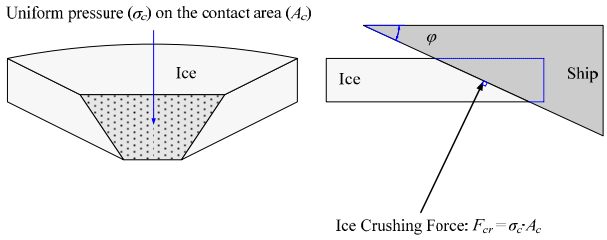


Fig. 2.6 Calculation of the ice crushing force

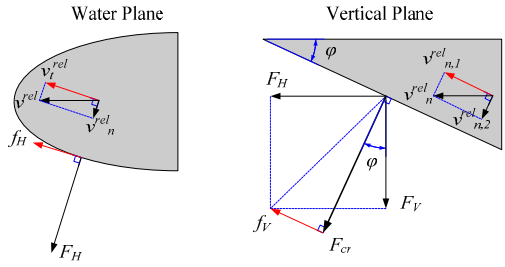


Fig. 2.7 Decomposed force and velocity components

### *2.2.3 Ice bending failure*

If the vertical component of the contact force between ice and hull ($F_V$, shown in Fig. 2.7) exceeds the bending failure load of ice cover, $P_f$, given in Equation (2.7), the ice wedge (as shown in Fig. 2.3) will be broken from the edge of the ice:

$$P_f = C_f \left(\frac{\theta}{\pi}\right)^2 \sigma_f h_i^2 \qquad (2.7)$$

where $\theta$ is the opening angle of the idealized ice wedge shown in Fig. 2.8, $\sigma_f$ is the flexural strength of the ice, $h_i$ is the thickness of the ice, and $C_f$ is an empirical

parameter. Equation (2.7) accounts for the opening angle, and it is an empirical equation (introduced by Kashtelyan (Kerr, 1975), applied in Wang (2001), Liu et al. (2006), and Nguyen et al. (2009)). Thus, the constant $C_f$ must be obtained from measurements.

The geometrical idealization of the ice wedge in contact with the hull is illustrated in Fig. 2.8, where the bending crack is determined by the interpolation of the icebreaking radius at the first and last contact node (i.e., $R_f$ and $R_l$). The icebreaking radius $R$ is found by the expression given in Wang (2001) (based on information from Enkvist (1972) and Varsta (1983)):

$$R = C_l \cdot l \cdot \left(1.0 + C_v \cdot v^{rel}{}_{n,2}\right) \tag{2.8}$$

where $v^{rel}{}_{n,2}$ is the relative normal velocity between the contact surface and the hull node (illustrated in Fig. 2.7), $C_l$ and $C_v$ are two empirical parameters obtained from field measurements, and $l$ is the characteristic length of the ice:

$$l = \left( \frac{E h_i^3}{12\left(1-\nu^2\right)\rho_w g} \right)^{\frac{1}{4}} \tag{2.9}$$

where $E$ is the elastic modulus of ice, $\nu$ is the Poisson's ratio, $\rho_w$ is the density of water, $g$ is the acceleration of gravity.

Based on these assumptions and simplifications, the icebreaking pattern and the continuous icebreaking forces can be determined using a step-by-step procedure.

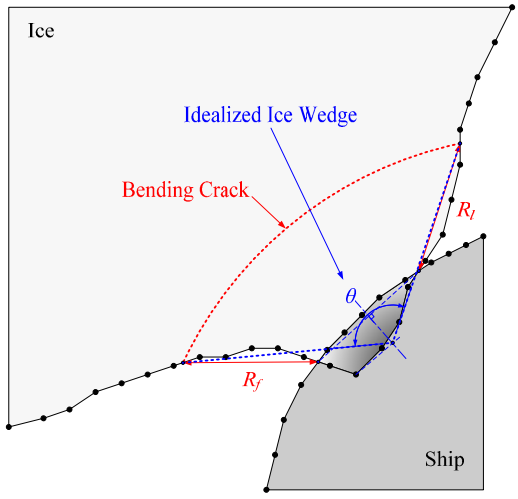


Fig. 2.8 Geometrical idealization of the ice wedge in contact with the hull

### *2.2.4 Ship's motion*

The simulation of ship's motion is conducted in three degrees of freedom, that is, in surge, sway and yaw directions. The ship's motion in global coordinate system can be described by the Newton's second law:

$$\begin{aligned} m \cdot \dot{u}_g &= FX_g \\ m \cdot \dot{v}_g &= FY_g \\ I_z \cdot \dot{r} &= N \end{aligned} \tag{2.10}$$

where $FX_g$, $FY_g$ are the forces in surge and sway directions; $N$ is the yaw moment; $m$ is the mass of the ship; $I_z$ is the moment of inertia in yaw direction; $u_g$, $v_g$ and $r$ are the velocities in surge, sway and yaw, respectively; the dot notation denotes the derivative with respect to time.

The forces and velocities can be translated into the ship coordinate system by:

$$\begin{aligned} FX_g &= FX \cdot \cos(\psi) - FY \cdot \sin(\psi) \\ FY_g &= FX \cdot \sin(\psi) + FY \cdot \cos(\psi) \end{aligned} \tag{2.11}$$

$$\begin{aligned} u_g &= u \cdot \cos(\psi) - v \cdot \sin(\psi) \\ v_g &= u \cdot \sin(\psi) + v \cdot \cos(\psi) \end{aligned} \tag{2.12}$$

where $\psi$ is the heading angle of the ship (as shown in Fig. 2.9).

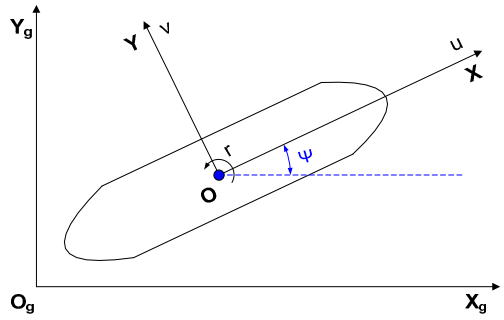


Fig. 2.9 The coordinate system used for the simulation of ship's motion

The accelerations in the ship coordinate system are obtained by differentiating Eq. (2.12):

$$\begin{aligned} \dot{u}_g &= \dot{u}\cdot\cos(\psi) - \dot{v}\cdot\sin(\psi) - \left(u\cdot\sin(\psi) + v\cdot\cos(\psi)\right)\cdot r \\ \dot{v}_g &= \dot{u}\cdot\sin(\psi) + \dot{v}\cdot\cos(\psi) + \left(u\cdot\cos(\psi) - v\cdot\sin(\psi)\right)\cdot r \end{aligned} \tag{2.13}$$

By inserting Eqs. (2.11) and (2.13) into Eq. (2.10), the ship's motion in the ship coordinate system can then be described by:

$$\begin{aligned} m\cdot\dot{u} &= FX + m\cdot v\cdot r \\ m\cdot\dot{v} &= FY - m\cdot u\cdot r \\ I_z\cdot\dot{r} &= N \end{aligned} \tag{2.14}$$

To define the forces and moment terms, Eq. (2.14) is then substituted by a general matrix form of the linear coupled differential equations of motion:

$$\left(\mathbf{M}+\mathbf{A}\right)\cdot\ddot{\mathbf{x}}(t) + \mathbf{B}\cdot\dot{\mathbf{x}}(t) + \mathbf{C}\cdot\mathbf{x}(t) = \mathbf{F}(t) \tag{2.15}$$

where the added mass coefficients are calculated by the boundary element method, and the damping and restoring terms are taken as zero in this simulation. Fig. 2.10 shows an example of the ship geometry model used in the hydrodynamic and open water resistance calculations (Bertram, 2000) which are carried out before the simulation in ice.

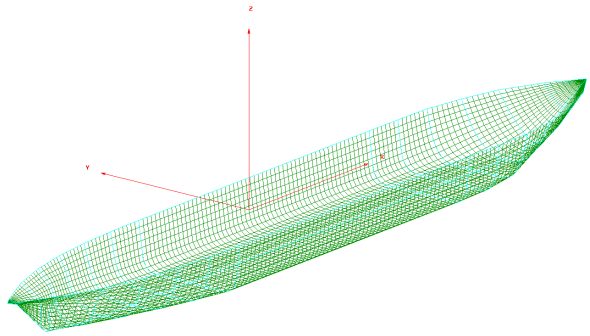

Fig. 2.10 Ship geometry model of MT Uikku used in the hydrodynamic and open water resistance calculations

The forces and moments that result from the ice, propeller, rudder and open water are considered in this simulation. Eq. (2.16) shows the decomposed components of the forces and moment acting on the ship:

$$\begin{aligned} F_1 &= F_1^i + F_1^p + F_1^r + F_1^{ow} + m\cdot v\cdot r \\ F_2 &= F_2^i + F_2^p + F_2^r + F_2^{ow} - m\cdot u\cdot r \\ F_6 &= F_6^i + F_6^p + F_6^r + F_6^{ow} \end{aligned} \tag{2.16}$$

where the subscripts 1, 2 and 6 refer to the directions of surge, sway and yaw, the superscripts *i*, *p*, *r* and *ow* refer to the ice, propeller, rudder and open water, respectively.

A step-by-step numerical integration method is then applied to solve the equations of motion that are established above. According to Newmark's method, the general integral equations are given by:

$$\begin{aligned}\dot{\mathbf{x}}(t_{k+1}) &= \dot{\mathbf{x}}(t_k) + (1-\lambda)\cdot\ddot{\mathbf{x}}(t_k)\cdot\Delta t + \lambda\cdot\ddot{\mathbf{x}}(t_{k+1})\cdot\Delta t \\ \mathbf{x}(t_{k+1}) &= \mathbf{x}(t_k) + \dot{\mathbf{x}}(t_k)\cdot\Delta t + \left(\frac{1}{2}-\beta\right)\cdot\ddot{\mathbf{x}}(t_k)\cdot\Delta t^2 + \beta\cdot\ddot{\mathbf{x}}(t_{k+1})\cdot\Delta t^2\end{aligned} \tag{2.17}$$

These equations are obtained by a Taylor-series expansion in which the residual term is approximated by the quadrature formulas. The weighting terms $\lambda$ and $\beta$ are free parameters in the quadrature formulas that are determined by the requirements related to stability and accuracy. If a linear acceleration is assumed within the time interval $\Delta t$, Eq. (2.17) can be translated into:

$$\begin{aligned}\dot{\mathbf{x}}(t_{k+1}) &= \dot{\mathbf{x}}(t_k) + \frac{1}{2}\ddot{\mathbf{x}}(t_k)\cdot\Delta t + \frac{1}{2}\ddot{\mathbf{x}}(t_{k+1})\cdot\Delta t \\ \mathbf{x}(t_{k+1}) &= \mathbf{x}(t_k) + \dot{\mathbf{x}}(t_k)\cdot\Delta t + \frac{1}{3}\ddot{\mathbf{x}}(t_k)\cdot\Delta t^2 + \frac{1}{6}\ddot{\mathbf{x}}(t_{k+1})\cdot\Delta t^2\end{aligned} \tag{2.18}$$

where

$$\ddot{\mathbf{x}}(t_{k+1}) = (\mathbf{M}+\mathbf{A})^{-1}\left(\mathbf{F}(t_{k+1}) - \mathbf{B}\cdot\dot{\mathbf{x}}(t_{k+1}) - \mathbf{C}\cdot\mathbf{x}(t_{k+1})\right) \tag{2.19}$$

This is a popular method because it leads to continuity in the acceleration, velocity and displacement. By inserting Eq. (2.19) into Eq. (2.18), this method can be translated into an explicit form:

$$\mathbf{x}(t_{k+1}) = \left(\frac{6}{\Delta t^2}(\mathbf{M}+\mathbf{A}) + \frac{3}{\Delta t}\mathbf{B} + \mathbf{C}\right)^{-1}\cdot\left(\mathbf{F}(t_{k+1}) + (\mathbf{M}+\mathbf{A})\cdot\mathbf{a}_k + \mathbf{B}\cdot\mathbf{b}_k\right) \tag{2.20}$$

where

$$\begin{aligned}\mathbf{a}_k &= \frac{6}{\Delta t^2}\mathbf{x}(t_k) + \frac{6}{\Delta t}\dot{\mathbf{x}}(t_k) + 2\ddot{\mathbf{x}}(t_k) \\ \mathbf{b}_k &= \frac{3}{\Delta t}\mathbf{x}(t_k) + 2\dot{\mathbf{x}}(t_k) + \frac{1}{2}\ddot{\mathbf{x}}(t_k)\cdot\Delta t\end{aligned} \tag{2.21}$$

### *2.2.5 Interdependence between the ship's motion and the ice loads*

As shown in Eq. (2.20), the forces and moment $F(t_{k+1})$ at time step *k+1* are unknown at time step *k* due to the interdependence between the ice loads and the ship's motion.

Thus, iterations are performed at each time step until the accuracy is acceptable. The convergence criterion is based on the change of forces and moment from iteration step *i* to iteration step *i+1*, which can be expressed by:

$$\sqrt{\left(F_1^{i+1}-F_1^i\right)^2+\left(F_2^{i+1}-F_2^i\right)^2+\left(F_6^{i+1}-F_6^i\right)^2}\Big/\sqrt{\left(F_1^i\right)^2+\left(F_2^i\right)^2+\left(F_6^i\right)^2}<\varepsilon \qquad (2.22)$$

where $\varepsilon$ is a small, positive number on the order of $10^{-3}$.

## 2.3 Convergence test

The effects of the applied discretization size (the distance between adjacent ice or hull nodes, as shown in Fig. 2.3) and time step length on the simulated global and local ice loads, as well as the computation time are tested, respectively.

A 30-min icebreaking run of MT Uikku is simulated for each test. The specified ice thickness is 0.3 m, and the ship is set to move straightly ahead at full power. Different values of the discretization size of ice nodes (1600, 800, 400, 200, 100, 50, 25 mm) and the time step length (0.032, 0.016, 0.008, 0.004, 0.002, 0.001, 0.0005 s) are applied. The ice resistance encountered by the ship (global ice load), the mean value of ice-induced frame loads (local ice load on Frame 196.5, divided by the frame spacing) and the computation time are plotted in Figs. 2.11 to 2.16, as a function of the discretization size and time step length, respectively.

It is found that the simulated global ice load converges quite well when the discretization size or the time step length decreases. The deviation is not so big even if a big discretization size or time step length is used. The convergence of local ice load is acceptable, but not as quick as that of global ice load. This is because the local ice load is more sensitive to the contact and icebreaking patterns, as compared with the global ice load which is an integrated value of local ice loads over the hull area. As shown in Figs. 2.13 and 2.16, the computation time increases with the decreasing discretization size and time step length, the time step length in particular has a direct influence on the computation time. To achieve a balance between the computation time and the convergence, a discretization size of 50 mm and a time step length of 0.001 s are finally applied in the simulation program.

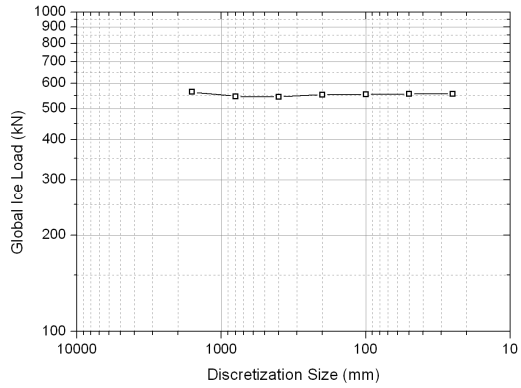


Fig. 2.11 Simulated global ice load as a function of discretization size

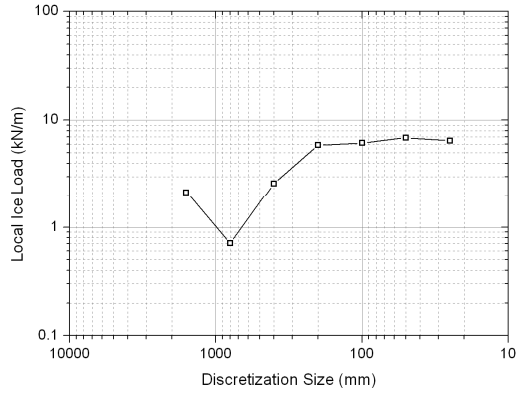


Fig. 2.12 Simulated local ice load as a function of discretization size

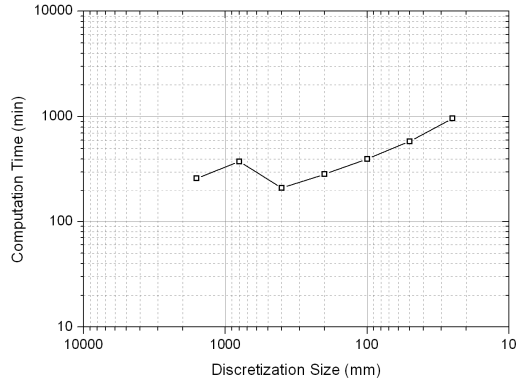


Fig. 2.13 The computation time as a function of discretization size

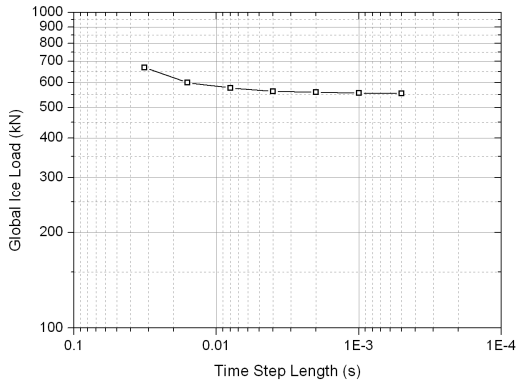


Fig. 2.14 Simulated global ice load as a function of time step length

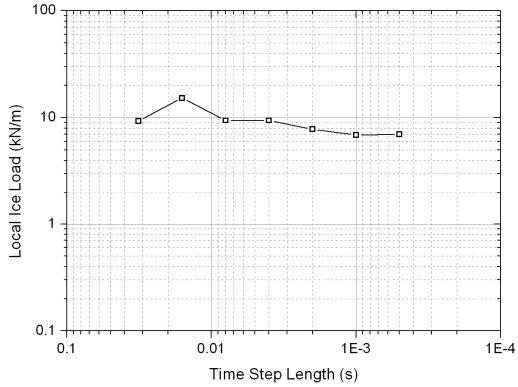


Fig. 2.15 Simulated local ice load as a function of time step length

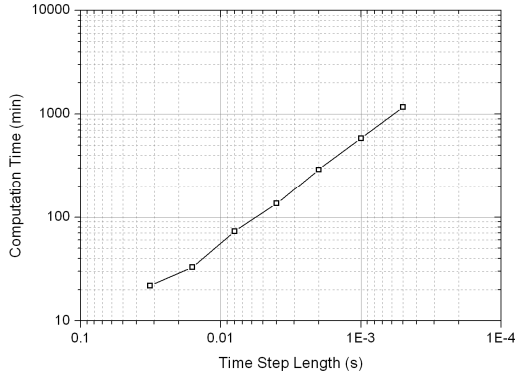


Fig. 2.16 The computation time as a function of time step length

## 2.4 Comparative study

As introduced in Section 2.2, the applied icebreaking model is based on the empirical data, so the simulated icebreaking forces should, to a certain extent be comparable to the empirical estimate. Fig. 2.17 shows a 1-min time history of simulated icebreaking forces for Tor Viking II (ice thickness: 0.5 m, constant ship speed: 5 m/s). The mean value of instantaneous icebreaking forces is then compared with the breaking ice resistance proposed by Lindqvist (1989), by changing different parameters. Fig. 2.18 shows the mean value of simulated icebreaking forces as a function of ice thickness, under the influence of the empirical parameter, $C_f$ (defined in Eq. (2.7)). It is found that the correlation between simulated breaking ice resistance and the ice thickness is in general consistent with Lindqvist's formulation. The fluctuation of simulation results is due to the influence of $C_f$ and the different icebreaking patterns.

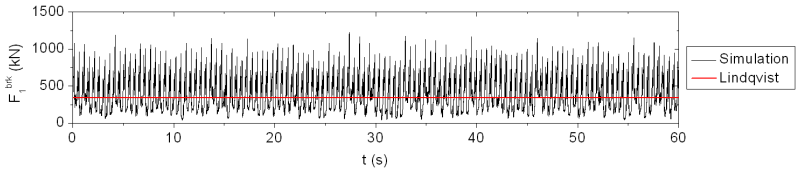


Fig. 2.17 An example of the time history of simulated icebreaking forces and the breaking ice resistance proposed by Lindqvist (1989)

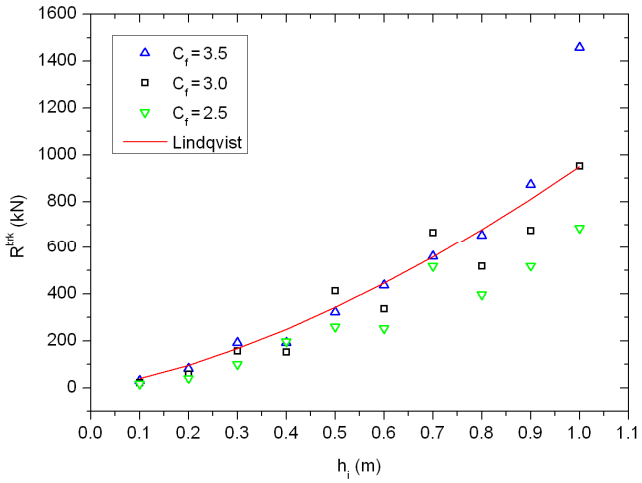


Fig. 2.18 Comparison of the breaking ice resistance between the specified simulations and Lindqvist's formulation

As shown in Fig. 2.19, the occurrence of shoulder crushing (i.e. the ice is continuously crushed by hull shoulder without bending failure) can result in the increased breaking ice resistance at bow shoulder, which may considerably impair the ship's performance in ice. The shoulder crushing is also observed in full-scale trials, but it is difficult to

learn about its actual effect on ice resistance. In this respect, the present numerical method can provide some supplementary information on that. As shown in Figs. 2.20 and 2.21, the simulated breaking ice resistance in 0.5 m thick ice is about 8% higher than in 0.6 m thick ice due to shoulder crushing. Herein, the occurrence and the extent of shoulder crushing are determined by the geometry of simulated icebreaking pattern which is dependent on the ice condition (especially the ice thickness), the hull shape and the ship's motion.

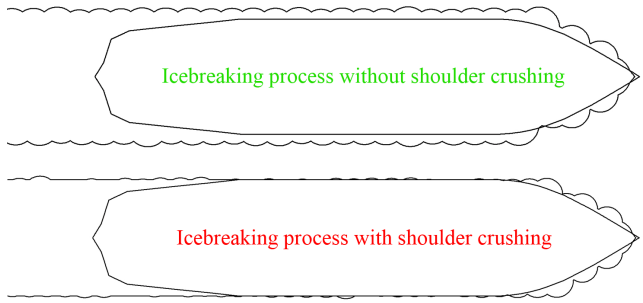


Fig. 2.19 Two different icebreaking patterns

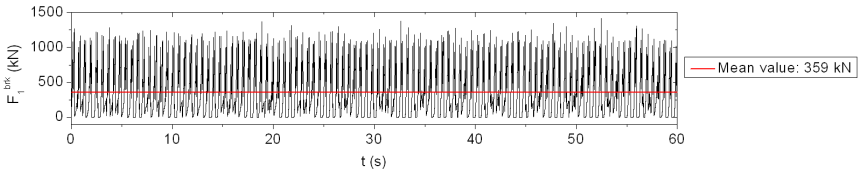


Fig. 2.20 A 1-min time history and the mean value of simulated icebreaking forces in 0.6 thick ice, without shoulder crushing

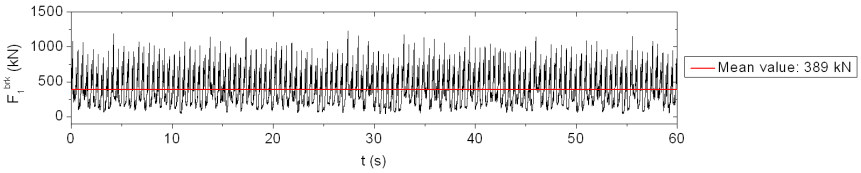


Fig. 2.21 A 1-min time history and the mean value of simulated icebreaking forces in 0.5 thick ice, with shoulder crushing

Fig. 2.22 shows a comparison between the simulated h-v plots and the h-v curve determined from full-scale measurements (Riska et al., 2001). Two sets of empirical parameters ($C_f$ and $C_l$, defined in Eqs. (2.7) and (2.8) respectively) are applied in the simulations. The simulation results are in general consistent with the measured parabolic regression curve. It is considered that the numerical method can be used for the prediction of ship's overall performance in level ice.

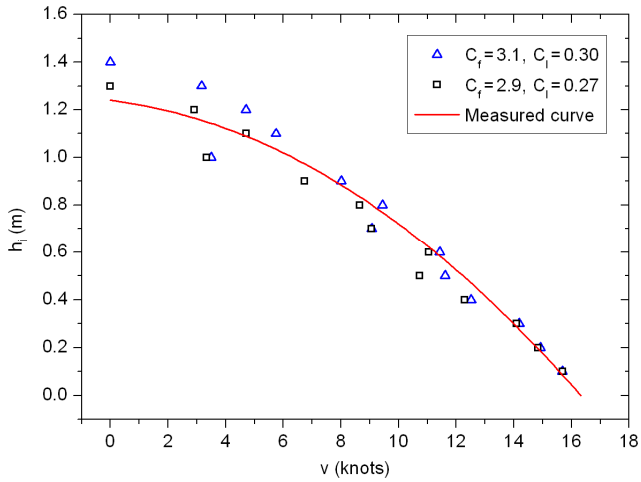


Fig. 2.22 Comparison of the h-v curve between the specified simulations and the full-scale measurements presented by Riska et al. (2001)

## 2.5 Statistical variation of the ice properties

The ice loading process has a clear stochastic nature due to variations in the ice conditions and in the icebreaking processes of ships. The ice model is then extended to more complex ice conditions by considering random ice properties. The main random variables used in this model are ice thickness, ice crushing pressure and ice flexural strength, by referring to the semi-empirical method (Kujala, 1994). Herein, the referenced data of ice properties specifically come from sites in the Baltic Sea. For a more general use, it is necessary to have a good understanding of the present stage-of-knowledge of sea ice properties (which can refer to the excellent review work recently done by Timco and Weeks (2010)).

### *2.5.1 Statistical variation of the ice thickness*

The thickness of the ice cover is highly variable, which is caused by thermal and mechanical factors. The thermal factor is a continuous component and is related to changes in air temperature and snow cover above the ice surface. The mechanical factors are discrete components that are caused by the rafting, ridging, and opening of leads and polynyas.

The existing data of the ice thickness variations are very limited. In Kujala (1994), the relevant data characterizing Baltic Sea ice were reviewed. Fig. 2.23 shows an example of the distribution of pack ice thickness that was measured at 10 m intervals along a line of 1 km length on March 1975 on the Bothnian Bay (a survey that was reproduced from Udin (1976) and Leppäranta (1981)). Two distinct groups of data can be seen in Fig. 2.23. The lower values indicate the distribution of the level ice, and the thickness values

that are higher than 0.8 m are assumed to represent deformed (ridged or rafted) ice (Leppäranta, 1981).

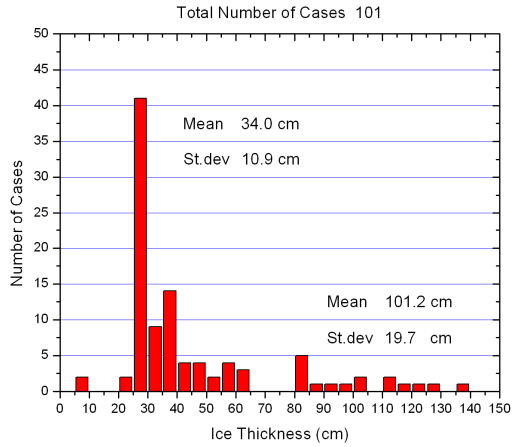


Fig. 2.23 Distribution of the ice thickness as measured at 10 m intervals along a line of 1 km length on March 1975 on the Bothnian Bay (digitized from Kujala (1994))

The situation is further complicated when the prevailing ice thickness variations are observed in full-scale ice load measurements during the normal operations of a ship. Then the definition of the ice thickness is usually based on visual observations of the upper and lower limit of the level ice thickness occurring on the sea area covered by the voyage of the ship. For ice ridges, the occurrence probability and height of the sail are usually the only parameters that can be observed routinely during the voyages (Kujala, 1994).

### *2.5.2 Statistical variation of the ice crushing strength*

As discussed in Section 2.2.2, the definition of effective crushing strength is used to determine the contact force in ice–hull interaction. The statistical variation of ice crushing strength is then considered by using the measured statistical data on ice crushing pressure.

In Kujala (1994), a formulation of the ice crushing pressure in statistical terms was introduced. The resulting crushing pressure is a gamma-distributed variable with small contact areas (< 0.001 $m^2$) and a normally distributed variable with larger contact areas. As the contact area increases, the mean value of the crushing pressure asymptotically approaches a constant value, and the standard deviation, $\sigma_p$, decreases as a function of the contact area, $A$:

$$\sigma_p = \frac{0.065}{\sqrt{A}} \tag{2.23}$$

where $\sigma_p$ is given in MPa, $A$ is given in $m^2$.

By comparing this calculation with the field measurements obtained by Riska et al. (1990), the mean value and the standard deviation of ice crushing strength are then identified as 2.3 and 0.65 MPa in the Monte Carlo simulation described below.

### *2.5.3 Statistical variation of the ice flexural strength*

The strength properties of the ice are sensitive to a number of physical parameters such as the temperature, grain size, crystallographic orientation, porosity, brine content and strain rate. Thus, the strength of the ice under bending is typically studied by conducting on-site flexural strength tests. As discussed in Kujala (1994), the flexural strength is not a basic material property because it is usually determined from the measured failure force by applying linear bending theory with homogenous and isotropic material properties throughout the ice thickness. The advantage of field testing is that the natural variations of the ice properties throughout the thickness of the ice are included in the test results.

Fig. 2.24 shows a histogram of the measured flexural strength values of Baltic Sea ice (data from Kujala (1994)). The mean value (0.58 MPa) and standard deviation (0.11 MPa) of the ice flexural strength given in Fig. 2.24 are then used in the Monte Carlo simulation described below.

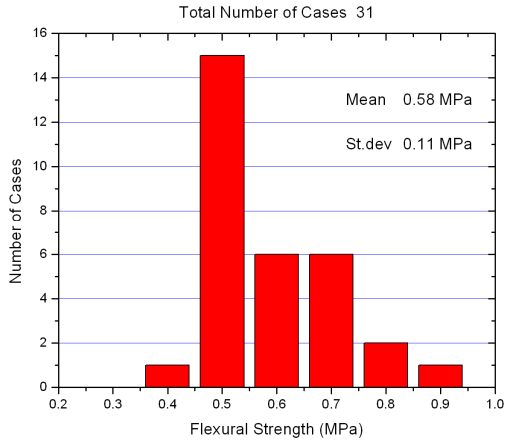


Fig. 2.24 Distribution of the measured flexural strength values of Baltic Sea ice (digitized from Kujala (1994))

### *2.5.4 Monte Carlo simulation*

The Monte Carlo method is applied to predefine an ice field where the ice thickness, ice crushing strength and ice flexural strength are randomly generated using a certain specified probability distribution along the sailing route of the ship. If a normal distribution is assumed, and the correlation between these three variables is neglected,

then the cumulative distribution function (CDF), $F(X)$, and its inverse CDF $F^{-1}(U)$ can be expressed by:

$$F(X) = \frac{1}{\sqrt{2\pi \cdot \sigma}} \cdot \int_{-\infty}^{X} \exp\left( \frac{-(s-\mu)^2}{2\sigma^2} \right) \cdot ds$$
$$U \sim U(0,1) \qquad (2.24)$$
$$X = F^{-1}(U)$$

where $\mu$ and $\sigma$ are the mean value and the standard deviation of random variable $X$, $U$ is a randomly generated number between 0 and 1.

Because there is no information about the correlation of the spatial ice properties, the sensitivity of a possible correlation is investigated by sampling the properties at the spatial points with different intervals. As shown in Eq. (2.24), if a particular mean value and standard deviation are given, then a random value of $X$ can be generated. Using the statistical values that are introduced in Sections 2.5.1 to 2.5.3, the ice thickness, ice crushing strength and ice flexural strength can be randomized along the route by the following procedure: (1) a series of sampling points are fixed along the route, with a certain interval; (2) a random value of the ice property is generated for each sampling point independently; and (3) the intermediate value between two adjacent points is determined by linear interpolation.

Fig. 2.25 shows a random sample of the varying ice properties along a 10 km route, where it is assumed that the ice thickness ($h_i$), ice crushing strength ($\sigma_c$) and ice flexural strength ($\sigma_f$) follow a normal probability distribution and they are independent on each other. Fig. 2.26 shows three simulated icebreaking runs in which the ice properties are randomized at different intervals (25, 50 and 100 m). The 10-minute time histories of the calculated forward speed of the ship (at the same thrust) are also shown in Fig. 2.27. These results show that, by decreasing the interval between two adjacent sampling points, the randomness of the simulated icebreaking pattern increases while the excursion of the calculated ship speed decreases.

As previously introduced, the spatial correlation of the ice properties is neglected between two adjacent sampling points. Therefore, a relatively long interval (50 m) is finally used in the simulation program. The fine tuning of the spatial sampling point can be done by comparing the time histories of simulated ship speed (as shown in Fig. 2.27) with the relevant record from full-scale voyages, and the issues of correlation remain for further analysis.

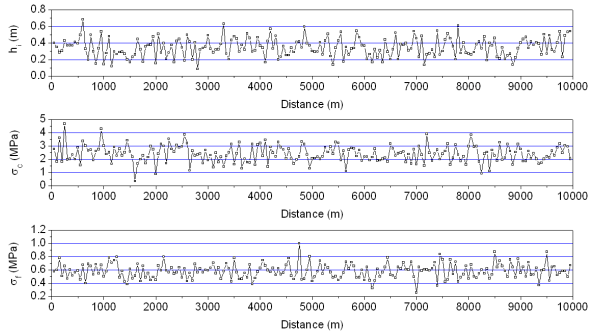


Fig. 2.25 A random sample of the varying ice properties along a 10 km route

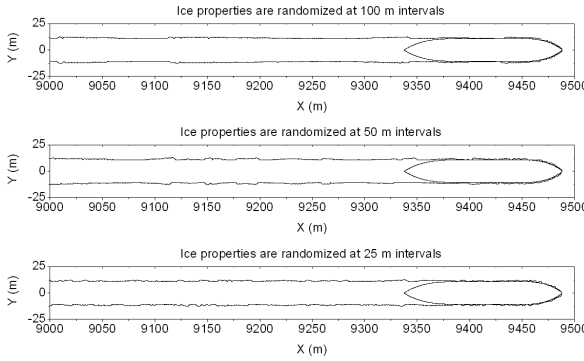


Fig. 2.26 Simulated icebreaking runs under randomly varying ice conditions

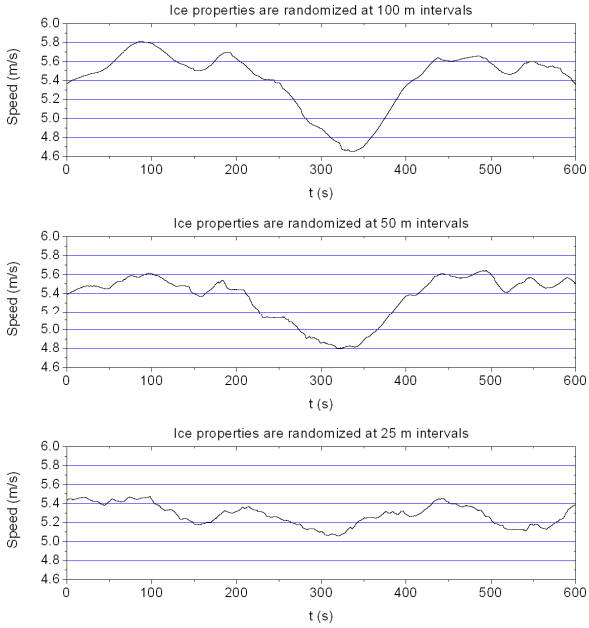


Fig. 2.27 Time histories of the calculated ship speed (at the same thrust)

# Chapter 3

# Ship's Performance in Level Ice

A case study with an icebreaker, Tor Viking II, is carried out to investigate the ship's performance in level ice. *Paper 1* and *Paper 2* are associated with this subject. In *Paper 1*, the speed that the ship can attain in ice is investigated, by comparing the simulation results with the h-v curves determined from field measurements. *Paper 2* focuses on the turning performance which is measured by the turning circle diameter.

## 3.1 General

Ship performance in ice consists of ability to break ice and to maneuver in ice. At early design phase some analytical methods can be applied to determine the level ice performance of an icebreaking ship. As mentioned in Chapter 1, these methods are at best semi-empirical and should be used cautiously, especially beyond the range of validity. The analytical methods can not account for the details of hull shape. When the design proceeds, more exact calculations or model tests should be carried out to finalize the hull shape and to ensure an adequate maneuvering performance which can not be verified by the analytical methods.

For the present numerical method, the 3D ship geometry (see e.g. Fig. 2.9) is considered in the hydrodynamic calculations, and the 2D hull shape (see e.g. Fig. 2.3) is considered in ice–hull interaction. In this chapter, the level ice performance of a Swedish multi-purpose icebreaker, Tor Viking II (as shown in Fig. 3.1), is investigated by comparing the simulation results with the field measurements obtained by Riska et al. (2001).

Fig. 3.1 Icebreaker Tor Viking II (www.ils.fi)

The main dimensions of Tor Viking II are presented in Table 3.1. The specification values of the vessel in ice are: (1) minimum forward speed of 3.0 knots in 1.0 m thick level ice; (2) minimum speed astern of 3.0 knots in 0.5 m thick level ice; and (3) the turning circle diameter less than 500 m in 0.5 m thick level ice. The level ice capability of Tor Viking II was tested in ice fields of two thicknesses, and the test results met the above requirements.

Table 3.1 Main dimensions of Tor Viking II

| | | |
|---|---|---|
| Length over all | 83.7 | m |
| Length between perpendiculars | 75.2 | m |
| Breadth, moulded | 18.0 | m |
| Draught, maximum icebreaking | 6.5 | m |
| Deadweight | 2,528 | ton |
| Power output | 13.4 | MW |

## 3.2 Forward speed

In the simulation with a free-running model, the ship's motion is obtained by solving the equations of motion in which the thrust and the global ice load both are identified. Fig. 3.2 shows a time history of simulated forward speed in 0.6 m thick ice, where the ship is moving at full power and the starting forward speed is 4.0 m/s. The speed that the ship can attain in 0.6 m thick ice is then determined as 5.68 m/s. As shown in Fig. 3.3, the total ice forces encountered by the ship consist of a time varying component and an almost constant component. The time varying component is due to the continuous icebreaking process which is numerically detected, while the constant component is the submersion and friction resistance derived from Lindqvist's formulation (Lindqvist, 1989).

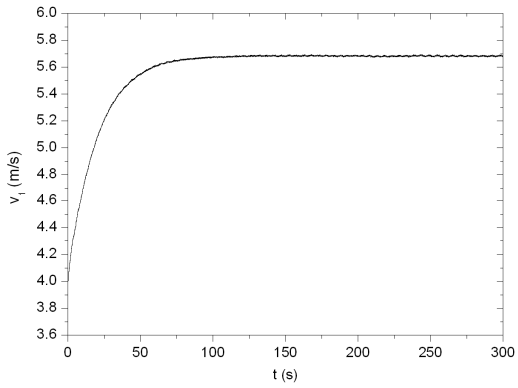


Fig. 3.2 A simulated time history of the forward speed of the ship, from a starting speed to the full speed (in 0.6 m thick ice)

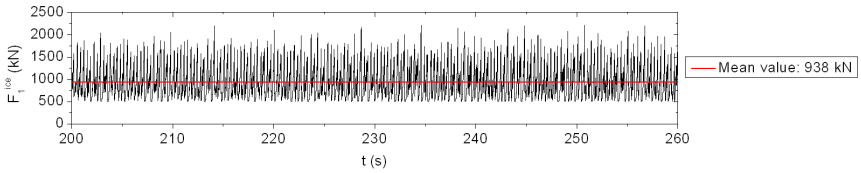


Fig. 3.3 A simulated time history of the ice forces encountered in surge direction (in 0.6 m thick ice)

Ship's performance in level ice is usually measured by the h-v curve. As shown in Fig. 3.4, the simulation results agree well with the full-scale measurements (Riska et al., 2001). It is also found that the forward speed of the ship may be considerably slowed down (see e.g. the simulation result in 0.5m or 1.0 m thick ice) due to the occurrence of shoulder crushing, as discussed in Section 2.4. In a certain full-scale ice trial, the natural variation of ice thickness is inevitable. If a reasonable range of variation is defined, this effect can also be included in the simulations.

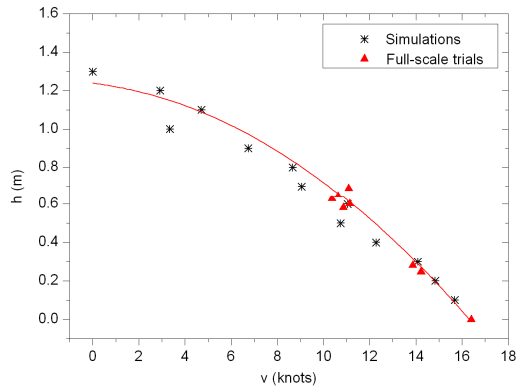


Fig. 3.4 Comparison of the h-v curve between the present simulations and the full-scale tests presented by Riska et al. (2001)

## 3.3 Turning circle

Fig. 3.5 shows a simulated turning circle in 0.6 m thick ice, where $D_t$ denotes the turning circle diameter which is a measure of the ship's maneuverability in ice. In this simulation, the ship starts moving straightly ahead at full power. The rudders are then assumed to be turned to the full angle (45º) instantly, and the ship starts turning freely with a constant rudder angle. As shown in Fig. 3.6, the forward speed is sharply slowed down when the ship starts turning. As compared to Fig. 3.3, the time history of the ice forces shown in Fig. 3.7 is quite different, and the mean force is also increased due to the continuous crushing at hull shoulder.

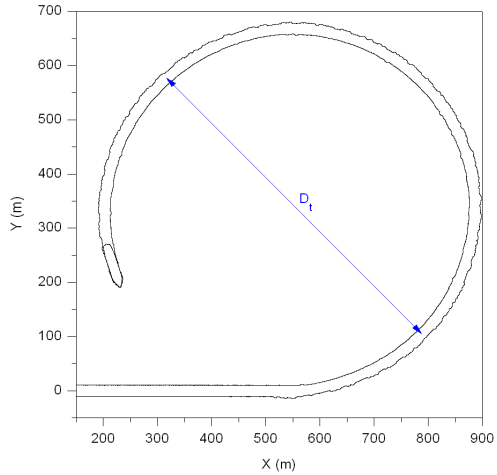


Fig. 3.5 A simulated turning circle (in 0.6 m thick ice)

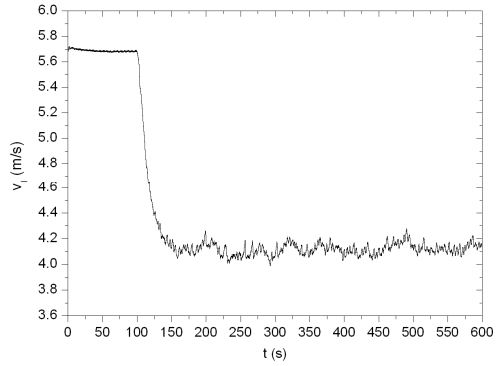


Fig. 3.6 A simulated time history of the forward speed of the ship, from straight going to turning freely with a constant rudder angle (in 0.6 m thick ice)

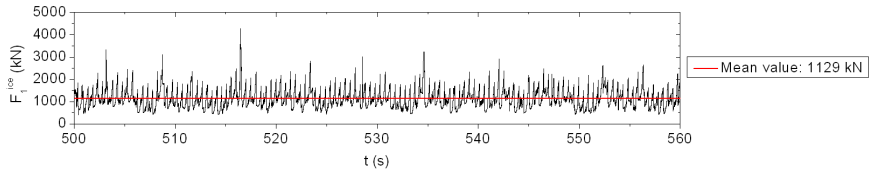


Fig. 3.7 A simulated time history of the ice forces encountered in surge direction, during turning operation (in 0.6 m thick ice)

As shown in Fig. 3.8, the simulated values of turning circle diameter in different ice thicknesses are comparable to full-scale measurements. But it is also found that the calculated turning circle diameters in thicker ice (e.g. 0.8 m and 0.9 m) deviate from the trend established by measurements or simulations. This is attributed to the different icebreaking patterns described below.

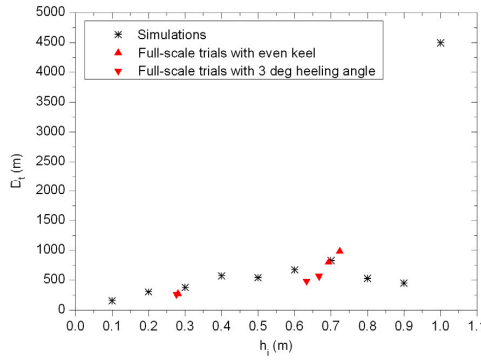


Fig. 3.8 Comparison of the turning circle diameter between the present simulations and the full-scale tests presented by Riska et al. (2010)

## 3.4 Influence of shoulder crushing on ship's performance

As discussed in Section 2.4, the continuous ice crushing at bow shoulder can result in the increased breaking ice resistance, and it is found in Section 3.2 that the forward speed of the ship may be considerably slowed down due to the occurrence of shoulder crushing. In turning operations, this effect is more notable because the aft shoulder can also be in contact with ice.

As shown in Fig. 3.9 and Figs. 3.10 to 3.12, it happens often in both full scale and the simulations that only occasionally some ice floes are broken by bending at the aft shoulder and sometimes the ice edge is just crushed. The corresponding time histories of the heading angle are also shown in Figs. 3.13 to 3.15. It can be clearly seen that the simulated turning process is very sensitive to the occurrence of shoulder crushing, and if it happens the turning process will be considerably slowed down. In 0.7 m thick ice (as shown in Figs. 3.10 and 3.13), shoulder crushing happens intermittently, so a devious time history of the heading angle comes up. In 0.9 m thick ice (as shown in Figs. 3.11 and 3.14), shoulder crushing seldom happens, so the ship has a more rapid turning process even than in 0.7 m thick ice. In 1.0 m thick ice (as shown in Figs. 3.12 and 3.15), shoulder crushing happens all the time, so the turning process becomes very slow.

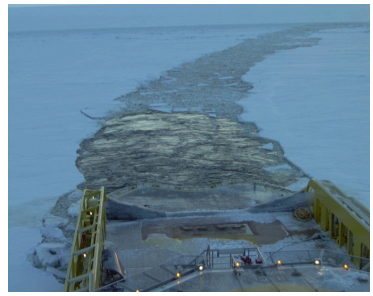

Fig. 3.9 Full-scale ship turning in ice

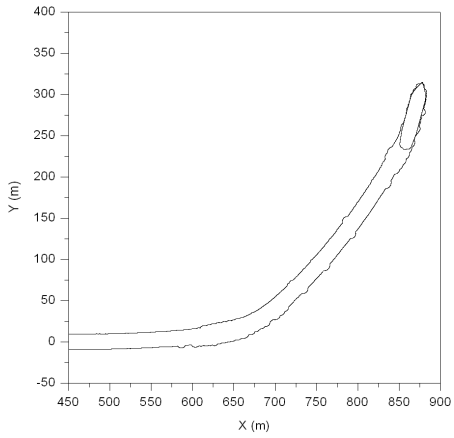


Fig. 3.10 Simulated ship turning in 0.7 m thick ice

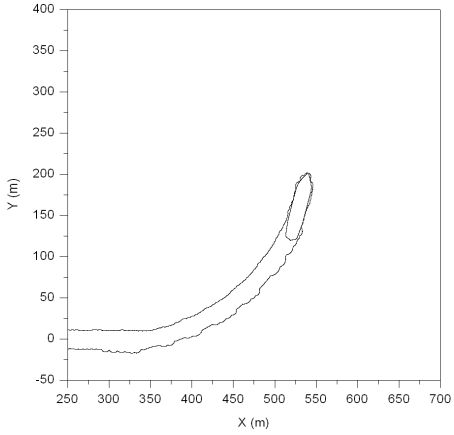


Fig. 3.11 Simulated ship turning in 0.9 m thick ice

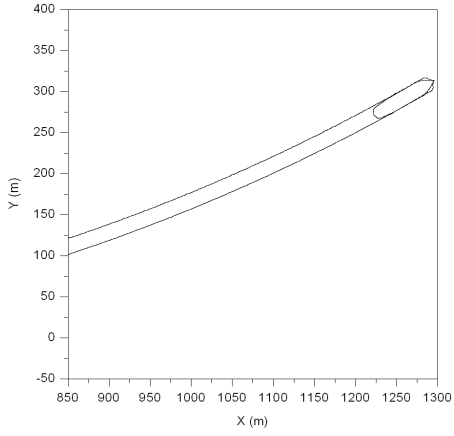


Fig. 3.12 Simulated ship turning in 1.0 m thick ice

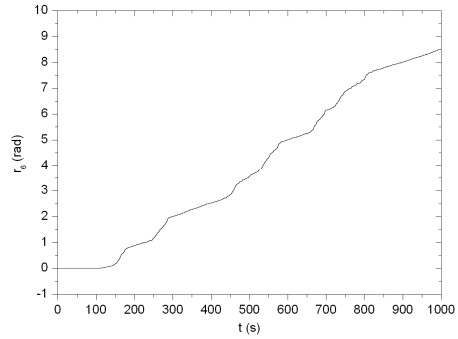


Fig. 3.13 Simulated time history of the heading angle in 0.7 m thick ice

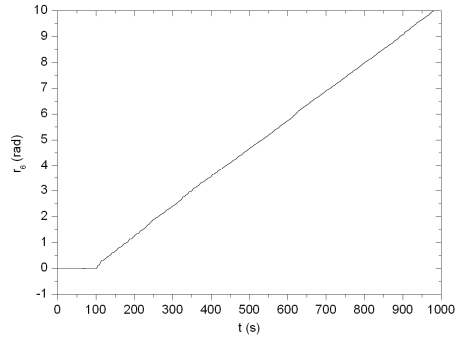


Fig. 3.14 Simulated time history of the heading angle in 0.9 m thick ice

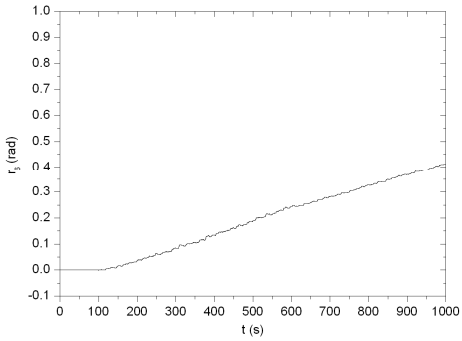


Fig. 3.15 Simulated time history of the heading angle in 1.0 m thick ice

Fig. 3.16 shows the simulated turning circle in 0.7 m thick ice. As compared with Fig. 3.5 (in 0.6 m thick ice), the turning track can not be taken as a circle due to the intermittent crushing. During the full-scale ice trials (Riska et al., 2001), the turning operations with 3 deg heeling angle were also tested, and the measured turning circle diameters in thicker ice also show a deviation from the trend in even keel condition (as shown in Fig. 3.8). This may be attributed to the reduced shoulder crushing as it occurs in the simulations, but more validation of the data is needed.

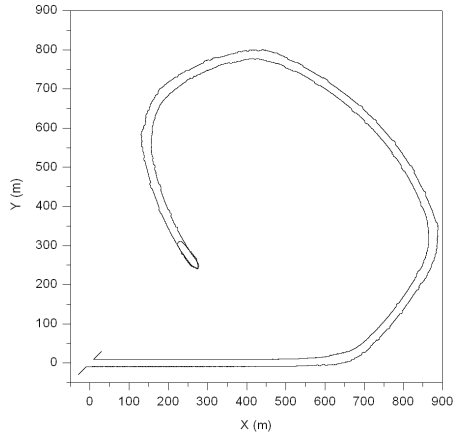


Fig. 3.16 Simulated turning circle in 0.7 m thick ice

# Chapter 4

# Probabilistic and Spatial Distribution of Local Ice Loads around the Hull

A case study with an icebreaking tanker, MT Uikku, is carried out to investigate the probabilistic and spatial distribution of local ice loads around the hull. *Paper 3* and *Paper 4* are associated with this chapter. In *Paper 3*, the origin of the probabilistic variation of local ice loads is investigated, by considering the variations in the external ice conditions and in the icebreaking processes of the ship. The probabilistic distribution of ice-induced peak loads on a frame is then analyzed and compared with field measurements. In *Paper 4*, the simulation results on the spatial distribution of local ice loads around the hull are presented.

## 4.1 General

The ice loading process has a clear stochastic nature due to variations in the ice conditions and in the icebreaking processes of ships. The statistical characteristics of the local ice loads on ships have been studied almost exclusively on the basis of full-scale measurements.

MT Uikku (as shown in Fig. 4.1) is a double-hull icebreaking motor tanker that is owned by Neste Shipping and Kvaerner Masa-Yard's joint venture company, Nemarc. The main dimensions of MT Uikku are presented in Table 4.1. The ship was constructed to meet the standards of the highest Finnish-Swedish Ice Class, IA Super. In 1998, the hull was strengthened for voyages in the Arctic Sea. After strengthening, the hull was stronger than the Finnish-Swedish Ice Class IA Super demands (Kujala et al., 2009). In 1998, MT Uikku was instrumented to measure the ice loads from different parts of the hull during the ARCDEV voyage (Kotisalo and Kujala, 1999). In 2003, three voyages were made between the Gulf of Finland and the Bothnian Bay (Hänninen, 2003), and the statistical characteristics of the ice loads measured on the bow area were discussed in Kujala et al. (2009) in which the analyzed data were gathered from the sensors that were mounted on frame 196.5 (as shown in Fig. 4.2).

A case study with MT Uikku is then carried out by using the simulation program. In this study, the thickness and strength properties of the ice encountered by the ship are assumed to be constant or randomly generated using the Monte Carlo method. The statistical data on the strength properties of Baltic Sea ice (as introduced in Section 2.5) are applied in this simulation. The ice-induced frame loads (see e.g. Fig. 4.2) are analyzed using the line load on the frame. This is obtained by dividing the normal force on the frame by the frame spacing (0.35 m), the units are thus in kN/m. As shown in Fig. 4.3, a frame on the bow area (frame 196.5) and another frame on the bow shoulder area (frame 175.5) are selected for the comparison between the simulation results and the field measurements obtained by Kotisalo and Kujala (1999) and Hänninen (2003).

Fig. 4.1 Icebreaking tanker MT Uikku (personal.inet.fi/koti/jaakko.vahala)

Table 4.1 Main dimensions of MT Uikku

| | | |
|---|---|---|
| Length over all | 164.4 | m |
| Length between perpendiculars | 150.0 | m |
| Breadth, moulded | 22.2 | m |
| Draught | 12.0 | m |
| Deadweight | 15,750 | ton |
| Power output | 11.4 | MW |

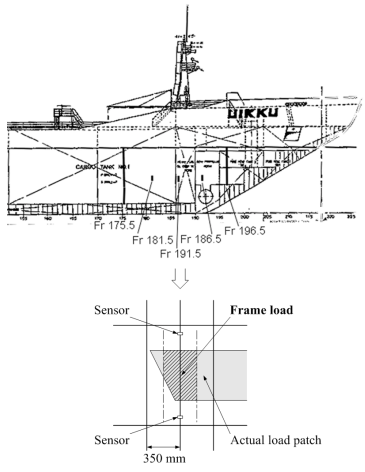


Fig. 4.2 A side view of MT Uikku (bow area)

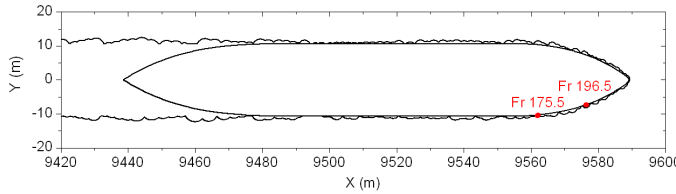


Fig. 4.3 Two frames selected for the comparison between the simulation results and field measurements

It should be noted that the submersion and sliding processes of the broken ice are not simulated by this numerical method. The effects of the submersion and sliding processes on the global ice loads are derived from Lindqvist's formulation, in which the bow is assumed to be completely covered by ice, and the bottom is covered for 70% of the length of the ship (Lindqvist (1989)). If the calculated submersion and friction resistance (less than 1000 kN) is divided evenly among all frames (the frame spacing is 350 mm, as shown in Fig. 4.2), the load value for each frame will be less than 5 kN. Therefore, it is assumed that the ice-induced frame loads, especially the peak loads on the frame, are primarily determined by the icebreaking process.

## 4.2 Probabilistic distribution of ice-induced frame loads

The origin of the probabilistic variation in ice loading has been attributed earlier to the variations in the ice types and ice properties. In the following simulations, the level ice with uniform and varying properties is considered while other ice types (e.g. ice ridge and brash ice) are not taken into account.

### *4.2.1 Simulation in uniform ice conditions*

In this section, the thickness and strength properties of the ice that is encountered by the ship are assumed to be constant during an icebreaking run.

Fig. 4.4 shows the 10-min time histories of the calculated ice loads on frame 196.5, which consists of six icebreaking runs in which different constant values for the ice thickness (0.30 to 0.40 m) are simulated. The simulated frame loads are very sensitive to the given ice thickness. This result is not unexpected because it is concluded in *Paper 1* that the simulated icebreaking pattern is very sensitive to the ice thickness. Under certain ice conditions, it is possible that the specified frame is never in contact with the ice during the relevant icebreaking pattern. Thus, as shown in Fig. 4.4, the ice loads can maintain a value of zero during the entire icebreaking run.

Fig. 4.5 shows three icebreaking runs that are simulated with different thrusts, and the calculated mean values of ship speed varied between 2.90 and 5.67 m/s. The simulated frame loads are also sensitive to the motion of the ship because the icebreaking pattern is also dependent on the relative velocity between the hull and the ice wedges that are in contact.

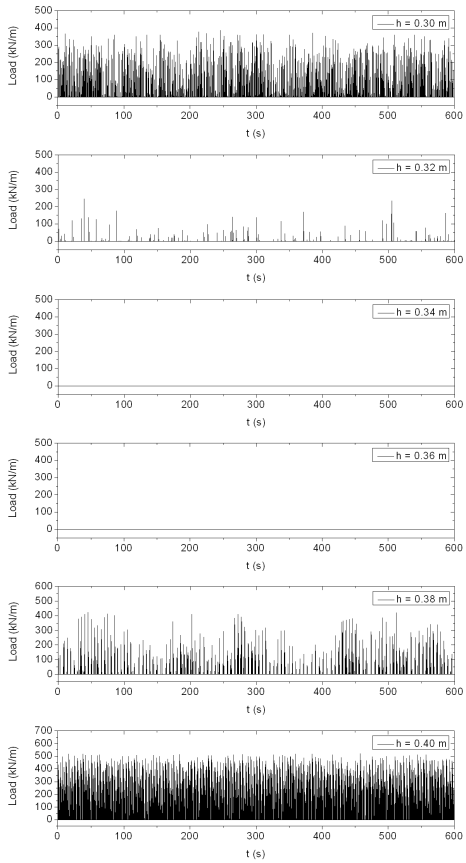


Fig. 4.4 Time histories of the simulated ice loads on frame 196.5 with different constant values of the ice thickness (h)

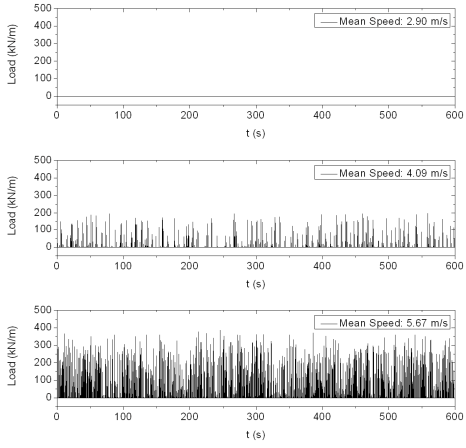


Fig. 4.5 Time histories of the simulated ice loads on frame 196.5 with different mean values of ship speed (dependent on the given thrust)

Individual ice loads need to be separated when studying the time histories of ice loads. The Rayleigh separation method (as introduced in Vuorio et al. (1979) and Kujala et al. (2009)) is used in this study to collect the peak loads within a certain time interval. Fig. 4.6 shows the occurrence frequency of the peak loads as a function of the ice thickness, where the frequency is calculated by dividing the number of peaks by the time interval (10 min). As shown in this figure, the frequency of the peak loads can vary from 0 to about 2 Hz due to a small variation in the ice thickness, and it is uncertain whether this frequency will increase or decrease. This is because a small change of both the ice conditions and the motion of the ship can lead to a chain of changes in the icebreaking patterns around the hull, which may totally change the locations of the contact zones (as shown in Fig. 2.3).

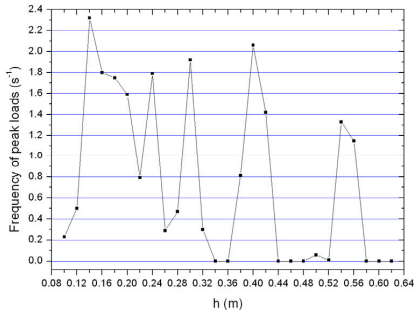


Fig. 4.6 Frequency of the simulated peak loads on frame 196.5 as a function of the ice thickness (h)

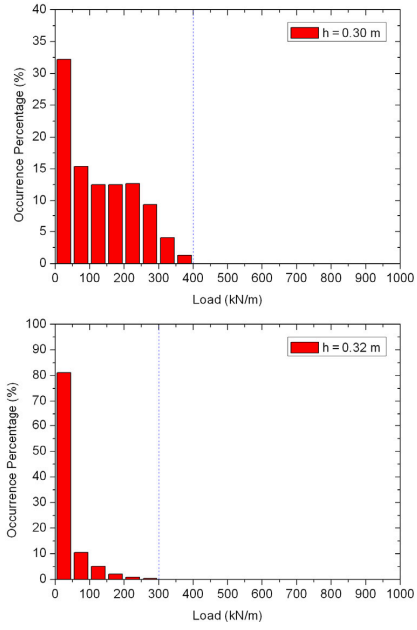


Fig. 4.7 Distributions of the simulated peak loads on frame 196.5 with different constant values of the ice thickness (h)

Fig. 4.7 shows the distributions of the peak loads which are plotted in the form of histogram. It is found that the simulated peak loads are scattered although the external ice conditions are fixed. This is attributed to the variation in the contact and icebreaking patterns. The contact and icebreaking patterns are determined by the interaction between ship and ice, which is a continuously varying process and can increase the variation of ice-induced frame loads.

### *4.2.2 Simulation in randomly varying ice conditions*

In this section, the thickness and strength properties of the ice that is encountered by the ship are randomized along the route. The statistical data that are applied in this study are presented in Table 4.2.

Table 4.2 Statistical data on the ice properties

| | Mean | Std. |
|---|---|---|
| Ice thickness | 0.340 m | 0.109 m |
| Ice crushing strength | 2.30 MPa | 0.65 MPa |
| Ice flexural strength | 0.58 MPa | 0.11 MPa |

In Kujala et al. (2009), the exponential, gamma and Weibull distributions were fitted to the measured peak loads on frame 196.5, and it was found that the Weibull distribution with a shape factor of 0.75 gave the best fit to the measured statistical distributions. In this study, the distributions of the simulated peak loads on the same frame are then analyzed using the Weibull probabilistic model.

The cumulative distribution function of the 2-Parameter Weibull distribution is given by:

$$F(x) = 1 - \exp\left(-\left(x/\lambda\right)^{k}\right) \tag{4.1}$$

where $k$ is the shape factor and $\lambda$ is the scale factor of the distribution.

Fig. 4.8 shows the fitted distributions to the simulated peak loads (recorded in a period of 12 hours), where $x_i$ are the ordered values of peak loads ( $x_i$ =1, 2, 3… kN/m); $F_i$ are the cumulative probabilities of $x_i$ ; ln() is the natural logarithm function. If $x_i$ exactly follow a Weilbull distribution, the $\ln(-\ln(1-F_i))$ versus $\ln(x_i)$ plot should be a straight line with a slope equal to the shape factor of Weibull distribution. As shown in this figure, the Weibull distribution (shape factor $k$ = 0.75) which was found to give the best fit to the measured data can also be fitted to the simulation results. But, it seems that a smaller shape factor is better fitted for the low peak loads and a bigger shape factor is better fitted for the high peak loads.

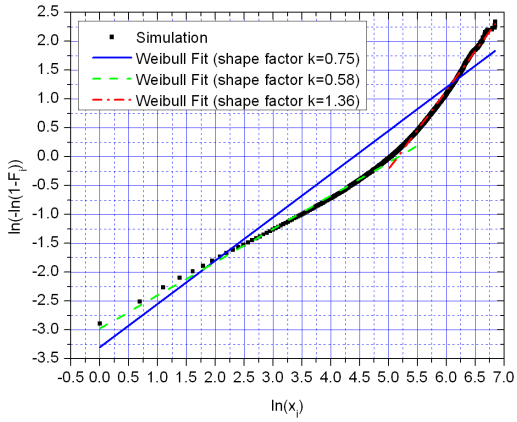


Fig. 4.8 Distributions of the simulated peak loads (recorded in a period of 12 hours) on frame 196.5 and fitted probability distributions by using the Weibull model

In this simulation, the thickness and strength properties of the ice are randomized by the normal distribution, while the simulated peak loads on a frame are found to approximately fit a Weibull distribution. This is because there is an internal source of the probabilistic variation in ice loading due to the icebreaking processes of the ship, other than the external ice conditions.

Fig. 4.9 shows the variation of the contact between frame 196.5 and the ice in a period of 10 min. Herein the contact length is the load length within the frame area, and the variation of the contact length is attributed to the time varying icebreaking process of the ship. The frame spacing is 0.35 m on the bow area of MT Uikku. So, it means that the frame is fully in contact with ice when the contact length equals to 0.35 m.

Fig. 4.10 shows a 10-min time history of the ice loads simulated in a randomly varying ice condition. The load peaks are separated in two groups, where the peaks indicated by red squares are in accordance with full contact while the peaks indicated by green squares are in accordance with varying contact length.

Fig. 4.11 shows the probabilistic distribution of simulated peak loads (recorded in a period of 12 hours), where $P_i$ are the occurrence percentages of the peak loads that are varying from $x_{i-1}$ to $x_i$. In the situation that the frame is fully in contact with ice, the distribution of simulated peak loads is dominated by the variations in the thickness and strength properties of the ice which are assumed to be normally distributed along the route. As a whole, it is dependent on the variations in both the external variables and the contact and icebreaking patterns, which results in the different distributions between the low peak loads and the high peak loads shown in Fig. 4.8.

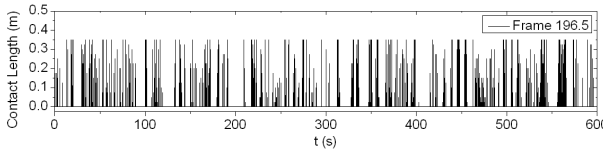


Fig. 4.9 Time varying contact length between frame 196.5 and the ice (average ice thickness: 0.34 m)

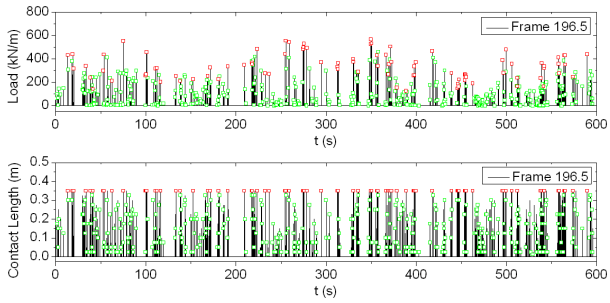


Fig. 4.10 A 10-min history and separated peak values of the ice loads simulated in a randomly varying ice condition (average ice thickness: 0.34 m)

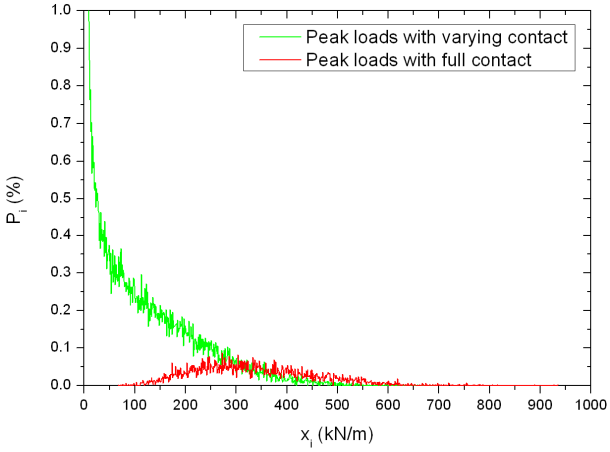


Fig. 4.11 Probabilistic distribution of the simulated peak loads (recorded in a period of 12 hours) on frame 196.5 with varying or full contact

### *4.2.3 Comparison with field measurements*

Fig. 4.12 shows a 10-min time history of simulated ice loads on frame 196.5, where the ice properties were randomly sampled along the route, the average ice thickness is 0.125 m (with a standard deviation of 0.0625 m), and the average ship speed is 5.43 m/s. The simulated ice loading process has a clear stochastic nature due to variations in the ice conditions and in the contact and icebreaking patterns. Fig. 4.13 shows a 10-min time history of measured ice loads on frame 196.5, where the measurement was performed during the ARCDEV voyage (Kotisalo and Kujala, 1999) under various ice conditions.

As shown by these two figures, the simulated ice loading history is comparable to the measurements even though the actual ice conditions in-service may be much more complex than the level ice (with varying thickness and strength properties) simulated here.

Fig. 4.14 shows an example of the distribution of measured peak loads on frame 196.5, which is plotted in the form of logarithmic histogram (data from Hänninen (2003)). This measurement was performed in a thin level ice condition, where the average ice thickness is 0.125 m, the average ship speed is 5.55 m/s, and the time interval is 10 min. The same scenario is applied to the simulations. Fig. 4.15 shows the distribution of simulated peak loads on frame 196.5, which are obtained from three simulated icebreaking runs. As shown by these two figures, the simulated distribution form is similar to the measured one, except for the very low peak loads (less than 40 kN/m). This is because in field measurements numerous of small peaks might be induced by the electronic noise, open water and brash ice (Kujala et al., 2009), which are not included in the simulated frame loads. It is found that the simulated maximum ice loads in the 10-min time interval are comparable to the measured value, and the variation of simulated load maxima is due to the scatter of sampled ice properties and the variation in the contact and icebreaking patterns. More simulation samples are thus needed for the statistical analysis of the maximum ice load within a certain period (as described in *paper 5*).

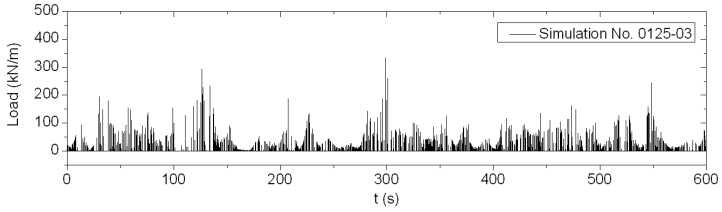


Fig. 4.12 A 10-min time history of simulated ice loads on frame 196.5 (average ice thickness: 0.125 m, average ship speed: 5.43 m/s)

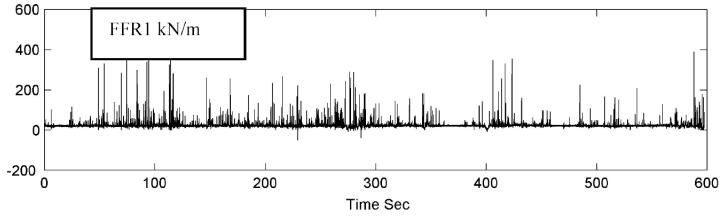


Fig. 4.13 A 10-min time history of measured ice loads on frame 196.5 (reproduced from Kotisalo and Kujala (1999), different types of ice conditions)

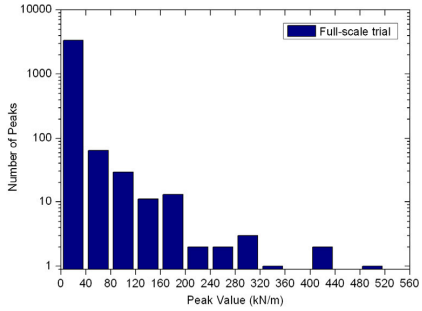


Fig. 4.14 Distribution of the peak loads on frame 196.5, measured in a 10 min full-scale trial (data from Hänninen (2003), average ice thickness: 0.125 m)

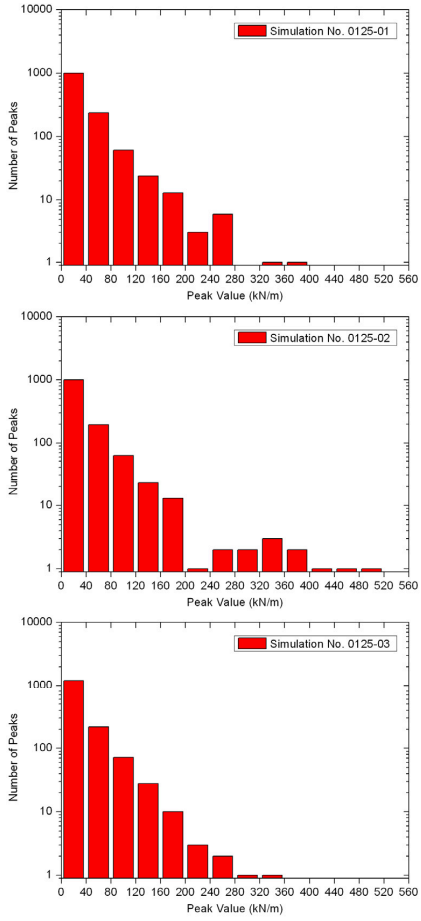


Fig. 4.15 Distribution of the peak loads on frame 196.5, obtained from three simulated icebreaking runs (average ice thickness: 0.125 m)

## 4.3 Spatial distribution of local ice loads around the hull

The origins of ice loads on different hull areas are different. When the ship proceeds straight ahead, only the bow waterline is breaking ice. Other areas of the hull encounter hits from broken ice pieces. The midship and aft areas can break ice when the ship is maneuvering (e.g. turning) or going astern. As the ice loads on different hull areas are of different origins, it is clear that the magnitudes of the loads are also different. This is taken into account in most ice rules by dividing the ship hull into regions and giving so called hull area factor for each region.

In FSICR the ship hull is divided into forward, midship and aft regions, among which the forward region (bow) has the highest hull area factor (i.e. 1.0). This is because the dominant operational mode of a ship is moving straight ahead. Accordingly the long-term ice loads at the bow should be considerably higher than the short-term ice loads. The load level defined in the ice rules of course need to reflect the long-term ice loads. But it has been suggested by the model tests (Izumiyama, 2006) and numerical calculations (Valanto, 2007) that in turning operation the ice loads at aft shoulder are pronounced and may be higher than at the bow area. Thus for the aft shoulder, the safety reserve in the ice rules may be lower than elsewhere. Information on the spatial distribution of local ice loads around the hull can thus be used for more reliable design of the ship which is intended to have a good turning ability in ice.

As shown in Fig. 4.16, thirty frames on different hull areas of MT Uikku are selected at 10 m intervals, the frame spacing is assumed to be same and equal to 0.35 m on each hull area. The spatial distribution of local ice loads is then investigated in both straight going and turning operations.

Figs. 4.17 and 4.18 show the simulated time histories of the ice-induced frame loads on two different hull areas when the ship is turning with a 30º steering angle (of the Azipod propulsion system). Since the spatial distribution of local ice loads around the hull is investigated in this simulation, the thickness and strength properties of the ice are thus assumed to be uniform. The frame in Fig. 4.17 is at the bow, the simulated ice loads on bow frames are similar in both straight going and turning operations. As shown in Fig. 4.17, the simulated ice loading process consists of numerous short duration spike-like peaks. It is quite similar to the normal pattern of local ice loads obtained from full-scale trials which are usually performed in straight going mode. The frame in Fig. 4.18 is at aft shoulder, where the ice loading history is quite different from the bow frames. This is because the frame at aft shoulder is close to vertical, accordingly the ice edge in the outside of the turning circle (the starboard side shown in Fig. 4.16) can be continuously crushed by the aft shoulder without bending failure. In this situation, the band-like load peaks may occur, and the mean ice load may increase considerably. It should be noted that the mean ice load may be overestimated, as the buckling or shearing failure of the ice is neglected in this simulation while it occasionally takes place in practice.

The peak values with a non-exceedance probability of 99% (refer to Izumiyama et al. (2005)) and the time averages (mean ice loads) are then derived from the ice loading histories. Fig. 4.19 shows the spatial distribution of simulated peak loads on frames around the hull. Three different steering angles (5, 15 and 30 deg) are used for the simulation of turning operations, all of them can result in high loads at aft shoulder, which means the aft shoulder of MT Uikku may be equally or even more vulnerable to ice damage as compared to frames on the bow area, when this ship is turning in a considerably severe ice condition. It is also found that the steering angle has only a slight influence on the magnitude of high peak load at the aft shoulder, while it has a significant influence on the number of frames which are under this high load level. Fig. 4.20 shows the spatial distribution of simulated mean ice loads on frames around the hull. Herein the steering angle has a significant influence on the magnitude of the mean ice load at aft shoulder, and this magnitude can be much higher than that at the bow. It means that in turning operations the aft shoulder of MT Uikku may encounter much heavier turning resistance as compared with the bow area.

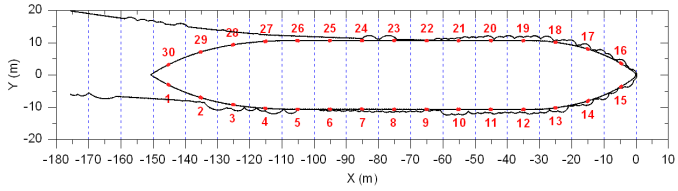


Fig. 4.16 Numbering of the frames on different hull areas of MT Uikku

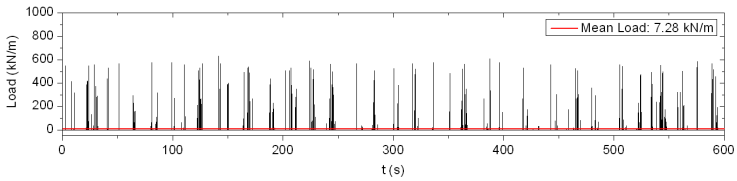


Fig. 4.17 A simulated time history of the local ice loads on frame 13 (uniform ice thickness: 0.34 m, steering angle: 30 deg)

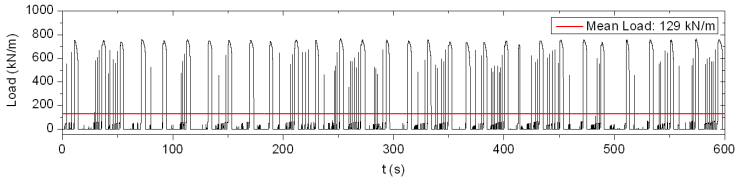


Fig. 4.18 A simulated time history of the local ice loads on frame 5 (uniform ice thickness: 0.34 m, steering angle: 30 deg)

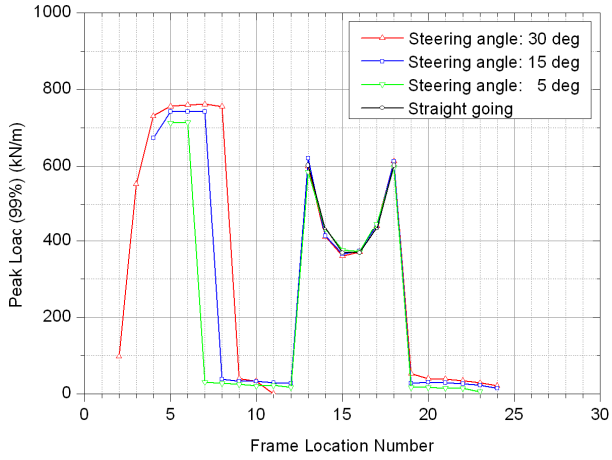


Fig. 4.19 Spatial distribution of simulated peak loads around the hull (uniform ice thickness: 0.34 m)

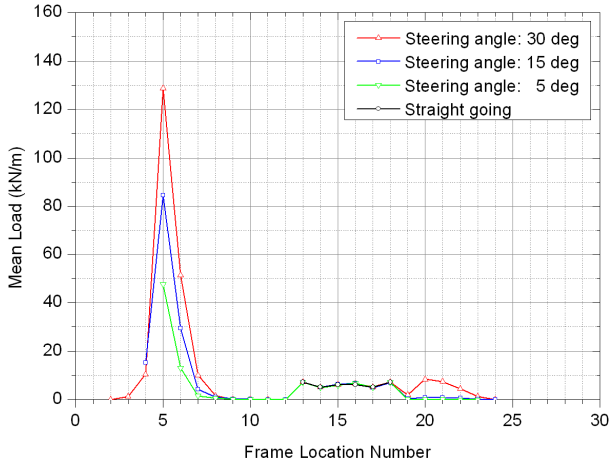


Fig. 4.20 Spatial distribution of simulated mean ice loads around the hull (uniform ice thickness: 0.34 m)

The spatial distribution of both peak loads and mean loads analyzed above are dependent on the different frame angles around the hull, as well as the shape of ship waterline. MT Uikku is an icebreaking tanker which has a larger length to beam ratio than conventional icebreaking ships (e.g. Tor Viking II). This hull form may develop high loads at aft shoulder. In a straight going test, e.g. the ARCDEV voyage in the Kara Sea (Kotisalo and Kujala, 1999), the measured load maximum at bow shoulder was about 50% higher than at the bow. As shown in Fig. 4.19 (frames 13 to 15, and frames 16 to 18), the simulated variation is quite close to this value. It can be expected that most other ice types, than the level ice simulated here, existing in the field would cause a similar load distribution form along the hull, even if the actual magnitude of the ice loads may be very different (Valanto, 2007). It is expensive and technically difficult to perform the ice load measurements around a wide hull area (such as that shown in Fig.

4.16) in field tests. The numerical simulation can thus compensate this shortage of field data.

# Chapter 5

# Short-Term Distribution of Maximum Ice Loads on a Frame

A case study with a chemical tanker, MS Kemira, is carried out to investigate the short-term distribution of maximum ice loads on a frame. In *Paper 5*, the correlation between the distribution of simulated load maxima and the ice thickness is analyzed. A potential way to evaluate the long-term ice load statistics based on short-term simulations is introduced.

## 5.1 General

Ice conditions and ship operations in ice vary in the short term from voyage to voyage and in the long term from winter to winter. Long-term ice load measurements conducted in the Baltic Sea consist mainly of 12-hour load maxima which are gathered during the normal operation of the ship over several years.

In this study, the full-scale measurements onboard MS Kemira (as shown in Fig. 5.1) are taken as reference. The main dimensions of MS Kemira are presented in Table 5.1. A detailed description of the full-scale measurements during the winters from 1985 to 1988 is given in Kujala (1989). In this report, the operation profile of the ship and the prevailing ice conditions are also summarized. The thickness values of the ice encountered by the ship are grouped in 9 classes: (1) 0.01 – 0.02 m; (2) 0.03 – 0.06 m; (3) 0.07 – 0.12 m; (4) 0.13 – 0.20 m; (5) 0.21 – 0.30 m; (6) 0.31 – 0.42 m; (7) 0.43 – 0.56 m; (8) 0.57 – 0.72 m; (9) > 0.73 m.


Fig. 5.1 Chemical tanker MS Kemira (www.flickr.com)

During the full-scale measurements, the actual ice conditions may include all possible variants of ice features within a 12 hours' voyage. In this numerical study, a number of 10-min voyages are simulated and the icebreaking loads on frame 127 are gathered. Within each voyage, the strength properties of the ice are assumed to be normally distributed along the route (as introduced in Section 2.5), the ice thickness is assumed to be uniformly or normally distributed. The 12-hour maximum load in a certain ice condition is then evaluated by fitting a Gumbel I asymptotic extreme value distribution (see e.g. Fig. 1.7) to the simulated 10-min load maxima.

Table 5.1 Main dimensions of MS Kemira

| | | |
|---|---|---|
| Length over all | 112.7 | m |
| Length between perpendiculars | 105.0 | m |
| Breadth, moulded | 17.5 | m |
| Draught, service | 6.6 | m |
| Deadweight | 8,145 | ton |
| Power output | 3.384 | MW |

## 5.2 Short-term distribution of simulated load maxima

Figs. 5.2 and 5.3 show the simulation results in the ice where the thickness is assumed to be normally distributed along the route. The specified mean value of the ice thickness, $m_h$, is 0.165 m, and the analysis is carried out with different values of the standard deviation, $\sigma_h$. As shown in Fig. 5.2, the Gumbel I distribution is well fitted to the simulated 10-min load maxima, $w$, with a given $\sigma_h$. A mean value of measured 12-hour load maxima in the level ice assigned to ice thickness class 4 (0.13 – 0.20 m) is shown in Fig. 5.3 (data from Kujala (1989), with few data points recorded under level ice condition). It can be expected that if a reasonable variance of the ice thickness is defined, the simulation results can be used for a preliminary estimation of the maximum ice loads within a 12 hours' voyage in level ice.

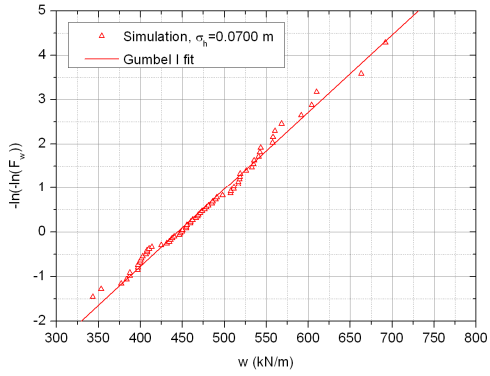


Fig. 5.2 Cumulative distribution of simulated 10-min load maxima, as plotted on Gumbel paper (average ice thickness: 0.165 m, number of samples: 72)

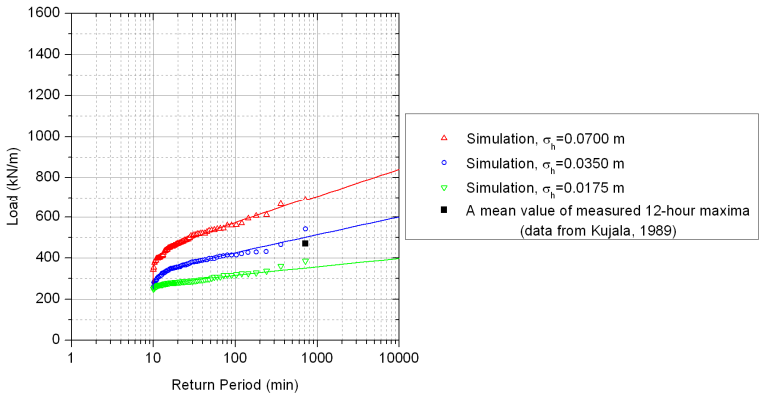


Fig. 5.3 Cumulative distribution of simulated 10-min load maxima, which is plotted as a function of the return period (average ice thickness: 0.165 m)

## 5.3 Correlation between the distribution of load maxima and the ice thickness

Fig. 5.4 shows the simulation results in the ice where the thickness is assumed to be uniformly distributed along the route. The Gumbel I distribution is fitted to the simulated 10-min load maxima, within each ice thickness class (except for class 8 and class 9, as the maximum icebreaking capacity of MS Kemira is about 0.5 m):

$$F_{W|H}(w|h_i) = \exp\left(-\exp\left(-\frac{1}{c_i}(w-u_i)\right)\right) \tag{5.1}$$

where the parameters $c_i$ and $u_i$ are related to the mean value, $\overline{w}$, and coefficient of variation, $k_\delta$, of $w$:

$$c_i = \overline{w}\frac{\sqrt{6}}{\pi}k_\delta \tag{5.2}$$

$$u_i = \overline{w} - \gamma c_i = \overline{w}\left(1 - \gamma\frac{\sqrt{6}}{\pi}k_\delta\right) \tag{5.3}$$

where $\gamma$ is Euler's constant, 0.577. The cumulative distribution function given in Eq. (5.1) is defined as conditional because the parameters $c_i$ and $u_i$ are correlated with the classified ice thickness, $h_i$.

As shown in Fig. 5.5, the correlation between $c_i$, $u_i$ and $h_i$ can be determined by an approximate linear or quadratic regression. The conditional cumulative distribution function can then be translated into:

$$F_{W|H}(w|h_i) = \exp\left(-\exp\left(-\frac{1}{k_c h_i}\left(w - k_{u,1}h_i - k_{u,2}h_i^2\right)\right)\right) \tag{5.4}$$

where the parameters $k_c$, $k_{u,1}$ and $k_{u,2}$ are determined from Fig. 5.5. It should be noted that these parameters are dependent on the hull shape and the frame angle. The assumed correlation in Fig. 5.5 is fit for a specified frame on a specified ship hull, herein further validations are needed.

The final cumulative distribution function of $w$ can be obtained by integrating the conditional cumulative distribution function over the relevant statistics of $h_i$:

$$F_W(w) = \int_0^{h_{max}} \exp\left(-\exp\left(-\frac{1}{k_c h_i}\left(w - k_{u,1}h_i - k_{u,2}h_i^2\right)\right)\right) f_{H_i}(h_i)\cdot \mathrm{d}h_i \tag{5.5}$$

where $f_{H_i}(h_i)$ is the probability density function of $h_i$, $h_{max}$ represents the maximum icebreaking capacity of the ship.

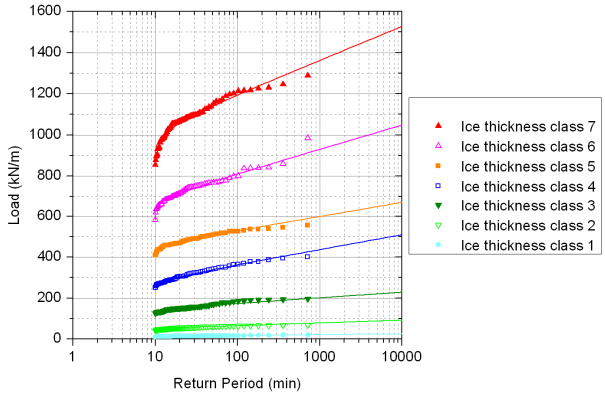


Fig. 5.4 Fitted Gumbel distribution to the simulated 10-min load maxima within each ice thickness class

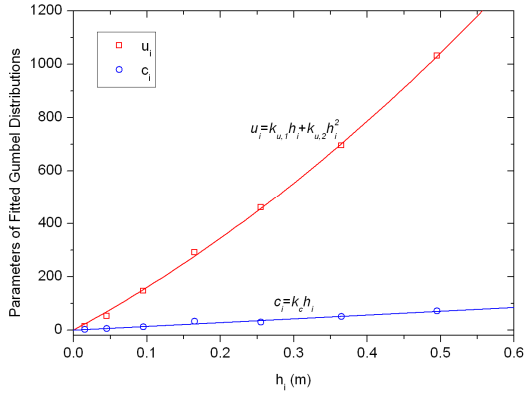


Fig. 5.5 Parameters of fitted Gumbel distribution as a function of the classified ice thickness

The empirical studies (e.g. Kujala, 1994) have shown that the best correlation between measured winter maximum ice load values and prevailing ice conditions is obtained when the equivalent level ice thickness is used to describe the annual ice conditions instead of parameters such as the maximum ice extent, fast or pack ice thickness. In view of this, Eq. (5.5) indicates a potential way to evaluate the long-term ice load statistics based on short-term simulations.

# Chapter 6

# Conclusions and Recommendations for Future Work

## 6.1 Conclusions

The present thesis focuses on a numerical model for simulating ice–hull interaction and ship maneuvers in level ice. This model is partly based on the empirical data, by which the observed phenomena of continuous icebreaking can be reproduced. In the simulation of a full-scale icebreaking run, the interdependence between the ice load and the ship's motion is considered, and the three degree-of-freedom rigid body equations of surge, sway and yaw are solved by numerical integration. The thickness and strength properties of the ice encountered by the ship are assumed to be constant or predefined based on the statistical data. Accordingly the global and local ice loads on ship hulls can be obtained in a deterministic or probabilistic way.

As far as we know the present numerical model is the first one to deal with multiple subjects including the ice–hull interaction, the overall performance of icebreaking ships and the statistics of local ice loads around the hull. The simulation results are discussed through three case studies, in which three ships in service are modeled and the corresponding field data are used for comparison. While field measurements will continue to be important in understanding the ice actions on ships, numerical methods can provide useful information, since they can be easily used to study the effect of different parameters.

The main contributions of the present work are summarized as follows:

1) The full-scale icebreaking process in level ice is continuously reproduced by considering the interdependence between the ice load and the ship's motion. The computation time and the accuracy can be effectively controlled by adjusting the discretization size of the ice and the time step length. The simulated icebreaking resistance is comparable to the empirical estimate and it is found that the occurrence of shoulder crushing can result in the increased resistance. Herein, the occurrence and the extent of shoulder crushing are determined by the geometry of simulated icebreaking pattern which is dependent on the ice condition (especially the ice thickness), the hull shape and the ship's motion. It is also observed in full-scale tests that sometimes the ice edge is just crushed by

hull shoulder without bending failure, but it is difficult to learn about its actual effect on ice resistance and ship's performance. In this respect, the present numerical method can provide some complementary information on that.

2) The global ice load encountered by the ship is obtained as an integrated value of local ice loads around the hull. The global ice load effects on ship's performance are investigated in both straight going and turning operations. The calculated speed that the ship can attain in ice and the turning circle diameter agree well with full-scale measurements. It is found that the forward speed of the ship can be considerably slowed down due to the occurrence of shoulder crushing. In turning operations, this effect is more notable because the aft shoulder can also be in contact with ice. It happens often in both full scale and the simulations that only occasionally some ice floes are broken by bending at aft shoulder and sometimes the ice edge is just crushed. The simulation results to a certain extent reflect the complexity of icebreaking process and the influence of an alternative hull shape on ship's maneuvering performance in ice.

3) A randomly varying ice condition is considered in the numerical simulation of ice–hull interaction. The thickness and strength properties of the ice encountered by the ship can be predefined based on the statistical data and the Monte Carlo method. The origin of the probabilistic variation of local ice loads is investigated, by considering the variations in the external ice conditions and in the icebreaking processes of the ship.

4) The probabilistic distribution of ice-induced peak loads on a frame is analyzed referring to field measurements. It is found that the Weibull distribution which is found to give the best fit to the measured data can also be fitted to the simulation results, with a smaller shape factor better fitted for the low peak loads and a bigger shape factor better fitted for the high peak loads. This is because the distribution of high peak loads is dominated by the variations in the thickness and strength properties of the ice which are assumed to be normally distributed along the route, while the distribution of low peak loads is dominated by the variation of icebreaking patterns which may change the contact length between a given frame and the ice edge from zero to the whole frame spacing.

5) The spatial distribution of local ice loads around the hull is investigated in both straight going and turning operations. The simulation results agree with previous experimental and numerical studies, that the turning operation may develop a high load level on the aft shoulder area. It is also found that the aft shoulder may encounter much heavier turning resistance as compared with the bow area. This is dependent on the different frame angles around the hull, as well as the shape of waterline. It can be expected that this hull form with a larger length to beam ratio than conventional icebreaking ships may develop high loads at aft shoulder.

Information on the distributions of local ice loads around the hull can be used for more effective design of ice-going ships both in terms of overall operation and from the structural point of view. It is expensive and technically difficult to perform the full-scale ice load measurements around a wide hull area. The present numerical method can thus compensate the shortage of field data.

6) For the first time, a preliminary way to evaluate the long-term ice load statistics based on short-term simulations is proposed. The Gumbel I asymptotic extreme value distribution is fitted to the simulated 10-min load maxima under a predefined ice condition referring to field measurements and the statistical data on the strength properties of Baltic Sea ice. The correlation between the distribution of simulated load maxima and the ice thickness is summarized, and the long-term cumulative distribution can thus be obtained by the integration over the long-term statistics of ice thickness.

In brief, a new numerical method is developed and applied in this thesis to predict both global and local ice loads on ship structures. It is demonstrated that this method can supplement field and laboratory measurements by providing more detailed information about the following issues:

1) The continuous icebreaking process and its effect on ice resistance and ship's performance: the occurrence of shoulder crushing can result in the increased ice resistance and impair ship's performance.

2) The origin of the probabilistic variation of local ice loads: the variation in the contact and icebreaking patterns is found to be an internal factor, other than the external ice conditions.

3) The spatial distribution of local ice loads around the hull: the turning operation may develop a high load level on the aft shoulder area.

4) The correlation between the short-term distribution of maximum ice loads on a frame and the ice thickness: a reasonable correlation is found and the long-term cumulative distribution can be obtained by the integration over the long-term statistics of ice thickness.

## 6.2 Recommendations for future work

In this section, several considerations which are of interest and of importance in relation to the present thesis are presented. However, they are not conducted due to the time constraints. These may be the subjects for future studies:

1) Empirical data are used in the present numerical model to estimate the bearing capacity and the breaking length of a floating ice sheet. Empirical models for

these predictions are usually the very simplified ones which assume that the ice structure acts as an elastic, homogeneous, isotropic plate on an elastic foundation, while other models (e.g. FEM model) tend to bring more uncertainties on the ice properties, fracture criterion, fluid–ice interaction (see e.g. Sawamura et al. (2008)), and so on. Further studies on these issues would be beneficial to improve the modeling of ice–hull interaction.

2) In the present numerical model, the ice is assumed to be uniformly crushed on the contact surface, and a constant ice pressure (i.e. effective ice crushing strength) is used to calculate the contact force between ice and hull. If relevant data are provided, the pressure–area relationship can easily be considered in refining the ice loading process.

3) The present numerical model focuses on the icebreaking process. The effects of the submersion and sliding of broken ice on the global ice load are derived from Lindqvist's formulation, while their effects on the local ice load are not taken into account. Due to the complexity of fluid–ice interaction, it is difficult for a simulation program to exactly detect the flow of individual ice pieces after they are broken from the ice edge. Specialized model tests would help to get a better understanding of that.

4) Heave, roll and pitch motions of the ship are not taken into account in the present simulation. An improved simulation program including 6DOF ship motions, is now under development at CeSOS.

5) Spatial correlation of the thickness and strength properties of the ice along the route and the correlation between different ice properties are not considered in predefining a random ice field. This can easily be taken into account if the relevant information is provided.

6) Station-keeping of a moored ship in drifting level ice is also of interest, a case study has been carried out by using the simulation program and considering a heading controller (Zhou et al., 2011). Further work would be done on these issues. In addition, the influence of different hull shapes on ship's performance and on the distribution of local ice loads around the hull, the thrust or propulsion efficiency in ice and the different maneuvering methods are not discussed in the present thesis. These issues remain for further analysis.

# References


Bertram, V., 2000. Practical ship hydrodynamics. Butterworth Heinemann, Oxford, UK.

Browne, R. and Norhamo, L., 2007. Background notes to "propeller ice interaction loads". International Association of Classification Societies (IACS) Unified Requirements for Polar Ships.

Bulat, V., 1982. The effect of snow cover on ice resistance. The Naval Architect, November 1982, pp. E.253.

Cammaert, A. and Muggeridge, D., 1988. Ice interaction with offshore structures. Van Nostrand Reinhold, New York, USA.

Carter, D., 1983. Ship resistance to continuous motion in level ice. Report No. TP3679E, Transportation Development Centre, Transport Canada, Montreal, Canada.

Corlett, E.C.B. and Snaith, G.R., 1964. Some aspects of icebreaker design. Transactions of Royal Institution of Naval Architects (RINA), Vol. 106, No. 4, pp. 389-413.

Crago, W.A., Dix, P.J. and German, J.G., 1971. Model icebreaking experiments and their correlation with full-scale data. Transactions of Royal Institution of Naval Architects (RINA), Vol. 113, No. 4, pp. 83-108.

Daley, C., 2001. Oblique ice collision loads on ships based on energy methods. Oceanic Engineering International, Vol. 5, No. 2, pp. 67-72.

Edwards, R.Y.J. et al., 1976. Influence of major characteristics of icebreaker hulls on their powering requirements and maneuverability in ice. Transactions of Society of Naval Architects and Marine Engineers (SNAME), Vol. 84, pp. 364-407.

Enkvist, E., 1972. On the ice resistance encountered by ships operating in the continuous mode of icebreaking. Report No.24, Swedish Academy of Engineering Science in Finland, Helsinki, Finland.

Enkvist, E., Varsta, P. and Riska, K., 1979. The ship-ice interaction. Proceedings of 5$^{th}$ International Conference on Port and Ocean Engineering under Arctic Conditions (POAC), Trondheim, Norway.

Enkvist, E., 1983. A survey of experimental indications of the relation between the submersion and breaking components of level ice resistance to ships. Proceedings of 7th International Conference on Port and Ocean Engineering under Arctic Conditions (POAC), Espoo, Finland.

Ettema, R., Stern, F. and Lazaro, J., 1987. Dynamics of continuous-mode icbreaking by a polar-class icebreaker hull. Report No. 314, Iowa Institute of Hydraulic Research, June 1987.

Ferris, L.W., 1959. The proportions and forms of icebreakers. Transactions of Society of Naval Architects and Marine Engineers (SNAME), Vol. 67, pp. 6-25.

FSICR, 2008. [Finnish-Swedish Ice Class Rules, 2008]. Finnish Maritime Administration Bulletin No. 10/10.12.2008.

Frederking, R., 1999. The local pressure–area relation in ship impact with ice. Proceedings of 15th International Conference on Port and Ocean Engineering under Arctic Conditions (POAC), Helsinki, Finland.

Frederking, R., 2003. Determination of local ice pressures from ship transits in ice. Proceedings of 13rd International Offshore and Polar Engineering Conference (ISOPE), Honolulu, Hawaii, USA.

Frederking, R., Kubat, I., Collins, A. and Suominen, M., 2005. SAFEICE database description. Report for Deliverable D2-4 of SAFEICE Project, September 2005.

German, J.G., 1959. Design and construction of icebreakers. Transactions of Society of Naval Architects and Marine Engineers (SNAME), Vol. 67, pp. 26-69.

Gürtner, A., 2009. Experimental and numerical investigations of ice-structure interaction. Ph.D. thesis, Norwegian University of Science and Technology, Trondheim, Norway.

Hänninen S., 2003. Ship based observations on board MT Uikku during the winter 2003. Report for Deliverable D8 of IRIS Project, November 2003.

Hänninen, S., 2004. Inventory list of data sources about ship hull ice loads and damages. Report for Deliverable D2-1 of SAFEICE Project, December 2004.

Izumiyama, K., Wako, D., Shimoda, H. and Uto, S., 2005. Ice load measurement on a model ship hull. Proceedings of 18th International Conference on Port and Ocean Engineering under Arctic Conditions (POAC), New York, USA.

Izumiyama, K., 2006. Description of local ice loading and hull area factors based on model test results. Report for Deliverable D3-1 of SAFEICE Project, 2006.

Jansson, J.E., 1956a. Ice-breakers and their design, Part I. European Shipbuilding, No. 5, pp. 112-128.

Jansson, J.E., 1956b. Ice-breakers and their design, Part II. European Shipbuilding, No. 6, pp. 143-151.

Johansson, B.M. and Mäkinen, E., 1973. Icebreaking model tests: systematic variation of bow lines and main dimensions of hull forms suitable for the Great Lakes. Marine Technology, Vol. 10, No. 3, pp. 236-243.

Johnson, H.F., 1946. Development of ice-breaking vessels for the U.S. Coast Guard. Transactions of Society of Naval Architects and Marine Engineers (SNAME), Vol. 54, pp. 112-151.

Jones, S.J., 1989. A review of ship performance in level ice. Proceedings of 8th International Conference on Offshore Mechanics and Arctic Engineering (OMAE), New York, USA.

Jones, S.J., 2004. Ships in ice – a review. 25th Symposium on Naval Hydrodynamics, St. John's, Newfoundland and Labrador, Canada, August 2004.

Jordaan, I., Li, C., Sudom, D., Stuckey, P. and Ralph, F., 2005. Principles for local and global ice design using pressure–area relationships. Proceedings of 18th International Conference on Port and Ocean Engineering under Arctic Conditions (POAC), Potsdam, New York, USA.

Juurmaa, K. and Segercrantz, H., 1981. On propulsion and its efficiency in ice. Proceedings of 6th STAR Symposium, Society of Naval Architects and Marine Engineers (SNAME), New York, USA.

Juva, M. and Riska, K., 2002. On the power requirement in the Finnish-Swedish Ice Class Rules. Research Report No. 47, Winter Navigation Research Board, Finland and Sweden.

Kari, A., 1921. The design of icebreakers. Shipbuilding and Shipping Record, No. 18, December 1921, pp. 802-804.

Kashteljan, V.I., Poznyak, I.I. and Ryvlin, A.Y., 1968. Ice resistance to motion of a ship. Sudostroyeniye, Leningrad.

Kendall, K., 1978. Complexities of compression failure. Proceedings of the Royal Society, London, UK, A361, pp. 245-263.

Kitagawa, H. et al., 1986. A study of ship performance in ice-covered waters (1st Report) – Effect of parallel mid-body. Report No. LM-AVR-14, NRC, Institute for Marine Dynamics.

Korzhavin, K.N., 1971. Action of ice on engineering structures. Translation No. TL260, U.S. Army CRREL.

Koskinen, P. and Jussila, M., 1991. Long term measurements of ice loads on propeller blade of M/S Gudingen. Research Notes No.1260, Technical Research Centre of Finland, Espoo, Finland, [in Finnish, paraphrased in Riska, 2010a].

Kotisalo, K. and Kujala, P., 1999. Ice load measurements onboard MT Uikku during the ARCDEV voyage. Proceedings of 15th International Conference on Port and Ocean Engineering under Arctic Conditions (POAC), Espoo, Finland.

Kotras, T.V., Baird, A.V. and Naegle, J.W., 1983. Predicting ship performance in level ice. Transactions of Society of Naval Architects and Marine Engineers (SNAME), Vol. 91, pp. 329-349.

Kujala, P., 1989. Results of long-term measurements on board chemical tanker Kemira in the Baltic Sea during the winters 1985 to 1988. Research Report No. 47, Winter Navigation Research Board, Finland and Sweden, 1989.

Kujala, P., 1994. On the statistics of ice loads on ship hull in the Baltic. Mechanical Engineering Series No. 116, Ship Laboratory, Helsinki University of Technology, Finland.

Kujala, P., 1996. Semi-empirical evaluation of long term ice loads on a ship hull. Marine Structures, Vol. 9, pp. 849-871.

Kujala, P., Suominen, M. and Riska, K., 2009. Statistics of ice loads measured on MT Uikku in the Baltic. Proceedings of 20$^{th}$ International Conference on Port and Ocean Engineering under Arctic Conditions (POAC), Lulea, Sweden.

Kurdjumov, V. and Kheisin, D., 1976. Hydrodynamic model of the impact of a solid on ice. Prikladnaja Mekhanika, Vol. 12, No. 10, pp. 103-109, [in Russian, paraphrased in Riska, 2010a].

Lensu, M., 2002. Short term prediction of ice loads experienced by ice going ships. Report No. M-269, Ship Laboratory, Helsinki University of Technology, Finland.

Leppäranta, M., 1981. On the structure and mechanics of pack ice in the Bothnian Bay. Dissertation in Finnish Marine Research No. 248, Helsinki, pp. 3-86.

Leppäranta, M., 2005. The drift of sea ice. Praxis Publishing, Chichester, UK.

Lewis, J.W. and Edwards, R.Y.J., 1970. Methods for predicting icebreaking and ice resistance characteristics of icebreakers. Transactions of Society of Naval Architects and Marine Engineers (SNAME), Vol. 78, pp. 213-249.

Lewis, J.W., Debord, F.W. and Bulat, V.A., 1982. Resistance and propulsion of ice-worthy ships. Transactions of Society of Naval Architects and Marine Engineers (SNAME), Vol. 90, pp. 249-276.

Lindqvist, G., 1989. A straightforward method for calculation of ice resistance of ships. Proceedings of 10th International Conference on Port and Ocean Engineering under Arctic Conditions (POAC), Lulea, Sweden.

Liu, J.C., Lau, M. and Williams, F.M., 2006. Mathematical modeling of ice–hull interaction for ship maneuvering in ice simulations. Proceedings of 7th International Conference and Exhibition on Performance of Ships and Structures in Ice (ICETECH), Banff, Alberta, Canada.

Lubbad, R. and Løset, S., 2011. A numerical model for real-time simulation of ship-ice interaction. Cold Regions Science and Technology Vol. 65, pp. 111-127.

Marchenko, N., 2009. Experiences of Russian Arctic navigation. Proceedings of 20th International Conference on Port and Ocean Engineering under Arctic Conditions (POAC), Lulea, Sweden.

Marquis, G., Koski, K. and Koskinen, P., 2008. Fatigue design methodology for propellers operating in ice (Rev. 2). Research Report No. VTT-R-00717-08, Technical Research Centre of Finland, Espoo, Finland.

Martio, J., 2007. Numerical simulation of vessel's maneuvering performance in uniform ice. Report No. M-301, Ship Laboratory, Helsinki University of Technology, Finland.

Masterson, D.M. and Frederking, R.M.W., 1993. Local contact pressures in ship/ice and structure/ice interactions. Cold Regions Science and Technology, Vol. 21, pp. 169-185.

Milano, V.R., 1973. Ship resistance to continuous motion in ice. Transactions of Society of Naval Architects and Marine Engineers (SNAME), Vol. 81, pp. 274-306.

Mäkinen, E., Lahti, A. and Rimppi, M., 1975. Influence of friction on ice resistance; search for low friction surfaces. Proceedings of Transactions of Society of Naval Architects and Marine Engineers (SNAME) Ice Technical Symposium, Montreal, Canada.

Nguyen, D.T., Sørbø, A.H. and Sørensen, A.J., 2009. Modeling and control for dynamic positioned vessels in level ice. Proceedings of 8th Conference on Manoeuvring and Control of Marine Craft, Guarujá, Brazil.

Popov, Y., Faddeev, O., Kheisin, D. and Yakovlev, A., 1968. Strength of ships sailing in ice. Technical Translation No. FSTC-HT-23-96-68, U.S. Army Foreign Science and Technology Centre, Washington, USA.

Poznyak, I.I. and Ionov, B.P., 1981. The division of icebreaking resistance into components. Proceedings of 6th STAR Symposium, Society of Naval Architects and Marine Engineers (SNAME), New York, USA.

Riska, K., 1987. On the mechanics of the ramming interaction between a ship and a massive ice floe. Publications No. 43, Technical Research Centre of Finland, Espoo, Finland.

Riska, K., Rantala, H. and Joensuu, A., 1990. Full scale observations of ship-ice contact. Report No. M-97, The Laboratory of Naval Architecture and Marine Engineering, Helsinki University of Technology, Finland.

Riska, K., Daley, C. and Hayward, R., 1996. Ship–ice interaction – Determination of bow forces and hull response due to head-on and glancing impact between a ship and an ice floe. Report to Transport Canada, TP12734E.

Riska, K., Wilhelmson, M., Englund, K. and Leiviskä T., 1998. Performance of merchant vessels in ice in the Baltic. Research Report No. 52, Winter Navigation Research Board, Helsinki, Finland, [Development of the powering requirements for FSICR Project].

Riska, K., Leiviskä, T., Nyman, T., Fransson, L., Lehtonen, J., Eronen, H. and Backman, A., 2001. Ice performance of the Swedish multi-purpose icebreaker Tor Viking II. Proceedings of 16th International Conference on Port and Ocean Engineering under Arctic Conditions (POAC), Ottawa, Canada.

Riska, K., 2007a. Definition of ice loading for the Finnish-Swedish Ice Class Rules. Report for Deliverable D7-2 of SAFEICE Project, October 2007.

Riska, K., 2007b. Definition of ice loading for the Finnish-Swedish Ice Class Rules. Report for Deliverable D7-3 of SAFEICE Project, December 2007.

Riska, K., 2010a. Design of ice breaking ships. Encyclopedia of Life Support Systems (EOLSS), Developed under the Auspices of the UNESCO, Eolss Publishers, Oxford, UK, [http://www.eolss.net].

Riska, K., 2010b. Ship-ice interaction in ship design: theory and practice. Encyclopedia of Life Support Systems (EOLSS), Developed under the Auspices of the UNESCO, Eolss Publishers, Oxford, UK, [http://www.eolss.net].

Runeberg, R., 1988/89. On steamers for winter navigation and ice-breaking. Proceedings of Institution of Civil Engineers, Vol. 97, Pt. III, pp. 277-301.

Sanderson, T., 1988. Ice mechanics, risk to offshore structures. Graham & Trotman, London, UK.

Sawamura, J., Riska K. and Moan T., 2008. Finite Element Analysis of fluid–ice interaction during ice bending. Proceedings of 19th International Symposium on Ice (IAHR), Vancouver, British Columbia, Canada.

Sawamura, J., Tsuchiya, H., Tachibana, T. and Osawa, N., 2010. Numerical modeling for ship maneuvering in level ice. Proceedings of 20th International Symposium on Ice (IAHR), Lahti, Finland.

Scarton, H.A., 1975. On the role of bow friction in icebreaking. Journal of Ship Research, Vol. 19, pp. 34-39.

Schneider, P.J. and Eberly, D.H., 2002. Geometric tools for computer graphics. Morgan Kaufmann Publishers, San Francisco, USA.

Shimanskii, Y.A., 1938. Conditional standards of ice qualities of a ship. Transactions of Arctic Research Institute, Northern Sea Route Administration Publishing House, Vol. 130, Leningrad. Translation T-381-01 by Engineering Consulting and Translation Centre (ECTC), New York, USA.

Simonson, D.R., 1936. Bow characteristics of icebreaking. Journal of American Society of Naval Engineers, Vol. 48, No. 2, pp. 249-254.

Su, B., Riska, K. and Moan, T., 2010a. A numerical method for the prediction of ship performance in level ice. Cold Regions Science and Technology, Vol. 60, pp. 177-188.

Su, B., Riska, K. and Moan, T., 2010b. Numerical simulation of ship turning in level ice. Proceedings of 29th International Conference on Offshore Mechanics and Arctic Engineering (OMAE), Shanghai, China.

Su, B., Riska, K. and Moan, T., 2011a. Numerical simulation of local ice loads in uniform and randomly varying ice conditions. Cold Regions Science and Technology, Vol. 65, pp. 145-159.

Su, B., Riska, K. and Moan, T., 2011b. Numerical study of ice-induced loads on ship hulls. Marine Structures, in press.

Su, B., Riska, K. and Moan, T., 2011c. Numerical simulation of ships operating in level ice. Submitted to 21st International Conference on Port and Ocean Engineering under Arctic Conditions (POAC), Montreal, Canada.

Tatinclaux, J.C., 1984. Model tests on two models of WTGB 140-ft icebreakers. Report No. 84-3, U.S. Army CRREL.

Timco, G.W. and Weeks, W.F., 2010. A review of the engineering properties of sea ice. Cold Regions Science and Technology, Vol. 60, pp. 107-129.

Timco, G.W., 1986. A new type of model ice for refrigerated towing tankers. Cold Regions Science and Technology, Vol. 12, pp. 175-195.

Tuhkuri, J., 1996. Experimental investigations and computational fracture mechanics modeling of brittle ice fragmentation. D.Sc. thesis, Acta Polytechnica Scandinavica, Mechanical Engineering Series No. 120.

Udin, I., 1976. Sea Ice-75. Ground Truth Report No. 16:2, Winter Navigation Research Board. Norrköping.

Valanto, P., 2001. The resistance of ships in level ice. Transactions of Society of Naval Architects and Marine Engineers (SNAME), Vol. 109, pp. 53-83.

Valanto, P., 2007. Spatial distribution of numerically predicted ice loads on ship hulls in level ice. Report for Deliverable D6-3 of SAFEICE Project, May 2007.

Vance, G.P., 1975. A scaling system for ships modeled in ice. Proceedings of Transactions of Society of Naval Architects and Marine Engineers (SNAME) Ice Technical Symposium, Montreal, Canada.

Vance, G.P., 1980. Analysis of the performance of a 140-ft Great Lakes icebreaker: USCGC Katmai Bay. Report No. 80-8, U.S. Army CRREL.

Vance, G.P., Goodwin, M.J. and Gracewski, A.S., 1981. Full scale icebreaking test of the USCGC Katmai Bay. Proceedings of 6$^{th}$ STAR Symposium, Society of Naval Architects and Marine Engineers (SNAME), New York, USA.

Varsta, P., 1983. On the mechanics of ice load on ships in level ice in the Baltic Sea. Publications 11, Technical Research Centre of Finland, Espoo, Finland.

Varsta, P., 1984. Determination of ice loads semi-empirically. In Ship Strength and Winter Navigation, Technical Research Centre of Finland, VTT Symposium 52, pp.177-182.

Vuorio, J., Riska, K. and Varsta, P., 1979. Long term measurements of ice pressure and ice-induced stresses on the icebreaker SISU in winter 1978. Research Report No. 28, Winter Navigation Research Board, Finland and Sweden.

Vinogradov, I.V., 1946. Vessels for Arctic navigation (icebreakers). Library of Congress, No. (VM) 451.VS. Paraphrased in Ferris, 1959.

Virtanen et al., 1975. Great Lakes ore carrier series ice resistance model tests – draft variation. Test Report No. A-34 to U.S., Wärtsilä Icebreaking Model Basin, Department of Commerce, Maritime Administration.

Watson, A., 1959. Operation of Department of Transport icebreakers in Canada. Transactions of Society of Naval Architects and Marine Engineers (SNAME), Vol. 67, pp. 140-161.

Wadhams, P., 2002. Ice in the ocean. Gordon and Breach Science Publishers, London, UK.

White, R.M., 1970. Prediction of icebreaker capability. Transactions of Royal Institution of Naval Architects (RINA), Vol. 112, No. 2, pp. 225-251.

Zhan, P.B., Humphreys, D. and Phillips, L., 1987. Full-scale towed resistance trial of the USCGC mobile bay in uniform level ice. Transactions of Society of Naval Architects and Marine Engineers (SNAME), Vol. 95, pp. 45-77.

Zhou, L., Su, B., Riska, K. and Moan, T., 2011. Numerical simulation of moored ship in level ice. Submitted to 30th International Conference on Offshore Mechanics and Arctic Engineering (OMAE), Rotterdam, The Netherlands.

# Appendix

## Paper 1

## A numerical method for the prediction of ship performance in level ice

Biao Su, Kaj Riska and Torgeir Moan

Published in *Cold Regions Science and Technology*, Vol. 60 (2010), pp. 177-188

Cold Regions Science and Technology 60 (2010) 177–188

Contents lists available at ScienceDirect

Cold Regions Science and Technology

journal homepage: www.elsevier.com/locate/coldregions

# A numerical method for the prediction of ship performance in level ice

Biao Su [a,*], Kaj Riska [a,b], Torgeir Moan [a]

[a] Centre for Ships and Ocean Structures, Norwegian University of Science and Technology, Trondheim, Norway
[b] ILS Oy, Helsinki, Finland

ARTICLE INFO

*Article history:*
Received 29 September 2009
Accepted 16 November 2009

*Keywords:*
Numerical simulation
Continuous icebreaking
Ice force
Ice resistance
Ship maneuvers

ABSTRACT

A numerical method is introduced to simulate ship maneuvers in level ice. The coupling between continuous ice forces and ship motions is considered, and the three degree-of-freedom rigid body equations of surge, sway and yaw are solved by numerical integration. The numerical analysis is validated by comparison with the ship performance data from the ice trails of icebreaker AHTS/IB Tor Viking II. A good agreement is achieved.



## 1. Introduction

Ship operations in ice infested waters have increased significantly in the last decades due to the increased hydrocarbon exploration and exploitation as well as ship transport in the arctic region. Parallel developments have resulted in a suite of engineering tools for ice-worthy ship performance evaluation at the design stage, although present methods are subjected to significant uncertainty.

A typical operating scenario of interest for an ice region would require the ship to maintain a reasonable speed in the level ice of a certain thickness, and to be assured of making progress in much thicker ice. In practice, the ship must also be able to operate in snow-covered ice, and to transit certain ridge and rubble configurations. Furthermore, the ship must have a verifiable turning ability in the specified ice conditions (Kim et al., 2005).

Above all, ship performance in level ice is of most concern, and usually measured by ice thickness–ship velocity curve (h–v curve). The h–v curve is usually determined from full-scale trials and model tests. In early design, some empirical formulas for the calculation of ice resistance and ship propulsion can be used to give a direct figure of h–v curve. The purpose of this paper is to establish a numerical method partly based on empirical data to simulate both the continuous-mode icebreaking and ship motions. Then the ice thickness–ship velocity curve as well as the time series of ice forces is obtained. Finally, the numerical results of a real icebreaker AHTS/IB Tor Viking II are discussed and compared with measured data (Riska et al., 2001).

## 2. Simulation of icebreaking pattern

### 2.1. Review

The resistance encountered by a ship transitting a level sheet of ice depends primarily on the processes, by which its hull breaks and displaces ice. First, when the ice sheet contacts the hull, crushing happens. The crushing force will keep growing with an increasing contact area until its vertical component is great enough to cause a bending failure of ice. After the ice floes have been broken from the ice sheet, the advance of ship forces them to turn on edge until parallel with the hull. Then, the floes will become submerged and slide along the hull until they cannot maintain contact with the hull. In some hull zones, typically at the stem and at the shoulders which have large slope angles (almost vertical), crushing may be the only failure mode (Lindqvist, 1989). This can lead to a significant ice resistance.

Early research on level ice resistance was usually carried out based on this break-displace process (see e.g. Fig. 1). Although it may be questionable (Enkvist et al., 1979), most of the ice resistance formulas were established on this assumption (e.g. Enkvist, 1972; Lewis et al., 1982; Lindqvist, 1989).

In an attempt to simulate continuous icebreaking pattern and real-time ice forces, Izumiyama et al. (1992) proposed a simulation strategy for the force of an advancing level ice acting on a fixed cone structure. The ice failure model was based on the plastic limit theory, and the size of the broken ice floes was randomly generated from an assumed normal distribution which was observed from the model tests. Wang (2001) followed a similar strategy, and the ice-cone interaction was simulated computationally by a geometric grid method based on the mechanical ice failure model, which was derived from the empirical formula proposed by Kashtelian (given by

* Corresponding author. Tel.: +47 41602417; fax: +47 73595528.
*E-mail address:* biao@ntnu.no (B. Su).

0165-232X/$ – see front matter © 2009 Elsevier B.V. All rights reserved.
doi:10.1016/j.coldregions.2009.11.006

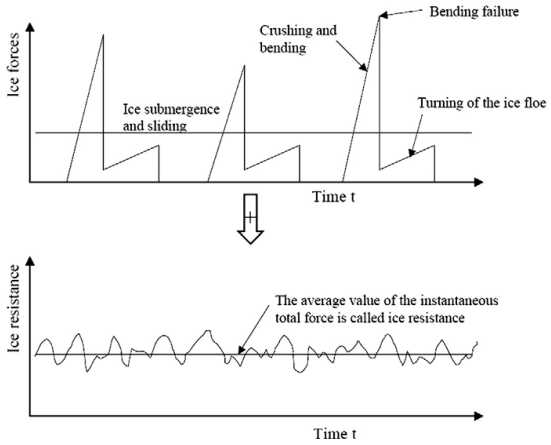


**Fig. 1.** Idealized time histories of ice forces and the definition of ice resistance (Riska, 2007).

Kerr, 1975) and calculations by Varsta (1983). Nguyen et al. (2009) have applied this derived ice failure model to ice-ship interaction. Sawamura et al. (2008) simulated the dynamic response of floating ice due to a rapid forcing and obtained the bending behaviour of floating ice, then they proposed a continuous contact procedure to calculate the repetitive ice forces.

In this paper, the continuous-mode icebreaking is simulated by using an ice failure model similar to that derived in Wang (2001). However a more refined contact procedure is introduced herein, because we need to solve the coupling problem between ice forces and ship motions, while Wang (2001) only considered a stationary rotational symmetric structure.

### 2.2. Contact area

The 2D ship hull and ice edge are discretized into a number of nodes in the established simulation program. As shown in Fig. 2, the discretized ship hull is a closed polygon. At each time step, the program will collect the ice nodes which are inside this hull polygon. Then, every contact zone can be found. To check the ice node whether it is inside the hull polygon, some effective computer geometric tools are adopted. The detailed algorithm can be found in Schneider and Eberly (2002).

Ice wedges involved in the break-displace process are determined by the bending cracks, which are idealized and described by a single parameter, i.e. icebreaking radius. The icebreaking radius is found by the expression given in Wang (2001) (based on information from Enkvist, 1972; and Varsta, 1983):

$$R = C_l l(1.0 + C_v v_n^{rel}) \tag{1}$$

where, $v_n^{rel}$ is the relative normal velocity between ice and hull node; $C_l$ and $C_v$ are empirical parameters, $C_l$ has a positive value and $C_v$ has a negative value, both of them are tunable in the simulation program; $l$ is the characteristic length of ice:

$$l = \left(\frac{Eh_i^3}{12(1-\nu^2)\rho_w g}\right)^{\frac{1}{4}}. \tag{2}$$

As shown in Fig. 3, the ice wedge is idealized and determined by the interpolation of icebreaking radius at the first and last contact nodes (i.e. $R_f$ and $R_l$), the opening angle of ice wedge is marked as $\theta$. The contact zone is discretized by a number of triangles (the red marked triangles shown in Fig. 3) based on the hull nodes involved in contact. Then the contact area can be calculated as discussed below.

To calculate every contact area, we assume that the contact surface between hull and ice is flat. This implies that two cases must be considered. As shown in Fig. 4, $L_h$ is calculated from the distance between adjacent hull nodes, $L_c$ is calculated from the distance between the contacting ice nodes and hull nodes, $\varphi$ is the slope angle of ship hull, $h_i$ is ice thickness.

**Case 1**. $L_c * \tan(\varphi) \le h_i$

$$A_c = \frac{1}{2} L_h \frac{L_c}{\cos(\varphi)}. \tag{3}$$

**Case 2**. $L_c * \tan(\varphi) > h_i$

$$A_c = \frac{1}{2}\left(L_h + L_h \frac{L_c - h_i / \tan(\varphi)}{L_c}\right)\frac{h_i}{\sin(\varphi).} \tag{4}$$

### 2.3. Crushing force

Before bending failure, we assume that ice is just crushed on the contact surface, crushing force $F_{cr}$ is normal to the contact surface and determined by the ice crushing strength $\sigma_c$ (the mean value of crushing pressure, refer to Kujala, 1994) and contact area $A_c$:

$$F_{cr} = \sigma_c A_c. \tag{5}$$

As shown in Fig. 5, the crushing force has a horizontal component $F_H$ and vertical component $F_V$. Here, the frictional force is taken into account, which also has a horizontal component $f_H$ and vertical component $f_V$. To determine each component of frictional force, we assume that there is no vertical displacement of the ice wedge before bending failure. So, $f_H$ is proportional to the relative velocity component $v_t^{rel}$ and $f_V$ is proportional to the relative velocity component $v_{n,1}^{rel}$ (denoted as the red lines shown in Fig. 5):

$$f_H = \mu_i F_{cr} v_t^{rel} \Big/ \sqrt{(v_t^{rel})^2 + (v_{n,1}^{rel})^2} \tag{6}$$

$$f_V = \mu_i F_{cr} v_{n,1}^{rel} \Big/ \sqrt{(v_t^{rel})^2 + (v_{n,1}^{rel})^2} \tag{7}$$

$$F_H = F_{cr}\sin(\varphi) + f_V \cos(\varphi) \tag{8}$$

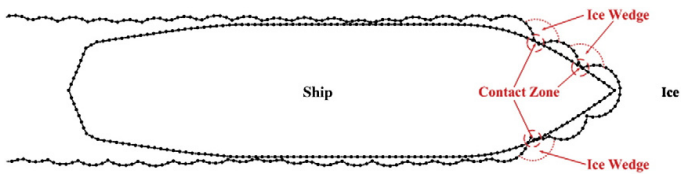


**Fig. 2.** Discretization of ship hull and ice edge.

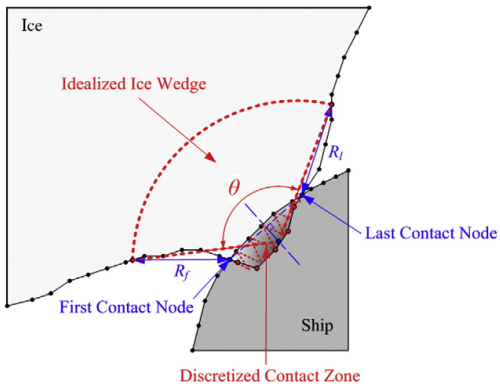


**Fig. 3.** Idealized ice wedge and discretized contact zone. (For interpretation of the references to color in this figure legend, the reader is referred to the web version of this article.)

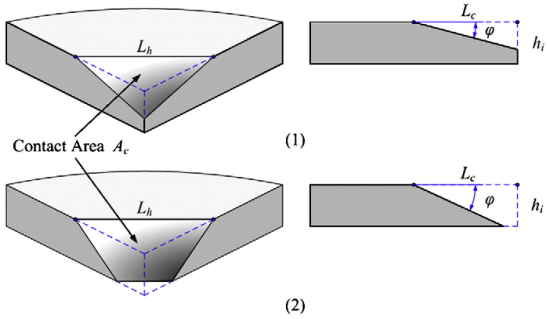


**Fig. 4.** Two cases of contact area calculation.

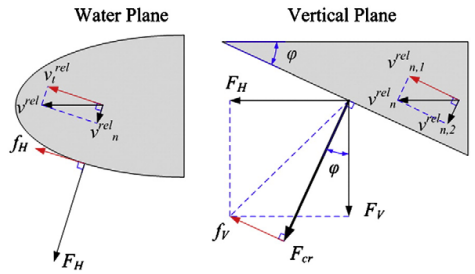


**Fig. 5.** Force and velocity components. (For interpretation of the references to color in this figure legend, the reader is referred to the web version of this article.)

$$F_V = F_{cr}\cos(\varphi) - f_V \sin(\varphi) \tag{9}$$

where $\mu_i$ is the frictional coefficient between ice and hull.

### 2.4. Bending failure

Kerr (1975) presented a critical survey of the studies on the bearing capacity of floating ice plates, in which Kashtelian's calculations for the direct determination of "failure load" $P_f$ are discussed. As introduced by Kerr (1975), Kashtelian's work is based on the observation that the carrying capacity is reached when the floating ice wedges are initially broken off, and the failure load for an ice wedge of opening angle $\theta$ is given by:

$$P_f = C_f \left(\frac{\theta}{\pi}\right)^2 \sigma_f h_i^2 \tag{10}$$

where, $\sigma_f$ is the flexural strength of ice; $h_i$ is ice thickness; $C_f$ is an empirical parameter. Eq. (10) accounts for the opening angle but it is an empirical equation. Thus the constant $C_f$ should be obtained from some measurements carried out. Quite small value (about 1) for this constant was proposed by Kashtelian, while in Nguyen et al. (2009) a value of 4.5 was used and validated by the empirical ice resistance formula.

Here, Eqs. (9) and (10) are used to check whether the ice wedge (shown in Fig. 3) is broken from the ice sheet. If $F_V < P_f$, no bending failure, the ice wedge is just crushed at the cusp; if $F_V \geq P_f$, bending failure happens, the ice wedge is crushed and cleared from the ice edge.

Based on these assumptions, the continuous icebreaking pattern and icebreaking forces can be determined step by step. Fig. 6 shows the time history of icebreaking forces. The mean ice resistance including crushing and bending components as proposed by Lindqvist (1989), is also marked (0.5 m ice thickness; 5 m/s ship speed).

Fig. 7 gives the power spectrum of the time series shown in Fig. 6. The dominant frequencies are identifiable, due to the periodic icebreaking processes. The ice wedges around the hull are not broken simultaneously, so there are more than one peaks of icebreaking force in each breaking process (as shown in Fig. 8).

The effect of the empirical parameters introduced above is investigated. Here, $C_f$ is the empirical parameter in bending failure calculation, which dominates the magnitude of icebreaking force. The results for different values of $C_f$ are given in Fig. 9, where $h$ is ice thickness. The value we choose for $C_f$ is 3.1, which gives a relatively reasonable mean icebreaking force as compared to the Lindqvist's ice resistance (shown in Fig. 10).

As shown in Figs. 9 and 10, the icebreaking forces obtained by the numerical method described above do not always increase with the increasing ice thickness. The irregularity in resistance values shown in Fig. 10 is due to changes in the nature of icebreaking pattern: sometimes crushing dominates and sometimes bending. Two cases of icebreaking pattern (shown in Fig. 11) may occur in the simulation. In

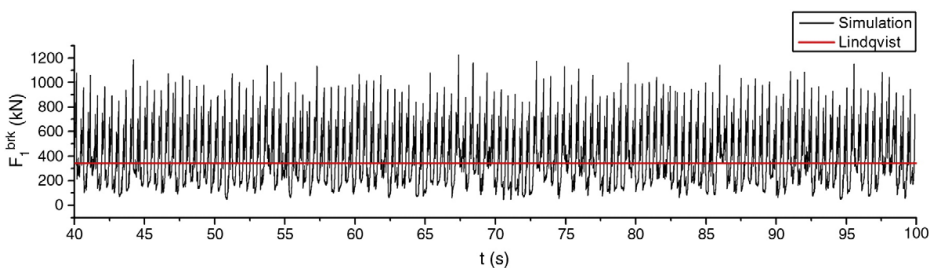


**Fig. 6.** Time history of icebreaking forces and the Lindqvist's ice resistance in a 0.5 m thick ice and a ship speed of 5 m/s.

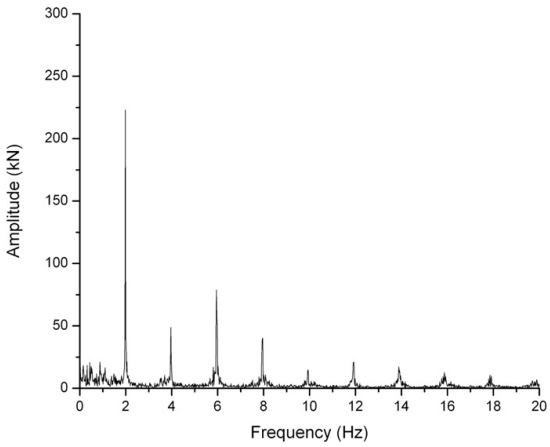


**Fig. 7.** Power spectrum corresponding to Fig. 6.

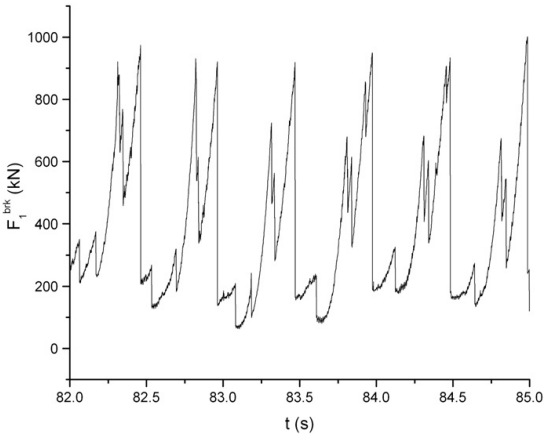


**Fig. 8.** Periodicity of icebreaking forces.

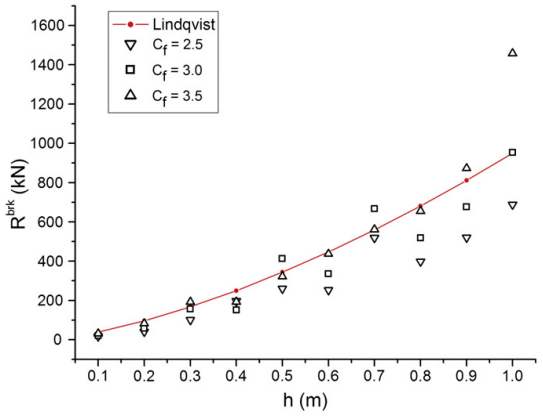


**Fig. 9.** Mean icebreaking forces and the Lindqvist's ice resistance with different values of ice thickness.

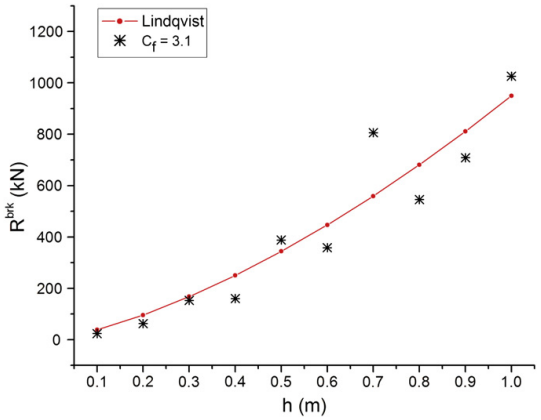


**Fig. 10.** Mean icebreaking forces and the Lindqvist's ice resistance with different values of ice thickness.

Case 2, some parts of the ice sheet are continuously crushed by the vertical parts of ship hull (i.e. shoulder crushing) without bending failure, then the icebreaking forces will become more severe. As shown in Fig. 12, the time series of icebreaking forces in these two cases are quite different, it has a larger mean value in Case 2, even if the ice thickness is bigger in Case 1 (0.6 m in Case 1 and 0.5 m in Case 2; 5 m/s ship speed in both cases).

## 3. Simulation of ship motions

### 3.1. Review

Ship maneuvers in ice are as yet not sufficiently analyzed because of the interdependence between ship motions and ice forces. Here, the surge, sway and yaw motions involved in ship maneuvers are simulated simultaneously, as well as icebreaking, the coupling problem between ship motions and ice forces is solved by iteration.

### 3.2. General equations of motion

Let $(X, Y, Z)$ be a right-handed coordinate system with $Z$ vertically upward, $X$ in the direction of forward motion, and the origin at the hull's center of gravity. Then, six linear coupled differential equations of motion can be written in the following form:

$$(\mathbf{M}+\mathbf{A})\ddot{\mathbf{r}}(t)+\mathbf{B}\,\dot{\mathbf{r}}(t)+\mathbf{C}\mathbf{r}(t)=\mathbf{F}(t). \tag{11}$$

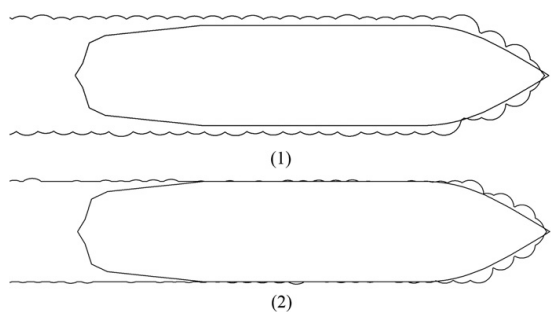


**Fig. 11.** Two cases of icebreaking pattern.

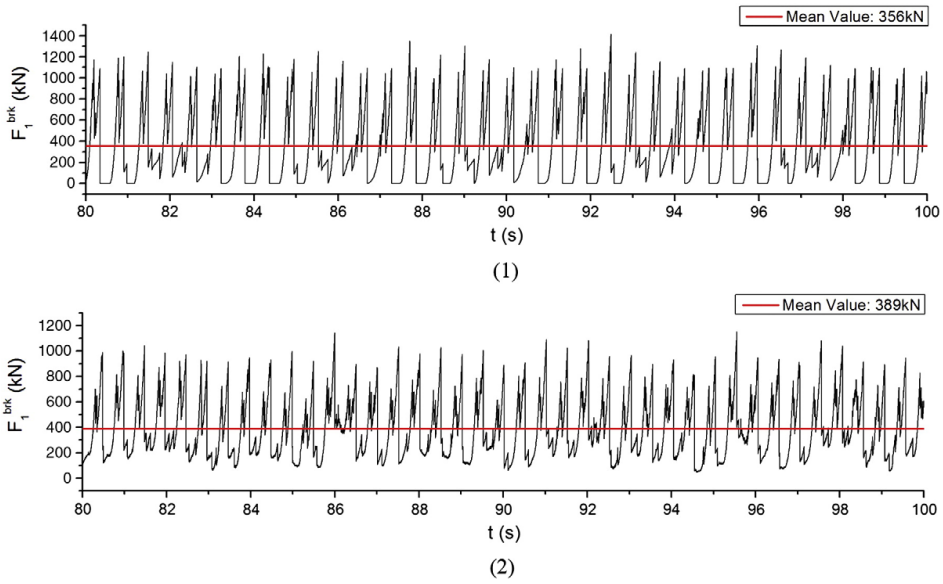


**Fig. 12.** Two cases of icebreaking force (Case 1: in a 0.6 m thick ice; Case 2: in a 0.5 m thick ice; a ship speed of 5 m/s in both cases).

If it is assumed that the ship has lateral symmetry, then the 3DOF (surge, sway and yaw) mass and added mass matrices are given by

$$\mathrm{M} = \begin{bmatrix} M & 0 & 0 \\ 0 & M & 0 \\ 0 & 0 & I_{66} \end{bmatrix} \tag{12}$$

$$\mathbf{A} = \begin{bmatrix} A_{11} & 0 & 0 \\ 0 & A_{22} & A_{26} \\ 0 & A_{62} & A_{66} \end{bmatrix} \tag{13}$$

where, $M$ is the mass of the ship; $I_{66}$ is the moment of inertia in $Z$ direction; the added mass coefficients are calculated from a given BEM program.

The damping and hydrostatic restoring coefficients are assumed to be zero in this 3DOF mode.

### 3.3. Excitation forces and moments

The icebreaking forces are obtained from the numerical simulation described in Section 2, and a semiempirical approach is applied to determine the forces and moments arising from the propeller, rudder and ambient water.

#### 3.3.1. Ice forces

The continuous icebreaking forces $\boldsymbol{F}^{brk}(t)$ are simulated at each time step, while the ice forces induced in the displacing process (turning, submerging and sliding) are calculated from the ice resistance formula, so the 3DOF ice force components can be expressed by:

$$F_1^{ice}(t) = F_1^{brk}(t) + R_s\left(1 + 9.4\frac{v^{rel}}{\sqrt{gL_{WL}}}\right) \times \frac{v_1^{rel}}{v^{rel}} \tag{14}$$

$$F_2^{ice}(t) = F_2^{brk}(t) + R_s\left(1 + 9.4\frac{v^{rel}}{\sqrt{gL_{WL}}}\right) \times \frac{v_2^{rel}}{v^{rel}} \tag{15}$$

$$F_6^{ice}(t) = F_6^{brk}(t) \tag{16}$$

where, $R_s$ is the submersion component of ice resistance, the detailed expression can be found in Lindqvist (1989); $v_1^{rel}$ and $v_2^{rel}$ are respectively the forward and transverse components of the relative velocity ($v^{rel}$) between ship and ice; $L_{WL}$ is the ship water line length.

Ice displacing forces are mainly induced by the momentum transfer and friction between ship hull and ice floes, which are related to the relative velocity between ship and ice. So, the ice displacing forces are approximated from the ice resistance formula by multiplying the ratios between $v_1^{rel}$, $v_2^{rel}$ and $v^{rel}$, as shown in Eqs. (14) and (15).

#### 3.3.2. Propeller and rudder forces

In early design and in the ice rules, the net thrust available to overcome ice resistance, $T_{net}$ can be estimated as:

$$T_{net} = T_B\left(1 - \frac{1}{3}\frac{v_1^{rel}}{v_{OW}} - \frac{2}{3}\left(\frac{v_1^{rel}}{v_{OW}}\right)^2\right) \tag{17}$$

where, $T_B$ is the bollard pull; $v_{ow}$ is open water speed; $v_1^{rel}$ is the forward component of the relative velocity between ship and ice.

So, the forces and moment arising from the propeller and rudder can simply be written as:

$$F_1^p(t) = T_{net} - \frac{1}{2}C_D\rho_w V_f^2 A_r \tag{18}$$

$$F_2^p(t) = \frac{1}{2}C_L\rho_w V_f^2 A_r \tag{19}$$

$$F_6^p(t) = \frac{1}{2}C_L\rho_w V_f^2 A_r \cdot x_r \tag{20}$$

where, $C_L$ and $C_D$ are the lift and drag coefficients of the rudder; $V_f$ is flow velocity; $A_r$ is rudder area; $x_r$ is the location of the rudder (Bertram, 2000).

#### 3.3.3. Hydrodynamic forces

The hydrodynamic forces due to the motion of the ship relative to the ambient water are considered. The effects of ambient current are


**Fig. 13.** Icebreaker AHTS/IB Tor Viking II.

**Table 1**
Ice characteristics.

| Parameter | Symbol | Value | Unit |
|---|---|---|---|
| Density | $\rho_i$ | 880 | kg/m$^3$ |
| Young's modulus | $E$ | 5400 | MPa |
| Poisson ratio | $\gamma$ | 0.33 | |
| Crushing strength | $\sigma_c$ | 2.3 | MPa |
| Flexural strength | $\sigma_f$ | 0.55 | MPa |
| Frictional coefficient | $\mu_i$ | 0.15 | |

thus incorporated by using relative velocities, while the effects of waves are neglected by assuming that the ambient water is totally covered by ice.

Empirical formulas are often used to calculate the current forces and moments on a ship (e.g. Faltinsen, 1990):

$$F_1^c(t) = \frac{0.075}{(\log_{10}Rn-2)^2}\frac{1}{2}\rho_w S_W v_1^{rel}\left|v_1^{rel}\right| \tag{21}$$

$$F_2^c(t) = \frac{1}{2}\rho_w \int_L C_D(x)D(x)v_2^{rel}(x)\left|v_2^{rel}(x)\right|dx \tag{22}$$

$$F_6^c(t) = \frac{1}{2}\rho_w \int_L C_D(x)D(x)v_2^{rel}(x)\left|v_2^{rel}(x)\right|xdx \tag{23}$$

where, the integration is over the length $L$ of the ship; $Rn$ is Reynolds number; $S_W$ is the wetted surface of the ship; $C_D(x)$ is the drag coefficient for cross-flow past an infinitely long cylinder with the cross-sectional area of the ship at the longitudinal coordinate $x$. $D(x)$ is the sectional draught.

The current force in surge direction $F_1^c(t)$ is not incorporated into the excitation force $F_1(t)$ when we use $T_{net}$ to calculate the propeller force, that is because the open water resistance in surge direction have been considered in the definition of $T_{net}$.

Then, the total excitation forces can be calculated as the sum of the ice, propeller and current forces:

$$F_1(t) = F_1^{ice}(t) + F_1^p(t) \tag{24}$$

$$F_2(t) = F_2^{ice}(t) + F_2^p(t) + F_2^c(t) \tag{25}$$

$$F_6(t) = F_6^{ice}(t) + F_6^p(t) + F_6^c(t). \tag{26}$$

**Table 2**
Ship characteristics.

| Parameter | Symbol | Value | Unit |
|---|---|---|---|
| Length between perpendiculars | $L_{PP}$ | 75.20 | m |
| Waterline length | $L_{WL}$ | 85.02 | m |
| Beam | $B$ | 18 | m |
| Draught | $D$ | 6.5 | m |
| Wetted surface area | $S$ | 1832.78 | m$^2$ |
| Displacement | $M$ | $5.79\times10^6$ | kg |
| Moment of inertia | $I_{66}$ | $2.07\times10^9$ | kg m$^2$ |
| Added mass coefficient | $A_{11}$ | $8.79\times10^5$ | kg |
| Added mass coefficient | $A_{22}$ | $5.55\times10^6$ | kg |
| Added mass coefficient | $A_{66}$ | $1.02\times10^9$ | kg m$^2$ |
| Added mass coefficient | $A_{26}$, $A_{62}$ | $1.77\times10^7$ | kg m |
| Propeller diameter | $D_P$ | 4.1 | m |
| Propulsion power | $P_D$ | 13440 | kW |
| Bollard pull | $T_B$ | 202 | t |
| Open water speed | $V_{OW}$ | 16.4 | kn |

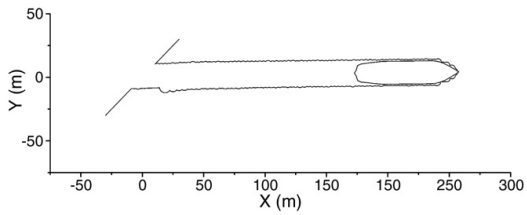


**Fig. 15.** Simulated ship transitting in ice.

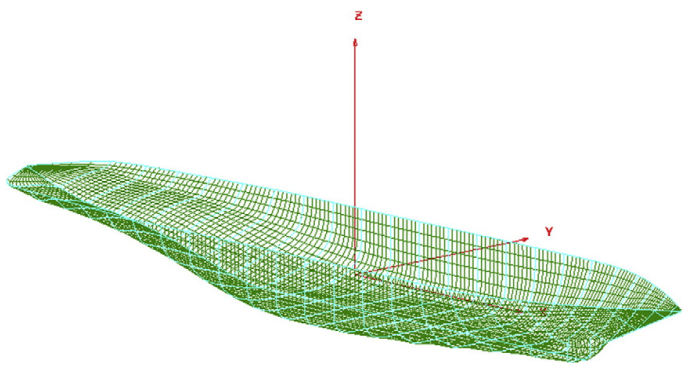


**Fig. 14.** Ship geometry model.

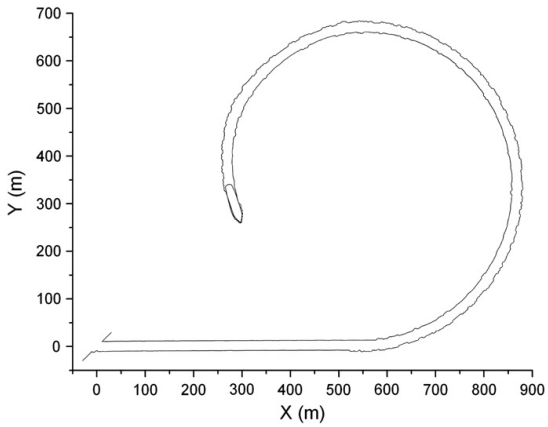


**Fig. 16.** Simulated ship turning in ice.

**Fig. 17.** Full-scale ship turning in ice.

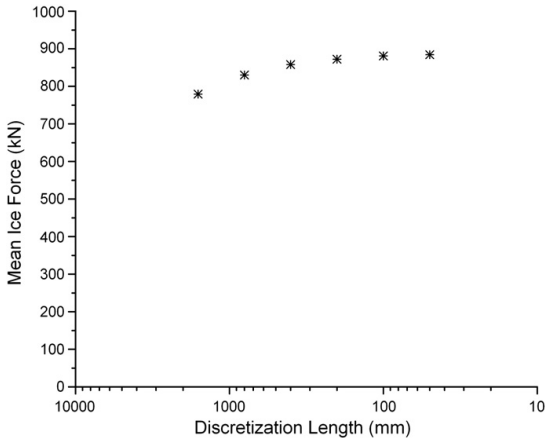


**Fig. 18.** Convergence of the mean ice force.

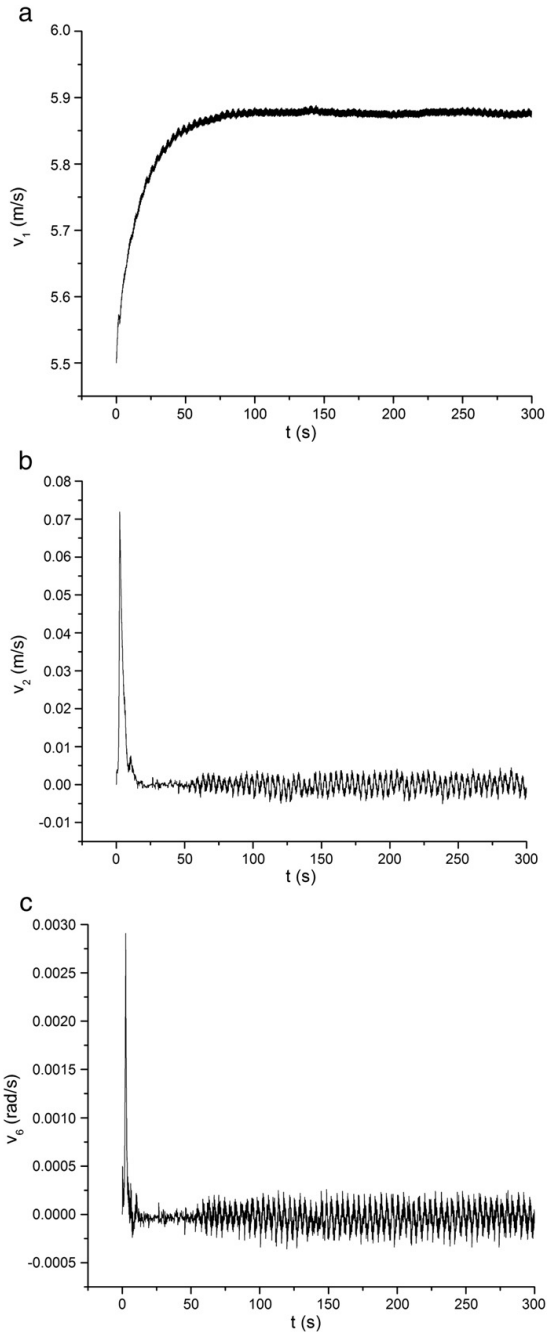


**Fig. 19.** Ship speed in transitting operation (in 0.6 m thick ice). a) Forward speed, b) Transverse speed, c) Turning rate.

### *3.4. Numerical integration of the equations of motion*

A step-by-step numerical integration method is applied to solve the equations of motion established above. According to

Newmark's method the general integral equations are given by:

$$\dot{\mathbf{r}}(t_{k+1}) = \dot{\mathbf{r}}(t_k) + (1-\lambda)\ddot{\mathbf{r}}(t_k)\delta t + \lambda\ddot{\mathbf{r}}(t_{k+1})\delta t \tag{27}$$

$$\mathbf{r}(t_{k+1}) = \mathbf{r}(t_k) + \dot{\mathbf{r}}(t_k)\delta t + \left(\frac{1}{2}-\beta\right)\ddot{\mathbf{r}}(t_k)\delta t^2 + \beta\ddot{\mathbf{r}}(t_{k+1})\delta t^2. \tag{28}$$

These equations above are obtained by a Taylor-series expansion where the residual term is approximated by the quadrature formulas. The weighting terms $\lambda$ and $\beta$ are free parameters in the quadrature formulas, which are determined by requirements related to stability and accuracy. If we assume a linear acceleration within the time interval $\delta t$, Eqs. (27) and (28) can be translated into:

$$\dot{\mathbf{r}}(t_{k+1}) = \dot{\mathbf{r}}(t_k) + \frac{1}{2}\ddot{\mathbf{r}}(t_k)\delta t + \frac{1}{2}\ddot{\mathbf{r}}(t_{k+1})\delta t \tag{29}$$

$$\mathbf{r}(t_{k+1}) = \mathbf{r}(t_k) + \dot{\mathbf{r}}(t_k)\delta t + \frac{1}{3}\ddot{\mathbf{r}}(t_k)\delta t^2 + \frac{1}{6}\ddot{\mathbf{r}}(t_{k+1})\delta t^2 \tag{30}$$

where

$$\ddot{\mathbf{r}}(t_{k+1}) = (\mathbf{M}+\mathbf{A})^{-1}(\mathbf{F}(t_{k+1}) - \mathbf{B}\dot{\mathbf{r}}(t_{k+1}) - \mathbf{C}\mathbf{r}(t_{k+1})). \tag{31}$$

This is a very popular method since it leads to continuity in acceleration, velocity and displacement. By inserting Eq. (31) into Eqs. (29) and (30), the method can be translated into an explicit form:

$$\mathbf{r}(t_{k+1}) = \left(\frac{6}{\delta t^2}(\mathbf{M}+\mathbf{A}) + \frac{3}{\delta t}\mathbf{B} + \mathbf{C}\right)^{-1}(\mathbf{F}(t_{k+1}) + (\mathbf{M}+\mathbf{A})\mathbf{a}_k + \mathbf{B}\mathbf{b}_k) \tag{32}$$

where

$$\mathbf{a}_k = \frac{6}{\delta t^2}\mathbf{r}(t_k) + \frac{6}{\delta t}\dot{\mathbf{r}}(t_k) + 2\ddot{\mathbf{r}}(t_k) \tag{33}$$

$$\mathbf{b}_k = \frac{3}{\delta t}\mathbf{r}(t_k) + 2\dot{\mathbf{r}}(t_k) + \frac{1}{2}\ddot{\mathbf{r}}(t_k)\delta t \tag{34}$$

In Eq. (32), the excitation forces $\mathbf{F}(t_{k+1})$ at time step $k+1$ is unknown at time step $k$ due to the interdependence between ship motion and ice force. So, iterations are performed at each time step, until the accuracy is acceptable. The convergence criterion is based on the change of excitation forces from one iteration to the next, which can be expressed by:

$$\sqrt{(F_1^{i+1}-F_1^i)^2 + (F_2^{i+1}-F_2^i)^2 + (F_6^{i+1}-F_6^i)^2} \Big/ \sqrt{(F_1^i)^2 + (F_2^i)^2 + (F_6^i)^2} < \varepsilon \tag{35}$$

where, $\varepsilon$ is a small, positive number, the magnitude of which is of the order $10^{-3}$.

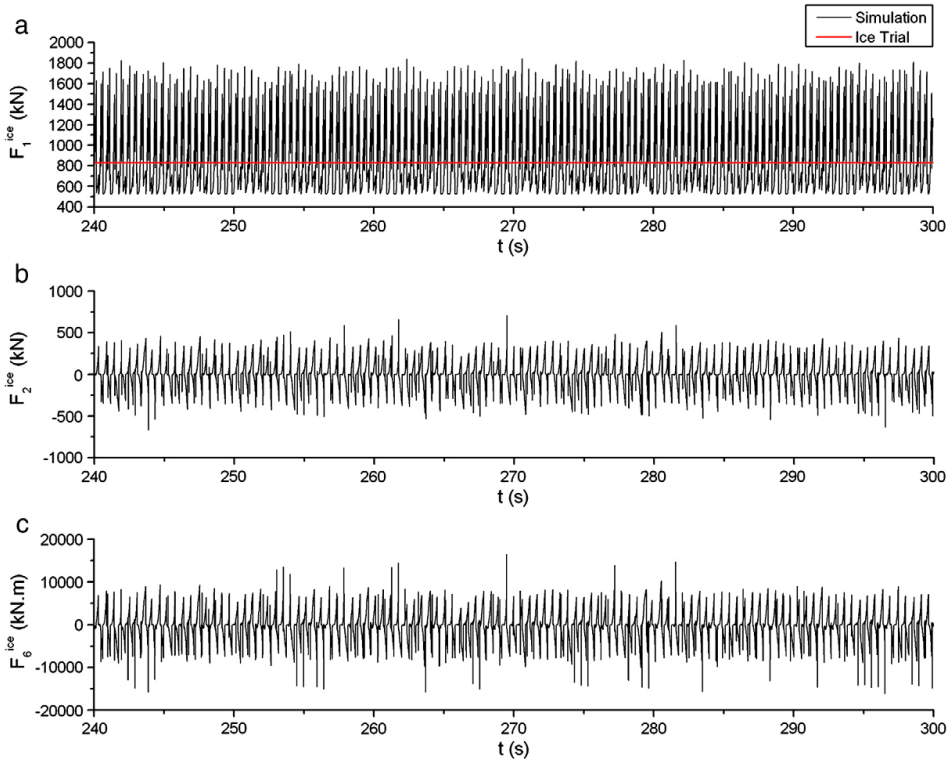


**Fig. 20.** Ice forces in transitting operation (in 0.6 m thick ice). a) Ice force in surge direction, b) Ice force in sway direction, c) Ice moment in yaw direction.

## 4. Numerical results

The numerical method introduced above is implemented in a computer program to simulate a full-scale ship operating in level ice, with the input including ice and ship characteristics, and the output including 3DOF instantaneous ice forces and ship motions. Then, some case studies with the Swedish multi-purpose icebreaker AHTS/IB Tor Viking II (as shown in Fig. 13) are performed to validate the numerical method.

### 4.1. Ice and ship characteristics

The level ice is assumed to be of a constant thickness and the material characteristics of ice are defined by the following constants in Table 1.

A 3D ship geometry (as shown in Fig. 14) is built for BEM calculations. The obtained 3DOF added mass coefficients (calculated in hydrostatic condition) and the main ship characteristics are given in Table 2.

### 4.2. Operating conditions

Transitting and turning operations are simulated in the numerical program (as shown in Figs. 15 and 16). Ice and current loads are the main environmental loads taken into consideration. In transitting operation, the propeller and rudder forces are just given in surge direction, while in turning operation the 3DOF propeller and rudder forces and moments are given.

The ice edge where the icebreaker enters is defined as an inclined straight line, which is not laterally symmetric (shown in Figs. 15 and 16). When the ship goes deep into ice, both the ice force and ship motion will be more stable and not significantly affected by the initial condition.

Fig. 17 also shows ship in full-scale turning in ice. It is clearly seen that the observed phenomena of icebreaking is quite well reproduced by the numerical method.

### 4.3. Convergence study

The effect of the discretization length (the distance between adjacent nodes) on the mean ice force is studied by changing the length. The results of this study are shown in Fig. 18.

As shown in Fig. 18, different values of discretization length (1600, 800, 400, 200, 100, 50 mm) are used, and the results show that the mean ice force converges quite well when the discretization length of ice nodes decreases.

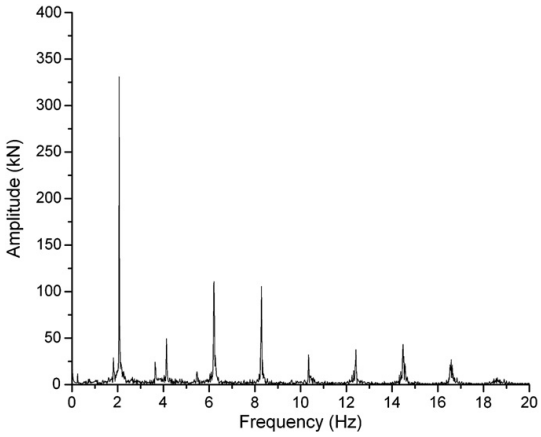


**Fig. 21.** Power spectrum corresponding to Fig. 19a.

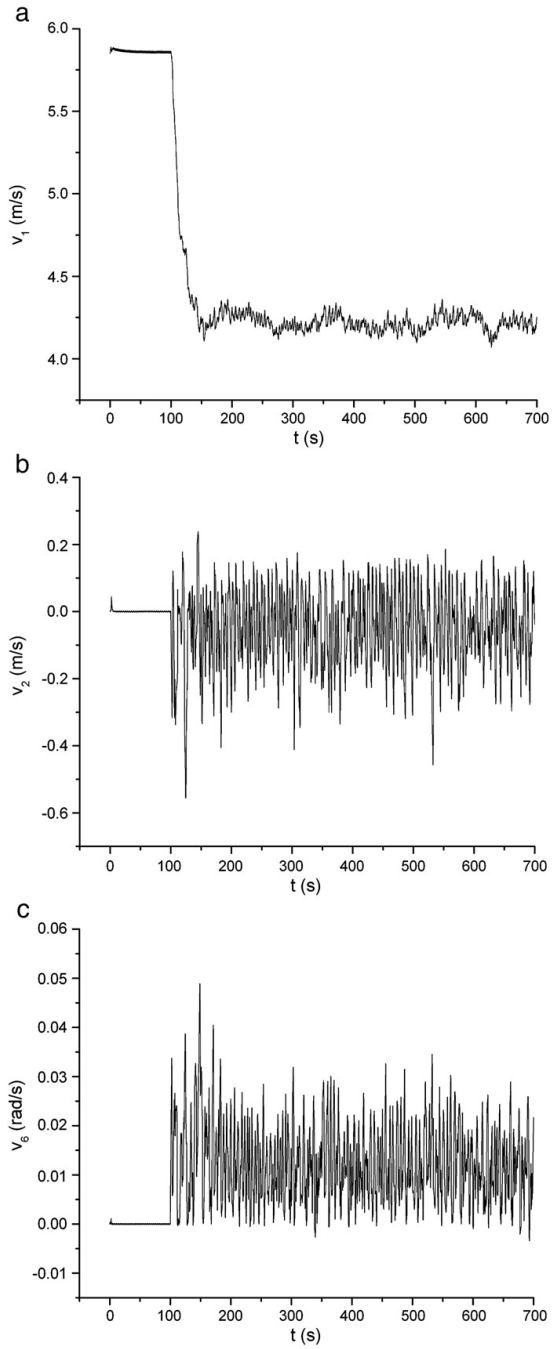


**Fig. 22.** Ship speed in turning operation (in 0.6 m thick ice). a) Forward speed, b) Transverse speed, c) Turning rate.

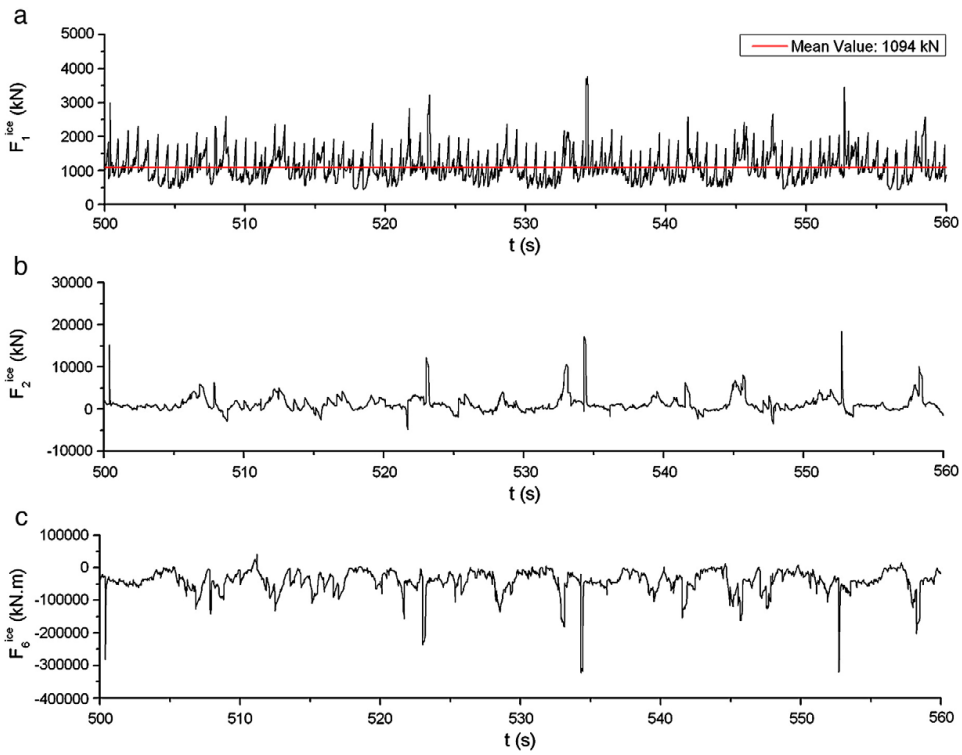


**Fig. 23.** Ice forces in turning operation (in 0.6 m thick ice). a) Ice force in surge direction, b) Ice force in sway direction, c) Ice moment in yaw direction.

### 4.4. Ice forces and ship motions

The instantaneous ice forces and ship motions in both transitting and turning operations have been calculated in the simulation program. A sample of the results is given in Figs. 19 to 25.

#### 4.4.1. Results in transitting condition

Fig. 19a–c shows the time series of 3DOF ship speed. The ship was moving with full propulsion and the starting forward speed was 5.5 m/s, after about 100 s, it achieved a more stable value. The starting transverse speed was zero, in the first 10 s it went up to a much higher value due to the non-symmetric ice edge, then decreased and started to oscillate around zero. The turning rate has the similar time series as transverse motion.

Fig. 20a–c shows the time series of 3DOF ice forces during the stable stage of ship motions. The ice resistance measured from the ice trials is 825 kN, which is also marked in Fig. 20a. The mean value of

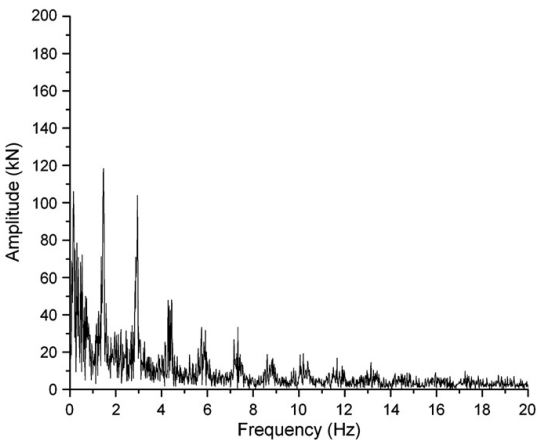


**Fig. 24.** Power spectrum corresponding to Fig. 23a.

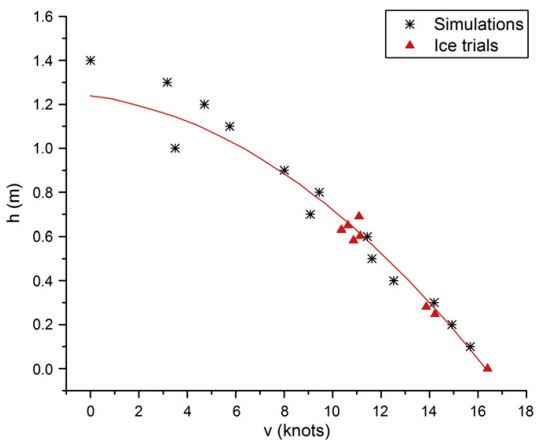


**Fig. 25.** The h–v curve.

simulated ice forces in surge direction is 881 kN, which is slightly higher than the measured value.

Fig. 21 gives the power spectrum of the time series shown in Fig. 20a, the dominant frequencies are identifiable, due to the periodic icebreaking processes and ship motions.

*4.4.2. Results in turning condition*

Fig. 22a–c shows the time series of 3DOF ship speed. The ship was moving in ice with full propulsion. At the time of 100s, both of the two rudders were turned to full angle (45°) and the ship started to turn in ice. As compared to Fig. 19a, the mean forward speed in turning operation is about 1.6 m/s lower than in transitting operation, but the amplitude of variation is much higher.

As compared to Fig. 20a–c, the time series of ice forces shown in Fig. 23a–c are quite different due to the continuous ice crushing on the shoulder of ship hull. The mean value of ice force is also higher in turning condition.

Due to the turning motions, low frequency components (lower than 1 Hz) come up, and become more important in the power spectrum (shown in Fig. 24).

*4.5. The h–v curve*

Ship performance in level ice is usually measured by the h–v curve. The icebreaking capability of Tor Viking II is 1.2 m thick level ice, and the specified value of ship speed in 1.0 m ice is 3.0 knots. The simulated h–v series are given in Fig. 25, as well as the parabolic regression curve determined from ice trial measurements (Riska et al., 2001). These two results show good consistency, and the deviation between the simulated h–v series is due to the two cases of icebreaking pattern introduced above. It is also seen that the required speed of 3.0 knots in 1.0 m ice is achieved with a good margin.

*4.6. The turning circle diameter*

The turning circle diameter $D_t$ is a measure of the ship maneuverability in ice, and the specified value of Tor Viking II is 500 m in 0.5 m thick ice. The simulated results of the turning circle diameters with different values of ice thickness are given in Fig. 26. The measured values from the ice trials (Riska et al., 2001) with the icebreaker on even keel and with a 3° heeling angle respectively, are also listed. As shown in Fig. 26, when the turning circle diameter is calculated in thicker ice, a deviation from the trend that was established by measurements occurs. This may be attributed to the crushing and bending phenomena at the aft shoulder area. It happens often in both full scale and the simulations that only occasionally some ice floes are broken by bending at the aft shoulder and sometimes the ice edge is just crushed (seen in Figs. 16 and 17). This effect of intermittent crushing will be investigated when this research proceeds.

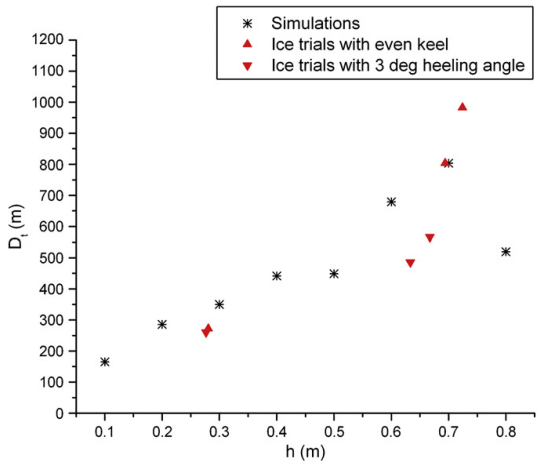


**Fig. 26.** The turning circle diameters with different values of ice thickness.

## 5. Conclusions

A numerical method for predicting ship performance in level ice is established based on empirical estimates of ice crushing pressure, ice bending failure and ice resistance. The accuracy of the numerical method is restricted by the empirical simplifications and assumptions made. But the advantage is that these can easily be tuned in the computer program if the improved data or models are achieved.

The full-scale data of Tor Viking II are used to validate the numerical results, and the agreement is found to be good. Following are the main conclusions from the numerical simulations:

(1) The observed phenomena of icebreaking can be well reproduced by the applied computer geometric tool, the sensitivity of which is investigated, and the accuracy is tunable;
(2) The icebreaking pattern is very sensitive to ice thickness, while the effect of ship speed is of less importance;
(3) Two cases of icebreaking pattern may occur in the simulations: in Case 1, the shoulder crushing does not happen, while it happens and results in a more severe icebreaking force in Case 2;
(4) The instantaneous 3DOF ice forces and ship motions can be efficiently determined by numerical integration;
(5) The simulated h–v series are non-monotonic, but have a similar variation as the full-scale data;
(6) The simulated turning circle diameter is close to the specified value, and the simulated results are also acceptable as compared to the measurements.

These conclusions are based on the simulation of a specific icebreaker. More hull shapes and environmental parameters should be investigated. Further work is needed on:

(1) The influence of heave, roll and pitch motions on ice forces and ship maneuvers (Ettema et al., 1987);
(2) The consideration of fluid–ice interaction and the effects of free surface between ship and ice;
(3) The regularity and irregularity in continuous icebreaking processes (Ettema et al., 1991).

## Acknowledgements

The authors acknowledge the support from the Rederi AB Transatlantic and Mr. Uno Haraldsson for the information about Tor Viking rudders, as well as the help from Mr. Xu Xiang in calculating ship characteristics.

## References

Bertram, V., 2000. Practical Ship Hydrodynamics. Butterworth-Heinemann, Oxford, UK.
Enkvist, E., 1972. On the Ice Resistance Encountered by Ships Operating in The Continuous Mode of Icebreaking. Report No.24, The Swedish Academy of Engineering Science in Finland. Helsinki, Finland.
Enkvist, E., Varsta, P., Riska, K., 1979. The ship–ice interaction. Proceedings of POAC 1979, pp. 977–1002.
Ettema, R., Stern, F., Lazaro, J., 1987. Dynamics of Continuous-Mode Icebreaking by a Polar-Class Icebreaker Hull. IIHR Report, Lowa Institude of Hydraulic Research, Lowa City, Lowa.
Ettema, R., Sharifi, K.P., Georgakakos, Stern, F., 1991. Chaos in continuous-mode icebreaking. Cold Regions Science and Technology 19, 131–144.
Faltinsen, O.M., 1990. Sea Loads on Ships and Offshore Structures. Cambridge University Press, Cambridge, UK.
Izumiyama, K., Kitagawa, H., Koyama, K., Uto, S., 1992. A numerical simulation of ice-cone interaction. Proceedings of IAHR 1992, pp. 188–199.

Kerr, A.D., 1975. The Bearing Capacity of Floating Ice Plates Subjected to Static or Quasi-static Loads, a Critical Survey. Research Report, vol. 333. Cold Regions Research and Engineering Laboratory, Hanover, New Hampshire, USA.

Kim, H.S., Ha, M.K., Williams, F.M., 2005. Speed-power performance of 95,000DWT Arctic tanker design. Journal of Offshore Mechanics and Arctic Engineering 127, 135–140.

Kujala, P., 1994. On the Statistics of Ice Loads on Ship Hull in the Baltic. Mechanical Engineering Series, vol. 116. Ship Laboratory, Helsinki University of Technology, Finland.

Lewis, J.W., DeBord, F.W., Bulat, V.A., 1982. Resistance and Propulsion of Ice-Worthy Ships. Transactions of SNAME, USA.

Lindqvist, G., 1989. A straightforward method for calculation of ice resistance of ships. Proceedings of POAC 1989, pp. 722–735.

Nguyen, D. T., Sørbø, A. H., Sørensen, A. J., 2009. Modelling and Control for Dynamic Positioned Vessels in Level Ice. Proceedings of 8th Conference on Manoeuvring and Control of Marine Craft (MCMC'2009), pp. 229–236, September 16–18, Guarujá, Brazil.

Riska, K., 2007. Arctic structures. Lecture Notes, Department of Marine Technology, Norwegian University of Science and Technology, Norway.

Riska, K., Leiviskä, T., Nyman, T., Fransson, L., Lehtonen, J., Eronen, H., Backman, A., 2001. Ice performance of the Swedish multi-purpose icebreaker Tor Viking II. Proceedings of POAC 2001, pp. 849–865.

Sawamura, J., Riska, K., Moan, T., 2008. Finite element analysis of fluid–ice interaction during ice bending. Proceedings of IAHR 2008, pp. 191–202.

Schneider, P.J., Eberly, D.H., 2002. Geometric Tools for Computer Graphics. Morgan Kaufmann Publishers, San Francisco, USA.

Varsta, P., 1983. On the mechanics of ice load on ships in level ice in the Baltic Sea. Publications 11, Technical Research Centre of Finland, Espoo, Finland.

Wang, S., 2001. A dynamic model for breaking pattern of level ice by conical structures. Ph.D. Thesis, Department of Mechanical Engineering, Helsinki University of Technology, Finland.

# Paper 2

# Numerical simulation of ship turning in level ice

Biao Su, Kaj Riska and Torgeir Moan

Published in the Proceedings of 29th International Conference on Offshore Mechanics and Arctic Engineering (OMAE 2010), Shanghai, China

Is not included due to copyright

# Paper 3

# Numerical simulation of local ice loads in uniform and randomly varying ice conditions

Biao Su, Kaj Riska and Torgeir Moan

Published in *Cold Regions Science and Technology*, Vol. 65 (2011), pp. 145-159

Cold Regions Science and Technology 65 (2011) 145–159

Contents lists available at ScienceDirect

Cold Regions Science and Technology

journal homepage: www.elsevier.com/locate/coldregions

# Numerical simulation of local ice loads in uniform and randomly varying ice conditions

Biao Su [a,*], Kaj Riska [a,b], Torgeir Moan [a]

[a] Centre for Ships and Ocean Structures, Norwegian University of Science and Technology, Trondheim, Norway
[b] ILS Oy, Helsinki, Finland

ARTICLE INFO

*Article history:*
Received 27 May 2010
Accepted 9 October 2010

*Keywords:*
Numerical simulation
Monte Carlo method
Icebreaking process
Ice conditions
Local ice loads
Statistical analysis

ABSTRACT

The ice loading process has a clear stochastic nature due to variations in the ice conditions and in the icebreaking processes of ships. The statistical characteristics of local ice loads are typically studied on the basis of field measurements. In this paper, a numerical method was applied to simulate a ship moving forward in either uniform or randomly varying ice conditions, where the thickness and strength properties of the ice encountered by the ship were assumed to be constant or randomly generated using the Monte Carlo method. The purpose of this simulation is to show the origin of the statistical variation in ice loading, which is difficult to identify in field measurements. To validate the numerical results, an icebreaking tanker, MT Uikku, was then modeled in a simulation program, the ice loading process was stochastically reproduced and the calculated amplitude values of the ice-induced frame loads were compared with the field measurements.


## 1. Introduction

The ice loading process has a clear stochastic nature due to variations in the ice conditions and in the icebreaking processes of ships. The statistical characteristics of the local ice loads on ships have been studied almost exclusively on the basis of full-scale measurements (e.g. Vuorio et al., 1979; Varsta, 1984; Kujala, 1994; Kujala et al., 2009). There have been many ship-ice load measurement campaigns conducted in Canada, US, Germany, Japan, Russia and Finland, but most of the data available for statistical analysis are from the Finnish sources (Hänninen, 2004; Frederking et al., 2005).

It is clear that the statistical variation in the ice conditions leads to the statistical variation of the ice loads, but the corresponding influence of the variation in the icebreaking processes is difficult to reveal by full-scale measurements. This is because the on-site ice conditions are always varying and uncontrollable. The separation of the origin of the statistical variation in ice loading into internal sources (due to the icebreaking process) and external sources (variation in encountered ice) is important in view of making long term predictions for ice loading.

A numerical method was introduced by Su et al. (2010a) to simulate the continuous icebreaking process. This method was based on empirical estimates of the ice crushing pressure, ice bending failure and ice resistance in which the observed phenomena of continuous icebreaking could be well reproduced. In the simulation program, a coupling between the continuous ice loads and the ship's motion was considered, and the three degree-of-freedom (3DOF) rigid body equations of surge, sway and yaw were solved using numerical integration. In an earlier study, Su et al. (2010a) investigated the global ice loads on ships (resistance) under uniform ice conditions. The numerical results were validated by the field measurements obtained by Riska et al. (2001).

In this paper, the ice model is extended to more complex ice conditions by considering random ice thickness and strength properties. This numerical method is applied to simulate a ship moving forward under uniform or randomly varying ice conditions with the purpose of determining the ice-induced frame loads. The local ice-structure load model is based on empirical data. Thus, this analysis especially shows the statistical variation of the loading process, which depends on the ice conditions and on the contact and icebreaking patterns.

A case study with an icebreaking tanker, MT Uikku, was carried out by using the simulation program. Firstly, the thickness and strength properties of the ice that is encountered by the ship are assumed to be constant during an icebreaking trial. In this case, the variation of the simulated local frame loads was intrinsically attributed to the varying icebreaking processes of the ship. Then, statistical data characterizing Baltic Sea ice (as reviewed by Kujala (1994)) were applied to randomize the ice conditions. The statistical characteristics of the simulated local frame loads were analyzed and compared with the field measurements obtained by Kotisalo and Kujala (1999) and Hänninen (2003).

## 2. Simulation of the icebreaking process

As previously mentioned, the numerical method that was introduced by Su et al. (2010a) is extended in this paper to simulate

* Corresponding author. Tel.: +47 41602417; fax: +47 73595528.
*E-mail address:* biao@ntnu.no (B. Su).

0165-232X/$ – see front matter © 2010 Elsevier B.V. All rights reserved.
doi:10.1016/j.coldregions.2010.10.004

the ice-ship interaction under more complex and variable ice conditions. In this section, this model is briefly described.

### 2.1. Simulation of the icebreaking pattern

In the simulation program, the 2D ship model and the edge of the ice were discretized into a number of nodes on the water plane (as shown in Fig. 1). At each time step, the computational geometric tools were applied to collect the contact zones along the ship hull. It was also assumed that the hull had a flat contact surface at each contact zone.

The ice wedges that were involved in the break-displace process were determined by the bending cracks, which were idealized and described by a single parameter, the icebreaking radius. The icebreaking radius $R$ was found by the expression given in Wang (2001) (based on information from Enkvist (1972) and Varsta (1983)):

$$R = C_l l\left(1.0 + C_v v_n^{rel}\right) \tag{1}$$

where $v_n^{rel}$ is the relative normal velocity between the ice and the hull node; $C_l$ and $C_v$ are two empirical parameters, $C_l$ has a positive value and $C_v$ has a negative value; $l$ is the characteristic length of the ice:

$$l = \left(\frac{Eh_i^3}{12(1-\nu^2)\rho_w g}\right)^{\frac{1}{4}}. \tag{2}$$

As shown in Fig. 2, the ice wedge was idealized and determined by the interpolation of the icebreaking radius at the first and last contact nodes (i.e., $R_f$ and $R_l$), and the opening angle of the ice wedge was denoted as $\theta$. The contact zone was discretized by a number of triangles (the triangles shown in red in Fig. 2) based on the hull nodes that were in contact. The contact area $A_c$ can then be calculated (Su et al., 2010a).

Before a bending failure occurs, we assume that the ice is only crushed on the contact surface. The crushing force $F_{cr}$ is normal to the contact surface and is calculated as the product of the effective crushing strength $\sigma_c$ and the contact area $A_c$, where the ice pressure on the contact surface is assumed to be uniform and equal to the effective crushing strength.

The frictional force was also taken into account (Su et al., 2010a). Thus, if the vertical component of the crushing and frictional forces $F_V$ exceeds the bending failure load $P_f$ given in Eq. (3), the ice wedge will be bent and cleared from the edge of the ice:

$$P_f = C_f\left(\frac{\theta}{\pi}\right)^2 \sigma_f h_i^2 \tag{3}$$

where $\theta$ is the opening angle of the idealized ice wedge shown in Fig. 2; $\sigma_f$ is the flexural strength of the ice; $h_i$ is the thickness of the ice; $C_f$ is an empirical parameter.

Eq. (3) accounts for the opening angle, but it is an empirical equation (introduced by Kashtelian and given in Kerr (1975)). Thus, the constant $C_f$ should be obtained from measurements.

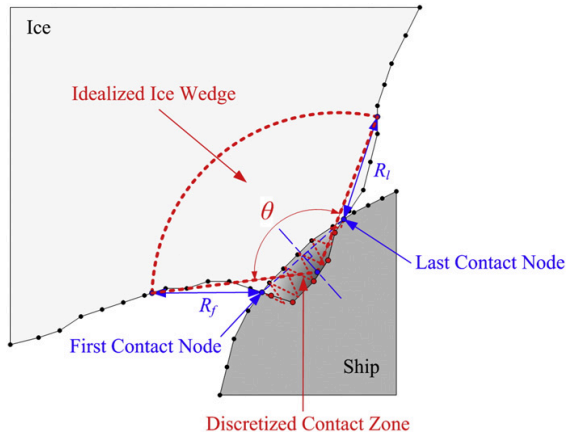


**Fig. 2.** Idealized ice wedge and discretized contact zone.

Based on these assumptions, the icebreaking pattern and continuous icebreaking forces can be determined using a step-by-step procedure. The effects of the empirical parameters (introduced above) on the mean icebreaking force were investigated and compared with Lindqvist's ice resistance (Lindqvist, 1989) in Su et al. (2010a).

### 2.2. Simulation of the ship's motion

This simulation is conducted in three degrees of freedom, that is, in surge, sway and yaw directions. The ship's motion in global coordinate system can be described by the Newton's second law:

$$\begin{aligned} m\dot{u}_g &= FX_g \\ m\dot{v}_g &= FY_g \\ I_z\dot{r} &= N \end{aligned} \tag{4}$$

where $FX_g$ and $FY_g$ are the forces in surge and sway directions; $N$ is the yaw moment; $m$ is the mass of the ship; $I_z$ is the moment of inertia in yaw direction; $u_g$, $v_g$ and $r$ are the velocities in surge, sway and yaw, respectively; the dot notation denotes the derivative with respect to time.

The forces and velocities can be translated into the ship coordinate system by:

$$\begin{aligned} FX_g &= FX\cos\psi - FY\sin\psi \\ FY_g &= FX\sin\psi + FY\cos\psi \end{aligned} \tag{5}$$

$$\begin{aligned} u_g &= u\cos\psi - v\sin\psi \\ v_g &= u\sin\psi + v\cos\psi \end{aligned} \tag{6}$$

where $\psi$ is the heading angle of the ship.

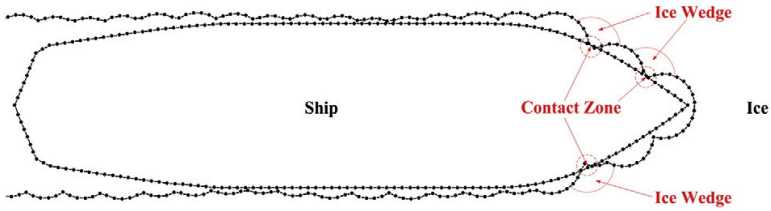


**Fig. 1.** Discretization of the ship hull and the edge of the ice.

The accelerations are then obtained by differentiating Eq. (6):

$$\begin{aligned}\dot{u}_g &= \dot{u}\cos\psi - \dot{v}\sin\psi - (u\sin\psi + v\cos\psi)r \\ \dot{v}_g &= \dot{u}\sin\psi + \dot{v}\cos\psi + (u\cos\psi - v\sin\psi)r.\end{aligned} \tag{7}$$

By inserting Eqs. (5) and (7) into Eq. (4), the ship's motion in the ship coordinate system can then be described by:

$$\begin{aligned}m\dot{u} &= FX + mvr \\ m\dot{v} &= FY - mur \\ I_z\dot{r} &= N\end{aligned} \tag{8}$$

To define the forces and moment terms, Eq. (8) is then substituted by a general matrix form of the linear coupled differential equations of motion:

$$(\mathbf{M}+\mathbf{A})\ddot{\mathbf{x}}(t) + \mathbf{B}\dot{\mathbf{x}}(t) + \mathbf{C}\mathbf{x}(t) = \mathbf{F}(t) \tag{9}$$

where the added mass coefficients were calculated by the boundary element method; the damping and restoring terms were taken as zero in this simulation.

The forces and moments that resulted from the ice, propeller, rudder and open water were considered in this simulation. Eq. (10) shows the decomposed components of the forces and moment acting on the ship:

$$\begin{aligned}F_1 &= F_1^i + F_1^p + F_1^r + F_1^{ow} + mvr \\ F_2 &= F_2^i + F_2^p + F_2^r + F_2^{ow} - mur \\ F_6 &= F_6^i + F_6^p + F_6^r + F_6^{ow}\end{aligned} \tag{10}$$

where the subscripts *1*,*2* and *6* refer to the directions of surge, sway and yaw; the superscripts *i*, *p*, *r* and *ow* refer to ice, propeller, rudder and open water, respectively.

A step-by-step numerical integration method was then applied to solve the equations of motion that were established above. According to Newmark's method, the general integral equations are given by:

$$\begin{aligned}\dot{\mathbf{x}}(t_{k+1}) &= \dot{\mathbf{x}}(t_k) + (1-\lambda)\ddot{\mathbf{x}}(t_k)\delta t + \lambda\ddot{\mathbf{x}}(t_{k+1})\delta t \\ \mathbf{x}(t_{k+1}) &= \mathbf{x}(t_k) + \dot{\mathbf{x}}(t_k)\delta t + \left(\frac{1}{2}-\beta\right)\ddot{\mathbf{x}}(t_k)\delta t^2 + \beta\ddot{\mathbf{x}}(t_{k+1})\delta t^2.\end{aligned} \tag{11}$$

These equations were obtained by a Taylor-series expansion in which the residual term was approximated by the quadrature formulas. The weighting terms $\lambda$ and $\beta$ are free parameters in the quadrature formulas that are determined by the requirements related to stability and accuracy. If a linear acceleration is assumed within the time interval $\delta t$, Eq. (11) can be translated into:

$$\begin{aligned}\dot{\mathbf{x}}(t_{k+1}) &= \dot{\mathbf{x}}(t_k) + \frac{1}{2}\ddot{\mathbf{x}}(t_k)\delta t + \frac{1}{2}\ddot{\mathbf{x}}(t_{k+1})\delta t \\ \mathbf{x}(t_{k+1}) &= \mathbf{x}(t_k) + \dot{\mathbf{x}}(t_k)\delta t + \frac{1}{3}\ddot{\mathbf{x}}(t_k)\delta t^2 + \frac{1}{6}\ddot{\mathbf{x}}(t_{k+1})\delta t^2\end{aligned} \tag{12}$$

where

$$\ddot{\mathbf{x}}(t_{k+1}) = (\mathbf{M}+\mathbf{A})^{-1}(\mathbf{F}(t_{k+1}) - \mathbf{B}\dot{\mathbf{x}}(t_{k+1}) - \mathbf{C}\mathbf{x}(t_{k+1})). \tag{13}$$

This is a popular method because it leads to continuity in the acceleration, velocity and displacement. By inserting Eq. (13) into Eq. (12), this method can be translated into an explicit form:

$$\mathbf{x}(t_{k+1}) = \left(\frac{6}{\delta t^2}(\mathbf{M}+\mathbf{A}) + \frac{3}{\delta t}\mathbf{B} + \mathbf{C}\right)^{-1}(\mathbf{F}(t_{k+1}) + (\mathbf{M}+\mathbf{A})\mathbf{a}_k + \mathbf{B}\mathbf{b}_k) \tag{14}$$

where

$$\begin{aligned}\mathbf{a}_k &= \frac{6}{\delta t^2}\mathbf{x}(t_k) + \frac{6}{\delta t}\dot{\mathbf{x}}(t_k) + 2\ddot{\mathbf{x}}(t_k) \\ \mathbf{b}_k &= \frac{3}{\delta t}\mathbf{x}(t_k) + 2\dot{\mathbf{x}}(t_k) + \frac{1}{2}\ddot{\mathbf{x}}(t_k)\delta t.\end{aligned} \tag{15}$$

### 2.3. Interaction between the ice loads and the ship's motion

The interaction between the rigid-body ship motions and the ice loads was considered in the simulation program (i.e., the calculated ship motions and ice loads were dependent on each other).

As shown in Eq. (14), the forces and moment $\boldsymbol{F}(t_{k+1})$ at time step $k+1$ are unknown at time step $k$ due to the interdependence between the ice loads and the ship's motion. Thus, iterations were performed at each time step until the accuracy was acceptable. The convergence criterion was based on the change of forces and moment from one iteration to the next, which can be expressed by:

$$\sqrt{(F_1^{i+1}-F_1^i)^2 + (F_2^{i+1}-F_2^i)^2 + (F_6^{i+1}-F_6^i)^2} \Big/ \sqrt{(F_1^i)^2 + (F_2^i)^2 + (F_6^i)^2} < \varepsilon \tag{16}$$

where $\epsilon$ is a small, positive number on the order of $10^{-3}$.

As discussed above, the icebreaking process was determined directly from empirical estimates of the ice crushing pressure, ice bending failure


**Fig. 3.** Icebreaking tanker MT Uikku.

and ice resistance. Thus, if variable environmental parameters are used in these empirical formulas (e.g. Eqs. (1) and (3)), then this simulation method can easily be applied to the randomly varying ice conditions.

## 3. Modeling of the ship

The ice loads acting on a ship can be treated in two ways: global and local (Izumiyama et al., 1999). The numerical method introduced above can be applied to gather local ice loads around a ship hull, and the global ice loads can be obtained as the integrated value of local loads. Su et al. (2010a,b) dealt with the global ice loads, and the numerical results were then validated by field measurements.

In this paper, an icebreaking tanker, MT Uikku (as shown in Fig. 3), was modeled in the simulation program, and the calculated local frame loads (denoted in Fig. 4) were investigated by comparison with full-scale measurements.

### 3.1. MT Uikku and field measurements

MT Uikku is a double-hull icebreaking motor tanker that is owned by Neste Shipping and Kvaerner Masa-Yard's joint venture company, Nemarc. The ship was constructed to meet the standards of the highest Finnish–Swedish Ice Class, IA Super. In 1998, the hull was strengthened for voyages in the Arctic Sea. After strengthening, the hull was stronger than the Finnish–Swedish Ice Class IA Super demands (Kujala et al., 2009). The primary dimensions of MT Uikku are presented in Table 1.

In 1998, MT Uikku was instrumented to measure the ice loads from different parts of the ship hull during the ARCDEV voyage (Kotisalo

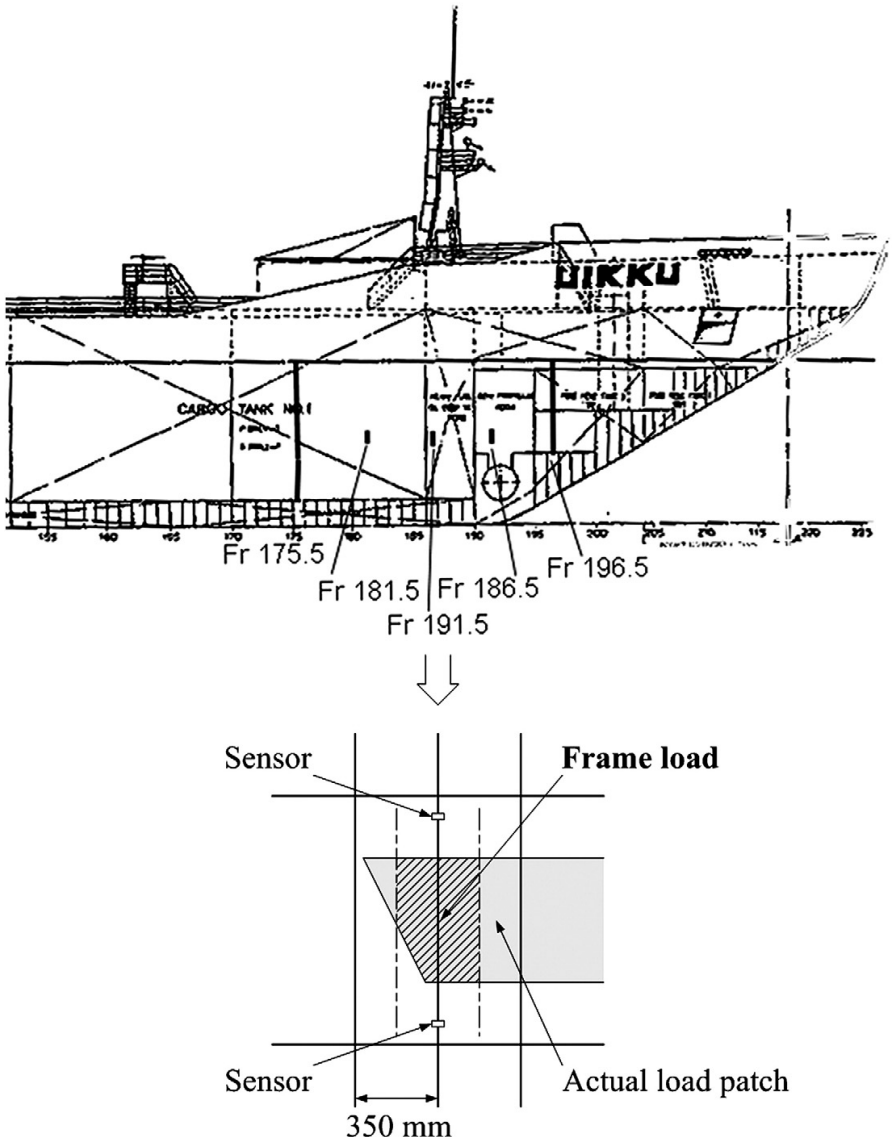


**Fig. 4.** A side view of MT Uikku (bow area).

**Table 1**
Primary dimensions of MT Uikku.

| | |
|---|---|
| Length over all | 164.4 m |
| Length between perpendiculars | 150.0 m |
| Breadth moulded | 22.2 m |
| Draught | 12 m |
| Displacement | 22,600 tons |
| Deadweight | 15,750 tons |
| Propulsion power | 11.4 MW |
| Speed | 17 knots |
| Block coefficient | 0.72 |

and Kujala, 1999). In 2003, three voyages were made between the Gulf of Finland and the Bothnian Bay (Hänninen, 2003), and the statistical characteristics of the ice loads measured on the bow area were discussed in Kujala et al. (2009) in which the analyzed data were gathered from the sensors that were mounted on frame 196.5 (as shown in Fig. 4).

### 3.2. Modeling of MT Uikku

Fig. 5 shows the 3D geometry model of MT Uikku, which was used in the hydrodynamic and open water resistance calculations.

During the simulation of the icebreaking process, the full-scale ship model of MT Uikku was discretized into a number of nodes on the water plane. As shown in Fig. 6, the edge of the ice was also discretized, and the ice thickness, ice crushing strength and ice flexural strength can be randomized along the sailing route of the ship (the X-axis as shown in this figure). Here, frame 196.5 on the bow area and frame 175.5 on the bow shoulder area were selected for the investigation of the local ice loads. Each of the load values was calculated by dividing the normal force on the frame by the frame spacing (350 mm); thus, the units are in kN/m.

It should be noted that the submersion and sliding processes of the broken ice were not simulated by this numerical method. The effects of the submersion and sliding processes on the global ice loads were calculated from the submersion component of Lindqvist's resistance. In calculating the submersion resistance, the bow was assumed to be completely covered by ice, and the bottom was covered for 70% of the length of the ship (Lindqvist (1989)). If the calculated submersion resistance (less than 1000 kN) is divided evenly among all frames (the frame spacing is 350 mm, as shown in Fig. 9), the load value for each frame will be less than 5 kN. Therefore, it was assumed that the ice-induced frame loads, especially the peak loads on the frame, were primarily determined by the breaking processes, and this analysis shows the variation of the ice loading process, which depends on the ice conditions and on the contact and icebreaking patterns.

## 4. Simulation in uniform ice conditions

The origin of the statistical variation in ice loading has been attributed earlier to the variations in the ice types and ice properties. In this simulation, the level ice with uniform and varying properties was considered while other ice types (e.g. ice ridge and ice floe) were not investigated.

Firstly (in this section), the thickness and strength properties of the ice that was encountered by the ship were assumed to be constant during an icebreaking trial.

Fig. 7 shows the 10-minute time histories of the calculated ice loads on frame 196.5, which are consisted of six icebreaking trials in

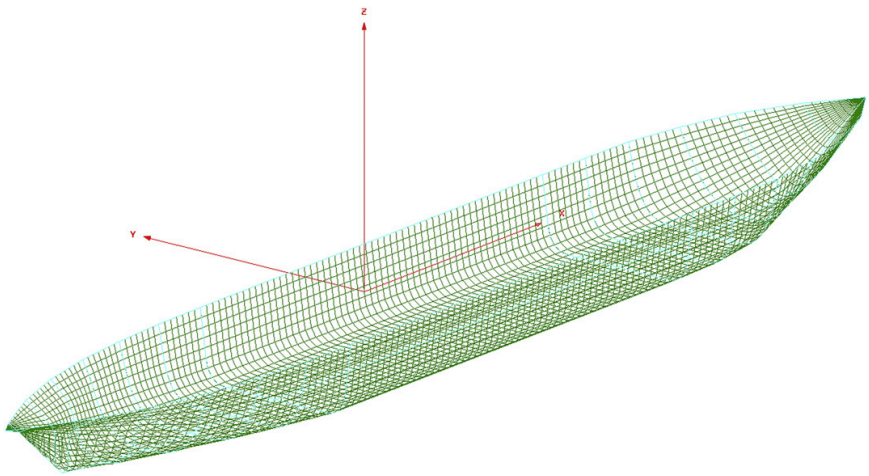


**Fig. 5.** Ship geometry model of MT Uikku used in the hydrodynamic and open water resistance calculations.

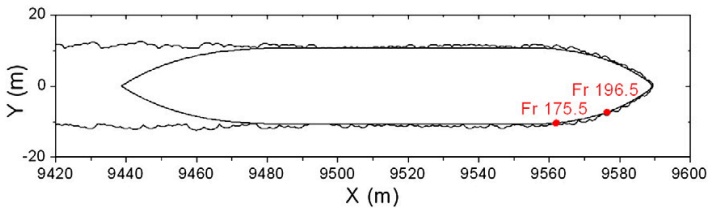


**Fig. 6.** Icebreaking model of MT Uikku.

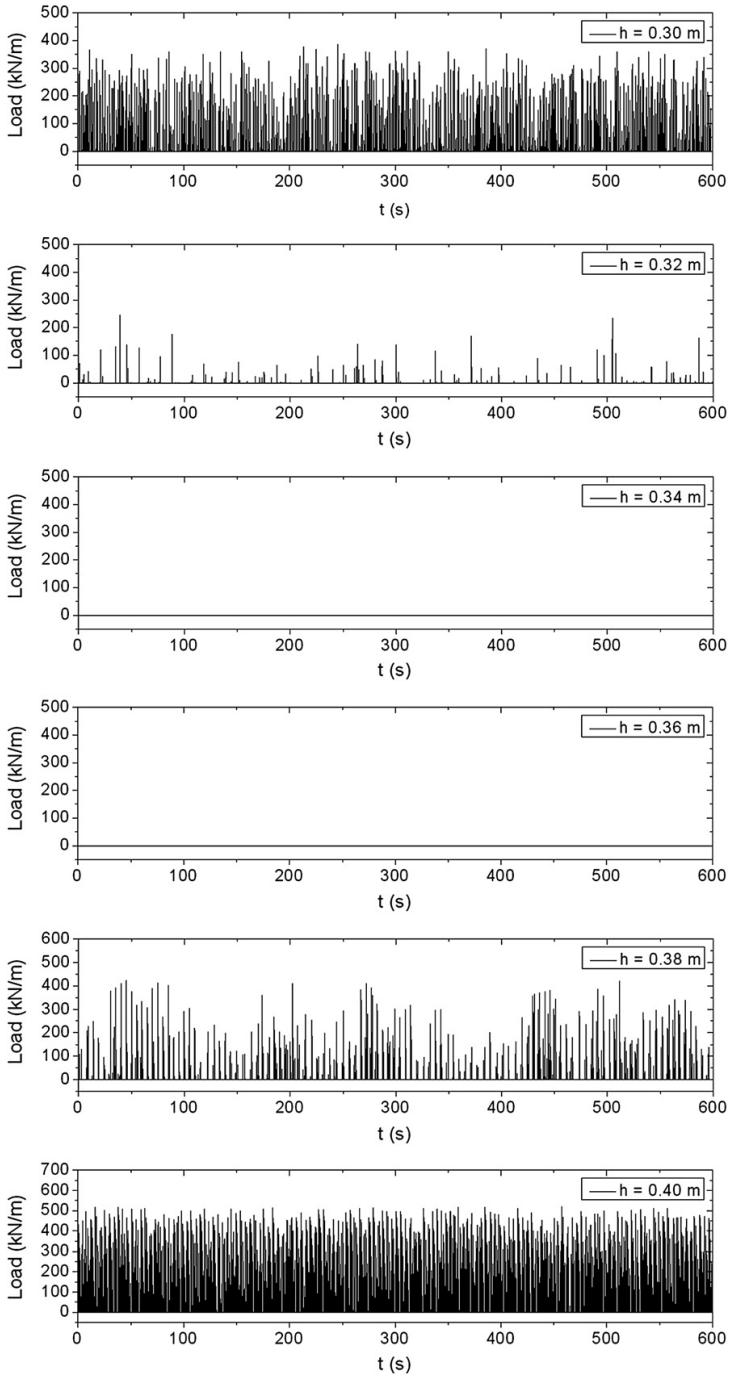


**Fig. 7.** Time histories of the calculated ice loads on frame 196.5 with different constant values of the ice thickness (h).

which different constant values for the ice thickness (0.3–0.4 m) were simulated. The simulated frame loads were very sensitive to the constant value of the ice thickness. This result is not unexpected because it was concluded by Su et al. (2010a) that the simulated icebreaking specified frame is never in contact with the ice during the relevant icebreaking pattern. Thus, as shown in Fig. 7, the ice loads can maintain a value of zero during the entire icebreaking trial.

Fig. 8 shows three icebreaking trials that were simulated with different thrusts, and the calculated mean values of ship speed varied between 2.90 and 5.67 m/s. The simulated frame loads were also

sensitive to the motion of the ship because the icebreaking pattern is also dependent on the relative velocity between the hull and the ice wedges that are in contact.

Individual ice loads need to be separated when studying the time histories of ice loads. The Rayleigh separation method was used in this paper to collect the peak loads within a certain time interval. Fig. 9 shows the occurrence frequency of the peak loads as a function of the ice thickness, where the frequency was calculated by dividing the number of peaks by the time interval (10 min). As shown in this figure, the frequency of the peak loads can vary from 0 to about 2 Hz due to a small variation in the ice thickness, and it is uncertain whether this frequency will increase or decrease. This is because a small change of both the ice conditions and the motion of the ship can lead to a chain of changes in the icebreaking patterns around the hull, which may totally change the locations of the contact zones (as shown in Fig. 1).

Fig. 10 shows the distributions of the peak loads which are plotted in the form of histogram. It was found that the simulated peak loads scattered although the external ice conditions were fixed. This is attributed to the variation in icebreaking pattern. The icebreaking pattern in this simulation is determined by the interaction between ship and ice, which is a continuously varying process and can increase the variation in ice-induced frame loads.

## 5. Simulation in randomly varying ice conditions

In this section, the thickness and strength properties of the ice that was encountered by the ship were randomized along the route.

The ice thickness was the primary variable that was used in this paper to describe the ice properties; the statistical characteristics of the ice crushing strength and ice flexural strength were also included. Based on existing data (reviewed by Kujala (1994)), the Monte Carlo method was applied to generate an ice field in which the thickness, crushing strength and flexural strength values were randomized along the route of the ship.

It should be noted that the referenced data of ice properties specifically came from sites in the Baltic Sea, because this simulation work was on the basis of the full-scale trials performed on the specific sea areas. For a more general use, it is necessary to have a good understanding of the present stage-of-knowledge of sea ice properties (which can refer to the excellent review work recently done by Timco and Weeks (2010)).

### 5.1. Statistical characteristics of the ice thickness

The thickness of the ice cover is highly variable, which is caused by thermal and mechanical factors. The thermal factor is a continuous component and is related to changes in air temperature and snow cover above the ice surface. The mechanical factors are discrete components that are caused by the rafting, ridging, and opening of leads and polynyas.

The existing data of the ice thickness variations are very limited. In Kujala (1994), the relevant data characterizing Baltic Sea ice were reviewed. Fig. 11 shows the distribution of the pack ice thickness that was measured at 10 m intervals along a line of 1 km length on March 1975 on the Bothnian Bay, a survey that was reproduced from Udin (1976) and Leppäranta (1981). Two distinct groups of data can be seen in Fig. 11. The lower values indicate the distribution of the level ice, and the thickness values that were higher than 0.8 m were assumed to represent deformed (ridged or rafted) ice (Leppäranta, 1981).

In full-scale ice load measurements, it is difficult to know the exact ice thickness distributions in the area that was covered by the voyage of the ship. In this paper, the ice load data that was measured during the two voyages of MT Uikku were utilized. The first one is the ARCDEV voyage made in the Arctic sea area (Kotisalo and Kujala, 1999), where the ice conditions that were encountered by MT Uikku

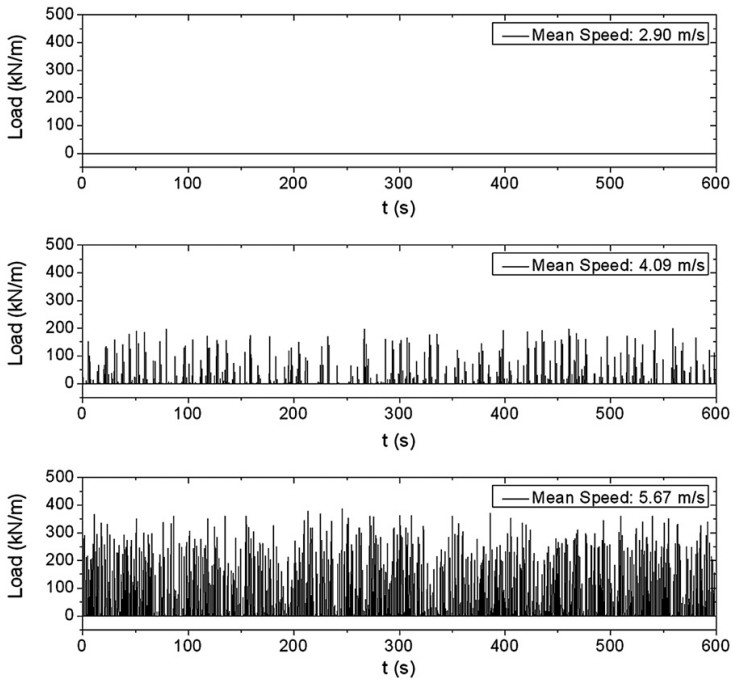


**Fig. 8.** Time histories of the calculated ice loads on frame 196.5 with different mean values of ship speed (dependent on given thrust).

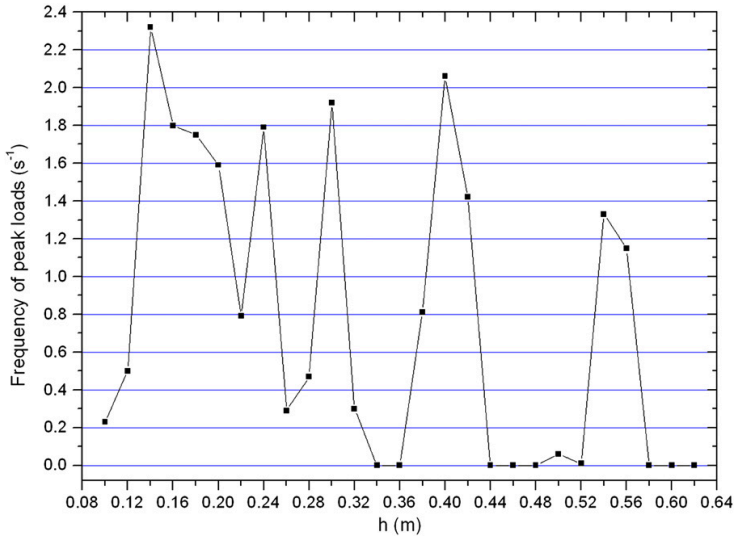


**Fig. 9.** Frequency of the calculated peak loads on frame 196.5 as a function of the ice thickness (h).

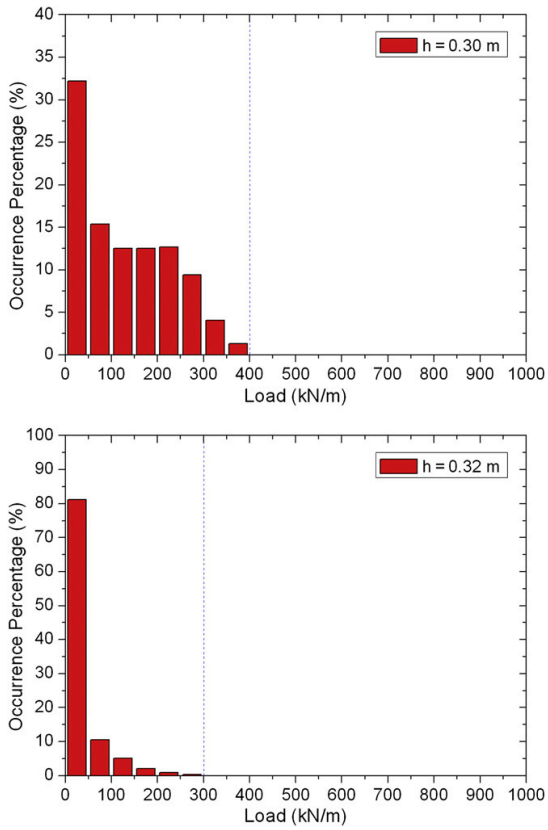


**Fig. 10.** Distributions of the calculated peak loads on frame 196.5 with different constant values of the ice thickness (h).

were difficult to clarify because the ship was in a convoy during this voyage. The second voyage was made between the Gulf of Finland and the Bothnian Bay (Hänninen, 2003), where the average level of the ice thickness was between 0.3 and 0.4 m. The observed mean value of the ice thickness during the second voyage is similar to the measurements that were made on the Bothnian Bay. Thus, the distribution of the level ice thickness given in Fig. 11 was used as the default value in the Monte Carlo simulation described below.

### 5.2. Statistical characteristics of the ice crushing strength

As discussed in Section 2.1, the definition of effective crushing strength was used to determine the contact force in the ship-ice interaction. The statistical variation of ice crushing strength was then considered by using the measured statistical data on ice crushing pressure.

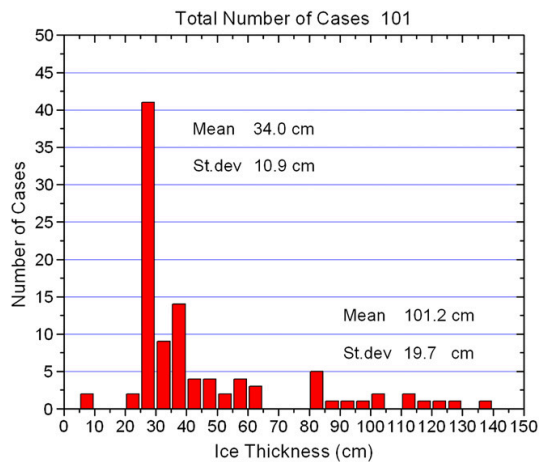


**Fig. 11.** Distribution of the ice thickness as measured at 10 m intervals along a line of 1 km length on March 1975 on the Bothnian Bay (Digitized from Kujala (1994)).

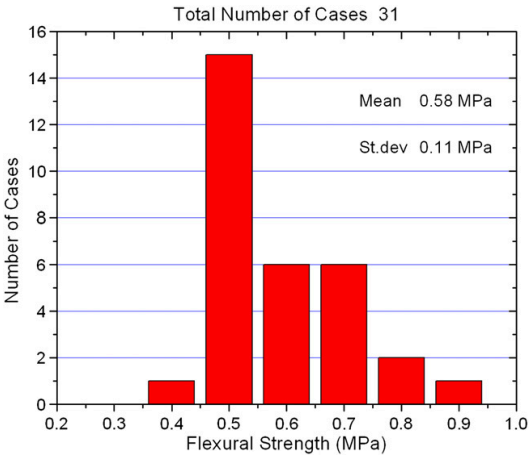


**Fig. 12.** Distribution of the measured flexural strength values of Baltic Sea ice (Digitized from Kujala (1994)).

In Kujala (1994), a formulation of the ice crushing pressure in statistical terms was introduced. The resulting crushing pressure is a gamma-distributed variable with small contact areas (<0.001 $m^2$) and a normally distributed variable with larger contact areas. As the contact area increases, the mean value of the crushing pressure asymptotically approaches a constant value, and the standard deviation $\sigma_p$ decreases as a function of the contact area $A$:

$$\sigma_p = \frac{0.065}{\sqrt{A}} \tag{17}$$

where $\sigma_p$ is given in MPa; $A$ is given in $m^2$.

By comparing this calculation with the field measurements obtained by Riska et al. (1990), the mean value and the standard deviation of ice crushing strength were then identified as 2.3 and 0.65 MPa in the Monte Carlo simulation described below.

### 5.3. Statistical characteristics of the ice flexural strength

The strength properties of the ice are sensitive to a number of physical parameters such as the temperature, grain size, crystallographic orientation, porosity, brine content and strain rate. Thus, the strength of the ice under bending is typically studied by conducting on-site flexural strength tests. As discussed in Kujala (1994), the flexural strength is not a basic material property because it is usually determined from the measured failure force by applying linear bending theory with homogenous and isotropic material properties throughout the ice thickness. The advantage of field testing is that the natural variations of the ice properties throughout the thickness of the ice are included in the test results.

Fig. 12 shows a histogram of the measured flexural strength values of Baltic Sea ice, which was also digitized from Kujala (1994). In this paper, the mean value (0.58 MPa) and standard deviation (0.11 MPa) of the ice flexural strength given in Fig. 12 was used in the Monte Carlo simulation described below.

### 5.4. Monte Carlo simulation

In this paper, a Monte Carlo simulation was applied to generate an ice field where the ice thickness, ice crushing strength and ice flexural strength were randomly generated using a certain specified probability distribution along the sailing route of the ship. If a normal distribution is assumed, and the correlation between these three variables is neglected, then the cumulative distribution function (CDF) $F(X)$ and its inverse CDF $F^{-1}(U)$ can be expressed by:

$$F(X) = \frac{1}{\sqrt{2\pi}\cdot\sigma}\int_{-\infty}^{X} e^{\left[\frac{-(s-\mu)^2}{2\sigma^2}\right]}ds \tag{18}$$

$$U \sim U(0,1) \tag{19}$$

$$X = F^{-1}(U) \tag{20}$$

where $\mu$ and $\sigma$ are the mean value and the standard deviation of random variable $X$; and $U$ is a randomly generated number between 0 and 1.

Because there is no information about the correlation of the spatial ice properties, the sensitivity of a possible correlation was investigated by sampling the properties at the spatial points at different intervals.

As shown in Eqs. (18)–(20), if a particular mean value and standard deviation are given, then a random value of $X$ can be generated. Using the statistical values that were introduced in Sections 5.1 to 5.3, the ice thickness, ice crushing strength and ice flexural strength can be randomized along the route.

Fig. 13 shows the randomized ice thickness along a 10 km route that was found using the following procedure: a) a series of sampling points were fixed along the route, the interval between two adjacent points was 50 m, the spatial correlation of the ice thickness was neglected; b) a random value of ice thickness was generated for each sampling point independently; and c) the intermediate value between two adjacent points was determined by linear interpolation. If the same procedure is applied to randomize the ice crushing strength and ice flexural strength, a more general ice field can be generated. Then, an icebreaking trial in the ice field can be simulated by the numerical method that was introduced in Section 2.

Fig. 14 shows three simulated icebreaking trials in which the statistical data introduced in Sections 5.1–5.3 were utilized and the ice properties were randomized at different intervals (25–100 m). The 10-minute time histories of the calculated forward speed of the ship (at the same thrust) are also shown in Fig. 15. The results show that, by decreasing the interval between two adjacent sampling points, the

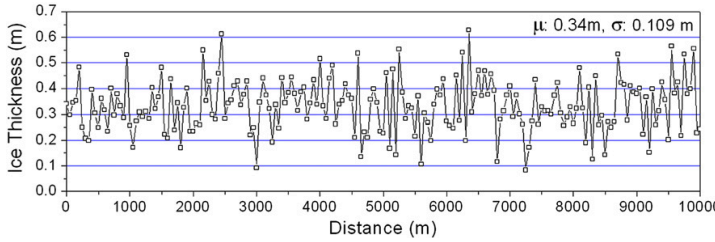


**Fig. 13.** Randomized ice thickness along a 10 km route.

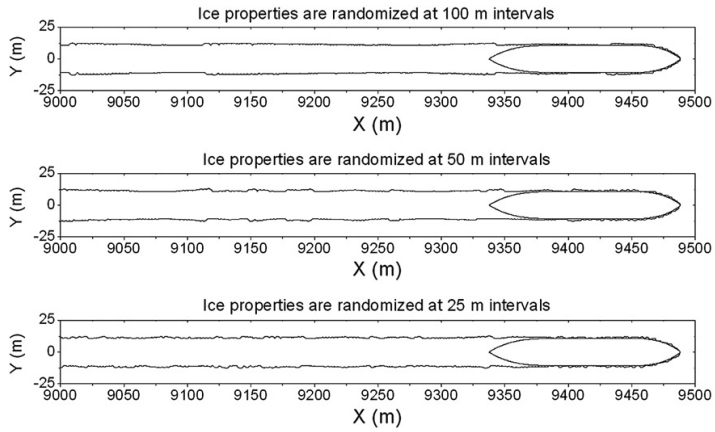


**Fig. 14.** Simulated icebreaking trials.

randomness of the simulated icebreaking pattern increases while the excursion of the calculated ship speed decreases.

As previously discussed, the spatial correlation of the ice properties was neglected between two adjacent sampling points. Therefore, a relatively long interval (50 m) was used in this simulation.

To verify the applied interval value, the excursion of the calculated ship speed (as shown in Fig. 15) can be compared with the available data from full-scale trials. Then, the spatial correlation of the ice properties can be investigated if the prevailing data are provided. The issues of correlation remain for further analysis.

Based on the assumptions and the randomizing procedures introduced above, a number of icebreaking trials were simulated. The final results are then presented statistically.

### 5.5. Statistical analysis

As described in Sections 5.1 to 5.4, the thickness and strength properties of the ice were randomized by the normal distribution. The statistical data that were applied in this simulation are given in Table 2.

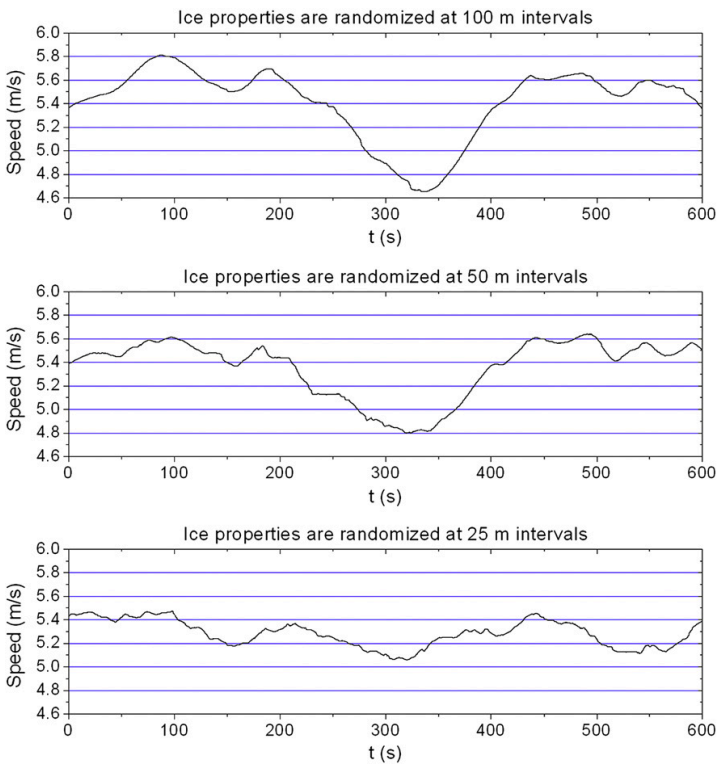


**Fig. 15.** Time histories of the calculated ship speed (at the same thrust).

**Table 2**
Statistical data of the ice properties.

| | Mean value | Standard deviation |
|---|---|---|
| Ice thickness | 0.340 m | 0.109 m |
| Ice crushing pressure | 2.30 MPa | 0.65 MPa |
| Ice flexural strength | 0.58 MPa | 0.11 MPa |

Fig. 16 shows the distributions of the recorded peak loads on frame 196.5 during three icebreaking trials simulated (each trail was simulated in a period of 30 min). It is found that the recorded peak loads fit a similar distribution, and the sampling error can simply be reduced by summing the results of each trial (as shown in Fig. 17).

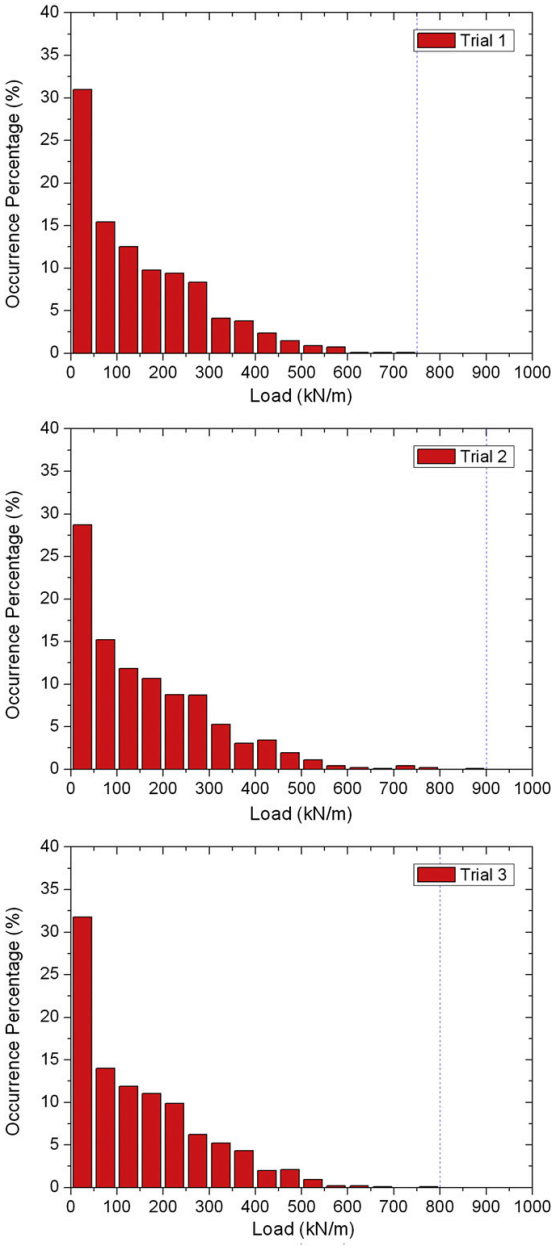


**Fig. 16.** Distributions of the peak loads on frame 196.5 during the different trials simulated.

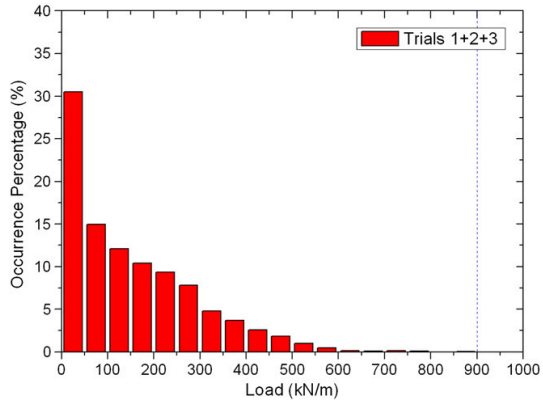


**Fig. 17.** Distributions of the peak loads on frame 196.5 by using the results of the three trials in Fig. 16.

In Kujala et al. (2009), the exponential, gamma and Weibull distributions were fitted to the measured peak loads on frame 196.5, and it was found that the Weibull distribution with a shape factor of 0.75 gave the best fit to the measured statistical distributions. In this paper, the distributions of the simulated peak loads on the same frame were then analyzed using the Weibull probabilistic model.

The cumulative distribution function of the Weibull distribution is given by:

$$F(x) = 1 - exp\left(-(x/\lambda)^k\right) \tag{21}$$

where $k$ is the shape factor; $\lambda$ is the scale factor of the distribution.

Fig. 18 shows the fitted distributions on the simulated peak loads (recorded in a period of 12 h), where $x_i$ are the ordered values of peak loads ($x_i = 1, 2, 3\ldots$ kN/m); $F_i$ are the cumulative probabilities of $x_i$; $ln()$ is the natural logarithm function. If $x_i$ exactly follow a Weibull distribution, the $ln(-ln(1-F_i))$ versus $ln(x_i)$ plot should be a straight line with a slope equal to the shape factor of Weibull distribution. As shown in this figure, the Weibull distribution (shape factor $k = 0.75$)

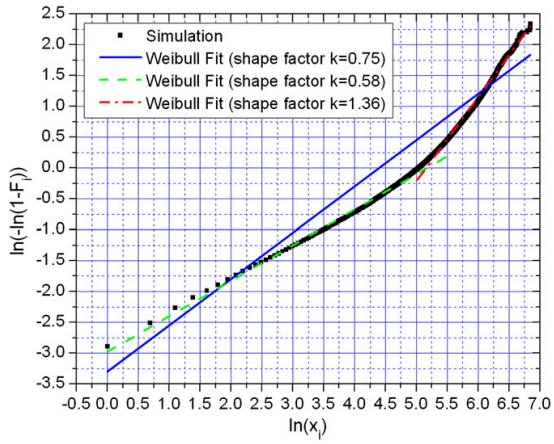


**Fig. 18.** Distributions of the simulated peak loads (recorded in a period of 12 h) on frame 196.5 and fitted probability distributions by using the Weibull model.

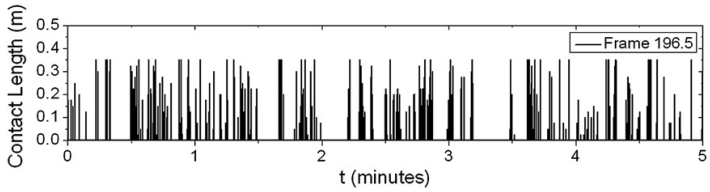


**Fig. 19.** Variation of the contact length between frame 196.5 and the ice in a period of 5 min.

which was found to give the best fit to the measured data can also be fitted to the simulated results. But, it seems that a smaller shape factor is better fitted for the low peak loads and a bigger shape factor is better fitted for the high peak loads.

In this simulation, the thickness and strength properties of the ice were randomized by the normal distribution, while the simulated peak loads on a frame were found to approximately fit a Weibull distribution. This is because there is an internal source of the statistical variation in ice loading due to the icebreaking processes of the ship, other than the external ice conditions (as discussed in Section 4).

Fig. 19 shows the variation of the contact between frame 196.5 and the ice in a period of 5 min simulated in the randomly varying ice conditions. Here, the contact length is the load length within the frame area, and the variations in the peak values of the contact length are attributed to the variations in the icebreaking patterns. As shown in Fig. 4, the frame spacing is 0.35 m on the bow area of MT Uikku. So, it means that the frame is fully in contact with ice when the contact length shown in Fig. 19 equals to 0.35 m. Fig. 20 shows the separated peak loads on frame 196.5 when this frame is fully in contact with ice. In this case, the load level is obviously high, and the distribution of the peak loads is dominated by the variations in the thickness and strength properties of the ice (since the contact length is constant in this case). Fig. 21 shows the separated peak loads on frame 196.5 with the varying contact length. In this case, the distribution of the peak loads is dependent on the variations in the external variables as well as the variations in the ice breaking patterns. Fig. 22 shows the distributions of the simulated peak loads (recorded in a period of 12 h) in these two cases, where $x_i$ are the ordered values of peak loads ($x_i = 1, 2, 3\ldots$ kN/m); $P_i$ are the occurrence percentages of the peak loads that are varying from $x_{i-1}$ to $x_i$. Then, the different distributions between the low peak loads and the high peak loads shown in Fig. 18 can be interpreted.

### 5.6. Comparison with field measurements

In an earlier study, Su et al. (2010a) investigated the global ice loads on ships (resistance) under uniform ice conditions, and the numerical results compared well with the field measurements obtained by Riska et al. (2001).

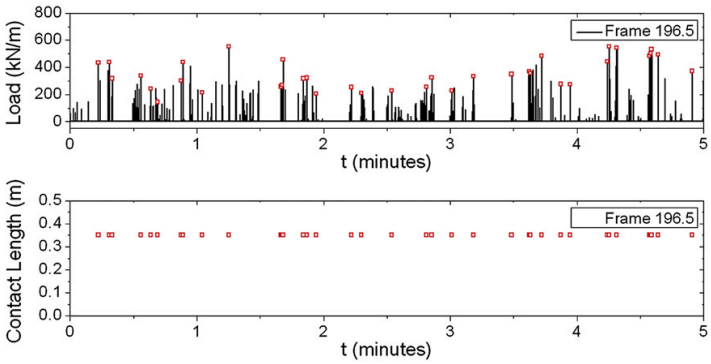


**Fig. 20.** Separated peak loads on frame 196.5 with full contact (peaks are indicated by red squares).

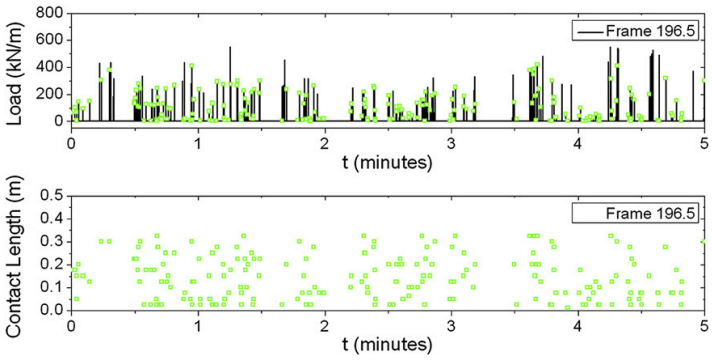


**Fig. 21.** Separated peak loads on frame 196.5 with varying contact (peaks are indicated by green squares).

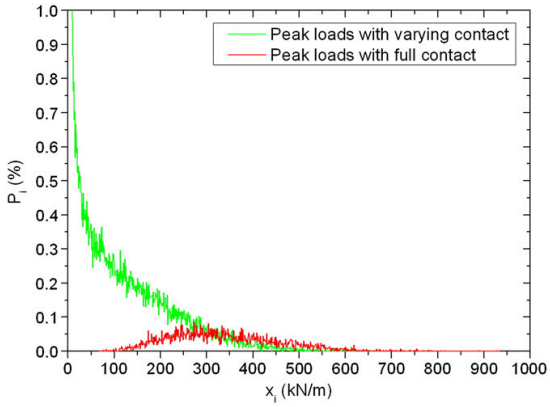


**Fig. 22.** Distributions of the simulated peak loads (recorded in a period of 12 h) on frame 196.5 with varying or full contact.

As compared with global ice load, the accuracy of simulated local ice load is more dependent on the empirical assumptions and the simplifications made. It should be noted that the ice pressure on the contact surface was assumed to be uniform and equal to the effective crushing strength. The fact that the ice pressure is not uniform will imply an uncertainty in the frame load.

Another uncertainty in comparing the simulated local ice loads with field measurements is that only the level ice condition was considered in this simulation while different types of ice might be encountered by the ship during the measurements.

In Section 3.1, two full-scale voyages of MT Uikku were introduced. During the ARCDEV voyage (Kotisalo and Kujala, 1999), the ice loads on both frame 196.5 and frame 175.5 were measured, but the actual ice conditions encountered by the ship were difficult to clarify. During the voyage that was made between the Gulf of Finland and the Bothnian Bay (Hänninen, 2003), the ice loads on frame 196.5 were measured, and the average thickness of the ice encountered by the ship was quite close to the measurements that were introduced in Section 5.1.

Therefore, the numerical results shown below were calculated under the same ice condition (given in Table 2), which referred to the second voyage.

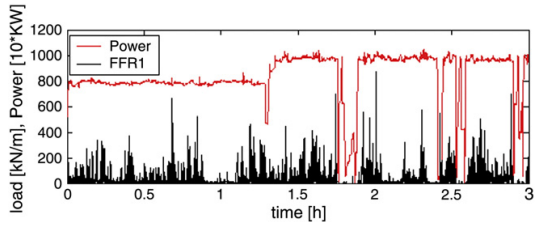


**Fig. 25.** A 3-hour time history of the measured ice loads on frame 196.5 (reproduced from Hänninen (2003), average ice thickness: 0.3–0.4 m).

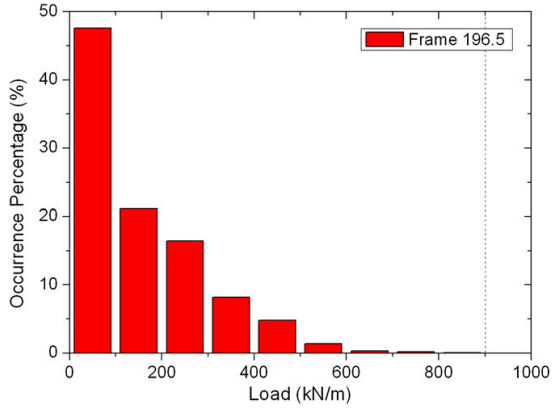


**Fig. 26.** Distributions of the calculated peak loads (recorded in a period of 2 h) on frame 196.5 (average ice thickness: 0.34 m).

As shown in Figs. 23 and 24, the simulated ice loading process had a significant stochastic nature, and the calculated amplitude values of the ice loads were comparable to the measurements shown in Fig. 25 (reproduced from Hänninen (2003)). As shown in Figs. 26 and 27, the peak values of the calculated ice loads were recorded in a period of 2 h, and the distributions of the peak loads were compared with the

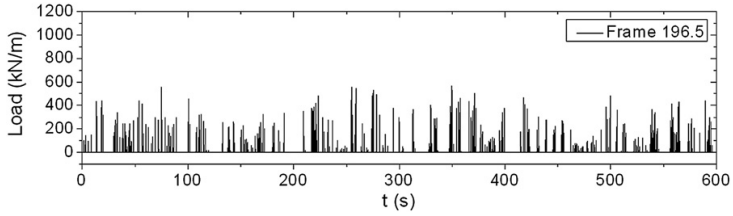


**Fig. 23.** A 10-minute time history of the calculated ice loads on frame 196.5 (average ice thickness: 0.34 m).

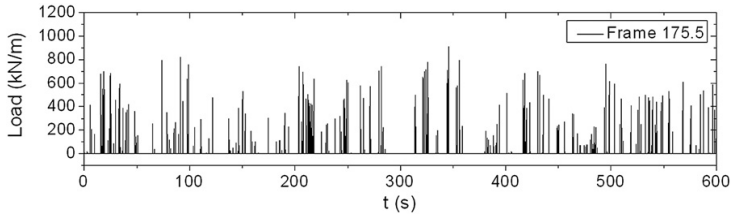


**Fig. 24.** A 10-minute time history of the calculated ice loads on frame 175.5 (average ice thickness: 0.34 m).

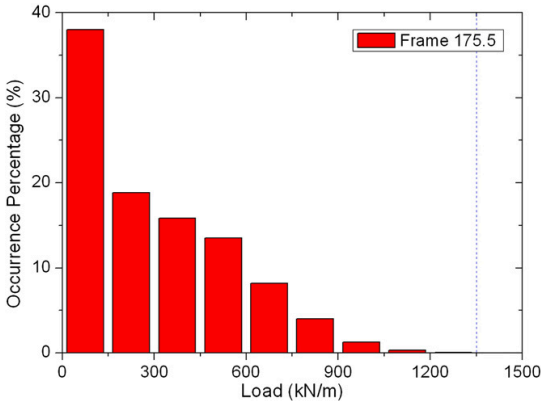


**Fig. 27.** Distributions of the calculated peak loads (recorded in a period of 2 h) on frame 175.5 (average ice thickness: 0.34 m).

measured statistical distributions. Fig. 28 shows an example of the measured peak load distributions on frame 196.5. The measured small peak loads were mostly induced by the noise, open water and broken ice, which were not included in the simulated frame loads. Therefore, the distributions of low peak loads were quite different between field measurement and the simulation while the distributions of high peak loads were similar.

The ice loads on frame 175.5 were not measured during the second voyage; therefore, the relevant results from the first voyage are shown in Fig. 29, in which the ice conditions were undefined.

From Figs. 26 and 27, it was found that the maximum values of the calculated ice loads on the bow shoulder area (frame 175.5) were larger than on the bow area (frame 196.5) under the same ice condition. Such loads were also measured in the field measurements (Kotisalo and Kujala, 1999). This may be interpreted as the effect of the frame angle. There have been several works done on the spatial distribution of ice loads around a ship hull. Some of them are experimental ones (e.g. Izumiyama et al., 1999), and some have been done numerically (e.g. Valanto, 2001). This issue will be investigated in future, as well as the different operations in ice.

## 6. Conclusions

In this paper, a numerical method was applied to simulate a ship moving forward in either uniform or variable ice conditions, where the thickness and strength properties of the ice that was encountered by the ship were assumed to be either constant or randomly generated using the Monte Carlo method.

Under the uniform ice conditions, the simulated peak loads on a frame scattered and were very sensitive to the prescribed ice conditions.

Under the randomly varying ice conditions, the thickness and strength properties of the ice were randomized by the normal distribution, while the simulated peak loads on a frame were found to approximately fit a Weibull distribution. This is because there is an internal source of the statistical variation in ice loading due to the icebreaking processes of the ship, other than the external ice conditions.

It is found that the statistical variation of the ice loading process is external caused by the variation in the ice conditions and internally caused by the variation in the contact and icebreaking patterns. In practice, this internal source of the variation in ice loading is difficult to identify, so it is taken as a main finding of this simulation.

To validate the numerical results, an icebreaking tanker, MT Uikku, was modeled in the simulation program. Statistical data characterizing Baltic Sea ice were also applied to randomize the ice conditions. The calculated amplitude values of the ice loads on two local frames were comparable to field measurements, the distributions of the recorded peak loads were also similar to the measured statistical distributions.

There are also some issues to be addressed more effectively:

a) Empirical data were used in this simulation to estimate the bearing capacity and the breaking length of a floating ice wedge. Empirical models for these predictions are usually the very simplified ones which assume that the ice structure acts as an elastic, homoge-

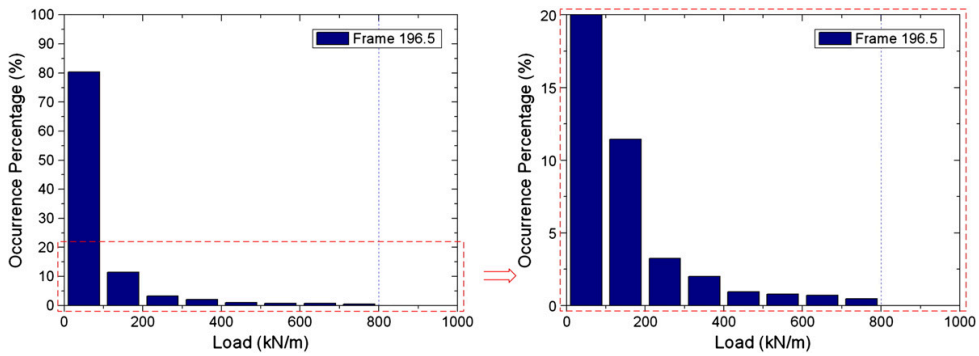


**Fig. 28.** An example of the measured peak load distributions on frame 196.5 (digitized from Kujala et al., 2009, maximal ice thickness over 0.5 m).

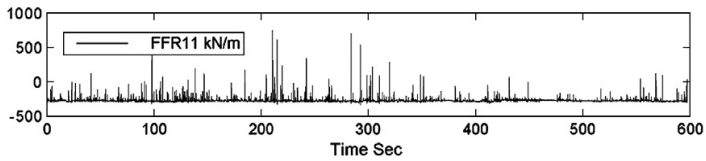


**Fig. 29.** A 10-minute time history of the measured ice loads on frame 175.5 (reproduced from Kotisalo and Kujala (1999), ice conditions undefined).

neous, isotropic plate on an elastic foundation, while other models (e.g. FEM model) tend to bring more uncertainties. Further studies on this issue would be beneficial to improve this simulation.

b) The simulated peak loads on the bow frame were found to approximately fit a Weibull distribution. This conclusion is based on the simulation of a specific icebreaking tanker moving forward in level ice, the referenced data of ice properties specifically came from sites on the Baltic Sea. To make a general conclusion, more hull shapes and ice types should be considered, and more comparisons and validations are needed.

c) The spatial distribution of ice loads around a ship hull was not discussed in this paper. This issue will be investigated in future.

## Acknowledgements

The authors wish to acknowledge the support of the Research Council of Norway through the Centre for Ships and Ocean Structures at the Norwegian University of Science and Technology in Trondheim, Norway.

## References

Enkvist, E., 1972. On the Ice Resistance Encountered by Ships Operating in The Continuous Mode of Icebreaking. Report No.24, The Swedish Academy of Engineering Science in Finland, Helsinki, Finland.

Frederking, R., Kubat, I., Collins, A., Suominen, M., 2005. SAFEICE Database Description. Report for Deliverable D2-4 of SAFEICE Project, September 2005.

Hänninen, S., 2003. Ship Based Observations on Board MT Uikku during the Winter 2003. Ship Laboratory, Helsinki University of Technology, Finland. (Unpublished).

Hänninen, S., 2004. Inventory List of Data Sources about Ship Hull Ice Loads and Damages. Report for Deliverable D2-1 of SAFEICE Project, December 2004.

Izumiyama, K., Wako, D., Uto, S., 1999. Ice Force Distribution around a Ship Hull. Proceedings of POAC 1999, 707–716.

Kerr, A.D., 1975. The Bearing Capacity of Floating Ice Plates Subjected to Static or Quasi-static Loads, a Critical Survey. Research Report 333, Cold Regions Research and Engineering Laboratory, Hanover, New Hampshire, USA.

Kotisalo, K., Kujala, P., 1999. Ice Load Measurements Onboard MT Uikku during the ARCDEV Voyage. Proceedings of POAC 1999, 974–987.

Kujala, P., 1994. On the Statistics of Ice Loads on Ship Hull in the Baltic. Mechanical Engineering Series No. 116, Ship Laboratory, Helsinki University of Technology, Finland.

Kujala, P., Suominen, M., Riska, K., 2009. Statistics of Ice Loads Measured on MT Uikku in the Baltic. Proceedings of POAC 2009.

Leppäranta, M., 1981. On the Structure and Mechanics of Pack Ice in the Bothnian Bay. Dissertation. In Finnish Marine Research No. 248, Helsinki, pp. 3–86.

Lindqvist, G., 1989. A straightforward method for calculation of ice resistance of ships. Proceedings of POAC 1989, 722–735.

Riska, K., Rantala, H., Joensuu, A., 1990. Full Scale Observations of Ship-Ice Contact. Report M-97, The laboratory of Naval Architecture and Marine Engineering, Helsinki University of Technology, Finland.

Riska, K., Leiviskä, T., Nyman, T., Fransson, L., Lehtonen, J., Eronen, H., Backman, A., 2001. Ice performance of the Swedish multi-purpose icebreaker Tor Viking II. Proceedings of POAC 2001, 849–865.

Su, B., Riska, K., Moan, T., 2010a. A numerical method for the prediction of ship performance in level ice. Cold Regions Science and Technology 60, 177–188.

Su, B., Riska, K., Moan, T., 2010b. Numerical Simulation of Ship Turning in Level Ice. Proceedings of OMAE 2010.

Timco, G.W., Weeks, W.F., 2010. A Review of the Engineering Properties of Sea Ice. Cold Regions Science and Technology 60, 107–129.

Udin, I., 1976. Sea Ice-75. Ground Truth Reprot. Winter Navigation Research Board. Report No. 16:2. Norrköping.

Valanto, P., 2001. On the cause and distribution of resistance forces on ship hulls moving in level ice. Proceedings of POAC 2001, 803–816.

Varsta, P., 1983. On the Mechanics of Ice Load on Ships in Level Ice in the Baltic Sea. Publications 11, Technical Research Centre of Finland, Espoo, Finland.

Varsta, P., 1984. Determination of Ice Loads Semiempirically. Ship Strength and Winter Navigation. Technical Research Centre of Finland. VTT Symposium, 52, pp. 177–182.

Vuorio, J., Riska, K., Varsta, P., 1979. Long Term Measurements of Ice Pressure and Ice-induced Stresses on the Icebreaker SISU in Winter 1978. Research Report No. 28, Winter Navigation Research Board, Finland and Sweden.

Wang, S., 2001. A Dynamic model for Breaking Pattern of Level Ice by Conical Structures. Ph.D. Thesis, Department of Mechanical Engineering, Helsinki University of Technology, Finland.

# Paper 4

# Numerical study of ice-induced loads on ship hulls

Biao Su, Kaj Riska and Torgeir Moan

Accepted for publication in *Marine Structures*, in press (2011)

Marine Structures xxx (2011) 1–21

Contents lists available at ScienceDirect

Marine Structures

journal homepage: www.elsevier.com/locate/marstruc

# Numerical study of ice-induced loads on ship hulls

Biao Su [a,*], Kaj Riska [a,b], Torgeir Moan [a]

[a] Centre for Ships and Ocean Structures, Norwegian University of Science and Technology, Trondheim, Norway
[b] ILS Oy, Helsinki, Finland

ARTICLE INFO

*Article history:*
Received 7 December 2010
Accepted 1 February 2011

*Keywords:*
Numerical simulation
Monte Carlo method
Design ice conditions
Level ice
Ice loads
Ship performance
Statistical analysis

ABSTRACT

A numerical model is introduced in this paper to investigate both global and local ice loads on ship hulls. This model is partly based on empirical data, by which the observed phenomena of continuous icebreaking can be well reproduced. In the simulation of a full-scale icebreaking trial, the interdependence between the ice load and the ship's motion is considered, and the three degree-of-freedom rigid body equations of surge, sway and yaw are solved by numerical integration. The variations in the level ice thickness and in the strength properties of ice can also be taken into account. The simulated ice loads on ship hulls are discussed through two case studies, in which the ship's performance, the statistics of ice-induced frame loads, and the spatial distribution of ice loads around the hull are analyzed and compared with field measurements. As far as we know the present paper is the first to integrate all the features above. It is hoped that further studies on this numerical model can supplement the field and laboratory measurements in establishing a design basis for the ice-going ships especially for ships navigating in the first-year ice.



## 1. Introduction

It is important to estimate both global and local ice loads on ships. The global ice load governs the ship's overall performance in ice, and it is an integrated effect of local ice loads over the hull area. Information on the distributions of local ice loads around the ship hull can be used for more effective design of ice-going ships both in terms of overall operation and from the structural point of view.

* Corresponding author. Tel.: +47 41602417; fax: +47 73595528.
*E-mail address:* biao@ntnu.no (B. Su).

0951-8339/$ – see front matter © 2011 Elsevier Ltd. All rights reserved.
doi:10.1016/j.marstruc.2011.02.008

Please cite this article in press as: Su B, et al., Numerical study of ice-induced loads on ship hulls, Marine Structures (2011), doi:10.1016/j.marstruc.2011.02.008

In an earlier study (Su et al. [1]), a numerical method was introduced by the authors to investigate the global ice load and the ship's performance in level ice. This method is partly based on the empirical data, by which the observed phenomena of continuous icebreaking can be reproduced. In the simulation of an icebreaking run, the interdependence between the ice load and the ship's motion is considered, and the three degree-of-freedom rigid body equations of surge, sway and yaw are solved by numerical integration. The full-scale hull shape of an icebreaker (Tor Viking II) was applied in a specific case study, and the estimated performance of the ship agreed well with the field measurements obtained by Riska et al. [2].

The ice model was then extended to more complex ice conditions by considering random ice thickness and strength properties (Su et al. [3]), with the purpose of identifying the origin of the statistical variation in local ice loads. A case study with an icebreaking tanker (MT Uikku) was performed by comparing the simulated frame loads with the field measurements obtained by Kotisalo and Kujala [4] and Hänninen [5].

In this paper, the method established is applied in the evaluation of: (1) ship's performance in level ice; (2) statistics of ice-induced frame loads; and (3) spatial distribution of ice loads around the hull. As far as we know the present paper is the first to integrate all the features above. It is hoped that further studies on this numerical model can supplement the field and laboratory measurements in establishing a design basis for the ice-going ships especially for ships navigating in the first-year ice.

## 2. Design basis for the ice-going ships

The basic structural design factors for ice-going ships are given in ice class rules, among others the "Finnish–Swedish Ice Class Rules" (FSICR). The design philosophy behind FSICR is based on both operative and safety aspects: the former is to ensure an adequate ship performance; and the latter is to guarantee an adequate strength of the hull and propulsion system. In this section, the practical approach to estimate the ship's performance and the design ice load on ship hull, as well as the design ice conditions are briefly described.

### 2.1. Design ice conditions

At sea the ice conditions may include all possible variants of ice features within one mile distance. The definition of design ice conditions is simplified in FSICR using the equivalent level ice thickness. Analysis of the hull damages caused by ice shows that this definition gives a roughly good estimate on the severity of ice conditions (Riska [6]).

Table 1 gives an example of the long-term data on the winter maximum equivalent level ice thickness in various parts of the Baltic Sea. The effect of ice ridges is included by multiplying the mean level ice thickness with a factor $k_r$ shown also in Table 1. This factor is obtained based on the occurrence probability ($P_r$) of ridges in an ice zone (Kujala [7]).

In FSICR the ships strengthened for navigation in ice are assigned to 4 ice classes: IA Super, IA, IB, and IC (FMA [8]). A maximum level ice thickness for each ice class is defined. This thickness varies linearly between 1.0 m for IA Super to 0.4 m for IC. Ice class IA Super is intended for independent navigation in difficult, but not in extreme Baltic ice conditions, while the other three ice classes are intended for navigation with the assistance of icebreakers when necessary. The selection of ice class should hence be made with the considerations of ice conditions, operational requirements and cost.

**Table 1**
Long-term data on the winter maximum equivalent thickness in various parts of the Baltic Sea (data from Kujala [7]).

| Sea area | Level ice thickness | | Ice ridge effect | | Equivalent ice thickness | |
|---|---|---|---|---|---|---|
| | Mean (m) | Std. (m) | $P_r$ | $k_r$ | Mean (m) | Std. (m) |
| Bothnian Bay | 0.474 | 0.164 | 0.50 | 1.28 | 0.607 | 0.210 |
| Bothnian Sea | 0.414 | 0.153 | 0.25 | 1.21 | 0.501 | 0.185 |
| Gulf of Finland | 0.404 | 0.140 | 0.25 | 1.21 | 0.489 | 0.170 |
| Baltic proper | 0.336 | 0.136 | 0.10 | 1.12 | 0.376 | 0.152 |

Please cite this article in press as: Su B, et al., Numerical study of ice-induced loads on ship hulls, Marine Structures (2011), doi:10.1016/j.marstruc.2011.02.008

### 2.2. Estimation of the ship's performance

The ship's performance in level ice is usually described by the speed ($v$) that the ship can attain in ice of a given thickness ($h$). Fig. 1 shows an example of the $h$–$v$ curves determined from field tests.

An empirical way to calculate the ship's speed in ice is to solve the equation between the net thrust and the ice resistance. The net thrust is the thrust available to overcome the ice resistance after the thrust used to overcome the open water resistance has been taken into account. Thus the net thrust, $T_{net}$, is defined as:

$$T_{net}(v) = T_{tot}(v)(1-t) - R_{ow}(v) \tag{1}$$

where $v$ is the ship's speed, $T_{tot}$ is the total thrust, $t$ is the thrust deduction factor, and $R_{ow}$ is the open water resistance.

In early design and in ice rules (i.e. FISCR) $T_{net}$ has been estimated by (Juva and Riska [9]):

$$T_{net}(v) = \left(1 - \frac{1}{3}\frac{v}{v_{ow}} - \frac{2}{3}\left(\frac{v}{v_{ow}}\right)^2\right)\cdot T_{pull} \tag{2}$$

where $v_{ow}$ is the maximum open water speed, and $T_{pull}$ is the bollard pull.

Research on the ice resistance can be found for example in Enkvist [10], Lewis et al. [11], Varsta [12], Lindqvist [13], Puntigliano [14], Riska et al. [15], and Valanto [16]. In FISCR, the formula of the resistance in a channel with brash ice and a consolidated layer is given, which is derived and modified based on the previous researches. The basic performance requirement for FSICR is a minimum speed of 5 knots in the specified ice channels. The power requirement of the propulsion machinery is thus calculated from the net thrust required to overcome the channel resistance. For an individual ship, the design values based on more exact calculations or model tests may be approved if the ship's parameter values are beyond the range defined in FSICR.

### 2.3. Estimation of the design ice load on ship hull

The ice load is a statistical quantity and thus the design load value must in principle be determined assuming a probability level or return period of the load. The load level in FSICR is, however, determined based on the experience from the hull damages caused by ice.

A more ambitious approach would be to define a certain risk or safety level. The design load value can be given by selecting a return period of occurrence for the load like once per lifetime, once per ice season, or once per voyage. The selected return period of the load must be in balance with the

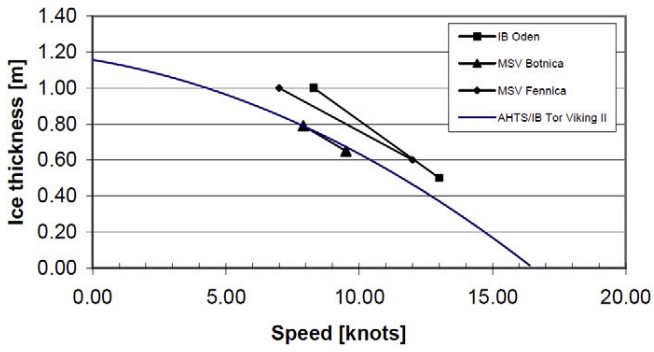


**Fig. 1.** The $h$–$v$ curves determined from the field tests of 4 vessels (reproduced from Riska et al. [2]).

Please cite this article in press as: Su B, et al., Numerical study of ice-induced loads on ship hulls, Marine Structures (2011), doi:10.1016/j.marstruc.2011.02.008

consequences of exceeding the allowable structural responses. This procedure of defining the design points requires thus (Riska [17]):

- Definition of the loads in probabilistic terms;
- Definition of the responses in terms of stresses, elastic deflections or permanent deflections and
- Definition of the limit states in order to ensure a consequent risk implied by the failure of different structural components (e.g. shell plating and frames).

Up to now the main source of ice load statistics is field measurement. Field measurements will continue to be important. However, numerical methods can provide useful information, since they can be easily used to study the effect of different parameters. The purpose of this paper is to establish and apply a numerical method to estimate both global and local ice loads on ships. The ship's performance in level ice and the statistics of ice-induced frame loads are investigated. The spatial distribution of local ice loads around the hull, which is usually difficult to gather by field tests, is also studied in this paper.

## 3. Numerical simulations

Research on the numerical modeling of ice–hull interaction and ship maneuvering in level ice can be found for example in Valanto [16], Martio [18], Liu et al. [19], Nguyen et al. [20], and Sawamura et al. [21]. For the simulation of full-scale icebreaking runs, a more integrated model was developed and improved by Su et al. ([1,3]). In this model the interdependence between the ice loads and the planar motion of the ship is considered. The simulation program is established to reproduce observed icebreaking patterns and the continuous ice loading processes in a uniform level ice and the ice with randomly varying thickness and strength properties. In this section, the numerical model is briefly described.

### 3.1. General description of the model

The methodology and assumptions used in the ice–hull interaction model are:

- The basic geometrical model (as shown in Fig. 2) includes the waterline of the ship and the edge of the ice both discretized;
- The motions (surge, sway and yaw) of the ship on the horizontal plane are taken into account and the icebreaking forces are assumed to act on the waterline;
- The contact zones around the hull and the resulting ice forces and icebreaking patterns are numerically detected based on the empirical estimates of ice crushing force and ice bending failure;
- Ice forces induced after the ice wedges are broken from the ice edge are taken into account by the Lindqvist's ice resistance formula (Lindqvist [13]);
- The hydrodynamic effects on the ship's motion (drag and added mass) are derived from a numerical calculation prior to the real-time simulation in ice (Fig. 3 shows an example of the ship geometry model used in the hydrodynamic calculations);
- Wave, wind and current forces are neglected as they are minor forces compared to ice forces;

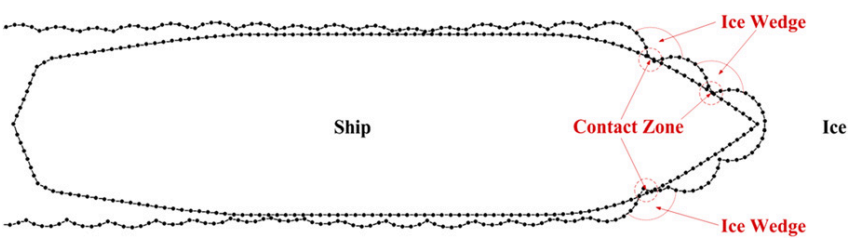


**Fig. 2.** Geometrical idealization of the ice–hull interaction.

Please cite this article in press as: Su B, et al., Numerical study of ice-induced loads on ship hulls, Marine Structures (2011), doi:10.1016/j.marstruc.2011.02.008

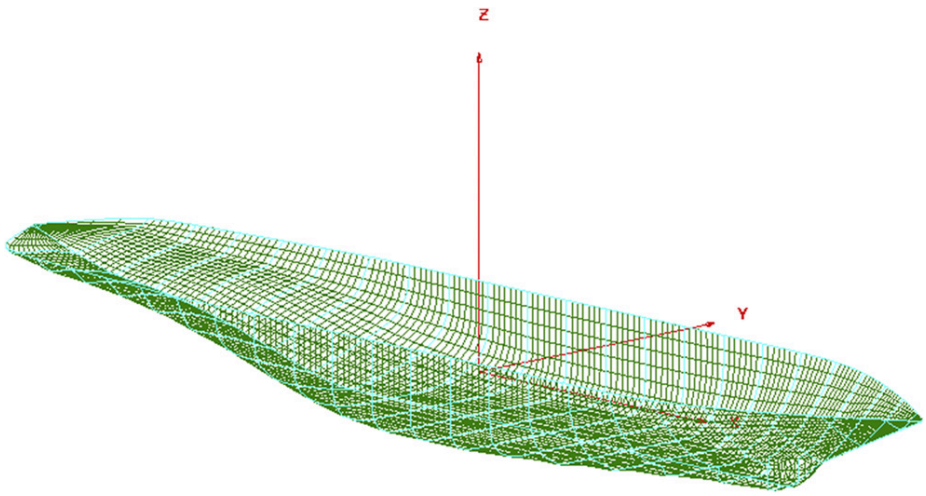


**Fig. 3.** Ship geometry model of Tor Viking II used in the hydrodynamic calculations.

- The rigid-body equations of motion are solved by numerical integration and
- Iterations are performed at each time step, considering the interdependence between the ship's motion and the ice loads.

The detailed description of the methodology can be found in Su et al. [1,3], while the empirical estimates of the ice crushing force, ice bending failure and the statistical variation of the ice properties are mainly described herein.

### 3.2. Ice crushing force

At each contact zone shown in Fig. 2, it is assumed that the ice is uniformly crushed on the contact surface. The crushing force, $F_{cr}$, is normal to the contact surface and calculated as the product of the effective ice crushing strength, $\sigma_c$, and the contact area, $A_c$. Fig. 4 shows the illustration of the contact area between ice and hull, where $\varphi$ is the frame angle, and the ice crushing pressure on the contact surface is assumed to be uniform and equal to the effective ice crushing strength. The frictional force is also taken into account, which is divided into two components, $f_H$ and $f_V$, according to the relative motion between ice and hull (the detailed description can be found in Su et al. [1]). The horizontal and vertical components of the total contact force between ice and hull are then illustrated in Fig. 5.

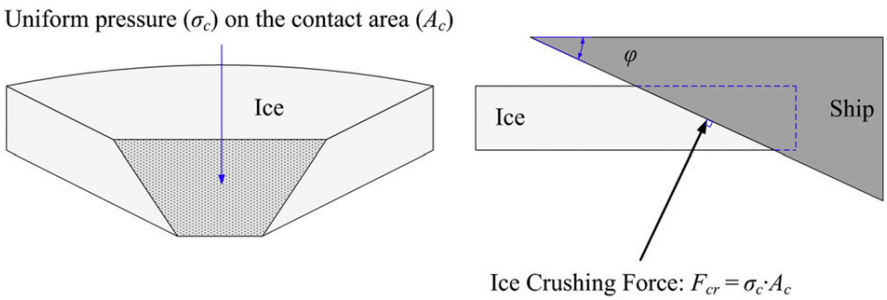


**Fig. 4.** Illustration of the contact area between ice and hull.

Please cite this article in press as: Su B, et al., Numerical study of ice-induced loads on ship hulls, Marine Structures (2011), doi:10.1016/j.marstruc.2011.02.008

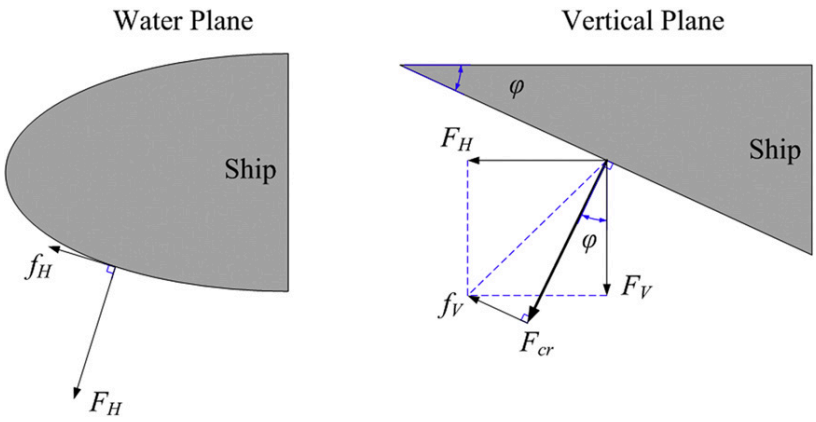


**Fig. 5.** Illustration of horizontal and vertical components of the contact force.

### 3.3. Ice bending failure

If the vertical component of the contact force between ice and hull ($F_V$, shown in Fig. 5) exceeds the bending failure load of ice cover, $P_f$, given in Eq. (3), the ice wedge (as shown in Fig. 2) will be broken from the edge of the ice:

$$P_f = C_f \left(\frac{\theta}{\pi}\right)^2 \sigma_f h_i^2 \tag{3}$$

where $\theta$ is the opening angle of the idealized ice wedge shown in Fig. 6, $\sigma_f$ is the flexural strength of the ice, $h_i$ is the thickness of the ice, and $C_f$ is an empirical parameter. Eq. (3) accounts for the opening angle,

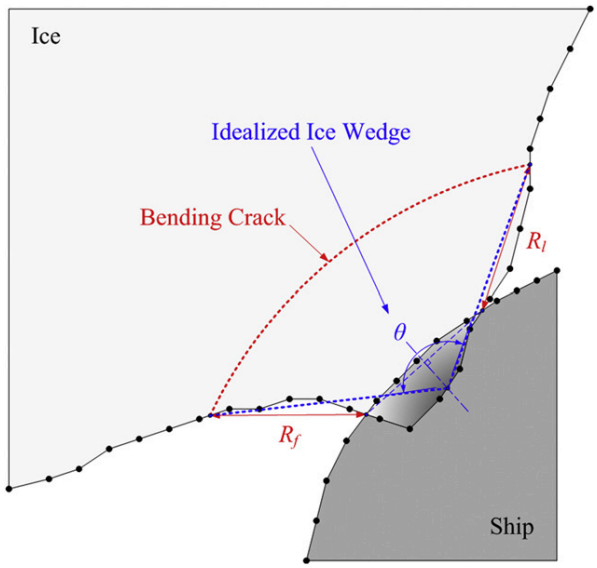


**Fig. 6.** Geometrical idealization of the ice wedge in contact with the hull.

Please cite this article in press as: Su B, et al., Numerical study of ice-induced loads on ship hulls, Marine Structures (2011), doi:10.1016/j.marstruc.2011.02.008

and it is an empirical equation (introduced by Kashtelyan (Kerr [22]), applied in Wang [23], Liu et al. [19], and Nguyen et al. [20]). Thus, the constant $C_f$ must be obtained from measurements.

The geometrical idealization of the ice wedge in contact with the hull is illustrated in Fig. 6, where the bending crack is determined by the interpolation of the icebreaking radius at the first and last contact node (i.e., $R_f$ and $R_l$). The icebreaking radius $R$ is found by the expression given in Wang [23] (based on information from Enkvist [10] and Varsta [12]):

$$R = C_l l\left(1.0 + C_v v_n^{rel}\right) \tag{4}$$

where $v_n^{\mathrm{rel}}$ is the relative normal velocity between the ice and the hull node, $C_l$ and $C_v$ are two empirical parameters obtained from field measurements, and $l$ is the characteristic length of the ice:

$$l = \left(\frac{Eh_i^3}{12(1-\nu^2)\rho_w g}\right)^{1/4} \tag{5}$$

Based on these assumptions and simplifications, the icebreaking pattern and the continuous icebreaking forces can be determined using a step-by-step procedure with a time step, $\Delta t$, equal to 0.001 s. The effects of the empirical parameters (in Eqs. (3) and (4)) on the mean icebreaking force were investigated and compared with the Lindqvist's ice resistance (Lindqvist [13]) in Su et al. [1]. It was found in Su et al. [3] that the variation in simulated local ice loads was noteworthy even if the ice properties (ice thickness and ice strength) were fixed. Thereafter the variation in the contact and icebreaking patterns was taken as an internal origin of the statistical variation in local ice loads, other than the external ice conditions.

### 3.4. Statistical variation of the ice properties

To reflect more complex ice conditions encountered in natural ice cover, the thickness and strength properties of the ice encountered by the ship can be randomly generated using the Monte Carlo method. Fig. 7 shows a random sample of the varying ice properties along a 10 km route, where it is

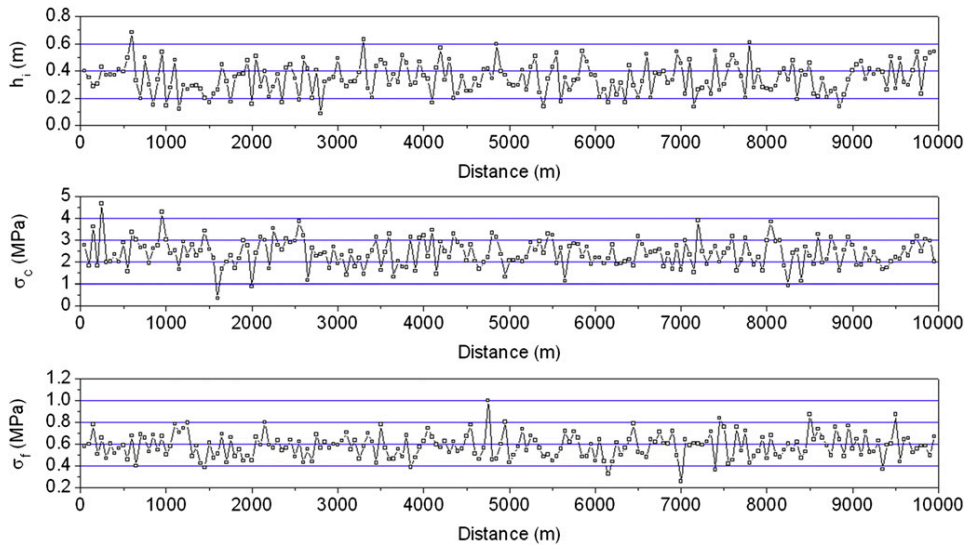


**Fig. 7.** A random sample of the varying ice properties along a 10 km route.

Please cite this article in press as: Su B, et al., Numerical study of ice-induced loads on ship hulls, Marine Structures (2011), doi:10.1016/j.marstruc.2011.02.008

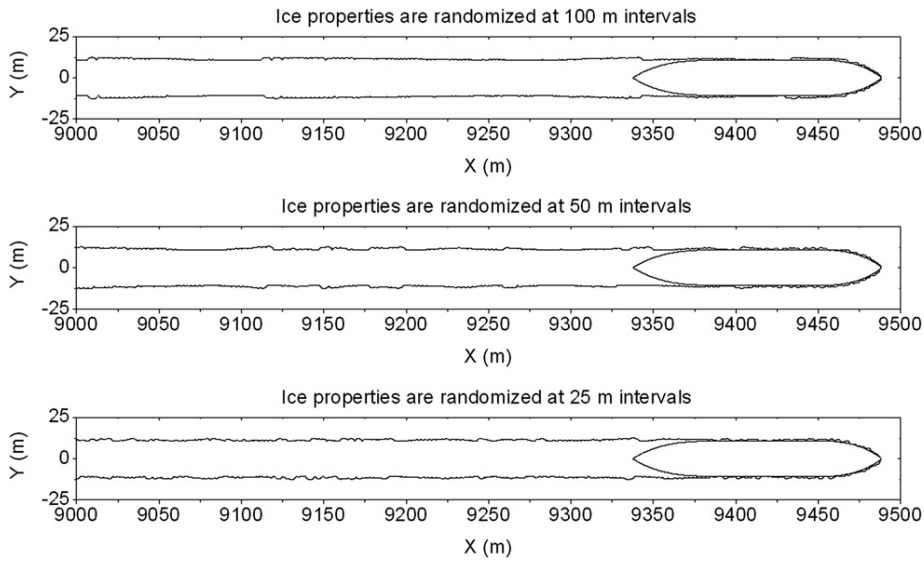


**Fig. 8.** Simulated icebreaking runs under randomly varying ice conditions.

assumed that the ice thickness, ice crushing strength and ice flexural strength follow a normal probability distribution and they are independent on each other.

The existing data on the correlation of the spatial ice properties are very limited. The sensitivity of a possible correlation can be investigated by sampling the properties at the spatial points at different intervals. Fig. 8 shows three simulated icebreaking runs in which the ice properties are randomized at different intervals (25, 50 and 100 m). The issues of correlation were briefly discussed in Su et al. [3], and it remains one of the topics for further analysis.

## 4. Ship's performance in level ice

A case study with an icebreaker, Tor Viking II, was carried out to investigate the total ice load and the ship's performance in level ice (the detailed descriptions can be found in Su et al. [1] and Su et al. [24]). In this study, the ice encountered by the ship was assumed to be uniform. The material characteristics of the ice are defined by the constants listed in Table 2. The main dimensions of Tor Viking II are presented in Table 3.

In the simulation with a free-running model, the ship's motion was obtained by solving the equations of motion in which the thrust and the global ice load both were identified. The speed that the ship can attain was then simulated in the ice of different thicknesses. As shown in Fig. 9, the simulated results agree well with the full-scale measurements (Riska et al. [2]). Fig. 10 shows a simulated turning

**Table 2**
Constant ice properties used in the simulations.

| | |
|---|---|
| Density | 880 kg/m$^3$ |
| Young's modulus | 5400 MPa |
| Poisson ratio | 0.33 |
| Crushing strength | 2.30 MPa |
| Flexural strength | 0.55 MPa |
| Frictional coefficient | 0.15 |

Please cite this article in press as: Su B, et al., Numerical study of ice-induced loads on ship hulls, Marine Structures (2011), doi:10.1016/j.marstruc.2011.02.008

**Table 3**
Main dimensions of Tor Viking II.

| | |
|---|---|
| Length overall | 83.7 m |
| Length between perpendiculars | 75.2 m |
| Breadth molded | 18.0 m |
| Draft | 6.5 m |
| Displacement | 5790 ton |
| Power output | 13.4 MW |

circle in level ice, where $D_t$ denotes the turning circle diameter which is a measure of the ship's maneuverability in ice. As shown in Fig. 11, the simulated values of turning circle diameter are also comparable to the measurements. Herein the deviation between the simulated results is due to the different icebreaking patterns. As discussed in Su et al. [1,24], if the shoulder crushing happens (i.e. the ice is continuously crushed by the hull shoulder without bending failure) both the forward speed and the turning rate of the ship will be considerably slowed down (see e.g. the simulated results in 1.0 m thick ice).

Through this case study, it can be expected that the numerical simulation can supplement full-scale tests to know more about: (1) the ship' performance in very severe ice conditions; (2) the influence of hull form and the icebreaking pattern on the ship's performance; and (3) the sensitivity of the ship' performance to various environmental parameters. These factors are closely linked to the overall design of ice-going ships.

## 5. Statistics of ice-induced frame loads

A case study with an icebreaking tanker, MT Uikku, was carried out to investigate the local ice load (the detailed descriptions can be found in Su et al. [3]). In this study, the thickness and strength properties of the ice encountered by the ship were assumed to be constant or randomly generated using the Monte Carlo method. The statistical data on the strength properties of Baltic Sea ice (given in Table 4, data from Kujala [7]) were applied in this simulation. The main dimensions of MT Uikku are presented in Table 5.

The ice-induced frame loads (see e.g. Fig. 12) were analyzed using the line load on the frame. This was obtained by dividing the normal force on the frame by the frame spacing (0.35 m), the units are thus in kN/m. As shown in Fig. 13, a frame on the bow area (frame 196.5) and another frame on the bow

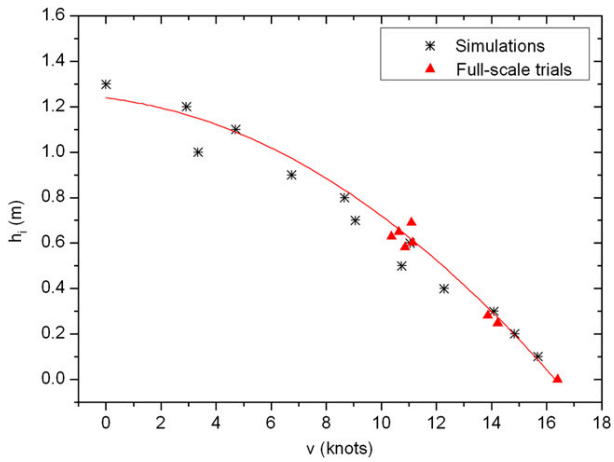


**Fig. 9.** Comparison of the $h$–$v$ curve between the present simulations and full-scale trials presented by Riska et al. [2].

Please cite this article in press as: Su B, et al., Numerical study of ice-induced loads on ship hulls, Marine Structures (2011), doi:10.1016/j.marstruc.2011.02.008

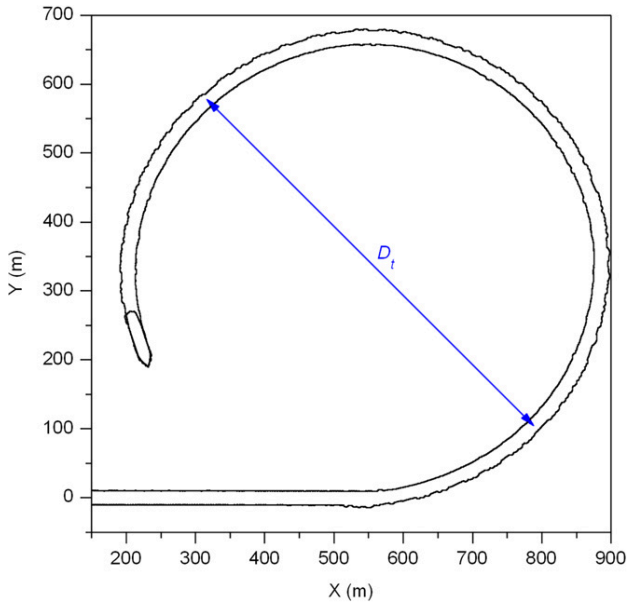


**Fig. 10.** A simulated turning circle in level ice.

shoulder area (frame 175.5) were selected for this study. The simulated results were then compared with the field measurements obtained by Kotisalo and Kujala [4] and Hänninen [5].

Fig. 14 shows a 10-min time history of simulated ice loads on frame 196.5, where the ice properties were uniform, the uniform ice thickness was 0.300 m, and the average ship speed is 5.43 m/s. It can be found that the simulated ice loading process varies with time even if the ice properties (ice thickness and ice strength) are fixed. This is due to the variation in the contact and icebreaking patterns (as discussed in Su et al. [3]).

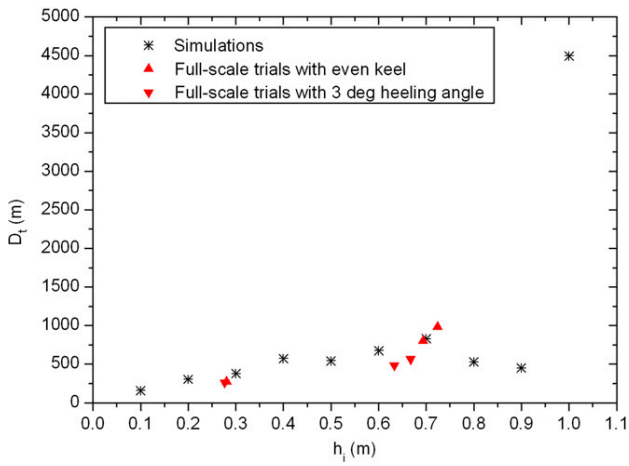


**Fig. 11.** Comparison of the turning circle diameter between the present simulations and full-scale trials presented by Riska et al. [2].

Please cite this article in press as: Su B, et al., Numerical study of ice-induced loads on ship hulls, Marine Structures (2011), doi:10.1016/j.marstruc.2011.02.008

**Table 4**
Statistical data on the ice strength properties used in the simulations.

| | Mean (MPa) | Std. (MPa) |
|---|---|---|
| Crushing strength | 2.30 | 0.65 |
| Flexural strength | 0.58 | 0.11 |

Fig. 15 shows a 10-min time history of simulated ice loads on frame 196.5, where the ice properties were randomly sampled along the route, the average ice thickness was 0.125 m (with a standard deviation of 0.0625 m), and the average ship speed is 5.43 m/s. The simulated ice loading process has a clear stochastic nature due to variations in the ice conditions and in the contact and icebreaking patterns. Fig. 16 shows a 10-min time history of measured ice loads on frame 196.5, where the measurement was performed during the ARCDEV voyage (Kotisalo and Kujala [4]) under various ice conditions. As shown by these two figures, the simulated ice loading history is comparable to the measurements even though the actual ice conditions in field may be much more complex than the level ice (with varying thickness and strength properties) simulated here.

Individual ice loads need to be separated when studying the ice load statistics. The Rayleigh separation method (as introduced in Vuorio et al. [25] and Kujala et al. [26]) was used in this paper to identify the peak loads within a certain time interval (i.e. 10 min). Fig. 17 shows an example of the distribution of measured peak loads on frame 196.5, which is plotted in the form of logarithmic histogram (data from Hänninen [5]). This measurement was performed in a thin level ice condition, where the average ice thickness is 0.125 m, the average ship speed is 5.55 m/s, and the time interval is 10 min. The same scenario was applied to the simulations. Fig. 18 shows the distribution of simulated peak loads on frame 196.5, which were obtained from three simulated icebreaking runs. As shown by these two figures, the simulated distribution form is similar to the measured one, except for the very low peak loads (less than 40 kN/m). This is because in field measurements numerous of small peaks might be induced by the electronic noise, open water and brash ice, which were not included in the simulated frame loads. It is found that the simulated load maxima in the 10 min time interval are comparable to the measured value, and the variation of simulated load maxima is due to the scatter of sampled ice properties and the variation in the contact and icebreaking patterns.

Ice conditions vary in the short term from voyage to voyage and in the long term from winter to winter. The short-term ice load statistics can be evaluated based on short-term simulations (as discussed in Su et al. [3]), while the evaluation of long-term ice loads should be combined with the long-term statistics of ice conditions. Empirical studies show that the best correlation between the measured winter maximum load values and the prevailing ice conditions in the Baltic Sea is obtained by using an equivalent level ice thickness (see e.g. Table 1) to describe the annual ice conditions instead of parameters such as the maximum ice extent, fast or pack ice thickness (Kujala [27]). Accordingly the long-term ice loads can be evaluated based on the long-term statistics of equivalent ice thickness. A simple example is given below to indicate the probable correlation between the extreme ice load, $w$, and the winter maximum equivalent ice thickness, $h_e$.

Firstly, 50 different values of $h_e$ were randomly generated by assuming that $h_e$ follows a normal probability distribution with the parameters defined in Table 1. As the long-term data of $h_e$ are given in various parts of the Baltic Sea, the operational profile of the ship should be taken into account. For the

**Table 5**
Main dimensions of MT Uikku.

| | |
|---|---|
| Length overall | 164.4 m |
| Length between perpendiculars | 150.0 m |
| Breadth molded | 22.2 m |
| Draft | 12.0 m |
| Displacement | 22,600 ton |
| Power output | 11.4 MW |

Please cite this article in press as: Su B, et al., Numerical study of ice-induced loads on ship hulls, Marine Structures (2011), doi:10.1016/j.marstruc.2011.02.008

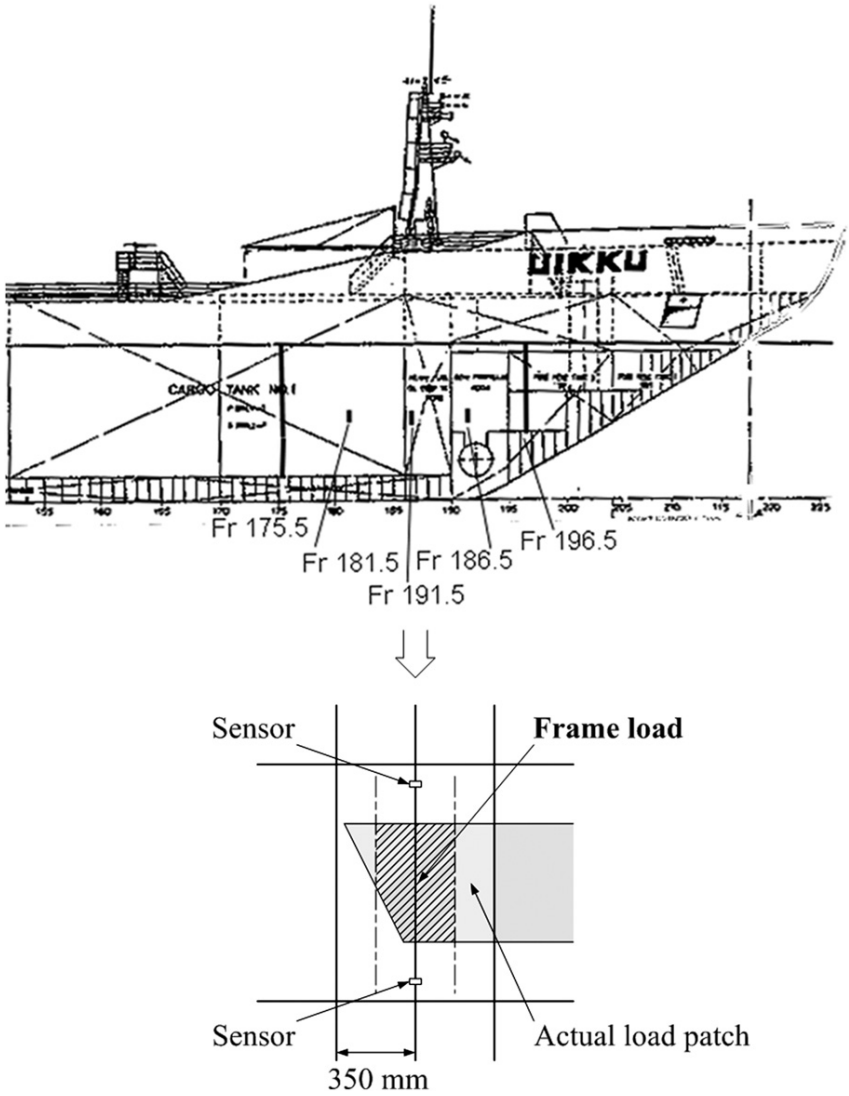


**Fig. 12.** A side view of MT Uikku (bow area).

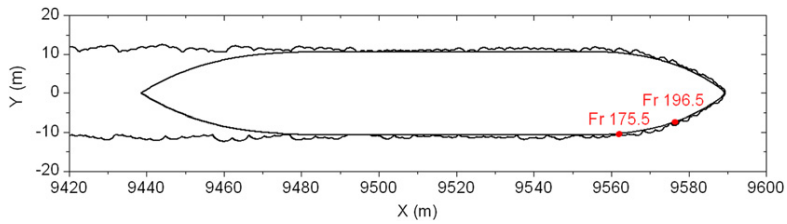


**Fig. 13.** Two frames selected for this study.

Please cite this article in press as: Su B, et al., Numerical study of ice-induced loads on ship hulls, Marine Structures (2011), doi:10.1016/j.marstruc.2011.02.008

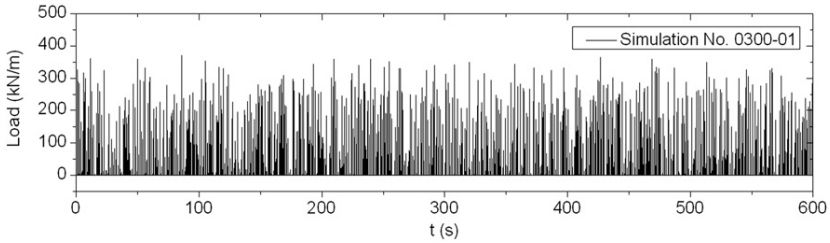


**Fig. 14.** A 10-min time history of simulated ice loads on frame 196.5 (uniform ice thickness: 0.300 m, average ship speed: 5.67 m/s).

purpose of simplification, only a given vessel (MT Uikku) and a given ice zone (Bothnian Bay) were considered in this example.

A 10-min voyage was then simulated for each deterministic value of $h_e$. The full propulsion power was used in each voyage and the ice strength properties, $\sigma_c$ and $\sigma_f$, were sampled along the route (see e.g. Fig. 7) by assuming that they are normally distributed and independent of $h_e$. The simulated maximum load in a 10-min voyage was then identified as an extreme ice load, $w$, which was combined with a winter maximum equivalent ice thickness, $h_e$. In the ice of a certain high thickness, the ship may get stuck and a specific frame may rarely be in contact with ice (as discussed in Su et al. [3]). The results from such samples are not included in the statistics.

Fig. 19 shows the simulated load maxima on frame 196.5 as a function of $h_e$. This result agrees with empirical studies (Kujala [27]), that the frame load $w$ increases almost linearly with the increasing value of $h_e$. The scatter of $w$ is due to the variations in sampled ice strength properties and in the contact and icebreaking patterns.

The long-term measurements indicate that a Gumbel I asymptotic extreme value distribution fits well on the measured extreme values of ice load (Vuorio et al. [25], Kujala and Vuorio [28], Kujala [29]). Fig. 20 shows the fitted distribution on simulated load maxima, as plotted on Gumbel paper. Fig. 21 shows the cumulative distribution of $w$ which is plotted as a function of the return period. As the long-term variation of winter maximum equivalent ice thickness is included in the statistics, this plot to a certain extent reflects the long-term variation of ice loads. If the operating time under the winter maximum ice conditions has been defined for a given ship, then this plot can be used for a preliminary prediction of the most probable extreme ice loads by extrapolating the fitted distribution to a certain period.

This example shows a simplified approach to estimate the long-term ice loads utilizing short-term simulations. It is based on the long-term statistics of winter maximum equivalent ice thickness. If the long-term statistics of the ice thickness encountered by a ship other than the winter maximum are known, then a refined approach for this estimation would be to define a conditional cumulative distribution function, $F_{W|H_i}(w|h_i)$, which can be determined by fitting a probability distribution on the

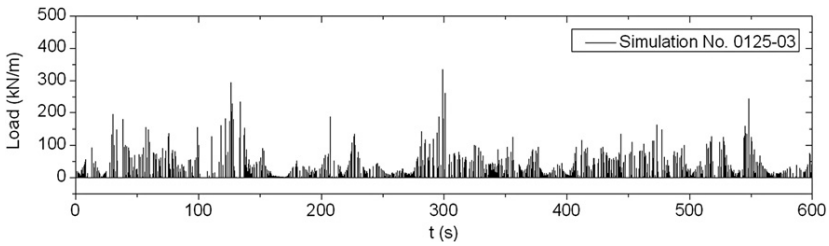


**Fig. 15.** A 10-min time history of simulated ice loads on frame 196.5 (average ice thickness: 0.125 m, average ship speed: 5.43 m/s).

Please cite this article in press as: Su B, et al., Numerical study of ice-induced loads on ship hulls, Marine Structures (2011), doi:10.1016/j.marstruc.2011.02.008

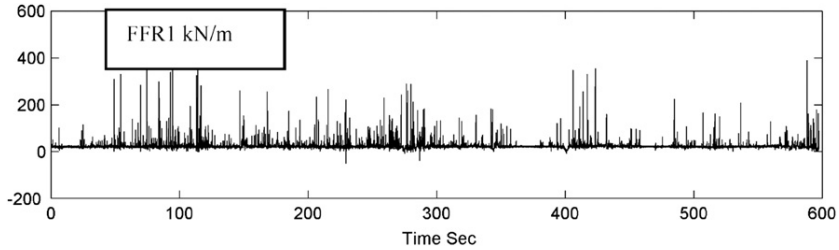


**Fig. 16.** A 10-min time history of measured ice loads on frame 196.5 (reproduced from Kotisalo and Kujala [4], different types of ice conditions).

simulated values of $w$ in the ice of randomly varying strength properties and a certain thickness, $h_i$. The long-term cumulative distribution function of extreme ice loads can then be obtained by integrating over the long-term statistics of $h_i$:

$$F_W(w) = \int_0^\infty F_{W|H_i}(w|h_i) f_{H_i}(h_i) dh_i \tag{6}$$

where $f_{H_i}(h_i)$ is the long-term probability density function of $h_i$. Up to now the operating time under the winter maximum ice conditions and the long-term statistics of the ice thickness are not well defined for a given ship navigating in a given ice zone. Specific data are needed for further studies.

## 6. Spatial distribution of ice loads around the hull

The origins of ice loads on different hull areas are different. When the ship proceeds straight ahead, only the bow waterline is breaking ice. Other areas of the hull encounter hits from broken ice pieces. The midship and aft areas can break ice when the ship is maneuvering (e.g. turning) or going astern. As the ice loads on different hull areas are of different origins, it is clear that the magnitudes of the loads are also different. This is taken into account in most ice rules by dividing the ship hull into regions and giving so called hull area factor for each region.

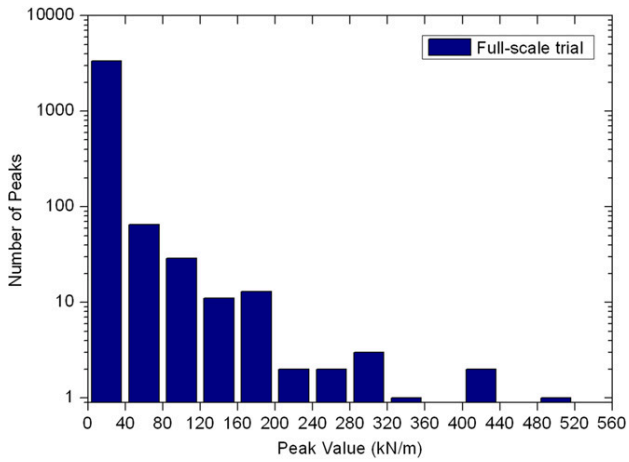


**Fig. 17.** Distribution of the peak loads on frame 196.5, measured in a 10 min full-scale trial (data from Hänninen [5], average ice thickness: 0.125 m).

Please cite this article in press as: Su B, et al., Numerical study of ice-induced loads on ship hulls, Marine Structures (2011), doi:10.1016/j.marstruc.2011.02.008

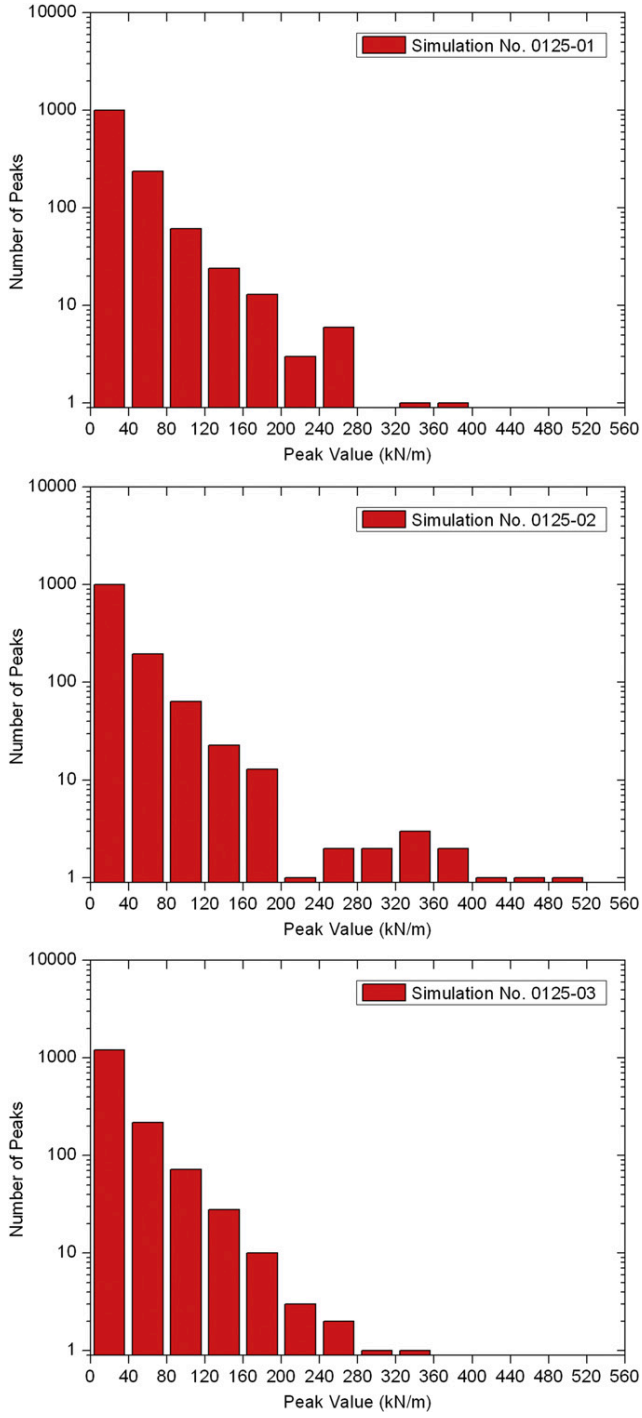


**Fig. 18.** Distribution of the peak loads on frame 196.5, obtained from three simulated icebreaking runs (average ice thickness: 0.125 m).

Please cite this article in press as: Su B, et al., Numerical study of ice-induced loads on ship hulls, Marine Structures (2011), doi:10.1016/j.marstruc.2011.02.008

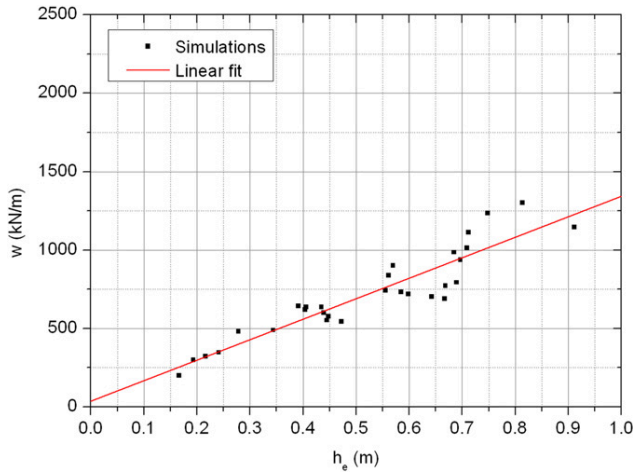


**Fig. 19.** Simulated load maxima on frame 196.5 as a function of $h_e$.

In FSICR the ship hull is divided into forward, midship and aft regions, among which the forward region (bow) has the highest hull area factor (i.e. 1.0). This is because the dominant operational mode of a ship is moving straight ahead. Accordingly the long-term ice loads at the bow should be considerably higher than the short-term ice loads. The load level defined in the ice rules of course need to reflect the long-term ice loads. But it has been suggested by the model tests (Izumiyama [30]) and numerical calculations (Valanto [31]) that in turning operation the ice loads at aft shoulder are pronounced and may be higher than at the bow area. Thus for the aft shoulder, the safety reserve in the ice rules may be lower than elsewhere. Information on the spatial distribution of local ice loads around the hull can thus be used for more reliable design of the ship which is intended to have a good turning ability in ice.

As shown in Fig. 22, thirty frames on different hull areas of MT Uikku were selected at 10 m intervals, and the frame spacing was assumed to be same and equal to 0.35 m on each hull area. The

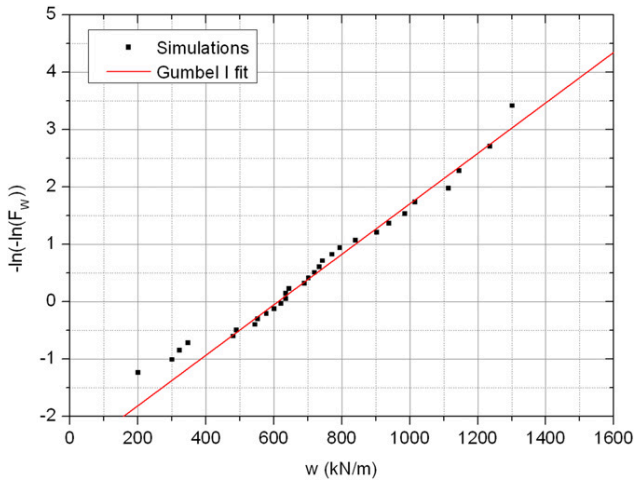


**Fig. 20.** The cumulative distribution of simulated load maxima on frame 196.5, as plotted on Gumbel paper.

Please cite this article in press as: Su B, et al., Numerical study of ice-induced loads on ship hulls, Marine Structures (2011), doi:10.1016/j.marstruc.2011.02.008

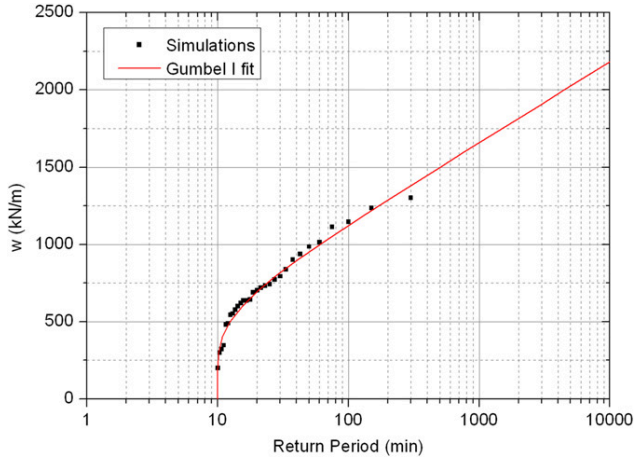


**Fig. 21.** The cumulative distribution of simulated load maxima on frame 196.5, which is plotted as a function of the return period.

spatial distribution of local ice loads was then investigated in both straight going and turning operations.

Figs. 23 and 24 show the simulated time histories of the ice-induced frame loads on two different hull areas when the ship was turning with a 30° steering angle (of the Azipod propulsion system). Since the spatial variation of local ice loads around the hull was investigated in this simulation, the thickness and strength properties of the ice were thus assumed to be uniform. The frame in Fig. 23 is at the bow, the simulated ice loads on bow frames are similar in both straight going and turning operations. As shown in Fig. 23, the simulated ice loading process consists of numerous short duration spike-like peaks. It is quite similar to the normal pattern of local ice loads obtained from full-scale trials which are usually performed in straight going mode. The frame in Fig. 24 is at aft shoulder, where the ice loading history is quite different from the bow frames. This is because the frame at aft shoulder is close to vertical, accordingly the ice edge in the outside of the turning circle (the starboard side shown in Fig. 22) would be continuously crushed by the aft shoulder without bending failure. In this situation, the band-like load peaks may occur, and the mean ice load may increase considerably. It should be noted that the mean ice load may be overestimated, as the buckling or shearing failure of the ice is neglected in this simulation while it occasionally takes place in practice.

The peak values with a non-exceedance probability of 99% (refer to Izumiyama et al. [32]) and the time averages (mean ice loads) were then derived from the ice loading histories. Fig. 25 shows the spatial variation of simulated peak loads on frames around the hull. Three different steering angles (5, 15 and 30°) were used for the simulation of turning operations, all of them would result in high

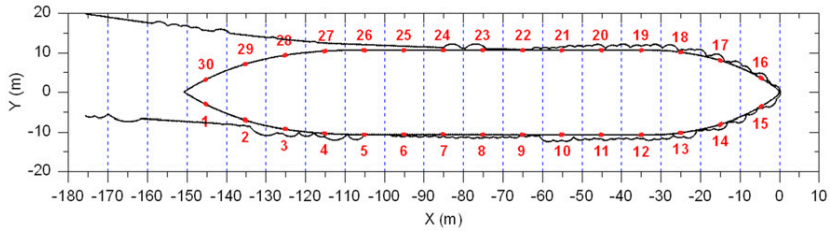


**Fig. 22.** Numbering of the frames on different hull areas of MT Uikku.

Please cite this article in press as: Su B, et al., Numerical study of ice-induced loads on ship hulls, Marine Structures (2011), doi:10.1016/j.marstruc.2011.02.008

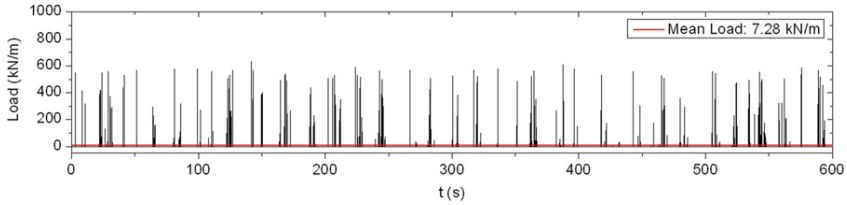


**Fig. 23.** A simulated time history of the local ice loads on frame 13 (uniform ice thickness: 0.34 m, steering angle: 30°).

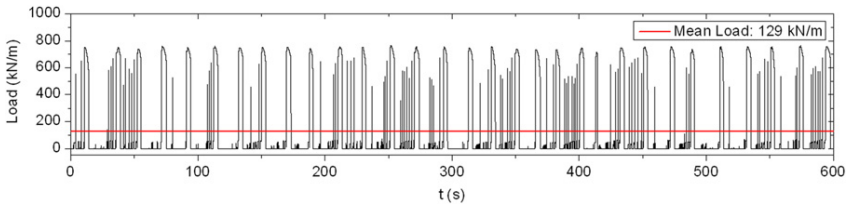


**Fig. 24.** A simulated time history of the local ice loads on frame 5 (uniform ice thickness: 0.34 m, steering angle: 30°).

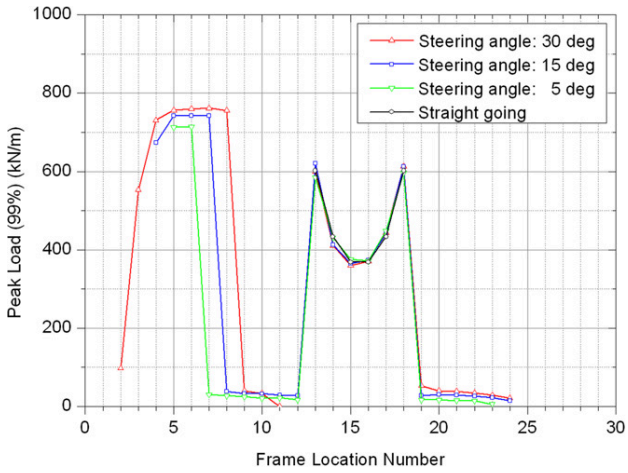


**Fig. 25.** Spatial distribution of simulated peak loads around the hull (uniform ice thickness: 0.34 m).

loads at aft shoulder, which means frames at the aft shoulder of MT Uikku may be equally or even more vulnerable to ice damage as compared to frames on the bow area, when this ship is turning in a considerably severe ice condition. It is also found that the steering angle has only a slight influence on the magnitude of high peak load at the aft shoulder, while it has a significant influence on the number of frames which are under this high load level. Fig. 26 shows the spatial variation of simulated mean ice loads on frames around the hull. Herein the steering angle has a significant influence on the magnitude of the mean ice load at aft shoulder, and this magnitude can be much higher than that at the bow. It

Please cite this article in press as: Su B, et al., Numerical study of ice-induced loads on ship hulls, Marine Structures (2011), doi:10.1016/j.marstruc.2011.02.008

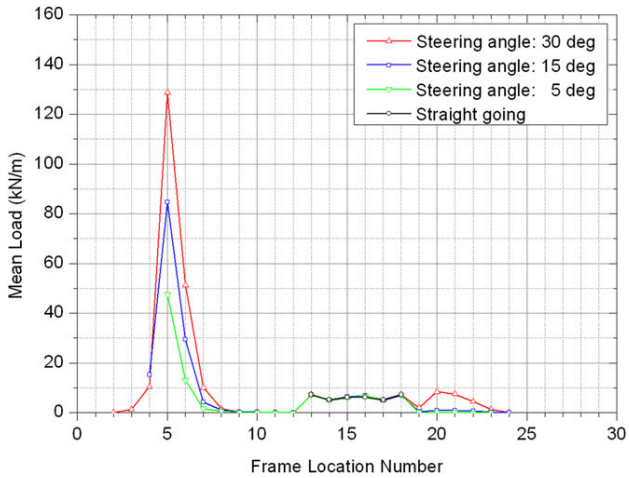


**Fig. 26.** Spatial distribution of simulated mean ice loads around the hull (uniform ice thickness: 0.34 m).

means that in turning operations the aft shoulder of MT Uikku may encounter much heavier turning resistance as compared with the bow area.

The spatial variation of both peak loads and mean loads analyzed above are dependent on the different frame angles around the hull, as well as the shape of ship waterline. MT Uikku is an ice-breaking tanker which has a larger length to beam ratio than conventional icebreaking ships (e.g. Tor Viking II). This hull form may develop high loads at aft shoulder. In a straight going test, e.g. the ARCDEV voyage in the Kara Sea (Kotisalo and Kujala [4]), the measured load maximum at bow shoulder was about 50% higher than at the bow. As shown in Fig. 25 (frames 13 to 15, and frames 16 to 18), the simulated variation is quite close to this value. It can be expected that most other ice formations, than the level ice simulated here, existing in the field would cause a similar load distribution form along the hull, even if the actual magnitude of the ice loads may be very different (Valanto [31]).

It is expensive and technically difficult to perform the ice load measurements around a wide hull area (such as that shown in Fig. 22) in field tests. The numerical simulation can thus compensate the shortage of field data to know more about: (1) the influence of hull form and the operational mode on the high load distributions around the hull; (2) the influence of hull form and the operational mode on the operating resistance encountered by different hull regions; and (3) the influence of ice failure mode and the icebreaking pattern on the operating resistance encountered by different hull regions. These factors are linked to the design of ice-going ships both in terms of overall operation and from the structural point of view.

## 7. Conclusions

(1) Empirical data are used in this numerical model to estimate the bearing capacity and the breaking length of a floating ice wedge. Empirical models for these predictions are based on the assumption that the ice cover acts as an elastic, homogeneous, isotropic plate on an elastic foundation. Further studies on this issue would be beneficial to improve the model.
(2) The observed phenomena of icebreaking can be well reproduced by the numerical method. The influence of global ice load on the ship's performance compares well with the full-scale measurements.
(3) The simulated ice loading histories on a frame are comparable to the full-scale measurements, the distributions of load peaks are similar to the measured statistical distributions. The long-term ice loads can be estimated based on the long-term statistics of ice conditions.

Please cite this article in press as: Su B, et al., Numerical study of ice-induced loads on ship hulls, Marine Structures (2011), doi:10.1016/j.marstruc.2011.02.008

(4) The simulated spatial variation of local ice loads around the hull agrees with previous experimental and numerical studies, that the turning operation may develop a high load level on the aft shoulder area.

The present studies are closely linked to the design basis for ice-going ships. It is indicated that the hull form, the operational mode, the icebreaking pattern and ice failure mode influence both global and local ice loads encountered by the ship. Further studies of these issues are planned, as well as the improvement of this numerical model by integrating the heave, roll and pitch motions of the ship and refining the ice forces induced after the ice pieces are broken by the hull.

## Acknowledgments

The authors wish to acknowledge the support of the Research Council of Norway through the Centre for Ships and Ocean Structures at the Norwegian University of Science and Technology in Trondheim, Norway.

## References

[1] Su B, Riska K, Moan T. A numerical method for the prediction of ship performance in level ice. Cold Regions Science and Technology 2010;60:177–88.
[2] Riska K, Leiviskä T, Nyman T, Fransson L, Lehtonen J, Eronen H, et al. Ice performance of the Swedish multi-purpose icebreaker Tor Viking II. In: 16th POAC international conference on port and ocean engineering under Arctic conditions; 2001. Ottawa, Ontario, Canada.
[3] Su B, Riska K, Moan T. Numerical simulation of local ice loads in uniform and randomly varying ice conditions. Cold Regions Science and Technology 2011;65:145–59.
[4] Kotisalo K, Kujala P. Analysis of ice load measurements onboard MT Uikku – results from the ARCDEV-voyage to Ob-bay, April–May 1998. Report No. D-50. Finland: Ship Laboratory, Helsinki University of Technology; 1999.
[5] Hänninen S. Ship based observations on board MT Uikku during the winter 2003; November 2003. Report for Deliverable D8 of IRIS Project.
[6] Riska K. Definition of ice loading for the Finnish–Swedish ice class rules; October 2007. Report for Deliverable D7–2 of SAFEICE Project.
[7] Kujala P. On the statistics of ice loads on ship hull in the Baltic. Mechanical Engineering Series No. 116. Finland: Ship Laboratory, Helsinki University of Technology; 1994.
[8] Fma. Finnish–Swedish ice class rules. Finnish Maritime Administration Bulletin; 2008. No. 10/10.12.2008.
[9] Juva M, Riska K. On the power requirement in the Finnish–Swedish ice class rules. Research Report No. 47. Finland and Sweden: Winter Navigation Research Board; 2002.
[10] Enkvist E. On the ice resistance encountered by ships operating in the continuous mode of icebreaking. Report No.24. Helsinki, Finland: Swedish Academy of Engineering Science in Finland; 1972.
[11] Lewis JW, DeBord FW, Bulat VA. Resistance and propulsion of ice-worthy ships. Transactions of SNAME, USA; 1982.
[12] Varsta P. On the mechanics of ice load on ships in level ice in the Baltic Sea. Publications 11. Espoo, Finland: Technical Research Centre of Finland; 1983.
[13] Lindqvist G. A straightforward method for calculation of ice resistance of ships. In: 10th POAC international conference on port and ocean engineering under Arctic conditions; 1989. Lulea, Sweden.
[14] Puntigliano FM. On the ship resistance under the design waterline in the continuous mode of icebreaking in level ice. In: 16th OMAE international conference on offshore mechanics and Arctic engineering; 1997. Yokohama, Japan.
[15] Riska K, Wilhelmson M, Englund K, Leivisk T. Performance of merchant vessels in the Baltic. Research Report No. 52. Finland and Sweden: Winter Navigation Research Board; 1997.
[16] Valanto P. The resistance of ships in level ice. Transactions of SNAME 2001;109:53–83.
[17] Riska K. Application of the SAFEICE Project results in developing the Finnish–Swedish ice class rules; December 2007. Report for Deliverable D7–3 of SAFEICE Project.
[18] Martio J. Numerical simulation of vessel's maneuvering performance in uniform ice. Report No. M-301. Finland: Ship Laboratory, Helsinki University of Technology; 2007.
[19] Liu JC, Lau M, Williams FM. Mathematical modeling of ice-hull interaction for ship maneuvering in ice simulations. In: 7th ICETECH international conference and exhibition on performance of ships and structures in ice; 2006. Banff, Alberta, Canada.
[20] Nguyen DT, Sørbø AH, Sørensen AJ. Modeling and control for dynamic positioned vessels in level ice. In: 8th conference on manoeuvring and control of marine craft; 2009. Guarujá, Brazil.
[21] Sawamura J, Tsuchiya H, Tachibana T, Osawa N. Numerical modeling for ship maneuvering in level ice. In: 20th IAHR international symposium on ice; 2010. Lahti, Finland.
[22] Kerr AD. The bearing capacity of floating ice plates subjected to static or quasi-static loads, a critical survey. Research Report No. 333. Hanover, New Hampshire, USA: Cold Regions Research and Engineering Laboratory; 1975.
[23] Wang S. A dynamic model for breaking pattern of level ice by conical structures. Ph.D. thesis. Finland: Department of Mechanical Engineering, Helsinki University of Technology; 2001.
[24] Su B, Riska K, Moan T. Numerical simulation of ship turning in level ice. In: 29th OMAE international conference on offshore mechanics and Arctic engineering; 2010. Shanghai, China.

Please cite this article in press as: Su B, et al., Numerical study of ice-induced loads on ship hulls, Marine Structures (2011), doi:10.1016/j.marstruc.2011.02.008

[25] Vuorio J, Riska K, Varsta P. Long term measurements of ice pressure and ice-induced stresses on the icebreaker Sisu in winter 1978. Research Report No. 28. Finland and Sweden: Winter Navigation Research Board; 1979.
[26] Kujala P, Suominen M, Riska K. Statistics of ice loads measured on MT Uikku in the Baltic. In: 20th POAC international conference on port and ocean engineering under Arctic conditions; 2009. Lulea, Sweden.
[27] Kujala P. Semi-empirical evaluation of long term ice loads on a ship hull. Marine Structures 1996;9:849–71.
[28] Kujala P, Vuorio J. Results and statistical analysis of ice load measurements on board icebreaker Sisu in winters 1979 to 1985. Research Report No. 43. Finland and Sweden: Winter Navigation Research Board; 1986.
[29] Kujala P. Results of long-term measurements on board chemical tanker Kemira in the Baltic Sea during the winters 1985 to 1988. Research Report No. 47. Finland and Sweden: Winter Navigation Research Board; 1989.
[30] Izumiyama K. Description of local ice loading and hull area factors based on model test results; 2005. Report for Deliverable D3–1 of SAFEICE Project.
[31] Valanto P. Spatial distribution of numerically predicted ice loads on ship hulls in level ice; May 2007. Report for Deliverable D6–3 of SAFEICE Project.
[32] Izumiyama K, Wako D, Shimoda H, Uto S. Ice load measurement on a model ship hull. In: 18th POAC international conference on port and ocean engineering under Arctic conditions; 2005. Potsdam, New York, USA.

Please cite this article in press as: Su B, et al., Numerical study of ice-induced loads on ship hulls, Marine Structures (2011), doi:10.1016/j.marstruc.2011.02.008

# Paper 5

# Numerical simulation of ships operating in level ice

Biao Su, Kaj Riska and Torgeir Moan

Submitted to 21st International Conference on Port and Ocean Engineering under Arctic Conditions (POAC 2011), Montreal, Canada

POAC'11
Montréal, Canada

Proceedings of the 21st International Conference on
**Port and Ocean Engineering under Arctic Conditions**
**July 10-14, 2011**
**Montréal, Canada**

POAC11-163

# Numerical Simulation of Ships Operating in Level Ice

Biao Su [1], Kaj Riska [1, 2], Torgeir Moan [1]

[1] Centre for Ships and Ocean Structures, NTNU, Trondheim, NORWAY

[2] ILS Oy, Helsinki, FINLAND

## ABSTRACT

A numerical model for simulating ship operations in level ice is presented. This model is partly based on empirical data, by which the observed phenomena of continuous icebreaking can be well reproduced. In the simulation of a full-scale icebreaking run, the interdependence between the ice load and the ship's motion is considered by solving the three degree-of-freedom rigid body equations of surge, sway and yaw by numerical integration. The variations in the level ice thickness and in the strength properties of ice can also be taken into account during the real-time simulations. The simulation results are discussed through three case studies, in which the ship's performance, the probabilistic and spatial variations of local ice loads around the hull and the short-term maximum ice loads on a frame are preliminarily analyzed and compared with field measurements conducted in the Baltic Sea. It is hoped that further studies on this numerical model can supplement the field and laboratory measurements in understanding the icebreaking processes and the resulting ice loads on ship hulls.

## INTRODUCTION

It is important to estimate both global and local ice loads on ships intended for the navigation in ice. The global ice load governs the ship's overall performance in ice, and it is an integrated effect of local ice loads over the hull area. Information on the distributions of local ice loads around the ship hull can be used for more effective design of ice-going ships both in terms of overall operation and from the structural point of view.

In an earlier study (Su et al., 2010a), a numerical method was introduced by the authors to investigate the global ice load and the ship's performance in level ice. This method is partly based on the empirical data, by which the observed phenomena of continuous icebreaking can be reproduced. In the simulation of an icebreaking run, the interdependence between the ice load and the ship's motion is considered, and the three degree-of-freedom rigid body equations of surge, sway and yaw are solved by numerical integration. The full-scale hull form of an icebreaker (Tor Viking II) was applied in a specific case study, and the estimated performance of the ship agreed well with the field measurements obtained by Riska et al. (2001).

The ice model was then extended to more complex ice conditions by considering random ice thickness and strength properties (Su et al., 2011), with the purpose of identifying the

probabilistic and spatial variations of local ice loads around the hull. A case study with an icebreaking tanker (MT Uikku) was performed by comparing the simulated peak loads on frames with the field measurements obtained by Kotisalo and Kujala (1999) and Hänninen (2003).

In this paper, the numerical model established and the previous simulation results are briefly described. A new case study with a chemical tanker (MS Kemira) is introduced by comparing the estimated 12-hour maximum ice loads on a frame with field measurements. The complementary information obtained on the icebreaking pattern, ice loading process and the short-term prediction of ice-induced loads on a frame are mainly discussed.

## NUMERICAL MODEL

Research on the numerical modeling of ice-hull interaction and ship maneuvering in level ice can be found for example in Valanto, 2001, Liu et al., 2006, Martio, 2007, Nguyen et al., 2009, Sawamura et al., 2010 and Lubbad and Løset, 2011. For the simulation of full-scale icebreaking runs, a more integrated model was developed and improved by Su et al. (2010a & 2011). In this model the interdependence between the ice loads and the planar motion of the ship is considered. The simulation program is established to reproduce observed icebreaking patterns and the continuous ice loading processes in a uniform level ice and the ice with randomly varying thickness and strength properties. In this section, the numerical model is briefly described.

### *General description of the model*

The methodology and assumptions used in the ice-hull interaction model are:

- the basic geometrical model (as shown in Figure 1) includes the waterline of the ship and the edge of the ice both discretized;
- the motions (surge, sway and yaw) of the ship on the horizontal plane are taken into account and the icebreaking forces are assumed to act on the waterline;
- the contact zones around the hull and the resulting ice forces and icebreaking patterns are numerically detected based on the empirical estimates of ice crushing force and ice bending failure;
- ice forces induced after the ice wedges are broken from the ice edge are taken into account by the Lindqvist's ice resistance formula (Lindqvist, 1989);
- the hydrodynamic effects on the ship's motion (drag and added mass) are derived from a numerical calculation before the simulation in ice;
- wave, wind and current forces are neglected as they are minor forces compared to ice forces;
- the rigid-body equations of motion are solved by numerical integration and
- iterations are performed at each time step, considering the interdependence between the ship's motion and the ice loads.

The detailed description of the methodology can be found in Su et al., 2010a & 2011, while the empirical estimates of the ice crushing force, ice bending failure and the statistical variation of the ice properties are mainly described herein.

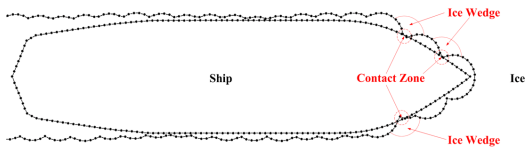

Figure 1. Geometrical idealization of the ice-hull interaction

***Ice crushing force***

At each contact zone shown in Figure 1, it is assumed that the ice is uniformly crushed on the contact surface. The crushing force, $F_{cr}$, is normal to the contact surface and calculated as the product of the effective ice crushing strength, $\sigma_c$, and the contact area, $A_c$. Figure 2 shows the illustration of the contact area between ice and hull, where $\varphi$ is the frame angle, and the ice crushing pressure on the contact surface is assumed to be uniform and equal to the effective ice crushing strength. The frictional force is also taken into account, which is divided into two components, $f_H$ and $f_V$, according to the relative motion between ice and hull. The horizontal and vertical components of the total contact force between ice and hull are then illustrated in Figure 3.

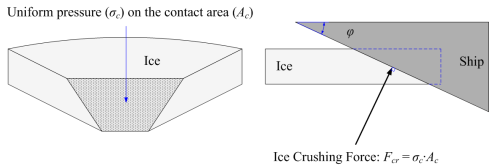

Figure 2. Illustration of the contact area between ice and hull

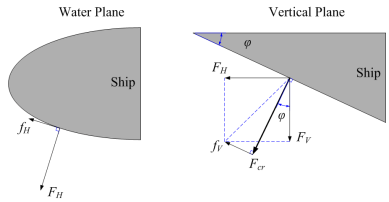

Figure 3. Illustration of horizontal and vertical components of the contact force

***Ice bending failure***

If the vertical component of the contact force between ice and hull ($F_V$, shown in Figure 3) exceeds the bending failure load of ice cover, $P_f$, given in Equation (1), the ice wedge (as shown in Figure 1 will be broken from the edge of the ice:

$$P_f = C_f \left( \frac{\theta}{\pi} \right)^2 \sigma_f h_i^2 \qquad (1)$$

where $\theta$ is the opening angle of the idealized ice wedge shown in Figure 4, $\sigma_f$ is the flexural strength of the ice, $h_i$ is the thickness of the ice, and $C_f$ is an empirical parameter. Equation (1) accounts for the opening angle, and it is an empirical equation (introduced by Kashtelyan (Kerr,

1975), applied in Wang, 2001, Liu et al., 2006, and Nguyen et al., 2009). Thus, the constant $C_f$ must be obtained from measurements.

The geometrical idealization of the ice wedge in contact with the hull is illustrated in Figure 4, where the bending crack is determined by the interpolation of the icebreaking radius at the first and last contact node (i.e., $R_f$ and $R_l$). The icebreaking radius $R$ is found by the expression given in Wang, 2001 (based on information from Enkvist, 1972 and Varsta, 1983):

$$R = C_l l\left(1.0 + C_v v^{rel}{}_n\right) \tag{2}$$

where $v^{rel}{}_n$ is the relative normal velocity between the ice and the hull node, $C_l$ and $C_v$ are two empirical parameters obtained from field measurements, and $l$ is the characteristic length of the ice:

$$l = \left(\frac{Eh_i^3}{12\left(1-\nu^2\right)\rho_w g}\right)^{\frac{1}{4}} \tag{3}$$

Based on these assumptions and simplifications, the icebreaking pattern and the continuous icebreaking forces can be determined using a step-by-step procedure with a time step, $\Delta t$, equal to 0.001 s. The effects of the empirical parameters (in Equations (1) and (2)) on the mean icebreaking force were investigated and compared with the Lindqvist's ice resistance (Lindqvist, 1989) in Su et al., 2010.

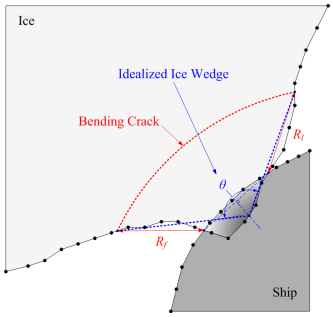


Figure 4. Geometrical idealization of the ice wedge in contact with the hull

***Statistical variation of the ice properties***

To reflect more complex ice conditions encountered in natural ice cover, the thickness and strength properties of the ice encountered by the ship can be randomly generated using the Monte Carlo method. Figure 5 shows a random sample of the varying ice properties along a 10 km route, where it is assumed that the ice thickness ($h_i$), ice crushing strength ($\sigma_c$) and ice flexural strength ($\sigma_f$) follow a normal probability distribution and they are independent on each other.

The existing data on the correlation of the spatial ice properties are very limited. The sensitivity of a possible correlation can be investigated by sampling the properties at the spatial points with different intervals. Figure 6 shows three simulated icebreaking runs in which the ice properties are randomized at different intervals (25, 50 and 100 m). The issues of correlation were briefly discussed in Su et al., 2011, and it remains one of the topics for further analysis.

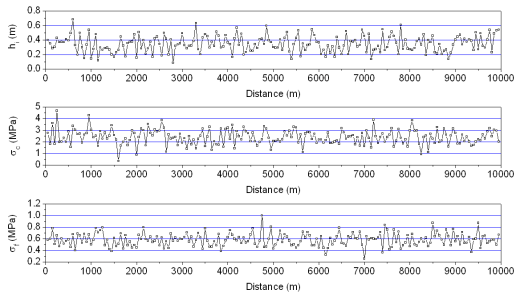


Figure 5. A random sample of the varying ice properties along a 10 km route

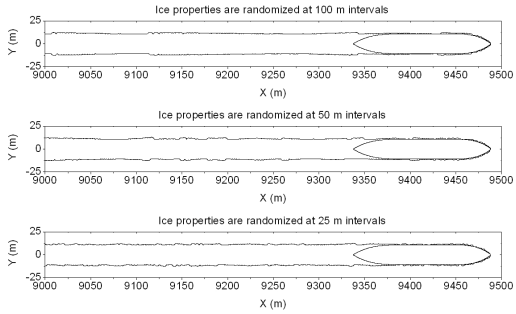


Figure 6. Simulated icebreaking runs under randomly varying ice conditions

## SHIP'S PERFORMANCE IN LEVEL ICE

A case study with an icebreaker, Tor Viking II, was carried out to investigate the total ice load and the ship's performance in level ice. In this study, the ice encountered by the ship was assumed to be uniform. The specified material characteristics of the ice and the main dimensions of the ship are given in Su et al., 2010.

In the simulation with a free-running model, the ship's motion was obtained by solving the equations of motion in which the thrust and the global ice load both were identified. The speed that the ship can attain was then simulated in the ice of different thicknesses. As shown in Figure 7, the simulation results agree well with the full-scale measurements (Riska et al., 2001). Figure 8 shows the simulated values of turning circle diameter which are also comparable to the measurements. Herein the deviation between the simulation results is due to the different icebreaking patterns shown in Figure 9. As discussed in Su et al., 2010a&b, if the shoulder crushing happens (i.e. the ice is continuously crushed by the hull shoulder without bending failure) both the forward speed and the turning rate of the ship will be considerably slowed down (see e.g. the simulation results in 1.0 m thick ice, as shown in Figure 7 and Figure 8).

The occurrence or non-occurrence of shoulder crushing is determined by the geometry of simulated icebreaking pattern, which is dependent on both the ice condition and the ship's motion. This phenomena was also observed in full-scale trials, but it is difficult to identify its actual effect on ship's performance because the actual ice conditions are usually uncontrollable. However, present simulation capability can account for shoulder crushing effects.

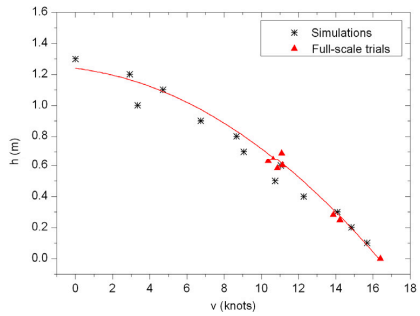


Figure 7. Comparison of the h-v curve between the present simulations and full-scale trials presented by Riska et al., 2001

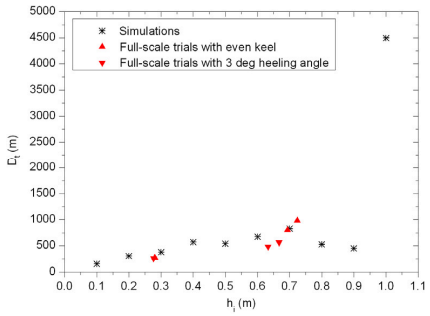


Figure 8. Comparison of the turning circle diameter between the present simulations and full-scale trials presented by Riska et al., 2010

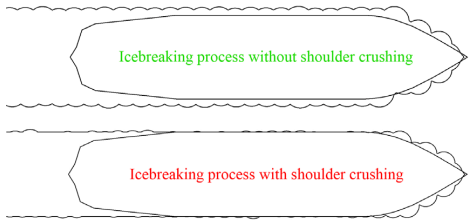


Figure 9. Two different icebreaking patterns

## PROBABILISTIC AND SPATIAL VARIATIONS OF LOCAL ICE LOADS

A case study with an icebreaking tanker, MT Uikku, was carried out to investigate the local ice load. In this study, the thickness and strength properties of the ice encountered by the ship were assumed to be constant or randomly generated using the Monte Carlo method. The statistical data on the strength properties of Baltic Sea ice (summarized by Kujala (1994)) were applied in this simulation, and the main dimensions of MT Uikku are given in Su et al., 2011.

In this study, the origin of the probabilistic variation of local ice loads was discussed. It was found that the variation of simulated ice loads on a frame was noteworthy even if the ice properties (i.e. ice thickness and ice strength) were fixed. Thereafter the variation in the contact and icebreaking patterns was taken as an internal origin of the probabilistic variation of local ice

loads, other than the external ice conditions. Figure 10 shows the variation of the contact between frame 196.5 and the ice in a period of 1 min simulated in the uniform ice. Here, the contact length is the load length within the frame area, and the variation of the contact length is attributed to the time varying icebreaking process of the ship. The frame spacing is 0.35 m on the bow area of MT Uikku. So, it means that the frame is fully in contact with ice when the contact length equals to 0.35 m.

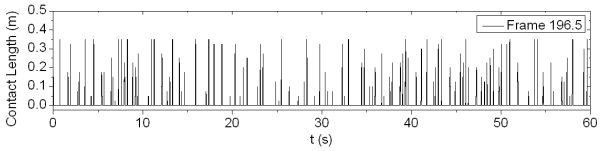


Figure 10. Time varying contact length between frame 196.5 and the ice (uniform ice thickness: 0.3 m)

Figure 11 shows a 10-min time history of the ice loads simulated in a randomly varying ice condition. The load values were calculated by dividing the normal force on the frame by the frame spacing (0.35 m); thus, the units are in kN/m. As shown in Figure 11, the load peaks are separated in two groups, where the peaks indicated by red squares are in accordance with full contact while the peaks indicated by green squares are in accordance with varying contact length.

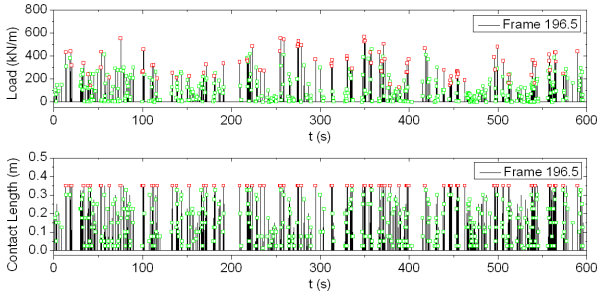


Figure 11. A 10-min history and separated peak values of the ice loads simulated in a randomly varying ice condition (average ice thickness: 0.34 m)

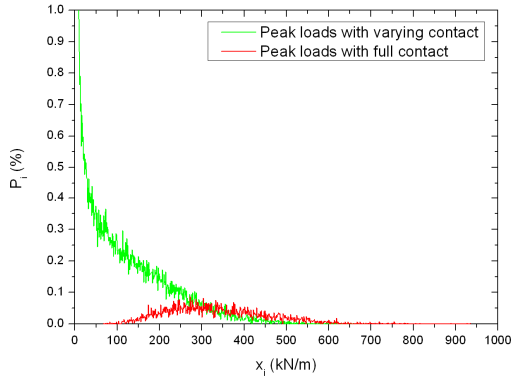


Figure 12. Probabilistic distribution of the simulated peak loads (recorded in a period of 12 hours) on frame 196.5 with varying or full contact

Figure 12 shows the probabilistic distribution of simulated peak loads (recorded in a period of 12 hours), where $x_i$ are the ordered values of peak loads ( $x_i$ =1, 2, 3… kN/m); $P_i$ are the occurrence percentages of the peak loads that are varying from $x_{i-1}$ to $x_i$ . In the situation that the frame is fully in contact with ice, the distribution of simulated peak loads is dominated by the variations in the thickness and strength properties of the ice which are assumed to be normally distributed along the route (see e.g. Figure 5). As a whole, it is dependent on the variations in both the external variables and the contact and icebreaking patterns.

As shown in Figure 13, 30 frames on different hull areas of MT Uikku were selected to investigate the spatial distribution of local ice loads in both straight going and turning operations. Figure 14 shows the simulated peak loads (with a non-exceedance probability of 99%, refer to Izumiyama et al., 2005) on different frames around the hull. This result agrees with previous experimental studies (e.g. Izumiyama et al., 2005), that the turning operation may develop a high load level on the aft shoulder area of the ship. It is expensive and technically difficult to perform the ice load measurements around a wide hull area in field tests. The present simulations can appreciably compensate this shortage of field data.

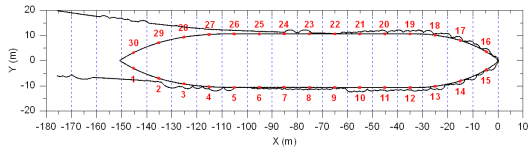


Figure 13. Numbering of the frames on different hull areas of MT Uikku

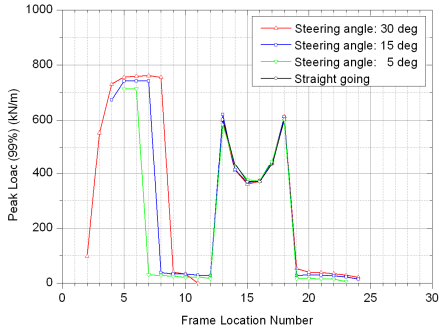


Figure 14. Spatial distribution of simulated peak loads around the hull (uniform ice thickness: 0.34 m)

## SHORT-TERM PREDICTION OF ICE-INDUCED LOADS ON A FRAME

Ice conditions and ship operations in ice vary in the short term from voyage to voyage and in the long term from winter to winter. Long-term ice load measurements conducted in the Baltic Sea consist mainly of 12-hour load maxima which are gathered during the normal operation of the ship over several years. A case study with a chemical tanker, MS Kemira, was carried out by using the simulation program. In this study, the statistical data on the strength properties of Baltic Sea ice were applied and the thickness of the ice encountered by the ship were classified referring

to the full-scale measurements onboard MS Kemira. The probable correlation between the simulated load maxima on a frame and the ice thickness is then discussed.

The main dimensions of MS Kemira and a detailed description of the full-scale measurements during the winters from 1985 to 1988 are given in Kujala, 1989. In this report, the operation profile of the ship and the prevailing ice conditions are also summarized. The thickness values of the ice encountered by the ship are grouped in 9 classes: (1) 0.01 – 0.02 m; (2) 0.03 – 0.06 m; (3) 0.07 – 0.12 m; (4) 0.13 – 0.20 m; (5) 0.21 – 0.30 m; (6) 0.31 – 0.42 m; (7) 0.43 – 0.56 m; (8) 0.57 – 0.72 m; (9) > 0.73 m.

During the full-scale measurements, the actual ice conditions may include all possible variants of ice features within a 12 hours' voyage. In this numerical study, a number of 10-min voyages were simulated and the icebreaking loads on frame 127 were gathered. Within each voyage, the strength properties of the ice were assumed to be normally distributed along the route (see e.g. Figure 5), the ice thickness was assumed to be uniformly or normally distributed. The 12-hour maximum load in a certain ice condition was then evaluated by fitting a Gumbel I asymptotic extreme value distribution on the simulated 10-min load maxima.

Figure 15 shows the simulation results in the ice where the thickness was assumed to be normally distributed along the route. The specified mean value of the ice thickness, $m_h$, was 0.165 m, and the analysis was carried out with different values of the standard deviation, $\sigma_h$. A mean value of measured 12-hour load maxima in the level ice assigned to ice thickness class 4 (0.13 – 0.20 m) is also denoted in this figure (data from Kujala, 1989 with few data points recorded under level ice condition). It can be expected that if a reasonable variance of the ice thickness is defined, the simulation results can be used for a preliminary estimation of the maximum ice loads within a 12 hours' voyage in level ice.

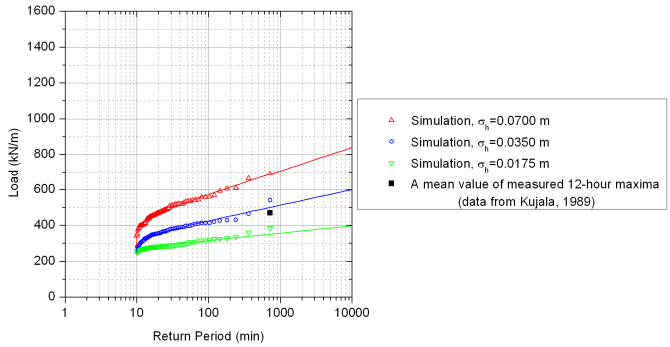


Figure 15. Simulated 10-min load maxima, and the comparison between the estimated and measured 12-hour load maxima (mean ice thickness: 0.165 m)

Figure 16 shows the simulation results in the ice where the thickness was assumed to be uniformly distributed along the route. The Gumbel I distribution is fitted to the simulated 10-min load maxima, $w$, within each ice thickness class (except for class 8 and class 9, as the maximum icebreaking capacity of MS Kemira is about 0.5 m):

$$F_{W|H}(w|h_i) = \exp\left(-\exp\left(-\frac{1}{c_i}(w-u_i)\right)\right) \qquad (4)$$

where the parameters $c_i$ and $u_i$ are related to the mean value, $\overline{w}$, and coefficient of variation, $k_\delta$, of $w$:

$$c_i = \overline{w}\frac{\sqrt{6}}{\pi}k_\delta \tag{5}$$

$$u_i = \overline{w} - \gamma c_i = \overline{w}\left(1 - \gamma\frac{\sqrt{6}}{\pi}k_\delta\right) \tag{6}$$

where $\gamma$ is Euler's constant, 0.577. The cumulative distribution function given in Equation (4) is defined as conditional because the parameters $c_i$ and $u_i$ are correlated with the classified ice thickness, $h_i$.

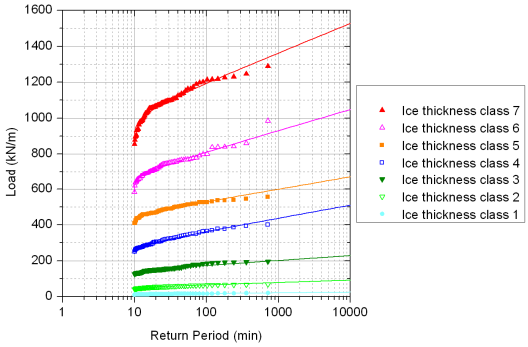


Figure 16. Fitted Gumbel distribution to the simulated 10-min load maxima within each ice thickness class

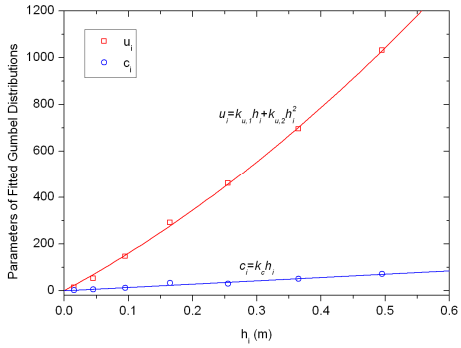


Figure 17. Parameters of fitted Gumbel distribution as a function of the classified ice thickness

As shown in Figure 17, the correlation between $c_i$, $u_i$ and $h_i$ can be determined by an approximate linear or quadratic regression. The conditional cumulative distribution function can then be translated into:

$$F_{W|H}(w|h_i) = \exp\left(-\exp\left(-\frac{1}{k_c h_i}\left(w - k_{u,1}h_i - k_{u,2}h_i^2\right)\right)\right) \tag{7}$$

where the parameters $k_c$ , $k_{u,1}$ and $k_{u,2}$ are determined from Figure 17. It should be noted that these parameters are dependent on the hull form and the frame angle. The assumed correlation in Figure 17 is fit for a specified frame on a specified ship hull, herein further validations are needed.

The final cumulative distribution function of $w$ can be obtained by integrating the conditional cumulative distribution function over the prevailing statistics of $h_i$ :

$$F_W(w) = \int_0^{h_{max}} \exp\left( -\exp\left( -\frac{1}{k_c h_i}\left( w - k_{u,1} h_i - k_{u,2} h_i^2 \right) \right) \right) f_{H_i}(h_i) \mathrm{d}h_i \qquad (8)$$

where $f_{H_i}(h_i)$ is the probability density function of $h_i$ , $h_{max}$ represents the maximum icebreaking capacity of the ship.

The empirical studies (e.g. Kujala, 1994) have shown that the best correlation between measured winter maximum ice load values and prevailing ice conditions is obtained when the equivalent level ice thickness is used to describe the annual ice conditions instead of parameters such as the maximum ice extent, fast or pack ice thickness. In view of this, Equation (8) indicates a potential way to evaluate the long-term ice load statistics based on short-term simulations.

## CONCLUSIONS

(1) Based on the empirical estimates of the bearing capacity and the breaking length of a floating ice wedge, the observed phenomena of continuous icebreaking can be reproduced by the simulation program.

(2) The global ice load effects on the ship's performance compare well with full-scale measurements.

(3) Information on the probabilistic and spatial variations of local ice loads and on the correlation between the short-term maximum ice loads acting on a frame and the prevailing ice conditions can be obtained by specifying the simulation parameters.

(4) A potential way to evaluate the long-term ice load statistics based on short-term simulations is introduced.

It is indicated by the present simulations that the hull form, the operational mode, the icebreaking pattern and ice failure mode influence both global and local ice loads encountered by the ship. Further studies of these issues are planned, as well as the improvement of this numerical model by considering the pressure–area relationship (see e.g. Jordaan et al., 2005), integrating the heave, roll and pitch motions of the ship and refining the ice forces induced after the ice pieces are broken by the hull.

## ACKNOWLEDGEMENTS

The authors wish to acknowledge the support of the Research Council of Norway through the Centre for Ships and Ocean Structures at the Norwegian University of Science and Technology in Trondheim, Norway.

## REFERENCES


Enkvist, E., 1972. On the Ice Resistance Encountered by Ships Operating in the Continuous Mode of Icebreaking. Report No.24, The Swedish Academy of Engineering Science in Finland, Helsinki, Finland.

Hänninen, S., 2003. Ship Based Observations on Board MT Uikku during the Winter 2003. Report for Deliverable D8 of IRIS Project, November 2003.

Izumiyama, K., Wako, D., Shimoda, H., and Uto, S., 2005. Ice Load Measurement on a Model Ship Hull. Proceedings of POAC 2005, pp. 635-645.

Jordaan, I., Li, C., Sudom, D., Stuckey, P., and Ralph, F., 2005. Principles for Local and Global Ice Design Using Pressure–Area Relationships. Proceedings of POAC 2005, pp. 375-385.

Kerr, A. D., 1975. The Bearing Capacity of Floating Ice Plates Subjected to Static or Quasi-static Loads, a Critical Survey. Research Report 333, Cold Regions Research and Engineering Laboratory, Hanover, New Hampshire, USA.

Kotisalo, K. and Kujala, P., 1999. Ice Load Measurements Onboard MT Uikku during the ARCDEV Voyage. Proceedings of POAC 1999, pp. 974-987.

Kujala, P., 1989. Results of Long-Term Measurements on Board Chemical Tanker Kemira in the Baltic Sea during the Winters 1985 to 1988. Research Report No. 47, Winter Navigation Research Board, Finland and Sweden, 1989.

Kujala, P., 1994. On the Statistics of Ice Loads on Ship Hull in the Baltic. Mechanical Engineering Series No. 116, Ship Laboratory, Helsinki University of Technology, Finland.

Lindqvist, G., 1989. A Straightforward Method for Calculation of Ice Resistance of Ships. Proceedings of POAC 1989, pp. 722-735.

Liu, J.C., Lau, M., and Williams, F.M., 2006. Mathematical Modeling of Ice-Hull Interaction for Ship Maneuvering in Ice Simulations. Proceedings of ICETECH 2006.

Lubbad, R., and Løset, S., 2011. A Numerical Model for Real-Time Simulation of Ship-Ice Interaction. Cold Regions Science and Technology 65 (2011), pp. 111-127.

Martio, J., 2007. Numerical Simulation of Vessel's Maneuvering Performance in Uniform Ice. Report No. M-301, Ship Laboratory, Helsinki University of Technology, Finland, 2007.

Nguyen, D.T., Sørbø, A.H., and Sørensen, A.J., 2009. Modeling and Control for Dynamic Positioned Vessels in Level Ice. 8th Conference on Manoeuvring and Control of Marine Craft, Guarujá, Brazil, 2009.

Riska, K., Leiviskä, T., Nyman, T., Fransson, L., Lehtonen, J., Eronen, H., and Backman, A., 2001. Ice Performance of the Swedish Multi-Purpose Icebreaker Tor Viking II. Proceedings of POAC 2001, pp. 849-865.

Sawamura, J., Tsuchiya, H., Tachibana, T., and Osawa, N., 2010. Numerical Modeling for Ship Maneuvering in Level Ice. Proceedings of IAHR 2010.

Su, B., Riska, K., and Moan, T., 2010a. A Numerical Method for the Prediction of Ship Performance in Level Ice. Cold Regions Science and Technology 60 (2010), pp. 177-188.

Su, B., Riska, K., and Moan, T., 2010b. Numerical Simulation of Ship Turning in Level Ice. Proceedings of OMAE 2010.

Su, B., Riska, K., and Moan, T., 2011. Numerical Simulation of Local Ice Loads in Uniform and Randomly Varying Ice Conditions. Cold Regions Science and Technology 65 (2011), pp. 145-159.

Valanto, P., 2001. The Resistance of Ships in Level Ice. Transactions of SNAME, 2001, Vol. 109, pp.53-83.

Varsta, P., 1983. On the Mechanics of Ice Load on Ships in Level Ice in the Baltic Sea. Publications 11, Technical Research Centre of Finland, Espoo, Finland.

Wang, S., 2001. A Dynamic Model for Breaking Pattern of Level Ice by Conical Structures. Ph.D. Thesis, Department of Mechanical Engineering, Helsinki University of Technology, Finland.

**R A P P O R T E R**
**UTGITT VED**
**INSTITUTT FOR MARIN TEKNIKK**
**(tidligere: FAKULTET FOR MARIN TEKNIKK)**
**NORGES TEKNISK-NATURVITENSKAPELIGE UNIVERSITET**

| Report No. | Author | Title |
|---|---|---|
| | Kavlie, Dag | Optimization of Plane Elastic Grillages, 1967 |
| | Hansen, Hans R. | Man-Machine Communication and Data-Storage Methods in Ship Structural Design, 1971 |
| | Gisvold, Kaare M. | A Method for non-linear mixed -integer programming and its Application to Design Problems, 1971 |
| | Lund, Sverre | Tanker Frame Optimalization by means of SUMT-Transformation and Behaviour Models, 1971 |
| | Vinje, Tor | On Vibration of Spherical Shells Interacting with Fluid, 1972 |
| | Lorentz, Jan D. | Tank Arrangement for Crude Oil Carriers in Accordance with the new Anti-Pollution Regulations, 1975 |
| | Carlsen, Carl A. | Computer-Aided Design of Tanker Structures, 1975 |
| | Larsen, Carl M. | Static and Dynamic Analysis of Offshore Pipelines during Installation, 1976 |
| UR-79-01 | Brigt Hatlestad, MK | The finite element method used in a fatigue evaluation of fixed offshore platforms. (Dr.Ing. Thesis) |
| UR-79-02 | Erik Pettersen, MK | Analysis and design of cellular structures. (Dr.Ing. Thesis) |
| UR-79-03 | Sverre Valsgård, MK | Finite difference and finite element methods applied to nonlinear analysis of plated structures. (Dr.Ing. Thesis) |
| UR-79-04 | Nils T. Nordsve, MK | Finite element collapse analysis of structural members considering imperfections and stresses due to fabrication. (Dr.Ing. Thesis) |
| UR-79-05 | Ivar J. Fylling, MK | Analysis of towline forces in ocean towing systems. (Dr.Ing. Thesis) |
| UR-80-06 | Nils Sandsmark, MM | Analysis of Stationary and Transient Heat Conduction by the Use of the Finite Element Method. (Dr.Ing. Thesis) |
| UR-80-09 | Sverre Haver, MK | Analysis of uncertainties related to the stochastic modeling of ocean waves. (Dr.Ing. Thesis) |
| UR-81-15 | Odland, Jonas | On the Strength of welded Ring stiffened cylindrical Shells primarily subjected to axial Compression |

| | | |
|---|---|---|
| UR-82-17 | Engesvik, Knut | Analysis of Uncertainties in the fatigue Capacity of Welded Joints |
| UR-82-18 | Rye, Henrik | Ocean wave groups |
| UR-83-30 | Eide, Oddvar Inge | On Cumulative Fatigue Damage in Steel Welded Joints |
| UR-83-33 | Mo, Olav | Stochastic Time Domain Analysis of Slender Offshore Structures |
| UR-83-34 | Amdahl, Jørgen | Energy absorption in Ship-platform impacts |
| UR-84-37 | Mørch, Morten | Motions and mooring forces of semi submersibles as determined by full-scale measurements and theoretical analysis |
| UR-84-38 | Soares, C. Guedes | Probabilistic models for load effects in ship structures |
| UR-84-39 | Aarsnes, Jan V. | Current forces on ships |
| UR-84-40 | Czujko, Jerzy | Collapse Analysis of Plates subjected to Biaxial Compression and Lateral Load |
| UR-85-46 | Alf G. Engseth, MK | Finite element collapse analysis of tubular steel offshore structures. (Dr.Ing. Thesis) |
| UR-86-47 | Dengody Sheshappa, MP | A Computer Design Model for Optimizing Fishing Vessel Designs Based on Techno-Economic Analysis. (Dr.Ing. Thesis) |
| UR-86-48 | Vidar Aanesland, MH | A Theoretical and Numerical Study of Ship Wave Resistance. (Dr.Ing. Thesis) |
| UR-86-49 | Heinz-Joachim Wessel, MK | Fracture Mechanics Analysis of Crack Growth in Plate Girders. (Dr.Ing. Thesis) |
| UR-86-50 | Jon Taby, MK | Ultimate and Post-ultimate Strength of Dented Tubular Members. (Dr.Ing. Thesis) |
| UR-86-51 | Walter Lian, MH | A Numerical Study of Two-Dimensional Separated Flow Past Bluff Bodies at Moderate KC-Numbers. (Dr.Ing. Thesis) |
| UR-86-52 | Bjørn Sortland, MH | Force Measurements in Oscillating Flow on Ship Sections and Circular Cylinders in a U-Tube Water Tank. (Dr.Ing. Thesis) |
| UR-86-53 | Kurt Strand, MM | A System Dynamic Approach to One-dimensional Fluid Flow. (Dr.Ing. Thesis) |
| UR-86-54 | Arne Edvin Løken, MH | Three Dimensional Second Order Hydrodynamic Effects on Ocean Structures in Waves. (Dr.Ing. Thesis) |
| UR-86-55 | Sigurd Falch, MH | A Numerical Study of Slamming of Two-Dimensional Bodies. (Dr.Ing. Thesis) |
| UR-87-56 | Arne Braathen, MH | Application of a Vortex Tracking Method to the Prediction of Roll Damping of a Two-Dimension |

| | | |
|---|---|---|
| | | Floating Body. (Dr.Ing. Thesis) |
| UR-87-57 | Bernt Leira, MK | Gaussian Vector Processes for Reliability Analysis involving Wave-Induced Load Effects. (Dr.Ing. Thesis) |
| UR-87-58 | Magnus Småvik, MM | Thermal Load and Process Characteristics in a Two-Stroke Diesel Engine with Thermal Barriers (in Norwegian). (Dr.Ing. Thesis) |
| MTA-88-59 | Bernt Arild Bremdal, MP | An Investigation of Marine Installation Processes – A Knowledge - Based Planning Approach. (Dr.Ing. Thesis) |
| MTA-88-60 | Xu Jun, MK | Non-linear Dynamic Analysis of Space-framed Offshore Structures. (Dr.Ing. Thesis) |
| MTA-89-61 | Gang Miao, MH | Hydrodynamic Forces and Dynamic Responses of Circular Cylinders in Wave Zones. (Dr.Ing. Thesis) |
| MTA-89-62 | Martin Greenhow, MH | Linear and Non-Linear Studies of Waves and Floating Bodies. Part I and Part II. (Dr.Techn. Thesis) |
| MTA-89-63 | Chang Li, MH | Force Coefficients of Spheres and Cubes in Oscillatory Flow with and without Current. (Dr.Ing. Thesis |
| MTA-89-64 | Hu Ying, MP | A Study of Marketing and Design in Development of Marine Transport Systems. (Dr.Ing. Thesis) |
| MTA-89-65 | Arild Jæger, MH | Seakeeping, Dynamic Stability and Performance of a Wedge Shaped Planing Hull. (Dr.Ing. Thesis) |
| MTA-89-66 | Chan Siu Hung, MM | The dynamic characteristics of tilting-pad bearings |
| MTA-89-67 | Kim Wikstrøm, MP | Analysis av projekteringen for ett offshore projekt. (Licenciat-avhandling) |
| MTA-89-68 | Jiao Guoyang, MK | Reliability Analysis of Crack Growth under Random Loading, considering Model Updating. (Dr.Ing. Thesis) |
| MTA-89-69 | Arnt Olufsen, MK | Uncertainty and Reliability Analysis of Fixed Offshore Structures. (Dr.Ing. Thesis) |
| MTA-89-70 | Wu Yu-Lin, MR | System Reliability Analyses of Offshore Structures using improved Truss and Beam Models. (Dr.Ing. Thesis) |
| MTA-90-71 | Jan Roger Hoff, MH | Three-dimensional Green function of a vessel with forward speed in waves. (Dr.Ing. Thesis) |
| MTA-90-72 | Rong Zhao, MH | Slow-Drift Motions of a Moored Two-Dimensional Body in Irregular Waves. (Dr.Ing. Thesis) |
| MTA-90-73 | Atle Minsaas, MP | Economical Risk Analysis. (Dr.Ing. Thesis) |
| MTA-90-74 | Knut-Aril Farnes, MK | Long-term Statistics of Response in Non-linear Marine Structures. (Dr.Ing. Thesis) |
| MTA-90- | Torbjørn Sotberg, MK | Application of Reliability Methods for Safety |

| | | |
|---|---|---|
| 75 | | Assessment of Submarine Pipelines. (Dr.Ing. Thesis) |
| MTA-90-76 | Zeuthen, Steffen, MP | SEAMAID. A computational model of the design process in a constraint-based logic programming environment. An example from the offshore domain. (Dr.Ing. Thesis) |
| MTA-91-77 | Haagensen, Sven, MM | Fuel Dependant Cyclic Variability in a Spark Ignition Engine - An Optical Approach. (Dr.Ing. Thesis) |
| MTA-91-78 | Løland, Geir, MH | Current forces on and flow through fish farms. (Dr.Ing. Thesis) |
| MTA-91-79 | Hoen, Christopher, MK | System Identification of Structures Excited by Stochastic Load Processes. (Dr.Ing. Thesis) |
| MTA-91-80 | Haugen, Stein, MK | Probabilistic Evaluation of Frequency of Collision between Ships and Offshore Platforms. (Dr.Ing. Thesis) |
| MTA-91-81 | Sødahl, Nils, MK | Methods for Design and Analysis of Flexible Risers. (Dr.Ing. Thesis) |
| MTA-91-82 | Ormberg, Harald, MK | Non-linear Response Analysis of Floating Fish Farm Systems. (Dr.Ing. Thesis) |
| MTA-91-83 | Marley, Mark J., MK | Time Variant Reliability under Fatigue Degradation. (Dr.Ing. Thesis) |
| MTA-91-84 | Krokstad, Jørgen R., MH | Second-order Loads in Multidirectional Seas. (Dr.Ing. Thesis) |
| MTA-91-85 | Molteberg, Gunnar A., MM | The Application of System Identification Techniques to Performance Monitoring of Four Stroke Turbocharged Diesel Engines. (Dr.Ing. Thesis) |
| MTA-92-86 | Mørch, Hans Jørgen Bjelke, MH | Aspects of Hydrofoil Design: with Emphasis on Hydrofoil Interaction in Calm Water. (Dr.Ing. Thesis) |
| MTA-92-87 | Chan Siu Hung, MM | Nonlinear Analysis of Rotordynamic Instabilities in Highspeed Turbomachinery. (Dr.Ing. Thesis) |
| MTA-92-88 | Bessason, Bjarni, MK | Assessment of Earthquake Loading and Response of Seismically Isolated Bridges. (Dr.Ing. Thesis) |
| MTA-92-89 | Langli, Geir, MP | Improving Operational Safety through exploitation of Design Knowledge - an investigation of offshore platform safety. (Dr.Ing. Thesis) |
| MTA-92-90 | Sævik, Svein, MK | On Stresses and Fatigue in Flexible Pipes. (Dr.Ing. Thesis) |
| MTA-92-91 | Ask, Tor Ø., MM | Ignition and Flame Growth in Lean Gas-Air Mixtures. An Experimental Study with a Schlieren System. (Dr.Ing. Thesis) |
| MTA-86-92 | Hessen, Gunnar, MK | Fracture Mechanics Analysis of Stiffened Tubular |

| | | |
|---|---|---|
| | | Members. (Dr.Ing. Thesis) |
| MTA-93-93 | Steinebach, Christian, MM | Knowledge Based Systems for Diagnosis of Rotating Machinery. (Dr.Ing. Thesis) |
| MTA-93-94 | Dalane, Jan Inge, MK | System Reliability in Design and Maintenance of Fixed Offshore Structures. (Dr.Ing. Thesis) |
| MTA-93-95 | Steen, Sverre, MH | Cobblestone Effect on SES. (Dr.Ing. Thesis) |
| MTA-93-96 | Karunakaran, Daniel, MK | Nonlinear Dynamic Response and Reliability Analysis of Drag-dominated Offshore Platforms. (Dr.Ing. Thesis) |
| MTA-93-97 | Hagen, Arnulf, MP | The Framework of a Design Process Language. (Dr.Ing. Thesis) |
| MTA-93-98 | Nordrik, Rune, MM | Investigation of Spark Ignition and Autoignition in Methane and Air Using Computational Fluid Dynamics and Chemical Reaction Kinetics. A Numerical Study of Ignition Processes in Internal Combustion Engines. (Dr.Ing. Thesis) |
| MTA-94-99 | Passano, Elizabeth, MK | Efficient Analysis of Nonlinear Slender Marine Structures. (Dr.Ing. Thesis) |
| MTA-94-100 | Kvålsvold, Jan, MH | Hydroelastic Modelling of Wetdeck Slamming on Multihull Vessels. (Dr.Ing. Thesis) |
| MTA-94-102 | Bech, Sidsel M., MK | Experimental and Numerical Determination of Stiffness and Strength of GRP/PVC Sandwich Structures. (Dr.Ing. Thesis) |
| MTA-95-103 | Paulsen, Hallvard, MM | A Study of Transient Jet and Spray using a Schlieren Method and Digital Image Processing. (Dr.Ing. Thesis) |
| MTA-95-104 | Hovde, Geir Olav, MK | Fatigue and Overload Reliability of Offshore Structural Systems, Considering the Effect of Inspection and Repair. (Dr.Ing. Thesis) |
| MTA-95-105 | Wang, Xiaozhi, MK | Reliability Analysis of Production Ships with Emphasis on Load Combination and Ultimate Strength. (Dr.Ing. Thesis) |
| MTA-95-106 | Ulstein, Tore, MH | Nonlinear Effects of a Flexible Stern Seal Bag on Cobblestone Oscillations of an SES. (Dr.Ing. Thesis) |
| MTA-95-107 | Solaas, Frøydis, MH | Analytical and Numerical Studies of Sloshing in Tanks. (Dr.Ing. Thesis) |
| MTA-95-108 | Hellan, Øyvind, MK | Nonlinear Pushover and Cyclic Analyses in Ultimate Limit State Design and Reassessment of Tubular Steel Offshore Structures. (Dr.Ing. Thesis) |
| MTA-95-109 | Hermundstad, Ole A., MK | Theoretical and Experimental Hydroelastic Analysis of High Speed Vessels. (Dr.Ing. Thesis) |
| MTA-96-110 | Bratland, Anne K., MH | Wave-Current Interaction Effects on Large-Volume Bodies in Water of Finite Depth. (Dr.Ing. Thesis) |

| | | |
|---|---|---|
| MTA-96-111 | Herfjord, Kjell, MH | A Study of Two-dimensional Separated Flow by a Combination of the Finite Element Method and Navier-Stokes Equations. (Dr.Ing. Thesis) |
| MTA-96-112 | Æsøy, Vilmar, MM | Hot Surface Assisted Compression Ignition in a Direct Injection Natural Gas Engine. (Dr.Ing. Thesis) |
| MTA-96-113 | Eknes, Monika L., MK | Escalation Scenarios Initiated by Gas Explosions on Offshore Installations. (Dr.Ing. Thesis) |
| MTA-96-114 | Erikstad, Stein O., MP | A Decision Support Model for Preliminary Ship Design. (Dr.Ing. Thesis) |
| MTA-96-115 | Pedersen, Egil, MH | A Nautical Study of Towed Marine Seismic Streamer Cable Configurations. (Dr.Ing. Thesis) |
| MTA-97-116 | Moksnes, Paul O., MM | Modelling Two-Phase Thermo-Fluid Systems Using Bond Graphs. (Dr.Ing. Thesis) |
| MTA-97-117 | Halse, Karl H., MK | On Vortex Shedding and Prediction of Vortex-Induced Vibrations of Circular Cylinders. (Dr.Ing. Thesis) |
| MTA-97-118 | Igland, Ragnar T., MK | Reliability Analysis of Pipelines during Laying, considering Ultimate Strength under Combined Loads. (Dr.Ing. Thesis) |
| MTA-97-119 | Pedersen, Hans-P., MP | Levendefiskteknologi for fiskefartøy. (Dr.Ing. Thesis) |
| MTA-98-120 | Vikestad, Kyrre, MK | Multi-Frequency Response of a Cylinder Subjected to Vortex Shedding and Support Motions. (Dr.Ing. Thesis) |
| MTA-98-121 | Azadi, Mohammad R. E., MK | Analysis of Static and Dynamic Pile-Soil-Jacket Behaviour. (Dr.Ing. Thesis) |
| MTA-98-122 | Ulltang, Terje, MP | A Communication Model for Product Information. (Dr.Ing. Thesis) |
| MTA-98-123 | Torbergsen, Erik, MM | Impeller/Diffuser Interaction Forces in Centrifugal Pumps. (Dr.Ing. Thesis) |
| MTA-98-124 | Hansen, Edmond, MH | A Discrete Element Model to Study Marginal Ice Zone Dynamics and the Behaviour of Vessels Moored in Broken Ice. (Dr.Ing. Thesis) |
| MTA-98-125 | Videiro, Paulo M., MK | Reliability Based Design of Marine Structures. (Dr.Ing. Thesis) |
| MTA-99-126 | Mainçon, Philippe, MK | Fatigue Reliability of Long Welds Application to Titanium Risers. (Dr.Ing. Thesis) |
| MTA-99-127 | Haugen, Elin M., MH | Hydroelastic Analysis of Slamming on Stiffened Plates with Application to Catamaran Wetdecks. (Dr.Ing. Thesis) |
| MTA-99-128 | Langhelle, Nina K., MK | Experimental Validation and Calibration of Nonlinear Finite Element Models for Use in Design of Aluminium Structures Exposed to Fire. (Dr.Ing. |

| | | |
|---|---|---|
| | | Thesis) |
| MTA-99-129 | Berstad, Are J., MK | Calculation of Fatigue Damage in Ship Structures. (Dr.Ing. Thesis) |
| MTA-99-130 | Andersen, Trond M., MM | Short Term Maintenance Planning. (Dr.Ing. Thesis) |
| MTA-99-131 | Tveiten, Bård Wathne, MK | Fatigue Assessment of Welded Aluminium Ship Details. (Dr.Ing. Thesis) |
| MTA-99-132 | Søreide, Fredrik, MP | Applications of underwater technology in deep water archaeology. Principles and practice. (Dr.Ing. Thesis) |
| MTA-99-133 | Tønnessen, Rune, MH | A Finite Element Method Applied to Unsteady Viscous Flow Around 2D Blunt Bodies With Sharp Corners. (Dr.Ing. Thesis) |
| MTA-99-134 | Elvekrok, Dag R., MP | Engineering Integration in Field Development Projects in the Norwegian Oil and Gas Industry. The Supplier Management of Norne. (Dr.Ing. Thesis) |
| MTA-99-135 | Fagerholt, Kjetil, MP | Optimeringsbaserte Metoder for Ruteplanlegging innen skipsfart. (Dr.Ing. Thesis) |
| MTA-99-136 | Bysveen, Marie, MM | Visualization in Two Directions on a Dynamic Combustion Rig for Studies of Fuel Quality. (Dr.Ing. Thesis) |
| MTA-2000-137 | Storteig, Eskild, MM | Dynamic characteristics and leakage performance of liquid annular seals in centrifugal pumps. (Dr.Ing. Thesis) |
| MTA-2000-138 | Sagli, Gro, MK | Model uncertainty and simplified estimates of long term extremes of hull girder loads in ships. (Dr.Ing. Thesis) |
| MTA-2000-139 | Tronstad, Harald, MK | Nonlinear analysis and design of cable net structures like fishing gear based on the finite element method. (Dr.Ing. Thesis) |
| MTA-2000-140 | Kroneberg, André, MP | Innovation in shipping by using scenarios. (Dr.Ing. Thesis) |
| MTA-2000-141 | Haslum, Herbjørn Alf, MH | Simplified methods applied to nonlinear motion of spar platforms. (Dr.Ing. Thesis) |
| MTA-2001-142 | Samdal, Ole Johan, MM | Modelling of Degradation Mechanisms and Stressor Interaction on Static Mechanical Equipment Residual Lifetime. (Dr.Ing. Thesis) |
| MTA-2001-143 | Baarholm, Rolf Jarle, MH | Theoretical and experimental studies of wave impact underneath decks of offshore platforms. (Dr.Ing. Thesis) |
| MTA-2001-144 | Wang, Lihua, MK | Probabilistic Analysis of Nonlinear Wave-induced Loads on Ships. (Dr.Ing. Thesis) |
| MTA-2001-145 | Kristensen, Odd H. Holt, MK | Ultimate Capacity of Aluminium Plates under Multiple Loads, Considering HAZ Properties. (Dr.Ing. Thesis) |

| | | |
|---|---|---|
| MTA-2001-146 | Greco, Marilena, MH | A Two-Dimensional Study of Green-Water Loading. (Dr.Ing. Thesis) |
| MTA-2001-147 | Heggelund, Svein E., MK | Calculation of Global Design Loads and Load Effects in Large High Speed Catamarans. (Dr.Ing. Thesis) |
| MTA-2001-148 | Babalola, Olusegun T., MK | Fatigue Strength of Titanium Risers – Defect Sensitivity. (Dr.Ing. Thesis) |
| MTA-2001-149 | Mohammed, Abuu K., MK | Nonlinear Shell Finite Elements for Ultimate Strength and Collapse Analysis of Ship Structures. (Dr.Ing. Thesis) |
| MTA-2002-150 | Holmedal, Lars E., MH | Wave-current interactions in the vicinity of the sea bed. (Dr.Ing. Thesis) |
| MTA-2002-151 | Rognebakke, Olav F., MH | Sloshing in rectangular tanks and interaction with ship motions. (Dr.Ing. Thesis) |
| MTA-2002-152 | Lader, Pål Furset, MH | Geometry and Kinematics of Breaking Waves. (Dr.Ing. Thesis) |
| MTA-2002-153 | Yang, Qinzheng, MH | Wash and wave resistance of ships in finite water depth. (Dr.Ing. Thesis) |
| MTA-2002-154 | Melhus, Øyvin, MM | Utilization of VOC in Diesel Engines. Ignition and combustion of VOC released by crude oil tankers. (Dr.Ing. Thesis) |
| MTA-2002-155 | Ronæss, Marit, MH | Wave Induced Motions of Two Ships Advancing on Parallel Course. (Dr.Ing. Thesis) |
| MTA-2002-156 | Økland, Ole D., MK | Numerical and experimental investigation of whipping in twin hull vessels exposed to severe wet deck slamming. (Dr.Ing. Thesis) |
| MTA-2002-157 | Ge, Chunhua, MK | Global Hydroelastic Response of Catamarans due to Wet Deck Slamming. (Dr.Ing. Thesis) |
| MTA-2002-158 | Byklum, Eirik, MK | Nonlinear Shell Finite Elements for Ultimate Strength and Collapse Analysis of Ship Structures. (Dr.Ing. Thesis) |
| IMT-2003-1 | Chen, Haibo, MK | Probabilistic Evaluation of FPSO-Tanker Collision in Tandem Offloading Operation. (Dr.Ing. Thesis) |
| IMT-2003-2 | Skaugset, Kjetil Bjørn, MK | On the Suppression of Vortex Induced Vibrations of Circular Cylinders by Radial Water Jets. (Dr.Ing. Thesis) |
| IMT-2003-3 | Chezhian, Muthu | Three-Dimensional Analysis of Slamming. (Dr.Ing. Thesis) |
| IMT-2003-4 | Buhaug, Øyvind | Deposit Formation on Cylinder Liner Surfaces in Medium Speed Engines. (Dr.Ing. Thesis) |
| IMT-2003-5 | Tregde, Vidar | Aspects of Ship Design: Optimization of Aft Hull with Inverse Geometry Design. (Dr.Ing. Thesis) |

| | | |
|---|---|---|
| IMT-2003-6 | Wist, Hanne Therese | Statistical Properties of Successive Ocean Wave Parameters. (Dr.Ing. Thesis) |
| IMT-2004-7 | Ransau, Samuel | Numerical Methods for Flows with Evolving Interfaces. (Dr.Ing. Thesis) |
| IMT-2004-8 | Soma, Torkel | Blue-Chip or Sub-Standard. A data interrogation approach of identity safety characteristics of shipping organization. (Dr.Ing. Thesis) |
| IMT-2004-9 | Ersdal, Svein | An experimental study of hydrodynamic forces on cylinders and cables in near axial flow. (Dr.Ing. Thesis) |
| IMT-2005-10 | Brodtkorb, Per Andreas | The Probability of Occurrence of Dangerous Wave Situations at Sea. (Dr.Ing. Thesis) |
| IMT-2005-11 | Yttervik, Rune | Ocean current variability in relation to offshore engineering. (Dr.Ing. Thesis) |
| IMT-2005-12 | Fredheim, Arne | Current Forces on Net-Structures. (Dr.Ing. Thesis) |
| IMT-2005-13 | Heggernes, Kjetil | Flow around marine structures. (Dr.Ing. Thesis |
| IMT-2005-14 | Fouques, Sebastien | Lagrangian Modelling of Ocean Surface Waves and Synthetic Aperture Radar Wave Measurements. (Dr.Ing. Thesis) |
| IMT-2006-15 | Holm, Håvard | Numerical calculation of viscous free surface flow around marine structures. (Dr.Ing. Thesis) |
| IMT-2006-16 | Bjørheim, Lars G. | Failure Assessment of Long Through Thickness Fatigue Cracks in Ship Hulls. (Dr.Ing. Thesis) |
| IMT-2006-17 | Hansson, Lisbeth | Safety Management for Prevention of Occupational Accidents. (Dr.Ing. Thesis) |
| IMT-2006-18 | Zhu, Xinying | Application of the CIP Method to Strongly Nonlinear Wave-Body Interaction Problems. (Dr.Ing. Thesis) |
| IMT-2006-19 | Reite, Karl Johan | Modelling and Control of Trawl Systems. (Dr.Ing. Thesis) |
| IMT-2006-20 | Smogeli, Øyvind Notland | Control of Marine Propellers. From Normal to Extreme Conditions. (Dr.Ing. Thesis) |
| IMT-2007-21 | Storhaug, Gaute | Experimental Investigation of Wave Induced Vibrations and Their Effect on the Fatigue Loading of Ships. (Dr.Ing. Thesis) |
| IMT-2007-22 | Sun, Hui | A Boundary Element Method Applied to Strongly Nonlinear Wave-Body Interaction Problems. (PhD Thesis, CeSOS) |
| IMT-2007-23 | Rustad, Anne Marthine | Modelling and Control of Top Tensioned Risers. (PhD Thesis, CeSOS) |
| IMT-2007-24 | Johansen, Vegar | Modelling flexible slender system for real-time simulations and control applications |
| IMT- | Wroldsen, Anders Sunde | Modelling and control of tensegrity structures. (PhD |

| | | |
|---|---|---|
| 2007-25 | | Thesis, CeSOS) |
| IMT-2007-26 | Aronsen, Kristoffer Høye | An experimental investigation of in-line and combined inline and cross flow vortex induced vibrations. (Dr. avhandling, IMT) |
| IMT-2007-27 | Gao, Zhen | Stochastic Response Analysis of Mooring Systems with Emphasis on Frequency-domain Analysis of Fatigue due to Wide-band Response Processes (PhD Thesis, CeSOS) |
| IMT-2007-28 | Thorstensen, Tom Anders | Lifetime Profit Modelling of Ageing Systems Utilizing Information about Technical Condition. (Dr.ing. thesis, IMT) |
| IMT-2008-29 | Berntsen, Per Ivar B. | Structural Reliability Based Position Mooring. (PhD-Thesis, IMT) |
| IMT-2008-30 | Ye, Naiquan | Fatigue Assessment of Aluminium Welded Box-stiffener Joints in Ships (Dr.ing. thesis, IMT) |
| IMT-2008-31 | Radan, Damir | Integrated Control of Marine Electrical Power Systems. (PhD-Thesis, IMT) |
| IMT-2008-32 | Thomassen, Paul | Methods for Dynamic Response Analysis and Fatigue Life Estimation of Floating Fish Cages. (Dr.ing. thesis, IMT) |
| IMT-2008-33 | Pákozdi, Csaba | A Smoothed Particle Hydrodynamics Study of Two-dimensional Nonlinear Sloshing in Rectangular Tanks. (Dr.ing.thesis, IMT) |
| IMT-2007-34 | Grytøyr, Guttorm | A Higher-Order Boundary Element Method and Applications to Marine Hydrodynamics. (Dr.ing.thesis, IMT) |
| IMT-2008-35 | Drummen, Ingo | Experimental and Numerical Investigation of Nonlinear Wave-Induced Load Effects in Containerships considering Hydroelasticity. (PhD thesis, CeSOS) |
| IMT-2008-36 | Skejic, Renato | Maneuvering and Seakeeping of a Singel Ship and of Two Ships in Interaction. (PhD-Thesis, CeSOS) |
| IMT-2008-37 | Harlem, Alf | An Age-Based Replacement Model for Repairable Systems with Attention to High-Speed Marine Diesel Engines. (PhD-Thesis, IMT) |
| IMT-2008-38 | Alsos, Hagbart S. | Ship Grounding. Analysis of Ductile Fracture, Bottom Damage and Hull Girder Response. (PhD-thesis, IMT) |
| IMT-2008-39 | Graczyk, Mateusz | Experimental Investigation of Sloshing Loading and Load Effects in Membrane LNG Tanks Subjected to Random Excitation. (PhD-thesis, CeSOS) |
| IMT-2008-40 | Taghipour, Reza | Efficient Prediction of Dynamic Response for Flexible amd Multi-body Marine Structures. (PhD-thesis, CeSOS) |
| IMT-2008-41 | Ruth, Eivind | Propulsion control and thrust allocation on marine vessels. (PhD thesis, CeSOS) |

| | | |
|---|---|---|
| IMT-2008-42 | Nystad, Bent Helge | Technical Condition Indexes and Remaining Useful Life of Aggregated Systems. PhD thesis, IMT |
| IMT-2008-43 | Soni, Prashant Kumar | Hydrodynamic Coefficients for Vortex Induced Vibrations of Flexible Beams, PhD thesis, CeSOS |
| IMT-2009-43 | Amlashi, Hadi K.K. | Ultimate Strength and Reliability-based Design of Ship Hulls with Emphasis on Combined Global and Local Loads. PhD Thesis, IMT |
| IMT-2009-44 | Pedersen, Tom Arne | Bond Graph Modelling of Marine Power Systems. PhD Thesis, IMT |
| IMT-2009-45 | Kristiansen, Trygve | Two-Dimensional Numerical and Experimental Studies of Piston-Mode Resonance. PhD-Thesis, CeSOS |
| IMT-2009-46 | Ong, Muk Chen | Applications of a Standard High Reynolds Number Model and a Stochastic Scour Prediction Model for Marine Structures. PhD-thesis, IMT |
| IMT-2009-47 | Hong, Lin | Simplified Analysis and Design of Ships subjected to Collision and Grounding. PhD-thesis, IMT |
| IMT-2009-48 | Koushan, Kamran | Vortex Induced Vibrations of Free Span Pipelines, PhD thesis, IMT |
| IMT-2009-49 | Korsvik, Jarl Eirik | Heuristic Methods for Ship Routing and Scheduling. PhD-thesis, IMT |
| IMT-2009-50 | Lee, Jihoon | Experimental Investigation and Numerical in Analyzing the Ocean Current Displacement of Longlines. Ph.d.-Thesis, IMT. |
| IMT-2009-51 | Vestbøstad, Tone Gran | A Numerical Study of Wave-in-Deck Impact usin a Two-Dimensional Constrained Interpolation Profile Method, Ph.d.thesis, CeSOS. |
| IMT-2009-52 | Bruun, Kristine | Bond Graph Modelling of Fuel Cells for Marine Power Plants. Ph.d.-thesis, IMT |
| IMT 2009-53 | Holstad, Anders | Numerical Investigation of Turbulence in a Sekwed Three-Dimensional Channel Flow, Ph.d.-thesis, IMT. |
| IMT 2009-54 | Ayala-Uraga, Efren | Reliability-Based Assessment of Deteriorating Ship-shaped Offshore Structures, Ph.d.-thesis, IMT |
| IMT 2009-55 | Kong, Xiangjun | A Numerical Study of a Damaged Ship in Beam Sea Waves. Ph.d.-thesis, IMT/CeSOS. |
| IMT 2010-56 | Kristiansen, David | Wave Induced Effects on Floaters of Aquaculture Plants, Ph.d.-thesis, IMT/CeSOS. |
| IMT 2010-57 | Ludvigsen, Martin | An ROV-Toolbox for Optical and Acoustic Scientific Seabed Investigation. Ph.d.-thesis IMT. |
| IMT 2010-58 | Hals, Jørgen | Modelling and Phase Control of Wave-Energy Converters. Ph.d.thesis, CeSOS. |

| | | |
|---|---|---|
| IMT<br>IMT<br>2010- 59 | Shu, Zhi | Uncertainty Assessment of Wave Loads and Ultimate Strength of Tankers and Bulk Carriers in a Reliability Framework. Ph.d. Thesis, IMT. |
| IMT<br>2010-60 | Shao, Yanlin | Numerical Potential-Flow Studies on Weakly-Nonlinear Wave-Body Interactions with/without Small Forward Speed, Ph.d.thesis, IMT. |
| IMT<br>2010-61 | Califano, Andrea | Dynamic Loads on Marine Propellers due to Intermittent Ventilation. Ph.d.thesis, IMT. |
| IMT<br>2010-62 | El Khoury, George | Numerical Simulations of Massively Separated Turbulent Flows, Ph.d.-thesis, IMT |
| IMT<br>2010-63 | Seim, Knut Sponheim | Mixing Process in Dense Overflows with Emphasis on the Faroe Bank Channel Overflow. Ph.d.thesis, IMT |
| IMT<br>2010-64 | Jia, Huirong | Structural Analysis of Intect and Damaged Ships in a Collission Risk Analysis Perspective. Ph.d.thesis CeSoS. |
| IMT<br>2010-65 | Jiao, Linlin | Wave-Induced Effects on a Pontoon-type Very Large Floating Structures (VLFS). Ph.D.-thesis, CeSOS. |
| IMT<br>2010-66 | Abrahamsen, Bjørn Christian | Sloshing Induced Tank Roof with Entrapped Air Pocket. Ph.d.thesis, CeSOS. |
| IMT<br>2011-67 | Karimirad, Madjid | Stochastic Dynamic Response Analysis of Spar-Type Wind Turbines with Catenary or Taut Mooring Systems. Ph.d.-thesis, CeSOS. |
| IMT -<br>2011-68 | Erlend Meland | Condition Monitoring of Safety Critical Valves. Ph.d.-thesis, IMT. |
| IMT –<br>2011-69 | Yang, Limin | Stochastic Dynamic System Analysis of Wave Energy Converter with Hydraulic Power Take-Off, with Particular Reference to Wear Damage Analysis, Ph.d. Thesis, CeSOS. |
| IMT –<br>2011-70 | Visscher, Jan | Application of Particla Image Velocimetry on Turbulent Marine Flows, Ph.d.Thesis, IMT. |